AFRL-VA-WP-TR-2007-3042

VERSATILE MEASUREMENT TECHNIQUES TO VALIDATE ANALYTICAL STRUCTURAL MECHANICAL MODELS

David Banaszak

Experimental Validation Branch (AFRL/VASV)
Structures Division
Air Vehicles Directorate
Air Force Materiel Command, Air Force Research Laboratory
Wright-Patterson Air Force Base, OH 45433-7542

MARCH 2007

Final Report for 03 January 2003 – 31 October 2006

AIR VEHICLES DIRECTORATE
AIR FORCE MATERIEL COMMAND
AIR FORCE RESEARCH LABORATORY
WRIGHT-PATTERSON AIR FORCE BASE, OH 45433-7542

NOTICE AND SIGNATURE PAGE

Using Government drawings, specifications, or other data included in this document for any purpose other than Government procurement does not in any way obligate the U.S. Government. The fact that the Government formulated or supplied the drawings, specifications, or other data does not license the holder or any other person or corporation; or convey any rights or permission to manufacture, use, or sell any patented invention that may relate to them.

This report was cleared for public release by the Air Force Research Laboratory Wright Site (AFRL/WS) Public Affairs Office and is available to the general public, including foreign nationals.

Copies may be obtained from the Defense Technical Information Center (DTIC) (http://www.dtic.mil).

AFRL-VA-WP-TR-2007-3042 HAS BEEN REVIEWED AND IS APPROVED FOR PUBLICATION IN ACCORDANCE WITH ASSIGNED DISTRIBUTION STATEMENT.

*//Signature//

DAVID L. BANASZAK, Project Engineer
Experimental Validation Branch
Structures Division

//Signature//

RICHARD L. ROLFES, Chief
Experimental Validation Branch
Structures Division

//Signature//

DAVID M. PRATT, PhD
Technical Advisor
Structures Division

This report is published in the interest of scientific and technical information exchange, and its publication does not constitute the Government's approval or disapproval of its ideas or findings.

*Disseminated copies will show "//signature//" stamped or typed above the signature blocks.

REPORT DOCUMENTATION PAGE

Form Approved
OMB No. 0704-0188

1. REPORT DATE *(DD-MM-YY)*	2. REPORT TYPE	3. DATES COVERED *(From - To)*
March 2007	Final	01/03/2003 – 10/31/2006

4. TITLE AND SUBTITLE
VERSATILE MEASUREMENT TECHNIQUES TO VALIDATE ANALYTICAL STRUCTURAL MECHANICAL MODELS

5a. CONTRACT NUMBER
In-house

5b. GRANT NUMBER

5c. PROGRAM ELEMENT NUMBER
0602201

6. AUTHOR(S)
David Banaszak

5d. PROJECT NUMBER
A0AN

5e. TASK NUMBER

5f. WORK UNIT NUMBER
0A

7. PERFORMING ORGANIZATION NAME(S) AND ADDRESS(ES)
Experimental Validation Branch (AFRL/VASV)
Structures Division
Air Vehicles Directorate
Air Force Materiel Command, Air Force Research Laboratory
Wright-Patterson Air Force Base, OH 45433-7542

8. PERFORMING ORGANIZATION REPORT NUMBER
AFRL-VA-WP-TR-2007-3042

9. SPONSORING/MONITORING AGENCY NAME(S) AND ADDRESS(ES)
Air Vehicles Directorate
Air Force Research Laboratory
Air Force Materiel Command
Wright-Patterson Air Force Base, OH 45433-7542

10. SPONSORING/MONITORING AGENCY ACRONYM(S)
AFRL-VA-WP

11. SPONSORING/MONITORING AGENCY REPORT NUMBER(S)
AFRL-VA-WP-TR-2007-3042

12. DISTRIBUTION/AVAILABILITY STATEMENT
Approved for public release; distribution unlimited.

13. SUPPLEMENTARY NOTES
Report contains color. PAO Case Number: AFRL/WS 07-0484, 06 Mar 2007.

14. ABSTRACT

The objective of this in-house work unit was to develop and improve structural measurement systems, facilities and techniques for the collection and analysis of static and dynamic loads data in an inexpensive, reliable and expeditious manner. The effort used state-of-the art instrumentation to collect and analyze data required to validly define the loads environment and provide the necessities for identification, prediction, prevention and control of vibration, static structural loads, dynamic flutter, acoustical loads and thermal stresses in areas of structural fatigue and damage. The Air Force needs common, versatile, advanced and inexpensive measurement systems to support numerous aerospace vehicles and aging aircraft. The approach includes environmental laboratory tests and flight tests of various types of flight data acquisition systems, sensors and components to ensure compliance with accuracy, life, flight worthiness, maintenance, size performance, weight, reliability and safety requirements of loads data collection systems. Measurement systems should maximize on-board memory, and minimize size, weight and power requirements. This effort illustrates AFRL measurement needs in the laboratory and in the field. Conduct in-house studies of new vibration and static testing and analysis techniques. Studies included purchasing or developing in-house software and conducting experimental programs utilizing Design of Experiments (DOE) to check current and proposed measurement techniques. This report contains papers that document the resultant projects conducted to validate new instrumentation.

15. SUBJECT TERMS
measurement, instrumentation, static, dynamics, loads, thermal, systems, structural data

16. SECURITY CLASSIFICATION OF:			17. LIMITATION OF ABSTRACT:	18. NUMBER OF PAGES	19a. NAME OF RESPONSIBLE PERSON (Monitor)
a. REPORT	b. ABSTRACT	c. THIS PAGE			David Banaszak
Unclassified	Unclassified	Unclassified	SAR	204	19b. TELEPHONE NUMBER *(Include Area Code)* N/A

Standard Form 298 (Rev. 8-98)
Prescribed by ANSI Std. Z39-18

TABLE OF CONTENTS

1.0 EXECUTIVE SUMMARY

The papers in this report are a result of an in-house work unit titled "Versatile Measurement Techniques to Validate Analytical Structural Mechanical Models"(A0AN0A) These efforts were conducted by engineers and technicians in the Structures Division of the Air Vehicle Directorate of the Air Force Research Laboratory (AFRL). Most work was completed in the Experimental Validation Branch (AFRL/VASV). The objective of this in-house work unit was to develop and improve structural measurement systems, facilities and techniques for the collection and analysis of static and dynamic loads data in an inexpensive, reliable and expeditious manner. The effort used state-of-the art instrumentation to collect and analyze data required to validly define the loads environment and provide the necessities for identification, prediction, prevention and control of vibration, static structural loads, dynamic flutter, acoustical loads and thermal stresses in areas of structural fatigue and damage. The Air Force needs common, versatile, advanced and inexpensive measurement systems to support numerous aerospace vehicles and aging aircraft. The approach includes environmental laboratory tests and flight tests of various types of flight data acquisition systems, sensors and components to ensure compliance with accuracy, life, flight worthiness, maintenance, size performance, weight, reliability and safety requirements of loads data collection systems. Measurement systems should maximize on-board memory, and minimize size, weight and power requirements. This effort illustrates AFRL's different structural measurement needs in the laboratory and in the field. Studies included purchasing or developing in-house software and conducting experimental programs utilizing design of experiments (DOE) to check current and proposed measurement techniques. This report contains a collection of papers that document the resultant projects conducted to validate use of new instrumentation procured and developed by AFRL during the period of 3 January 2003 through 31 October 2006.

Note to Reader: In addition to this hard copy report, a digital version with multimedia video can be requested from DTIC.

2.0 INTRODUCTION

Potential areas of instrumentation study based on the research and development needs of the Structures Division, Air Vehicle Directorate of the Air Force Research Laboratory (AFRL) included the following tasks: (1) Incorporate advance networking techniques using USB and firewire interfacing into transducer measurements systems using a networked digital computer based data acquisition system, (2) Redesign and purchase new damage dosimeters and update 12 Structures Division damage dosimeters to increase memory storage and increase channel count to a higher number, (3) Investigate mechanical end-to-end calibration techniques of measurement systems. This includes commercialization of the Remote Control Structural Exciter Air Force patent, (4) Integrate a Visual Crack Measurement System using Temperature Sensitive Paint with AFGROW crack length prediction software and investigation other non-contacting video measurement technology, (5) Integration of GPS technology into measurement systems, (6) Participate in seminars and technical committees including active participation in the Vehicle Instrumentation/Transducer Committee of the Telemetry Group of the Range Commanders Council, (7) Investigate advance signal analysis techniques (e.g. wavelets) for structural health monitoring data compression, signal de-noising and representing non-stationary non-guassian structural stochastic processes, (8) Purchase potential off-the-shelf data acquisition systems for evaluation.

For task (1), AFRL utilized USB based data acquisition with a laptop personal computer as shown in paper 3.9 and 3.10. For task (2) papers describing use of current dosimeters are included in papers 3.2, 3.3, 3.5, 3.6, 3.8 including completion of an AFRL in-house effort to measure vibratory data behind the engine of a C-130 of a North Carolina Air National Guard aircraft based in Charlotte. The results of task (3) of investigating mechanical end-to-end mechanical calibrations are the main subject of paper 3.2. Papers 3.1 and 3.4 illustrate applications of using temperature sensitive paint to track and create crack growth curves for structures during resonant vibration on an electrodynamics shaker described by task (4). For task (5) AFRL investigated integration of GPS technology into VASV's data acquisition systems. This is a feasible task that can use GPS receivers for dynamics data. For lower frequency static data a free NTP server will work but still needs to be implemented by AFRL engineers and technicians. For task (6), an AFRL/VASV engineer was a co-author of IRIG standard 121-06 titled "Instrumentation Engineers Handbook" that is available for use by all commericial and DOD engineers at the public Range Commanders Council website. Task (7) resulted in a SBIR topic that was rolled into another in-house effort. Lastly, task (8) included the loan and evaluation of a Fiber Bragg Grating system delivered to AFRL/ML on a small business innovative research (SBIR) contract to measure strain on a fiber at every 1 centimeter on the fiber. Evaluation of this system on three simple beams is described in paper 3.10.

Links to the papers are found in the table of contents and in section 3 of this report. Not all of these planned tasks were completed, but a summary of instrumentation developed and used on this in-house work unit during this effort are included in this report.

The Air Force Research Laboratory continuously needs to develop improved measurement systems, facilities and techniques for the collection and analysis of static, thermal and dynamic

loads data in an inexpensive, reliable and expeditious manner. This development provides the infrastructure to collect and analyze data to validate the loads environment of Air Force weapons systems. The data provides the necessities for identification, prediction, prevention and control of vibration, static structural loads, dynamic flutter, acoustical loads and thermal stresses in areas of structural fatigue and damage. The Air Force needs common, versatile, advanced and inexpensive measurement systems and analytical techniques to support unmanned air vehicles (e.g. sensor craft), space vehicles and life extension of aging aircraft.

With the advent of advanced computer technology, the need for valid measurements to validate advanced structural computer models such as Air Force Grow (AFGROW) and finite element analysis (FEA) models is constantly increasing for complex and sometimes even simple structures. Fortunately, the state-of-art in measurement technology is also constantly advancing and can acquire much more data in a quick and efficient manner. On-board data processing is even possible. Couple this with the reduced Air Force in-house resources to implement basic measurement installations such as strain measurement systems, and it is apparent that more must be done with less people. Resources are required to buy commercial-off-the-shelf (COTS) hardware and software to study and take advantage of the many new technologies that are available for making structural measurements.

A summary of recent Laboratory Management Reviews (LMRs) for this work unit (WU) follows:

(1) During a Laboratory Management Review (LMR) on 14 July 2004 the following progress and status was reported: Small Measurement Items being purchased in-house. U.S. Patent 6,575,620 awarded for "Method and Device for Visually Measurement Structural Fatigue using a Temperature Sensitive Coating. The reviewer's comments were: "Important WU. Need to focus, probably on high temperature. Work with Ken Leger to determine scope, approach and requirements."

(2) During a LMR on 8 September 2005 the following progress and status was reported: USB data acquisition systems used with laptop computer to collect temperature and strain data during evaluation of fiber optic sensors. Resulted in paper "Lab Evaluation of Fiber Optic EFPI Sensors for Extreme Environment Tests" presented at JSM2005 in Minneapolis. Fibers tested to 1600 °F. Flame Spray booth near completion with training scheduled for September 2005. Flame spray required for further evaluating high temperature mounting of fiber optic strain sensors, strain gages and thermocouples. Plasma spray capability planned. LabView PC based data acquisition system loaned to support cooperative research and development agreement (CRADA) effort with APR, Inc. Prepared peer reviewed Journal article for IEST based on ESTECH 2004 paper. The reviewer's comments were: "Summarize objective, approach, and tech challenges with crisp bullets - Survey future program test requirements to identify gaps between current instrumentation state of the art and future instrumentation requirements - Update milestones based on the survey defined above."

(3) During the final LMR on 31 August 2006, the following progress and status was reported: Flame Spray Facility on line during December 2005 for attaching high temperature sensors.

Provided support to Materials Directorate (ML) in evaluating FBG sensors for distributed strain sensing using optical fibers. ESTECH 2006 presentation titled "Autonomous Environmental Definition of C-130 Flap Well Skin Panel after Constraint Layer Damping Repair. 22nd Transducer Workshop presentation titled "Exploring Fiber Optic Strain Sensors for Testing Future Aerospace Structures". Objectives updated in accordance with comments provided during last LMR. The next milestone was to finish support to AFRL/ML in evaluation of FBG fiber optic sensors. The reviewers final comments were: "Work is support work to specific test projects and not research and does not require an R&D case file to continue - Close out this work unit."

Thus, as a result of the final LMR on 31 August 2006, this technical report shows all the paper and presentations that have been cleared for public release and represent the results of this in-house effort to advance instrumentation for the measurement of thermal, dynamics and loads data on Air Force aerospace systems through 31 October 2006.

3.0 TECHNICAL PAPERS AND PATENTS

The following ten cited technical papers and presentations are included as links in the table of contents.

1. “Crack Growth in Repaired Metallic Structures under Vibratory Loads”, Society for the Advancement of Material and Process Engineering (SAMPE) 2003 Proceedings, Banaszak, Ratwani and Baust, Long Beach, CA, 11-15 May 2003.
2. Challenges in Validating Strain Gage Flight Data from a Digital Damage Dosimeter" Institute of Environmental Sciences and Technology (IEST) 2003 Proceedings Design, Test, and Evaluation Product Reliability, ESTECH 2003 the 49th ATM, Banaszak and Brown, Phoenix, AZ, 18-21 May 2003.
3. " A Statistical Look at Damage Dosimeter Data from a Fighter Aircraft”, ASA 2003 Proceedings of the Section on Physical and Engineering Sciences, Banaszak and Brown San Francisco, CA 3-7 Aug 2003.
4. “Initiation and Growth of Cracks in Metallic Plates at Resonant Frequencies”, Banaszak and Ratwani, Fracture Mechanics 2003, Shanghai, China, 19-23 Aug 2003.
5. “Sonic Fatigue Damage Service Environment and Life Improvement from Dosimeter Data”, 2003 ASIP Poster Session Presentation, Rogers, L., Banaszak, Laird and Brown, Savannah, GA 2-4 Dec 2003.
6. “Autonomous Environmental Definition of C-130 Flap Well Skin Panel”, Banaszak, Brown and Laird, Journal of the IEST, Volume 1 No. 48 2005, pp50-61, Rolling Meadows, IL. and “Autonomous Environmental Definition of C-130 Flap Well Skin Panel” Institute of Environmental Sciences and 6B) Technology (IEST) 2004 Proceedings Design, Test, and Evaluation Product Reliability, ESTECH 2004 the 50th ATM, Banaszak, Brown and Laird, Las Vegas, NV, 25-28 Apr 04.
7. “Lab Evaluation of Fiber Optic EFPI Sensors for Extreme Environment Tests”, ASA 2005 Proceedings of the Section on Physical and Engineering Sciences, Banaszak and Kretz, ,Minneapolis, MN, 7-11 August 2005.
8. "Autonomous Environmental Definition of C-130 Flap Well Skin Panel After Constraint Layer Damping Repair” ESTECH 2006 the 52nd ATM of IEST, Banaszak and Parin, Phoenix, AZ, 8 May 2006 presentation.
9. "Exploring Fiber Optic Strain Sensors for Testing Future Aerospace Structures ", 22nd Transducer Workshop, Banaszak, Kretz and Fisher, Jun 06, Forth Worth, TX.
10. Evaluation of a Distributed Sensing System with Simple Bending Beams , 2nd DESS, Banaszak, Medina, Wright State University, 30 October 2006.

Referenced Patents: See http://www.uspto.gov/patft/index.html

1. Method and Device for Visually Measuring Structural Fatigue using a Temperature Sensitive Coating” US Patent Number: 6,575,620 B, Jun 10, 2003.
2. Remote Control Structural Exciter, US Patent Number: 5,804,697, Sep 8, 1998.

Section 3.1

Crack Growth in Repaired Metallic Structures under Vibratory Loads

SAMPE 2003 Paper

SAMPE = Society for the Advancement of Material and Process Engineering
At Long Beach CA
May 11-15, 2003

CRACK GROWTH IN REPAIRED METALLIC STRUCTURES UNDER VIBRATORY LOADS

David Banaszak and Henry D. Baust
Air Force Research Laboratory (AFRL), Wright Patterson Air Force Base, OH 45433

Mohan M. Ratwani, Ph. D
R-Tec, Rolling Hills Estates, CA 90274

ABSTRACT

Fatigue testing of metallic panels with and without bonded repair patches was carried out under vibratory loads on a shaker. The repair patches, made from a woven fiberglass laminate, were bonded to the panels with AF-163-2m adhesive. A layer of AVERY 1125 viscoelastic material was placed between adhesive layer and fiberglass patch. A visual crack measurement system using temperature sensitive paint was used to measure crack lengths at regular intervals. The test data indicated gradual reduction in resonant frequencies with crack propagation in panels with and without repair patches. Significant increase in crack growth lives of panels with repair patches was observed as compared to panels with no patches. AFGROW computer code was used to predict crack growth of panels with and without bonded patches. The stress intensity factors (SIF) in AFGROW code were modified to account for dynamic effects of vibratory loading.

KEYWORDS: Structural Analysis, Repair, Fatigue

1. INTRODUCTION

Composite patch repair is finding increasing use in repair of cracked metallic structures due to a number of advantages offered by the repair concept. The application of this concept to repair cracked metallic structures subjected to conventional mechanical fatigue loading is well established (References 1-8). However, the application of the concept to structures subjected to vibratory loads has been limited. Recent advances in the application of the concept to repairing metallic structures under vibratory loads (References 9-13) have provided new opportunities to apply this concept to: 1) Prevent acoustic fatigue failures from initiating during the life of an

aircraft, and 2) Retard the growth of the cracks that have already initiated. Some of the recent studies have shown that bonding of a fiberglass reinforcement (Reference 10-13) can enhance the fatigue life of metallic components subjected to vibratory loads. The enhancement in fatigue life due to bonding of composite reinforcements could occur due to - 1) an increase in stiffness and thereby decrease in stress response and increase in fatigue life, and 2) a retardation in crack initiation and growth of cracks due to load transfer to composite patch at crack initiation sites.

Analytical prediction of crack initiation and growth due to vibratory loads has always been a problem due to the complex nature of the loads and state of stress produced by the loads at the damage initiation sites. Past emphasis has been primarily on tests. This is often time-consuming and expensive. Recent advances in crack initiation and growth prediction methodology and software (e.g., AFGROW and NASGROW computer programs) have provided opportunities for analytical prediction of damage initiation and growth under vibratory loads. While the analytical techniques incorporated in AFGROW or NASGROW may not be directly applicable to life prediction under vibratory loads, they provide an excellent basis for developing analytical techniques for predicting damage initiation and growth under vibratory loads.

The present study was carried out to: 1) Identify potential benefits of bonded composite repairs under vibratory loads, and 2) Evaluate the capability of current analytical techniques to reliably predict the initiation and growth of cracks due to vibratory loads in structures with and without composite patches.

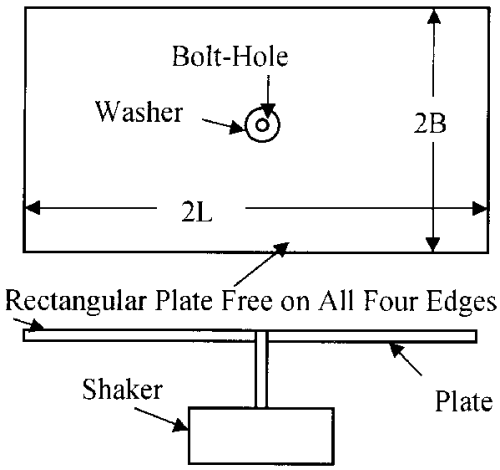

Figure 1a. Test specimen Geometry

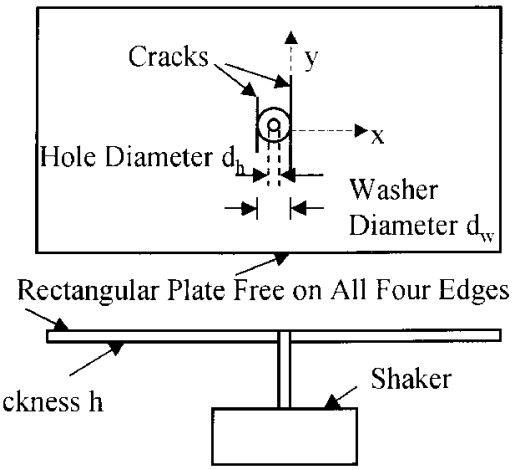

Figure 1b. Crack Initiation Locations

2. TEST PROGRAM

A comprehensive fatigue test database (References 10-13) on 2024-T3 aluminum panels with and without repair patches has been generated by the Wright-Patterson Air Force Base on aluminum specimens subjected to shaker excitation at resonant frequencies. Specimen configuration shown in Figure 1a was tested under vibratory loads in a shaker at resonant frequencies. Four series of test specimen with dimensions shown in Figure 2 were used. The figure also shows resonant test frequencies for test specimens without repair patch before crack initiation. The resonant frequencies decreased as cracks initiated and propagated. Each test series had at least 3 replicate tests.

Test Series	Width (mm)	Length (mm)	Thickness (mm)	Test Frequency (Hz)
1	85	180	1	110-112
2	85	180	3.2	330-336
3	170	360	1	27-28
4	170	360	3.2	82-83

Figure 2. Panel Dimensions and Resonant Frequencies on Panels Without Bonded Repair Patches Before Crack Initiation

A Visual Crack Measurement System (VCMS) using temperature sensitive paint, shown in Figure 3, was used to monitor initiation and growth of cracks. The details of VCMS are discussed in Reference 11.

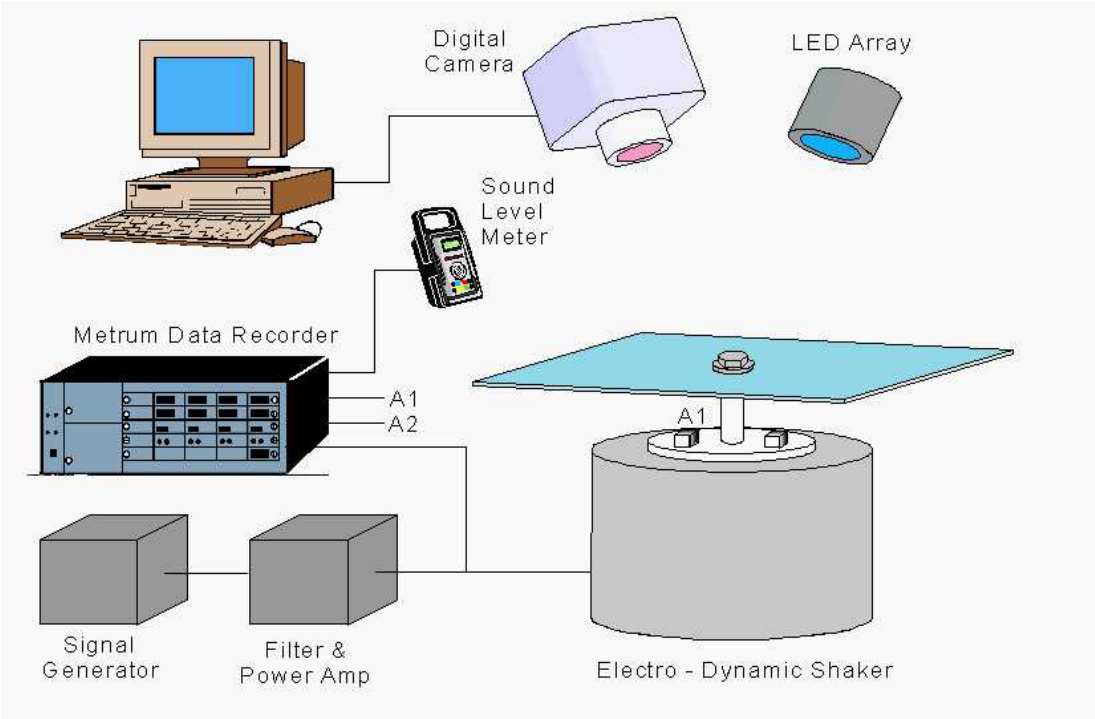

Figure 3. Schematic of Test Setup for Vibrating Panels Using Visual Crack Measurement System

After cracks were grown to approximately 25 mm, the test specimens were bonded with composite patches. The repair patches, made from a woven fiberglass laminate (Fiberite MXB-7701/7781 fiberglass prepreg), were bonded to the panels with AF-163-2m adhesive. A layer of AVERY 1125 viscoelastic material was placed between adhesive layer and fiberglass patch. All patches were 8 plies (3 of 40x70 mm; 3 of 40x65 mm and 3 of 40x60 mm).

All test specimens were bonded with same size patches irrespective of test specimen size and thickness. Typical small size specimens (180x85 mm) with a bonded repair patch are shown in Figure 4a. The repair patch width is almost the same as the width of the test specimen. Typical repair patches bonded to large size specimens (360x170 mm) are shown in Figure 4b. The repair patch covers only the central portion of the test specimen.

After bonding of repair patches testing was continued and crack growth measurements taken using VCMS. The tests indicated that the resonant frequencies of test specimens increased after bonding patches. As testing of bonded panels continued, resonant frequencies decreased with crack growth. Maximum tip deflections at the panel free ends (Figure 1a) were measured for computing strains and stresses.

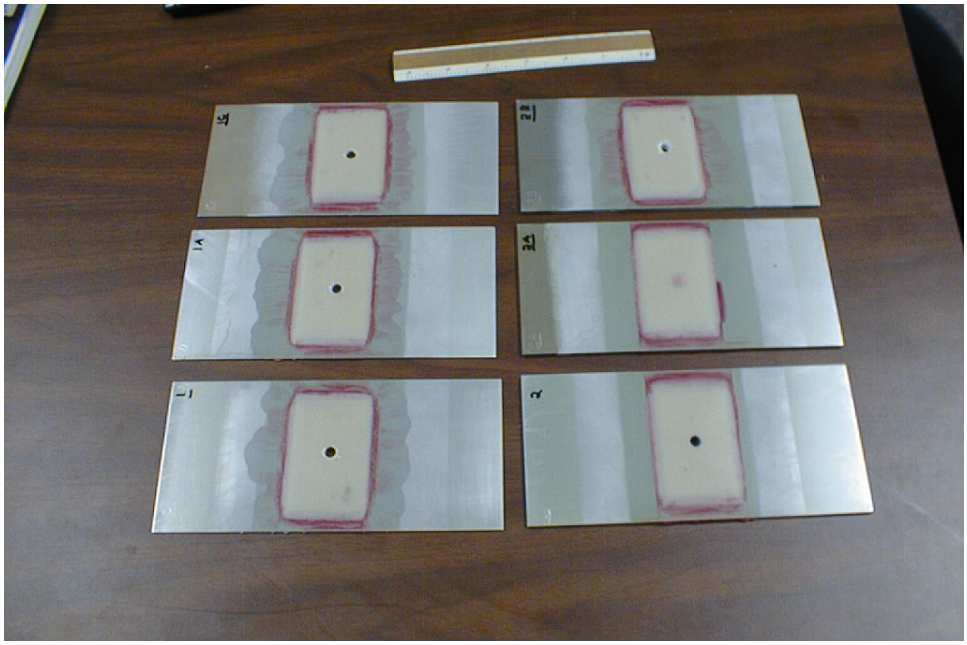

Figure 4a. Small Size (180x85 mm) Test Specimens with Repair Patches

Figure 4b. Large Size (360x170 mm) Test Specimens with Repair Patches

3. STRESS ANALYSIS

Analytical techniques to obtain resonant frequencies of cracked panels with and without bonded patches were developed and are reported in Reference 14. The analyses showed good agreement with test resonant frequencies. Dynamic stress analysis of vibrating panels shown in Figure 1a was developed in Reference 15. This analysis was used to obtain dynamic strains in the test panels. The predicted strains for various panels along with input g loading on the panel are shown in Figure 5. The figure also shows the test strains (Reference 10) obtained from maximum test deflections, shown in Figure 5, using simple beam theory. The agreement between predicted strains and test strains is very good. The stresses obtained from test strains were used in AFGROW computer code for crack growth predictions.

Specimen Size (mm)	Resonance Frequency	Input g Loading	Tip Displacement (mm)	Strains(μin/in) Predicted	Strains(μin/in) Test	Difference %
180x85x1	112	6	12.7	3,088	3,187	+3.1
180x85x3.2	348	6	4.45	3,377	3,346	-0.9
360x170x1	27	3	50.8	2,941	3,187	+7.7
360x170x3.2	83	3	17.15	3,101	3,226	+3.8

Figure 5. Comparison of Predicted and Test Strains

4. CRACK GROWTH IN PANELS WITHOUT COMPOSITE REPAIR PATCHES

In view of significant scatter in observed fatigue test data that included crack initiation, the test data were analyzed to investigate only crack growth behavior under vibratory loading. For each specimen of data series, the crack growth was plotted as a function of number of cycles after the first crack was detected in each specimen. Thus, for each specimen the time at which first crack was observed was considered as starting point with zero cycles and cycles were counted from this point onwards for comparing crack growth behavior.

A comparison of crack growth behavior in Test Series 1 and 2 is shown in Figure 6. The specimens in the tests are made from same material and have the same size (Length and Width). However, the thickness of Test Series 2 specimens is three times that of Test Series 1. The maximum strains in both the specimen series are almost the same as indicated in Figure 56. Hence, crack growth behavior is expected to be similar. However, Figure 6 indicates the crack growth in Test Series 1 to be much faster compared to Test Series 2. The resonant frequency of Test Series 2 specimens (330-336 Hz) is 3 times that for Test Series 1 specimens (110-112 Hz). It is shown in Reference 16 that higher frequency causes reduction in stress intensity factors, hence, slower crack growth. Also, in Series 2 thicker specimens under fully reversed bending cracks do not initiate in the same plane. Hence, instead of one crack on each side of specimen centerline there may be two parallel cracks that try to shield each other. This will reduce stress intensity factors and crack growth rate.

A comparison of crack growth in Test Series 1 and 3 is shown in Figure 7. Test specimen Series 1 and 3 are of same material and thickness with almost same maximum strains as indicated in

Figure 5. However, size of specimens (length and width) in Test Series 3 is twice that in Test Series 1. In view of similar strains in two specimen series, crack growth behavior is expected to be same. However, Figure 7 indicates the crack growth in Test Series 3 to be much faster as compared to Test Series 1. This is attributed to different test frequencies (resonant frequencies) of the test series. The resonant frequency of specimens in Test Series 1 (110-112Hz) is 4 times that for Test Series 3 (27-28 Hz).

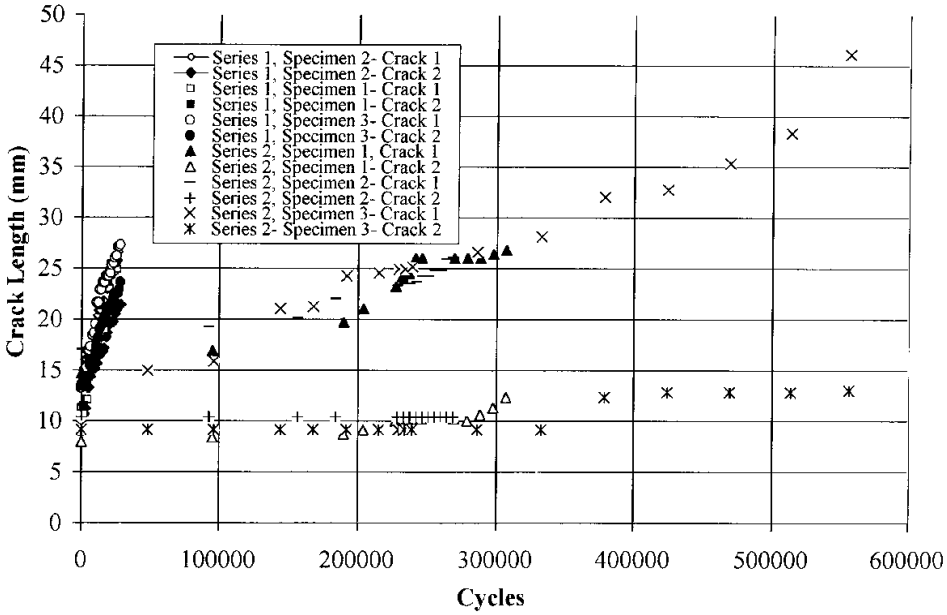

Figure 6. Comparison of Crack Growth in Series 1 and 2 Test Specimens

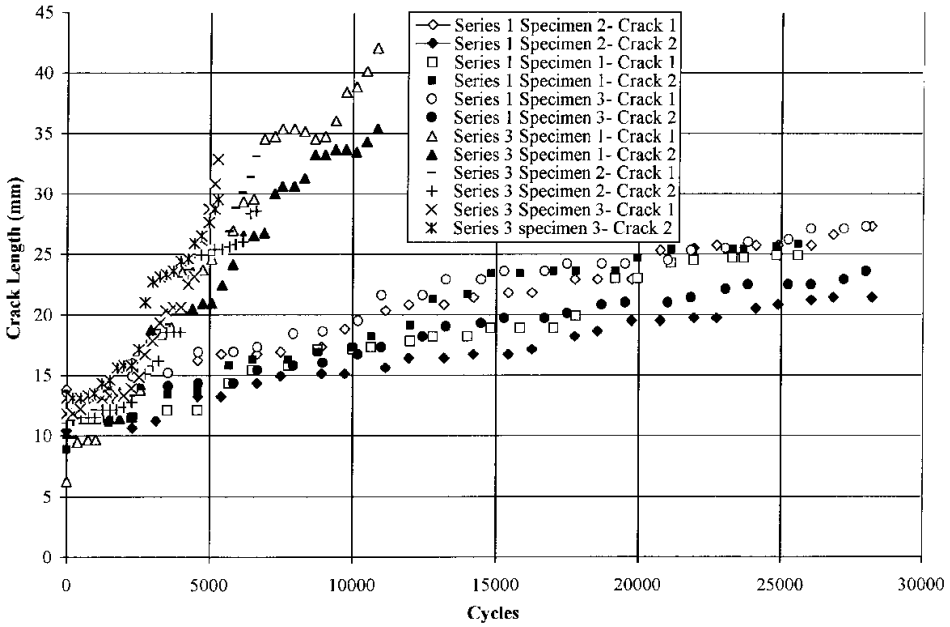

Figure 7. Comparison of Crack Growth in Series 1 and 3 Test Specimens

The review of crack growth data, indicated that a number of factors need to be considered in making crack growth predictions. The strains and corresponding stresses produced due to

vibratory loading (Figure 5) are an order of magnitude higher than one would expect from static analysis. Also, the bending moment in the panel varies from zero at free end to maximum value at the support. Current solutions for stress intensity factors, available in literature, are for the case of a constant moment applied to a panel. The use of such a solution to variable applied moment shall be an approximation. AFGROW computer program was used to predict crack growth in test specimens before bonding of repair patches and after bonding of repair patches. In making crack growth predictions with AFGROW, the following analysis cases were considered.

1. Use AFGROW computer code with present analytical capabilities.
2. Modify AFGROW stress intensity factors (SIFs) to account for the dynamic effects on SIFs. The dynamic effects on SIFs were considered based on the analysis reported in Reference 16.
3. Account for the effect of parallel cracks in the test specimens based on analysis of Reference 17. The test data have shown two cracks to grow one on each side of the central load application point (Figure 1b). Parallel cracks tend to shield each other and there by reduce SIFs.

Comparison of observed and predicted crack AFGROW growth in Series 1 specimens is shown in Figure 8. The AFGROW predictions are shown for the three analytical cases discussed above. The AFGROW predictions accounting for the dynamic and parallel crack effects agree well with test data initially up to 20-mm crack length. For larger crack lengths, observed crack growth is significantly slower. This is due to the fact that the bending SIF in AFGROW are for case of plate with constant far field moment. The present case of vibrating plate under consideration is subjected to zero moment at free end and maximum at the fixed end where cracks initiate. The SIF from AFGROW library will give higher value than for actual loading case. The error is likely to be higher for short span panels. The AFGROW analysis needs to be modified for the present bending case.

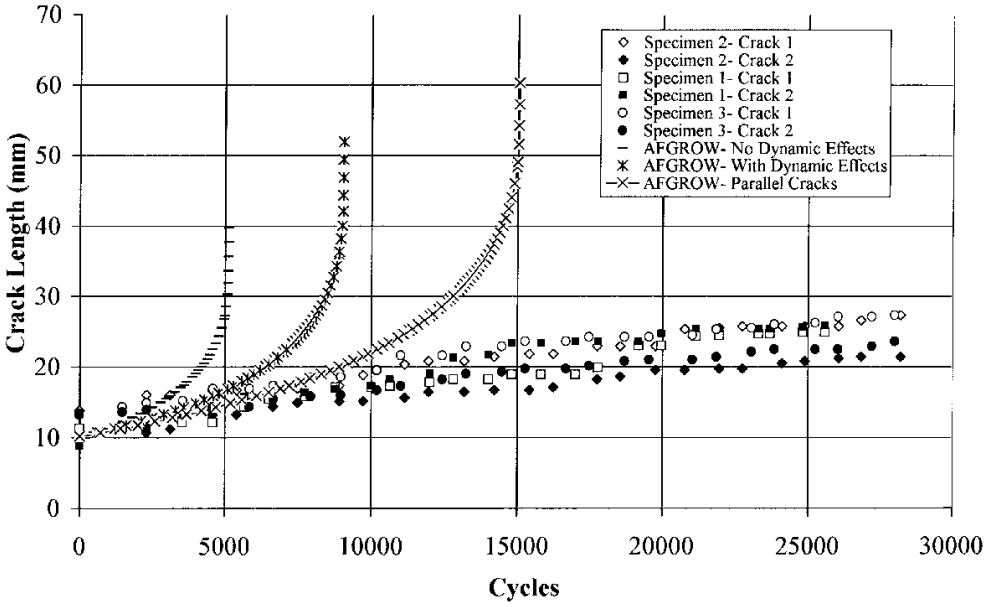

Figure 8. Observed and Predicted Crack Growth in Test Series 1 (185x85x1 mm) Specimens

A comparison of observed crack growth and AFGROW predicted crack growth in Series 3 specimens is shown in Figure 9. The AFGROW predictions are shown for the three analytical cases discussed above. The AFGROW predictions accounting for the dynamic effects agree well with test data initially up to about 30 mm crack length. However, for larger crack lengths observed crack growth is significantly slower. The modified AFGROW predictions accounting for dynamic and parallel crack effects agree well with test data. However, the slowing of crack growth exhibited by the test data is not predicted by analysis. This may be due to the fact that the bending stress intensity factors in AFGROW are for case of plate with far field applied constant moment. In the present case, the vibrating type plate under consideration is subjected to zero moment at free end and maximum at fixed end where cracks initiate.

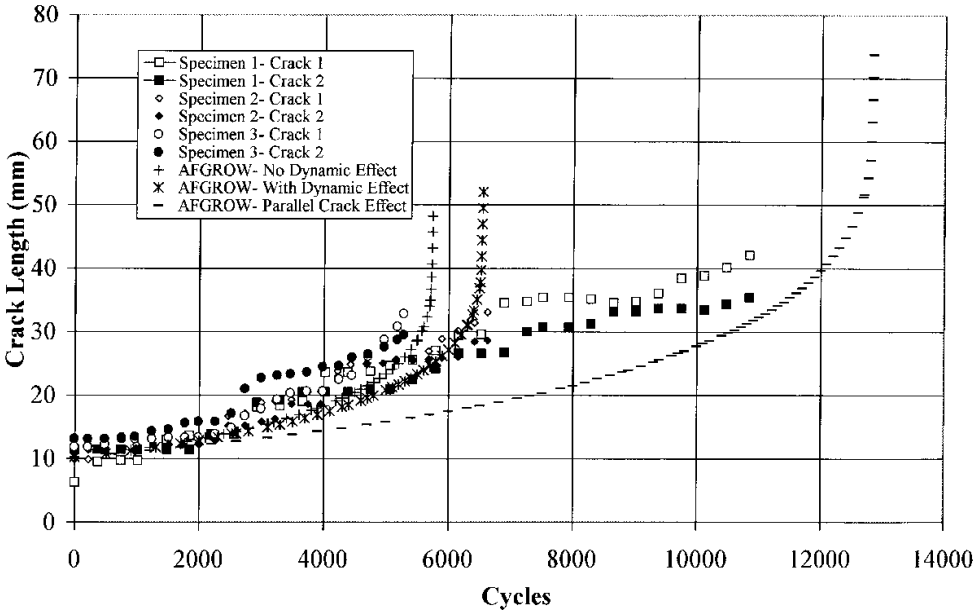

Figure 9. Observed and Predicted Crack Growth in Test Series 3 (360x170x1 mm) Specimens

5. CRACK GROWTH IN TEST SPECIMENS WITH BONDED COMPOSITE PATCHES

Crack growth data on test specimens, obtained after bonding of composite patches, were analyzed using AFGROW code. Test data from Test Series 1 and 2 could not be analyzed as the testing was conducted at a variety of stress levels. In these test series, it was not possible to grow cracks after a few million cycles and stress levels were increased to grow the cracks. The input load levels were gradually increased to 10g, 15g and 20g. The initial input load levels prior to bonding of composite patches were 6g. The damage occurred in test specimens at different stress levels and the patch experienced stiffness reduction and strength degradation under the high number of cycles. Hence, AFGROW analysis could not be directly applied to these test series. Test series 3 and 4 specimens were cycled at initial input load level of 3g after bonding of composite patches. AFGROW code was used to predict crack growth in these specimens after composite patches were bonded. The cycles were counted from the time testing was started after bonding of the patches.

AFGROW code bonded composite patch analysis was used for crack growth predictions. The composite patch stress intensity factors obtained from AFGROW code were modified to account for frequency effects based on Reference 16 analysis, and parallel crack effects based on Reference 17 analysis. Crack growth in Series 3 specimens is shown in Figure 10 along with AFGROW predictions. AFGROW predictions were made accounting for the effect of dynamic loads, parallel cracks and composite patches on SIF. The test data shows a large scatter. One specimen shows very short crack growth life. Total crack growth life of other two specimens agrees well with modified AFGROW predictions.

Crack growth in Test Series 4 specimens is shown in Figure 11 along with AFGROW predictions. AFGROW predictions were made accounting for the effect of dynamic loads, parallel cracks, and repair patches. Crack growth test data from one crack of Specimen 1 agrees well with AFGROW predictions. Other cracks show longer crack growth life as compared to AFGROW predictions.

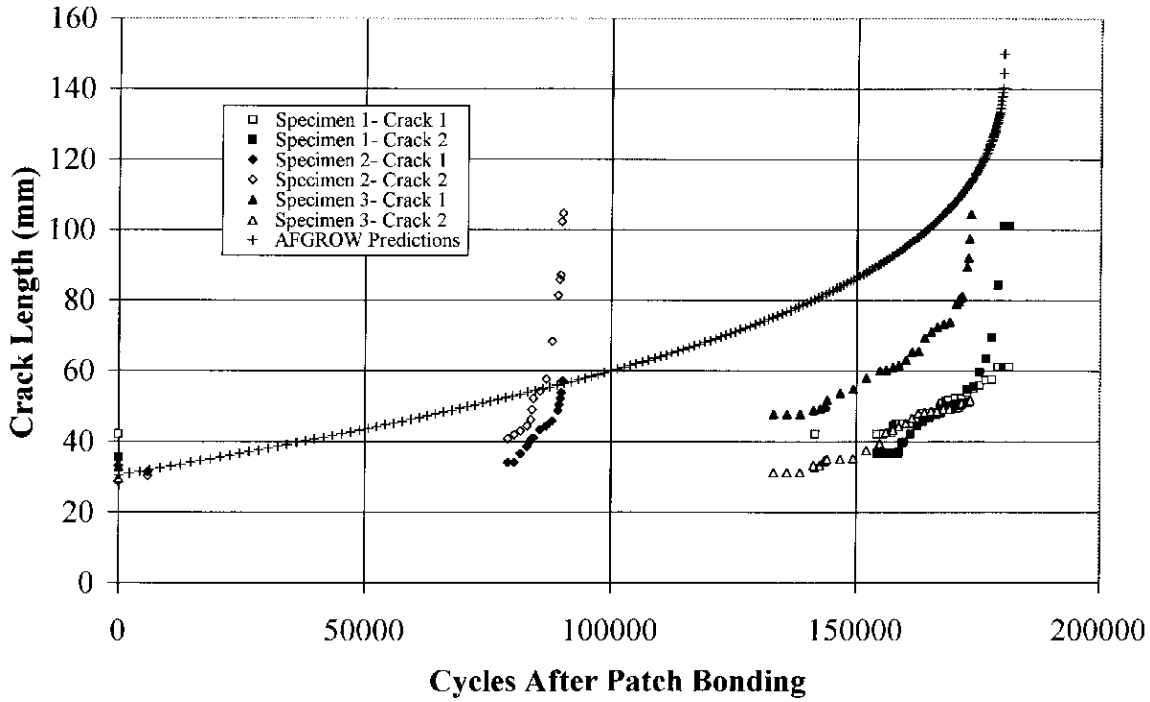

Figure 10. Observed and Predicted Crack Growth in Test Series 3 (1-mm Thick) Patched Specimen (Cycled at 3g)

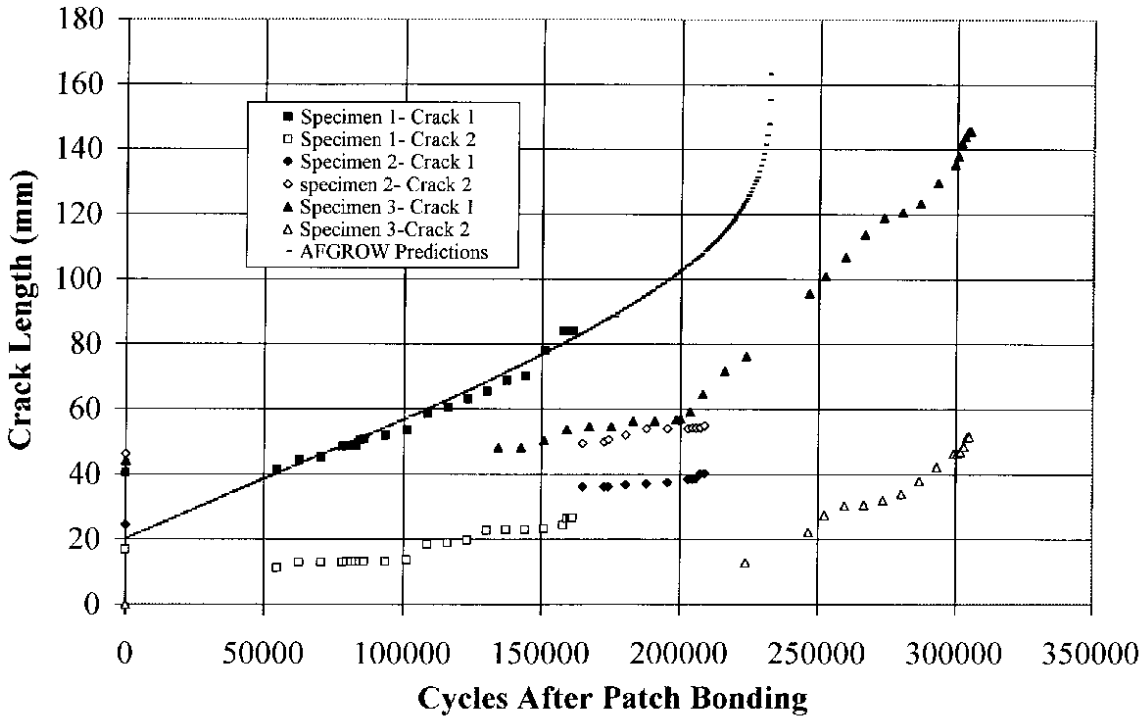

Figure 11. Observed and Predicted Crack Growth in Test Series 4 (3.2-mm Thick) Patched Specimen (Cycled at 3g)

A comparison of crack growth behavior in Series 3 specimen without repair patch (Figure 9) and with repair patch (Figure 10) shows significant increase in crack growth life. The number of cycles to grow crack from a length of about 30 mm to 45 mm in specimen without repair patch is about 6,000 cycles. The number of cycles to grow crack by same amount in specimen with repair patch is over 50,000.

6. CONCLUDING REMARKS

Crack growth data generated on aluminum panels with and without bonded repair patches under vibratory loads in a shaker have been analyzed. The trends in crack growth data are identified. It is shown that the resonant frequency has significant influence on crack growth rate. The higher resonant frequency reduces crack growth rate. The application of the crack growth computer code AFGROW to predict crack growth in panels subjected to vibratory loads was evaluated. It was determined that the stress intensity factor library in AFGROW code needs to be modified to account for the following factors-

1. Dynamic stresses
2. Influence of vibratory loads on stress intensity factors
3. Interaction between cracks
4. Stress intensity factors due to bending loads

7. REFERENCES

1. M. Heimerdinger, M.M. Ratwani and N.M. Ratwani, "Influence of Composite Repair Patch Dimensions on Crack Growth Life of Cracked Metallic Structures", Proceedings of Third FAA/DoD/NASA Conference on Aging Aircraft, Albuquerque, New Mexico (1999).
2. J. Helbling, R. Grover and M.M. Ratwani, "Analysis and Structural Test of Composite Reinforcement to Extend the Life of T-38 Lower Wing Skin", Proceedings Aircraft Structural Integrity Conference, San Antonio (1998).
3. J. Helbling, M. Heimerdinger and M.M. Ratwani, "Composite Patch Repair Applications to T-38 Lower Wing Skin", Proceedings of Second NASA/FAA/DoD Conference on Aging Aircraft, Williamsburg, Virginia (1998).
4. J. Helbling, M.M. Ratwani and M. Heimerdinger, "Analysis, Design and Test Verification of Composite Reinforcement for Multi-site Damage ", Proceedings of 20 International Conference on Aeronautical Fatigue Symposium, Seattle, Washington (1999).
5. J.J. Schubbe, "Thickness Effects on a Cracked Aluminum Plate with Composite Patch Repair", AFIT/DS/ENY/97-4 (1997).
6. A.A. Baker, "A Summary of Work on Applications of Advanced Fiber Composites at the Aeronautical Research Laboratory Australia", Composites, (1978).
7. J.B. Cockran, T. Christian and D.O. Hammond, "C-141 Repair of Metal Structure by Use of Composites", Proceedings of Aircraft Structural Integrity Conference, San Antonio, Texas (1988).
8. J. Mazza, "F-16 Fuel Vent Hole Repair Update," Proceedings of Aircraft Structural Integrity Conference, San Antonio, Texas (1996).
9. S. Ligoure, K. Hunter, R. Perez and T. Beier, "Flight Test Evaluation of Damped Composite Repairs for Sonic Fatigue", 40th AIAA/ASME/ASCE/AHS/ASC Structures, Structural Dynamics, and Materials Conference, St. Louis, (1999).
10. D. Banaszak, J.O. Lassiter and H.D. Baust, "Thermal-Optical Measurements in Structures with Damped Composite Repairs", The USAF Aircraft Structural Integrity Programs Conference, San Antonio, Texas, (1999).
11. D. Banaszak, G.A. Dale, N. Watkins and J.D. Jordan, "An Optical Technique for Detecting Fatigue Cracks in Aerospace Structures", 18th International Congress on Instrumentation in Aerospace Simulation, Toulouse, France, (1999).
12. D. Banaszak and G.A. Dale, "Two-Level Factorial Experiment for Crack Length Measurements of 2024-T3 Aluminum Plates Using Temperature Sensitive Paint and Electrodynamics Shakers", Proceeding of the Section on Physical and Engineering Sciences, American Statistical Association, (1999).
13. D. Banaszak, G.A. Dale and H.D. Baust, "Effectiveness of Damped Fiberglass Patches on Vibrating 2024-T3 Plates", Proceedings of SAMPE 2001 Conference, (2001).
14. M.M. Ratwani, M.J. Jacobson and D. Banaszak, "Resonant Frequencies of Vibrating Panels with Cracks and Bonded Composite Patches", Proceedings of 6th Joint FAA/DoD/NASA Conference on Aging Aircraft, San Francisco (2002).
15. M.M. Ratwani, "Development of Validated Crack Measurement System for Vibrating Structures", AFRL-VA-WP-TR-2002-3005 (2002).
16. E.S. Folias, "On the Steady State Transverse Vibrations of a Cracked Plate", Engineering Fracture Mechanics (1968).

17. M.M. Ratwani, "Wechselwirkung von Rissen (Interaction Between Cracks)", Institut fur Festkorpermechanik Research Report No. 5/72, Freiburg, West Germany (1972).

AUTHOR BIOGRAPHIES

David Banaszak received a Bachelor of Science (BS) in Electrical Engineering from the University of Wisconsin and a Master of Science (MS) in Applied Statistics from Wright State University. Dave works for the Air Vehicles Directorate of the AFRL. Dave does acoustic, vibration and loads measurements for numerous Air Force laboratory and field test programs. Dave is a member of the American Institute of Aeronautics and Astronautics (AIAA), Institute of Environmental Sciences and Technology (IEST) and American Statistical Association (ASA). Dave is also a member of the Vehicular Instrumentation/Transducer Subcommittee of the Range Commander's Council Telemetry Group. Currently Dave is President of the Greater Ohio Chapter of the IEST.

Dr. Ratwani was Director of the Aging Aircraft Project at Northrop Grumman Corporation (NGC), Military Aircraft Division and has over 30 years experience in aerospace structures. His expertise includes- aging systems restoration, software development for repairs, composite materials analysis and design, durability and damage tolerance of structures, and repair of aircraft structures. At Northrop, Dr. Ratwani was involved in life assessment of the F-5 and T-38 aircraft. Dr. Ratwani is the founder of R-Tec, where he has been principal investigator on several programs where he develops analytical techniques for bonded repair technology. His repair software was incorporated in US Air Force code AFGROW. He is author/co-author of over 100 technical papers and reports, and 5 textbooks. He taught special courses in composites, fatigue, and fracture for industries and universities in the USA and Europe. He was an invited lecturer at AGARD lecture series on aging aircraft.

Henry D. Baust received a BS in Electrical Engineering from the University of Iowa and a MS in Computer Science from Wright State University. His work for the Air Force evolves around wind tunnel testing. He has been involved with the design and installation of specialized measurement instrumentation, data systems, and control systems. Most recently he has been involved with optical flow field diagnostics systems. He is a member of IEEE.

Section 3.2

Challenges in Validating Strain Gage Flight Data from a Digital Damage Dosimeter

ESTECH 2003 Paper

ESTECH = Engineering Science and Technology
Annual meeting of the Institute of Environmental Sciences and Technology (IEST)
Phoenix, AZ
May 18-21, 2003

CHALLENGES IN VALIDATING FLIGHT DATA FROM A DIGITAL DAMAGE DOSIMETER

David Banaszak, Air Force Research Laboratory
Dansen L. Brown, Air Force Research Laboratory

Biography

David Banaszak received a Bachelor of Science (BS) in Electrical Engineering from the University of Wisconsin and a Master of Science (MS) in Applied Statistics from Wright State University. Dave works for the Air Vehicles Directorate of the Air Force Research Laboratory and does acoustic, vibration and loads measurements for numerous laboratory and field test programs. Dave is a member of the American Institute of Aeronautics and Astronautics, American Statistical Association and Vehicular Instrumentation/Transducer Subcommittee of the Range Commander's Council Telemetry Group. He is President of the Greater Ohio Chapter of the Institute of Environmental Sciences and Technology (IEST).

Dansen Brown has over 30 years experience in processing and analyzing dynamics data. He received Bachelor's and Master's degrees in Mathematics from Miami University (Oxford, Ohio) in the late '60s. He has worked for AFRL/VA since 1972, where he develops and maintains an advanced capability for the processing and analysis of dynamics data recorded during flight and ground tests conducted by the Structural Dynamics Branch of the Structures Division. He also frequently develops computer programs to recover, process, and analyze data recorded from other Air Force programs.

Abstract

The Air Force Research Laboratory (AFRL) sponsored development of on-board state-of-the-art digital data recorders called damage dosimeters to measure temperature and vibration data in areas of acoustic fatigue on aging aircraft such as the B-52, F-15, F-18, MD-88 and C-130. The Boeing Company designed the damage dosimeter to measure structural strains and temperatures on in-service aircraft to diagnose difficult-to-analyze structural conditions, such as acoustics and high cycle fatigue, requiring design of damped durability patches. The damage dosimeter is a rugged, small (fits in palm of hand), battery powered, lightweight (weighs less than 1.5 lb. (.69kg) without battery), data acquisition system that runs autonomously. The dosimeter measures 3 channels of strain at rates as high as 15 kilo-samples per second and a single channel of temperature at a rate of 1.3 samples per second. It only acquires data above a programmer defined rms strain threshold. For most tests, the dosimeter program stores 42 records of time history data each 0.3 seconds long and records and stores third octave records until its 4-Megabyte memory is filled. The damage dosimeter merges the functionality of both the analog signal conditioning, and a digital single board computer. Since the dosimeter requires installation of standard bonded strain gages and uses a series implementation of the Anderson Current Loop (ACL), a dosimeter measurement presents some technical calibration challenges. This paper shows AFRL investigated techniques to perform a system and physical (mechanical) end-to-end calibration of the three bonded strain gages connected in series. Techniques include inserting shunt calibration resistors in line for a system calibration and exciting the strain gages with a remote control structural exciter for a physical end-to-end calibration. The paper will present results from laboratory and C-130 calibration experiments.

Keywords

Calibration, Dosimeter, Data Acquisition, Vibration, Structures, Strain, Remote Control

Review of Dosimeter Operation

Motivation

Structural cracks in secondary structures, resulting from a high cycle fatigue (HCF), can result in costly inspection and repair. Often the repairs do not last because the structure continues to respond in a resonant fashion. The Durability Patch and Damage Dosimeter Program is an effort to resolve these problems with the application of compact, stand-alone, electronics and a damped bonded repair patch. Typical cracking of a secondary aircraft structure is shown in Banaszak, Brown and Trego (2002-ESTECH). To help design patches, Boeing developed a stand-alone data acquisition system (damage dosimeter) that can be easily installed on an aircraft to monitor temperature and dynamic characteristics of structures as presented by Haugse, Johnson, Smith, Rogers and Ryan (1999). This data provides the information required to design a repair. The damage dosimeter features include autonomous operation, on-board Fast Fourier Transform (FFT) computation and storage of third octave frequency spectra. The Anderson Current Loop (ACL) conditions strain gage signals to minimize

the power required to excite the dynamic gages and to eliminate the need to account for wire-length effects as described by Anderson (1995). A dosimeter, battery pack and block diagram is shown in figure 1. Smith and Searle (1998) give a complete description of the dosimeter.

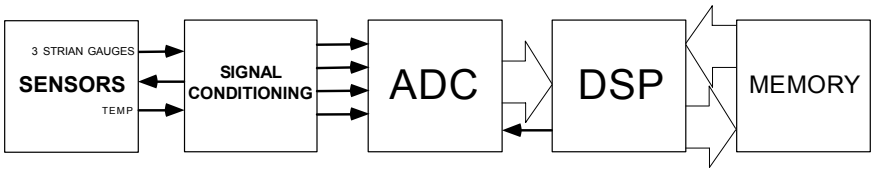

Figure 1. Damage Dosimeter and Battery Pack Overview and Block Diagram

Dosimeter Data Collection, Processing and Recording

The damage dosimeter operates in two modes: shop and acquisition. In acquisition mode the dosimeter acquires and stores data to non-volatile flash memory. During shop mode dosimeter data may be downloaded from its memory to a personal computer (PC) binary file. Once the battery pack is connected, all operations are autonomous (i.e. no human intervention is required) in acquisition mode.

During the first application of power, the dosimeter calculates the background noise level to determine an appropriate rms noise threshold. Below this threshold, the data will not be processed or recorded. The dosimeter powers down and remains off for about 99 seconds until powering up for acquiring a new record of data. When the dosimeter powers up again, the dosimeter enters acquisition mode and begins collecting strain and temperature data. Currently dosimeters acquire strain measurements at a rate of 7600 samples per second and temperature at about 1.3 samples per second. The strain data for each of the three gages is processed through a Fast Fourier Transform (FFT) analyzer to generate a Power Spectral Density (PSD). The PSD is then converted to 18 third octave frequency bands described more fully in Banaszak, Brown and Trego (2002-ESTECH).

Processed data sets are stored in non-volatile flash memory. Two types of data records are written: Standard Data Records (SDRs) and Strain Time-Histories (THs). The SDRs primarily consist of the rms strain levels for each of the 18 third octave frequency bands for each gage. In addition, the temperature, time stamp, and maximum strain for each gage are recorded with each SDR. SDRs are recorded only if the rms value of the time history is greater than the noise threshold.

The data acquisition, processing and recording process time line is as follows: The dosimeter acquires 2048 samples of three strain gages and 1 sample of temperature in about 0.3 second. The PSD is calculated. The rms value is computed and compared to the noise threshold. If the rms value is less than the threshold, the dosimeter powers off again for 99 seconds. If the rms value is above noise threshold, the 1/3-octave levels, computed from the PSD, are stored as a SDR record. The first 42 time-history data records are stored as TH records. Acquisition time is about .3 seconds and processing time is less than 1 second for each data cycle.

Dosimeter Programmability

The dosimeter can be reprogrammed to collect data without powering down during low threshold. This feature was used on the C-130 to better determine actual correlation of events between dosimeter data and the flight logs. For the C-130 installation described latter, after two flights of data were acquired during June 2002, the dosimeter only collected 17 and 1 record respectfully while operating in the above described autonomous mode with sleep cycles of 99 seconds. This may be due to the low level of strain not exceeding the first time computed threshold values. On the C-130 strain gage 1 had to be replaced with a check channel (350-ohm resistor). Based on earlier data found in Ikegami, et.el. (2001) for the C-130, this was the most active strain gage and strain gages 2 and 3 may not have had high enough strain levels to activate dosimeter data collection. For later flights the dosimeter had to be reprogrammed to continuously acquire data about 1.3 times per second as was done for F-15 data in Ikegama, et.el. (2001).

Software to Do Quick Look of the Data

Ikegami, Haugse, Trego, Rogers, and Maly (2001) describe the data format in memory. Strain time history records consists of 2048 sample points for each strain gage. The dosimeter is programmed to record the first 42 strain time history records. The strain time-histories contain the raw strain data for each of the three strain gages from one sample set. The SDRs consist of the rms strain levels for each of the 18 third octave frequency bands for each gage. After recording the first

42 records, the dosimeter continues to acquire data, compute an FFT and store third octave records in SDRs in the remaining memory locations. These data sets provide a characterization of the strain environment in the frequency domain.

AFRL developed software using LabVIEW™ virtual instruments (VIs) to get a quick look at downloaded binary data. The VI shows the desired TH or SDR records by displaying data from the raw dosimeter data file as shown in the figures that follow. AFRL is continuously improving the software to meet various user needs. The software provides engineers with the capability to quickly look at laboratory data while evaluating the dosimeter in the laboratory or in the field. The VI also allows the user to create spreadsheet files. Recent improvements include the ability to display probability density function (pdf), rain-flow and power spectral density (psd) plots based on the 2048-point time history records.

Calibration Provisions and Challenges

Calibration Provisions

As show in Banaszak, Brown and Trego (2002-ESTECH), strain calibrations are calculated based on equations for the ACL and the dosimeter analog to digital converter. For strain the micro strain (με) calibration equation is: με(K) =(K-2048)(counts) * 1.187 (με/counts), which implies that με(0) = -2048*(1.187) = -2430.976 με and με(4096) = 2430.976 με. K is the number of binary counts recorded on the dosimeter for each variable. These calibration equations are used in the LabVIEW™ quick look VIs.

Calibration Challenges

Calculating strain using equations is not a recommended practice. As stated in an Institute of Environmental Science and Technology (IEST) Recommended Practice by Himelblau, Piersol, Wise and Grundwig (1990): "An end-to-end mechanical calibration means a full calibration of the instrumentation from the actual physical input to the transducer to the output where the analog or digital signal will normally be analyzed. Mechanical calibrations are generally limited to data channels for accelerometers and microphone where the introduction of a known physical input is easily achieved." The Recommended Practice also states: "End-to-end mechanical calibrations are recommended for all accelerometer and microphone channels in the data acquisition system prior to each test. An end-to-end mechanical calibration of a given transducer channel generally constitutes a final check on the calibration of that channel".

For a damage dosimeter system, it appears difficult or impossible to perform an end-to-end mechanical calibration, since normally strain channel end-to-end mechanical calibrations cannot be accomplished due to the fact that gages are permanently mounted on the structure. Calibration of the strain gages used with the dosimeter present some interesting challenges: (1) The engineer is unable to easily get a real time look (e.g. using an oscilloscope) at the data signal input to the dosimeter especially when installed on the aircraft. Data must be recorded in memory and then downloaded into a personal computer for review. (2) The ACL technique is an excellent strain gage measurement technique, but is not the same as a standard strain gage bridge. A commercial off-the-shelf ACL laboratory signal conditioner is available from Trig-Tek (2001) that provides for shunt calibration of strain gages for static applications. For the dosimeter there was no provision for shunt calibration on the aircraft, i.e. no provision to simulate resistance changes on the installed strain gages. (3) AFRL's dosimeters are programmed to record only the first 42-0.3 second long time history records. The dosimeter is mainly designed to record many third octave data records. Any calibration signal must be captured during these time history records. (4) The dosimeter implements an auto-zeroing technique, which effectively filters out low frequencies and has an anti-aliasing filter to remove high frequencies. This impacts the appearance of a normal shunt calibration. (5) After installation on the aircraft as for a conventional strain gage it is very difficult to perform a mechanical end-to-end calibration of the measurement system. (6) As described by Banaszak, Brown and Trego (2002-JSM) root mean square (rms) values derived from third octave data may not be the same as rms values derived from time history data. So for evaluating calibration techniques, time histories are very important. This paper will focus on the 42 time history records.

Three Potential Calibration Techniques

This paper discusses 3 potential calibration techniques to attack these calibration challenges. The first technique uses a standard calibration shaker setup. The second uses shunt calibration resistors similar to conventional strain gage bridge calibration techniques. The third uses a remote control structural exciter as shown by Banaszak (2002). These three potential calibration techniques are not all inclusive. More calibration techniques can be found in instrumentation documents such as Interrange Instrumentation Group (IRIG) documents, Instrumentation Systems and Automation (ISA) handbooks and standards, Advisory Group for Aerospace Research and Development (AGARD) documents and IEST recommended practices. The three calibration techniques investigated in this paper are just a preliminary exploration of techniques that can be use to validate data in a damage dosimeter and will also be applicable to other digital data acquisition devices.

Laboratory Dosimeter Evaluation

As described by Banaszak, Brown and Trego (2002-ESTECH), AFRL set up a dosimeter evaluation laboratory to understand the operation of the dosimeter and to help obtain knowledge to use the dosimeters in field applications. Three strain gages (Measurement Group type CEA-13-062UW-350) were bonded to an aluminum plate and connected to the dosimeter. The plate was mounted on top of a shaker. Some data were recorded using sinusoidal excitation at the first bending mode of the plate, and some data were recorded while the plate was excited with pseudo random noise obtained from the spectrum analyzer to excite multiple vibration modes. The dosimeter data is then downloaded from memory to a PC for analysis. A plot of a typical sinusoidal time history of three strain gage channels using the latest version of AFRL's LabVIEW VI is show in figure 2. In addition to exciting strain gages using a shaker, AFRL evaluated the RCSE and shunt calibration techniques in the laboratory.

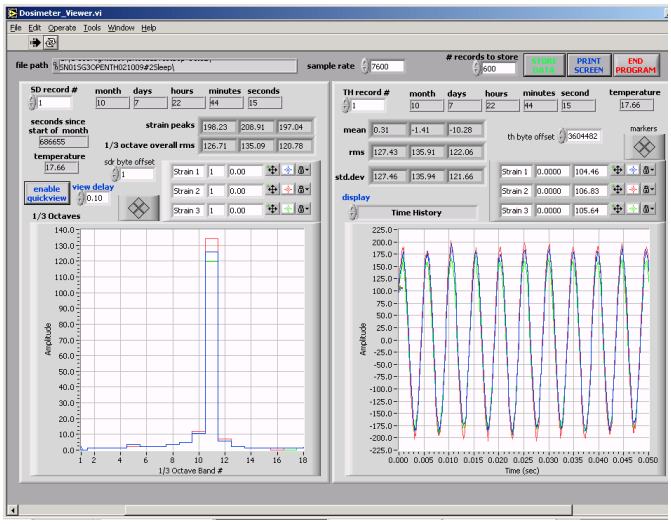

Figure 2. Typical Sine Wave Data –SN01-10 Oct 02

C-130 Aircraft Flight Test Installation

The Boeing Company used the dosimeter to collect dynamics data on the C-130 before completion of the durability patch contract. AFRL engineers continue collecting dosimeter data on the C-130 at the Air National Guard (ANG) Base in Charlotte, North Carolina. Detailed description of preliminary flight data measured using the damage dosimeter can be found in Ikegami, Haugse, Trego, Rogers, and Maly (2001). The dosimeter records the strain and temperature environment on the

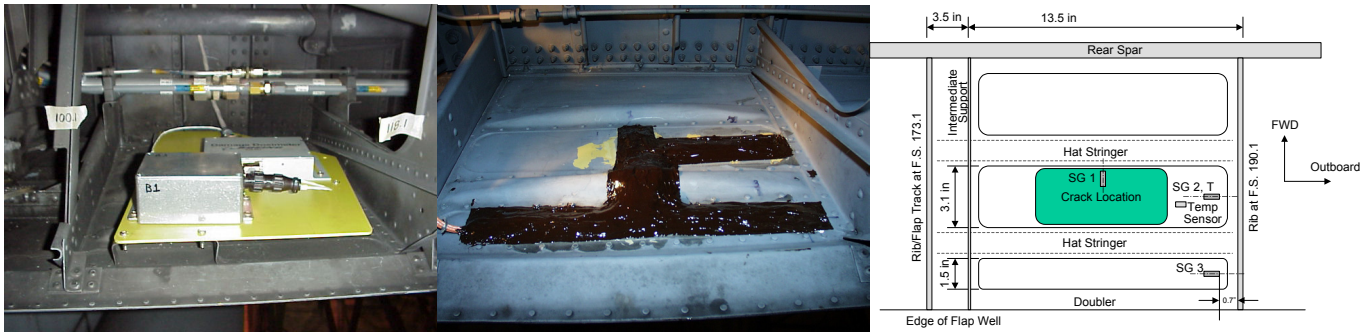

Figure 3. Damage Dosimeter Installation in C-130 as shown by Ikegami, et.el. (2001)

edge of the flap well of a C-130 aircraft that has experienced cracking. Turbulent airflow from the prop-wash causes high cycle fatigue in this region. Installation of the dosimeter, strain gages and temperature sensor in the C-130 wing flap well behind the outboard engine is shown in figure 3.

(1) Sine Comparison Calibration Using Shaker Excitation

Normally engineers can calibrate sensors by exciting a structure with a reference sensor with known calibration factors (sensitivity and frequency) and comparing its output to a sensor under test. A shaker in the laboratory excites a structure so that the sensor under test and the reference see the same mechanical response and the outputs of the two sensors can then be compared. However, in the field, shaker excitation of strain gages may be impossible or very difficult as shown by Banaszak (2002). Typical dosimeter recorder data using sine excitation on a shaker is shown in figure 2. Shaker excitation can also be random noise inputs and then the sensitivity and frequency response of the unknown sensor can be determined. This technique works well in the laboratory, but is usually not practical for a field installation such as the C-130.

It does however provide an excitation technique for the recommended mechanical end-to-end calibration. As shown in figure 2, the dosimeter records good time history and third octave data using this technique since the calibration signal is within the dosimeter data bandwidth. For example, in figure 2 the engineer sees most the data in third octave band 11 (i.e. start frequency = 51x3.71 = 189.1 hertz and end frequency = 64x3.71 = 233.44 hertz per Banaszak, Brown and Trego (2002-ESTECH)) and the rms level is about 130 με rms for each of the three strain gages. This agrees with the time history record that has a measured period of 5 milliseconds as shown in figure 2 or a frequency of 200 hertz. This is also the signal generator frequency into the shaker-excited plate that was used for this dosimeter measurement.

(2) System Calibration using a Shunt Calibration Resistor

A traditional technique for doing a system calibration of strain gages is by shunting the gage with a large resistor that will simulate the strain gage resistance change equivalent to a given microstrain (με). For example, for a 350ohm gage, a shunt resistance of 174,650 ohms is used to simulate a resistance change equivalent to 1000 με. With advice from Karl Anderson and Lyle Wells, AFRL designed a shunt calibration box to simulate 1000 με as shown in figure 4. The dosimeter

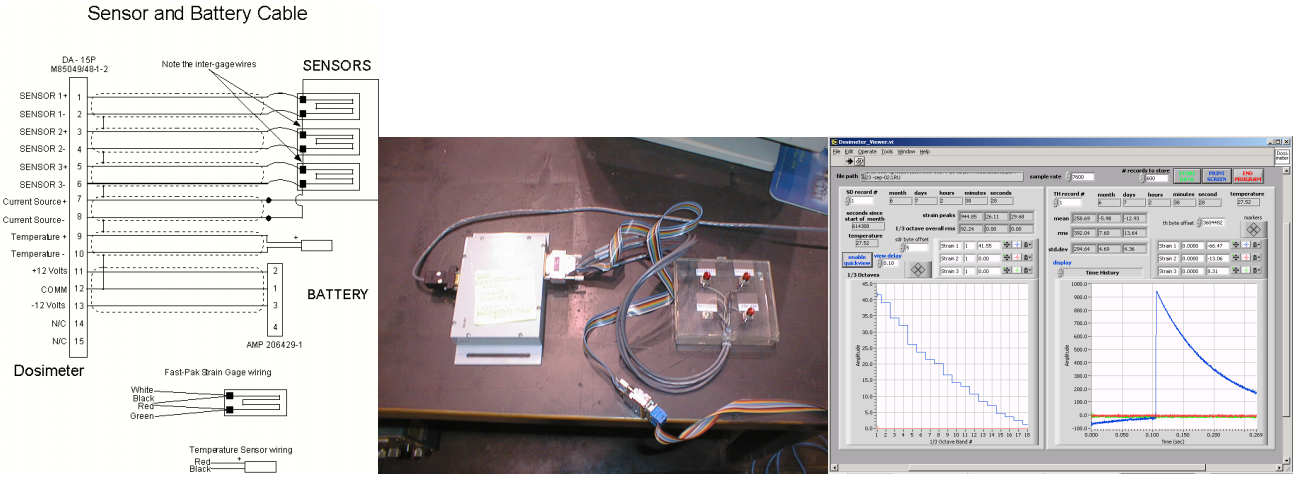

Figure 4. Dosimeter Cable, Shunt Calibration Box and Typical SG1 Output

wiring for connecting the strain gages to the dosimeter is shown in the left side of the figure. The shunt cal box is designed to shunt each of the strain gages and the internal reference resistor with a 174,650-ohm resistor in series with a push button switch to do a system calibration of 1000 με. The shunt calibration box connects inline with the dosimeter box as shown in the picture in figure 4. For example, for sensor 1 (SG 1), a switch and calibration resistor shunts pins 1 and 2. When the switch is pushed for SG 1, the reference resistor shunts the strain gage and produces a resistance change equivalent to 1000 με. A nice feature of the ACL is that a shunt calibration resistor across the internal 350-ohm reference resistor will produce an equal 1000 με change across all three strain gage signals simultaneously. AFRL evaluated this technique in the laboratory and on the C-130 with equally good results. Figure 4 shows the results displayed using the LabVIEW™ VI for strain gage 1. This calibration validated the calibration equations since the simulated step strain transition is 1000 με as expected. Similar results were seen for strain gage 2, strain gage 3 and the internal dosimeter reference resistor. This basically validated the use of the calculated ACL equations given above. The calibration time history record in figure 4 was collected in the field on the C-130 during June 02 to verify ground system operation of the dosimeter before a C-130 flight.

Similar plots were generated earlier by AFRL in the laboratory. This technique shows a rise and a fall time due to the auto-zeroing technique and anti-aliasing filters built into the dosimeter. This data can be used to estimate the low frequency and high frequency roll off of the dosimeter response. The dosimeter has a high frequency anti-alias filter and an autozeroing circuitry to remove static strain. By looking at the rise and fall times, an estimate of frequency response can be made of the low pass and high pass frequency bandwidths. For example, in figure 4 the rise time (t) is approximately 0.1060-0.1047 seconds = 1.3 milliseconds. Expanding the x scale of the time history plot in figure 4 makes this measurement easy. We can estimate that the low pass frequency cutoff for the dosimeter anti-aliasing filter is a minimum of 2.5/t = 2.5/1.3 ms = 1923 hertz. Also the pulse duration (T) is on the order of 0.200 seconds so an estimate for the minimum low frequency response frequency is .03/T = .03/.200 seconds = .15 hertz. Currently this is the quickest way to estimate the frequency response of the dosimeter.

During June 2002, the shunt calibration box was inserted in-line on the aircraft to record shunt calibration data during the first 42 time history records of the dosimeter. These calibration data were left on before recording flight data later

during September of 2002. As stated earlier, this technique works equally well in the laboratory and in the field. One challenge with the dosimeter is that calibration excitation needs to be timed precisely to capture the data during the time when the first 42 time history records are being recorded. Unfortunately, for this technique, the third octave data stored by the dosimeter may not be useful, since this static shunt calibration technique does not generate much energy within the passband of the dosimeter.

(3) Remote Control Structural Exciter

Banaszak (1998) patented a technique using a remote control structural exciter (RCSE) to stimulate structural transducers mounted in or on structures. As shown by Banaszak (2002) the technique of using a RCSE is one way to mechanically excite a structure on which a strain gage is already mounted. Figure 5 shows a laboratory set up where the three strain gages on a plate are excited with a RCSE. As seen by the middle graph in figure 5, the sinusoidal excitation induced by the RCSE is captured by the dosimeter in both the third octave and time history portions of the plot.

During June 2002, a small pager was taped to the bottom of the C-130 wing flap well with double sided tape at a location directly beneath strain gage 2 shown in figure 3. The objective of this test was to see if RCSE excitation could be observed for a strain gage in a field installation. An engineer activated the pager by a manual switch to vibrate the structure, but a remotely controlled pager would have provided a cleaner excitation. Due to the mass of the C-130 wing flap well skin, the amplitude of vibration induced by the pager was probably not very high. The engineer and technicians felt vibrations on the flap well skin with their hands. Also, the pager needed to be activated several times at the start of dosimeter operation to ensure that excitation data were recorded during one of the first 42 time histories. There was a significant amount of RTV covering the gages and panel, which might be damping out the vibration levels. The latest version of the LabVIEW™ VI allowed for viewing the psd of the time history. By keeping a written log of the pager on times and looking at the psds computed from the dosimeter time histories, the engineer correlated the RCSE pager signal excitation times with an observable, but very low, strain level at several dosimeter time history records. This is shown by the psd in the right hand side of figure 5 where there is a small peak of about 1 με rms at a frequency of 104 hertz during record number 23. This peak also shows up in record numbers 33, 38 and 42 and is close to the expected value of the RCSE frequency. However, this is such a low microstrain level that it is not observable in the third octave data computed from the psd. If a second reference sensor could have measured the strain more precisely, the input strain could have been measured and compared to the dosimeter measurement.

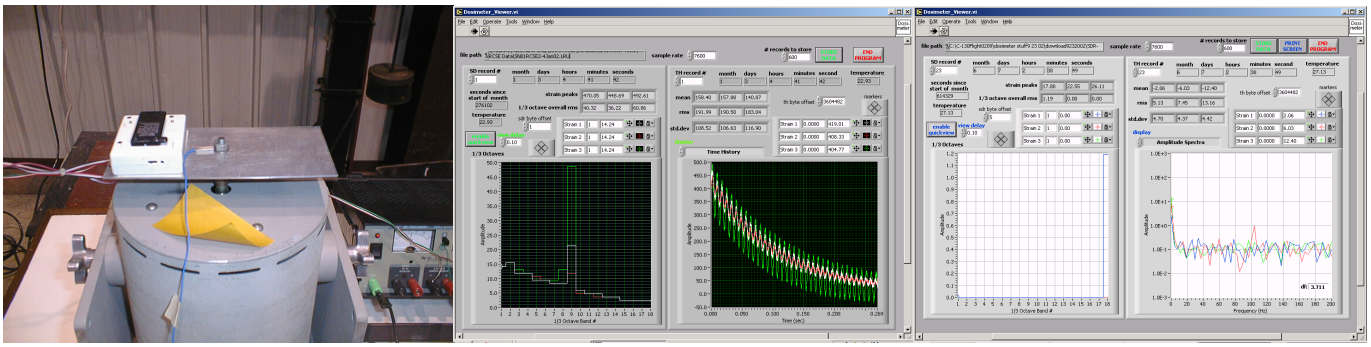

Figure 5. RCSE Calibration Test in the Laboratory on 4 January, Typical Laboratory Output, Typical C-130 Output

Discussion of Results

Of the three techniques discussed, ideally the best technique is using the RCSE. However, at this point in time, the excitation level is very low and much care and practice will be needed to make this a more useful technique. This technique will be tried again after RTV is removed from the C-130 and new strain gages are installed.

The shunt calibration technique gave a high-level calibration signal, but only simulates strain. This technique checks the electrical operation of the dosimeter system but not the mechanical interface between the gages and the structure. It does not provide a mechanical excitation as desired for an end-to-end calibration. Since the dosimeter is designed to zero out static strain, it is suggested that a dynamic shunt calibration as recommended by Mr. Lisle Wells be used to automatically switch the calibration resistor at a frequency rate within the bandpass of the dosimeter. Not only will this give sinusoidal time history records, but will also be viewable in the third octave data. Currently third octave data does not include DC components.

Previously AFRL engineers recommended the following dosimeter updates. The first is to increase the memory size, since there has been a dramatic increase in the capacity of non-volatile flash memory since the dosimeter was designed in 1996. This would allow more time history and standard data records. Removable or replaceable memory would be quicker for field applications. Other suggestions include: (1) Record static and dynamic strain simultaneously on each strain channel. (2) For dynamic measurements, use reusable integrated circuit piezoelectric strain sensors since they are much easier to install than conventional strain gages. (3) Store the standard deviation, mean, rms and peak value in the dosimeter memory. (4) Store setup, calibration factors and third octave bin definitions in a dosimeter header record. (5) The most important recommendation is to develop and require an end-to-end calibration technique for dosimeter strain channels after installation. The RCSE technique may be usable with strain gages not covered with RTV.

Summary and Conclusion

The damage dosimeter is a very useful tool to get quick response definition of dynamic strain frequencies on military and commercial aircraft. The dosimeter needs updating to be usable on requirements requiring static and dynamic measurements simultaneously. Calibration is an issue that is very important and is being continuously addressed by AFRL. Three calibration techniques to consider are (1) shaker excitation, (2) system shunt calibration and (3) mechanical end-to-end calibration using a remote control structural exciter. Preliminary results using the three calibration techniques have been briefly introduced. Each demonstrates the validity of damage dosimeter data. The shaker excitation technique is a good mechanical end-to-end calibration technique but is mostly only practical in the laboratory. The shunt calibration technique works equally well in the laboratory and in the C-130. It provides a good system calibration by simulating the change in resistance that is proportional to strain. Also the shunt calibration technique using a manual switch does not generate a signal that can be easily measured in the band pass of the dosimeter and is hard to measure on third octave plots. The RCSE technique is still a possibility for mechanical end-to-end calibration for the dosimeter system as recorded in a field installation such as on the C-130. Currently, off the shelf vibration pagers provide very low excitation levels, but with sensitive instruments such as the dosimeter, levels as low as 1 με are indeed measurable. More experiments will be attempted provided time is made available on the aircraft for investigating calibration techniques. The shunt calibration box will continue to be used as a system checkout. Both the shaker excitation and RCSE provide mechanical end-to-end calibration signals in the pass band of the dosimeter since they both provide dynamic calibration signals. Other calibration techniques are still available. For example, on the C-130 a static loading of the wing would be one excitation technique if the dosimeter were capable of measuring DC response. New calibration techniques are being developed and show promise to ensure the validity of data collected using the damage dosimeter. Currently, the most promising technique for providing a mechanical end-to-end calibration of strain gages mounted on structural components is the RCSE. The next time AFRL engineers can gain access to the C-130; they will conduct more RSCE experiments.

Acknowledgments

The authors thank David Smith of Integrity Design Engineering, Mr. Karl Anderson of Valid Measurements™ and Lyle Wells of Trig-Tek, Inc. in helping AFRL engineers to fully understand the damage dosimeter and possible calibration techniques. Also, special thanks are extended to Pat Huguenard for setting up AFRL laboratory evaluation equipment and to Chief Master Sergeant Michael Bigger and Master Sergeant Bob Bensley of the 145 Air Wing (145AW/LG) at the North Carolina ANG Base, who enthusiastically supported AFRL efforts to collect data on the C-130 using a damage dosimeter.

References

1. Anderson, K. F., (1995) "Practical Applications of Current Loop Signal Conditioning", Technical Memorandum: NASA-TM-4636, January, NASA Dryden Flight Research Facility, Edwards CA.
2. Banaszak, D., (2002) "End-to-End Mechanical Calibration of Strain Channels in Dynamic Health Monitoring Systems", Journal of the IEST Volume 45 2002 Annual Edition, pp 1134-120, Rolling Meadows, IL.
3. Banaszak, David (1998) Remote Control Structural Exciter, United States Patent Number 5,804,697, Sep 8.
4. Banaszak, D. Brown, D.L. and Trego, A., (2002), "Damage Dosimeter Third Octave and rms Time History Values, American Statistical Association 2002 Proceedings, Joint Statistical Meeting in NY, August, ASA, Alexandria, VA.
5. Banaszak, D., Brown, D.L. and Trego, A., (2002) "A Quick Look at Flight Data from a Digital Damage Dosimeter", ESTECH 2002 Proceedings, Apr28-May1, Anaheim, CA.
6. Haugse, E., Johnson, P.S., Smith, D. L., Rogers, L., Ryan, J., (1999) "Durability Patch & Damage Dosimeter: A Portable Battery Powered Data Acquisition Computer and Durability Patch Design Process", Third Joint FAA/DoD/NASA Conference on Aging Aircraft, Sep 20-23, Albuquerque, NM.

7. Himelblau, Harry, Piersol, Alan G., Wise, James H., and Grundwig, Max R. (1990) Handbook for Dynamic Data Acquisition and Analysis, Institute of Environment Sciences and Technology (IEST) Recommended Practice DTE012.1, 148-152, Mount Prospect, Il.
8. Ikegami, R., Haugse, E., Trego, A., Rogers, L, and Maly, J., (2001), Structural Technology and Analysis Program (STAP) Delivery Order Number: 004 Durability Patch, AFRL-VA-WP-TR-2001-3037, Air Force Research Laboratory, Wright Patterson AFB, OH.
9. Smith, Dave and Searle, Ian, (1998) " Damage Dosimeter: A portable Battery Powered Data Acquisition Computer." Western Regional Strain Gage Committee Paper, Dave Smith and Ian Searle, February 1998. (http://www.vm-usa.com)
10. Trig-Tek Inc., (2001) Instruction Manual Model 257A Dual ACL System, Anaheim, CA.

Section 3.3

A Statistical Look at Damage Dosimeter Data from a Fighter Aircraft

Presented at JSM 2003

JSM = Joint Statistical Meetings
San Francisco CA
August 3-7, 2003

A Statistical Look at Damage Dosimeter Data from a Fighter Aircraft

David Banaszak and Dansen L. Brown
Air Force Research Laboratory (AFRL), Structures Division, Wright Patterson AFB, OH 45433

KEYWORDS: Third Octave Data, Time History, Distribution, Correlations, Data Acquisition, Strain

ABSTRACT

The Air Force uses damage dosimeters, fabricated by The Boeing Company, to measure temperature and dynamic strains on aircraft. The dosimeter is a small, lightweight, battery powered data acquisition and processing system programmed to acquire and process data on-board the aircraft. Boeing used the dosimeter on a F-15 flight to compute and store 22,548 records during 14,616 seconds of operation (i.e. about 1.54 records per second). Boeing provided the Air Force with binary data from this flight. Each record contains a third octave spectrum (18 frequency bands) from each of 3 strain gages based on 2048 time samples in 0.3 seconds. The record also contains peak strains, temperature and time. The gages are in an area subject to structural cracking due to acoustics and high cycle fatigue. A computer program was developed to provide quick look at the third octave data and to store the computed rms, peak strains and temperatures in a spreadsheet for further statistical analysis. This paper contains a test description, time histories of root mean square (rms) data computed from the third octave spectra, distributions of the collected data and correlations between temperature and strains.

1. Introduction

1.1 Background and Theory

Typical secondary aircraft structural crack damage resulting from a high cycle fatigue (HCF) environment of greater than 10^6 cycles is shown in figure 1. This damage results in costly inspection and repair. Design of a durability repair patch requires information characterizing temperature, resonant response frequency and strain levels. The Air Force durability patch and damage dosimeter program resolves these problems by measuring the structure's operating environment with a compact, stand-alone, electronic device called a damage dosimeter and then applying a specifically-designed damped bonded repair patch. Roach (1998) shows an example of a composite bonded patch.

1.2 Review of Dosimeter Operation

The following review of dosimeter operation is included in Banaszak, Brown and Trego (2002-JSM). Banaszak, Brown and Trego (2002-ESTECH) described the Air Force sponsored flight tests using damage dosimeters, fabricated by The Boeing Company, to measure temperature and structural dynamic strains on B-52, F-15 and C-130 aircraft. The measurements diagnose difficult-to-analyze structural conditions, such as acoustics and high cycle fatigue, and support the durability patch design process to repair secondary structure cracks. The dosimeter is a rugged, small, lightweight data acquisition unit that runs autonomously off of battery power. It measures 3 channels of strain at a rate up to 15 kilo-samples per second and 1 channel of temperature at a rate of 1.3 samples per second. The dosimeter can be programmed to acquire data above a programmer defined root mean square (rms) strain threshold. It currently stores 42 time history records (0.3 seconds each) and computes and stores 29,544 third octave spectra (18 bands each) in its 4-megabyte memory. A LabVIEW™ virtual instrument (VI) program provides a quick look at the time history and third octave data and stores mean, rms and standard deviation values into a spreadsheet.

Banszak, Brown and Trego (2002-ESTECH) previously described dosimeter data acquisition, preliminary processing of the first 42 time history and third octave records for nine experimental cases, and some statistical analysis of the data. The dosimeter's normal data acquisition sequence includes first time threshold calculation, data collection, data processing, threshold comparison, and data recording. Acquired data are stored in memory. The dosimeter stores the peak strain value in third octave (SDR) records for each 2048 time history sample. For F-15 tests described below, the dosimeter was programmed to record SDR records continuously during the flight. The LabVIEW™ VI was used to view the third octave and 42 TH records. In addition to displaying the dosimeter TH and SDR records, the VI computes and displays the overall rms (σ_{SDR}) for each strain gage from the third octave records and mean(μ), root mean square (rms) and standard deviation(σ_{TH}) for the 2048 samples of the TH records. The VI also has an option to save the computed and recorded values for

the TH and SDR records to a spreadsheet compatible file.

Hardware and software details for the damage dosimeter can be found in Ikegami, Haugse, Trego, Rogers, and Maly (2001). A dosimeter photo and block diagram is shown in figures 2 and 3 respectfully. The dosimeter implements the Anderson Current Loop (ACL) signal conditioning technique described by Anderson (1995). Two types of data records are stored in the non-volatile memory of a dosimeter. A Strain Time History (TH) record consists of 2048 points of strain data sampled at 7600 samples per second for each of 3 channels. If the root mean square (rms) value of the data is above a predefined threshold, the dosimeter computes a Fast Fourier Transform (FFT) of each of the three strain time histories to generate a Power Spectral Density (PSD). The PSD is then integrated over 18 discrete third octave frequency bands to compress the strain data into contiguous third octave bands as described by Banaszak, Brown and Trego (2002-ESTECH). The 2048 points for the first 42 TH records above threshold are stored in the dosimeter's non-volatile flash memory. The third octave data are stored until memory is filled in Standard Data Records (SDRs).

1.3 Statistical Review

As noted by Bain and Englebert (1992), basic statistical property for any probability distribution of a random variable X (strain) is that

$$E(X^2) = rms^2 = \mu^2 + \sigma^2 \quad (1)$$

where, $E(X^2) = rms^2$ = Expectation (X^2), μ^2 is the mean square of X and σ^2 is the variance of X or σ is the standard deviation of X. For the dosimeter, let X equal one of the 2048 sample points of a stored TH record, then $E(X^2)=rms^2\mu^2$ and σ^2 are easy to compute. For a time history, μ^2 is the steady (DC) portion of the time history and σ^2 is alternating (AC) portion of the time history and $E(X^2) = rms^2$ is the total of the DC plus the AC portion of the time history. For the dosimeter, equation (1) is easily verified by using a spreadsheet for any dosimeter TH record by computing $E(X^2)$, μ^2 and σ^2. By design, the dosimeter's DC static component of the strain is $\mu^2 = 0$ so that $E(X^2)= rms^2 = 0 + \sigma^2 =\sigma^2$.

One-third octave bands are stored in up to 29,455 SDR records. The starting point of the third octave band distribution is programmable. Practical limits on the starting point are between 15 Hz and 75 Hz. Below 15 Hz, the width of the third octave band is less than the frequency increment of 3.71 Hz (= 7600Hz / 2048). Above 75 Hz, the final third octave band lies above the Nyquist frequency of 3800 Hz (= 7600Hz / 2). The dosimeter records third octave band rms values for each strain gage.

The three steps to compute the third octave overall rms are (1) square each band rms to get the mean square, (2) sum all resultant band rms^2s and (3) take the square root of that result to get to the overall rms. That is

$$\text{overall } rms^2 = \sum_{i=1}^{18} rms(i)^2 \quad (2)$$

where i is the band number. Equation (2) shows that bin center frequency knowledge is not required to compute the overall rms. But, remember that any energy outside the 1/3 octave bins (like the DC offset and frequencies greater than the maximum frequency band) are not included in the resulting third octave overall rms. Since the dosimeter is designed to have $\mu^2 = 0$, ideally the third octave overall rms value should equal the time history overall rms value.

Banaszak, Brown and Trego (2002-JSM) compared the rms levels of the 42 TH records with the first 42 SDR records by looking at the correlation and slope between the third octave standard deviation (σ_{SDR}) and the time history standard deviation (σ_{TH}). The dosimeter is designed to have $rms^2 = \sigma^2$ or $rms = \sigma$. They found that correlation between TH rms values and SDR rms values were highly dependent on the type of data that were recorded for each of 9 experimental cases. Based on that study and a look at data to date, the authors decided the best flight data to look at is from the F-15 flight test conducted by Boeing during December 2000.

2. Test Description of F-15 Flights by Boeing

As part of the Durability Patch Program, Boeing used a damage dosimeter on a F-15E for monitoring and recording structural strains during flight-testing. Boeing installed a dosimeter; three strain gages and a temperature sensor on the inside of the aircraft as shown by Ikegama, Haugse, Trego, Rogers and Maly (2001). The strain gages and temperature sensor were located on panel-1082. The dosimeter was installed in the door 47R in the lower center fuselage. Earlier F-15Es experienced fatigue cracking at several locations on the lower fuselage surface shown in figure 4 due to the high dynamic pressures and long dwell times during high-speed air-to-ground operations at low altitudes. The test program monitored strains on an adjacent external skin panel. This panel was part of the lower nacelle skin assembly and experiences high dynamic response during low altitude and high-speed maneuvers. The panel is made of 2024-T3 Aluminum. It is 0.071 inch thick with chem-milled pockets to 0.060 inch and 0.044 inch, and has experienced cracks in the former and in the panel

chem-mill boundary. On operational F-15 Es, this location is just aft of the LANTIRN Pod. The Dosimeter and battery pack were hard mounted to an existing flight test equipment shelf shown in figure 5. The dosimeter was activated prior to each flight and after each flight, the data were downloaded and the memory cleared. The dosimeter flights were flown during July 1999 – March 2001. The first four flight tests were unsuccessful due to problems with the system. The automatic triggering threshold never seemed to work, hence, the automatic triggering software was replaced with software that sampled and stored continuously as long as the battery was connected.

3. Data Analysis Process

3.1 Boeing Data Processing of F-15 Flight Data

The Damage Dosimeter provides the data required for durability patch design. It measures the vibration frequency and the temperature at which damage occurs in service. Third-octave-band distributions, strain PSDs and normalized cumulative rms plots should be analyzed as appropriate to determine the vibration frequency at which high cycle fatigue damage accumulates. Ikegama, Hauges, Trego, Rogers and Maly (2001) summarized dosimeter data for a typical recorded flight of the F-15 at St. Louis during December of 2000. All data looked reasonable. Figure 6 shows the total rms strain readings, based on third octave data, for the duration of the data collection cycle with temperature data overlaid.

The data is by record number, which for this case is proportional to time, since the dosimeter was program to continuously sample third octave records. For data where the strain is very low, (e.g. < 5 με), the aircraft is probably still on the ground. Also the temperature profile appears to follow the flight log.

Plotting the third-octave band distributions showed a more detailed picture of the frequency content for an individual record. Figures 7 and 8 are detailed pictures showing the third-octave band distributions for data records 8481 and 9332 where there were spikes in the rms as a function of record number.

3.2 AFRL Data Processing

AFRL used the same dosimeter binary data file as Ikegami, Haugse, Trego, Rogers and Maly (2001). AFRL data analysis process consisted of the following steps. 1) The LabVIEW™ VI described by Banaszak, Brown, Trego (2002-JSM) was used to save 22,548 records as a spreadsheet file, 2) soft® Excel was used to read the spreadsheet file. Line 1 of the file was deleted and the new data saved as an Excel worksheet file. 3) Next the time history information and inactive data records were removed from the excel files so that only data during flight remains (i.e. data record numbers (RN) 6873 to 19,243 were saved). 4) The worksheet data file was imported into SAS® JMP® which was used to get time history plots, distributions and correlations.

3.2.1 Definitions

In the following plots the label Octovl1 means the overall rms level computed from the third octave data for strain gage 1. Likewise octovl2 and octovl3 means the overall rms level computed from the third octave data from strain gage 2 and 3 respectfully.

3.2.2 Time Histories

Figure 9 shows a plot similar to figure 6 using the AFRL data processing described above. Now the x-axis is converted to minutes rather than record number. From the worksheet file above AFRL engineers determined that flight time was approximately 2 hours during record numbers 5873 to 19,243. During non-flight time (when strain was <= 5με), the third octave records were a value of 0 rms.

At first AFRL thought the dosimeter was not working since all the third octave records were zero, but this was actually just due to very low vibration during non-flight time. AFRL was also able to replicate third-octave plots as shown earlier in figures 7 and 8 where there was strain activity at a low frequency. The sudden peak in the rms values and the low frequency content of these records may be due to higher vibration levels or a data spike on the input. A complete time history would be very useful in determining validity of the third octave plots. AFRL laboratory experiments indicated that an intermittent open strain gage could cause a third octave plot with low frequency content.

3.2.3 Distribution of Collected Data During Flight

Using SAS® JMP® a distribution of the data can be found during the flight as shown in Figure 10. Here the distributions indicate that the strain peaks for strain gage 1 appear to be outliers (i.e. > 40 με). Otherwise the distributions of the rms values of strains appear to be Guassian for strain gages 2 and 3, but look very low for strain gage 1.

3.2.4 Correlation Between Temperature and Strain

One of the important considerations in the design of durability patches is to consider the correlation between different strain gages and

temperature. Using SAS® JMP® Multivariate analysis, the correlations and scatter plot shown in Figure 11 can be easily generated. In the plots there is little correlation between most combinations of the parameters. There is higher correlation between SG2 and SG3 (approx. .96). This may be evident by looking at the locations of the strain gages in Ikegama, Haugse, Trego, Rogers, and Maley (2001). That may mean that the two gages are in the same location.

4. Conclusions

The damage dosimeter is a useful tool to get quick response definition of thermal and dynamic strain frequencies on military and commercial aircraft. By continuously sampling third octave data throughout the entire flight, the data appears to make more sense and it is clearer as to when the aircraft was actually in flight. This also helps to eliminate time gaps in the data since now each a third octave record is recorded about once every 1.3 seconds. Lack of time histories for later records makes it difficult to determine the validity of the third octave data. There only appears to be correlations between the rms values of SG 2 and SG 3. Strain rms values during flight appear to have a guassian distribution for SG 2 and SG 3. The distribution for SG 1 looks questionable. Third octave data can be used for structural life prediction as long as we are sure that the underlying time history is valid.

Acknowledgments

David Smith and Karl Anderson helped to understand the dosimeter operation, Capt. Michael Myers an AFRL guided the dosimeter delivery to completion on contract F33615-95-D-3203 and Pat Huguenard set up laboratory evaluation equipment.

References

Anderson, K. F., (1995) "Practical Applications of Current Loop Signal Conditioning", Technical Memorandum: NASA-TM-4636, January, NASA Dryden Flight Research Facility, Edwards CA.

Bain & Englebert (1991) Introduction to Probability and Mathematical Statistics Second Edition, page 74, PWS-KENT, Boston, MA.

Banaszak, D., Brown, D. and Trego, A., (2002) "Damage Dosimeter Third Octave and Time History RMS Values", Annual Meeting of the American Statistical Association at the Joint Statistical Meeting (JSM) in New York, New York.

Banaszak, D., Brown, D. and Trego, A. (2002) "A Quick Look at Flight Data from a Digital Damage Dosimeter", Institute of Environmental Sciences and Technology ESTECH 2002 Proceedings, 48ATM, Anaheim, CA, IEST, Mount Prospect, IL.

Haugse, E., Johnson, P.S., Smith, D. L., Rogers, L., Ryan, J., (1999) "Durability Patch & Damage Dosimeter: A Portable Battery Powered Data Acquisition Computer and Durability Patch Design Process", Third Joint FAA/DoD/NASA Conference on Aging Aircraft, Sep 20-23, Albuquerque, NM.

Ikegami, R., Haugse E., Trego, A., Rogers, L., and Maly, J. , (2001),"Structural Technology and Analysis Program (STAP) Delivery Order Number: 004 Durability Patch", AFRL-VA-WP-TR-2001-3037 June.

Roach, Dennis P., (1998) "Bonded Composite Doublers for Commercial Aviation Use", *Aerospace Engineering*, pages 37-39, April.

SAS® Institute Inc. (2000) JMP® Introductory Guide Version 4, Gary, NC.

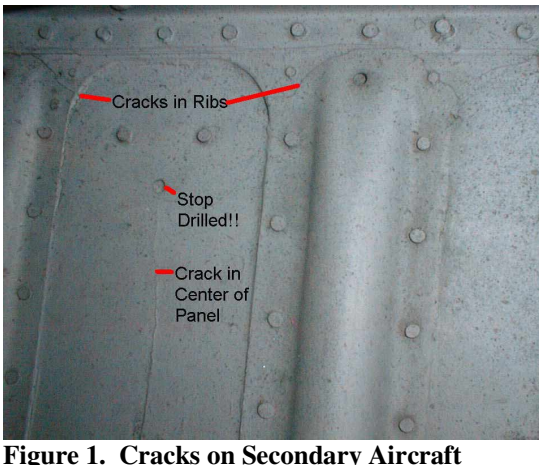

Figure 1. Cracks on Secondary Aircraft

Figure 2. Dosimeter and Battery Pack

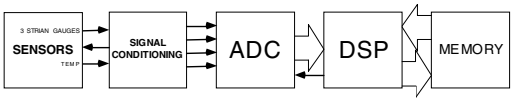

Figure 3. Dosimeter Block Diagram

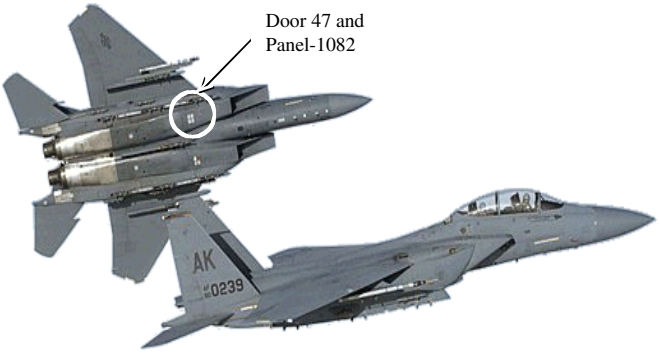

Figure 4. F-15E Critical Location, Dosimeter Installation

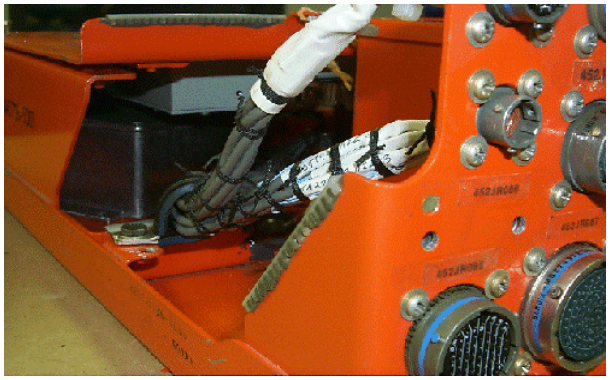

Figure 5. Dosimeter Installation Inside Equipment

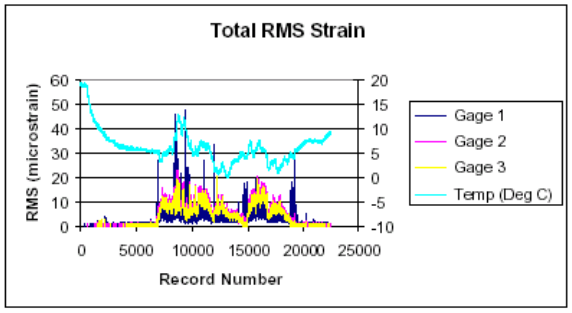

Figure 6. Total RMS as a Function of Record Number

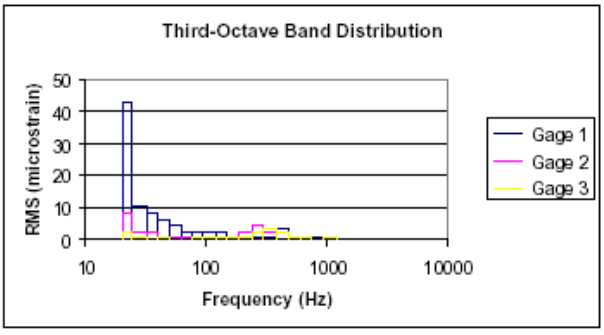

Figure 7. RMS Third-Octave Band Distribution for Record Number 8481

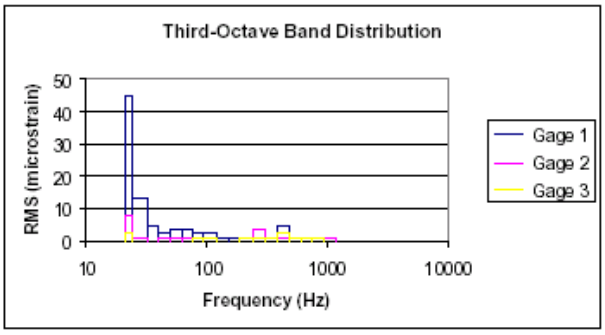

Figure 8. RMS Third-Octave Band Distribution for Record Number 9382

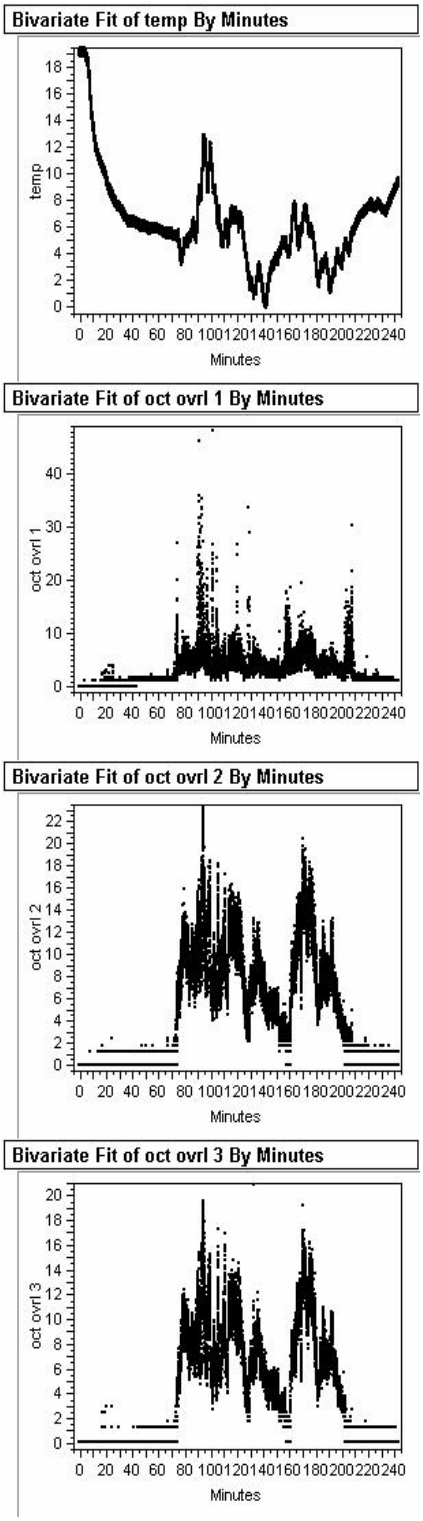

Figure 9. RMS Values as a Function of Minutes

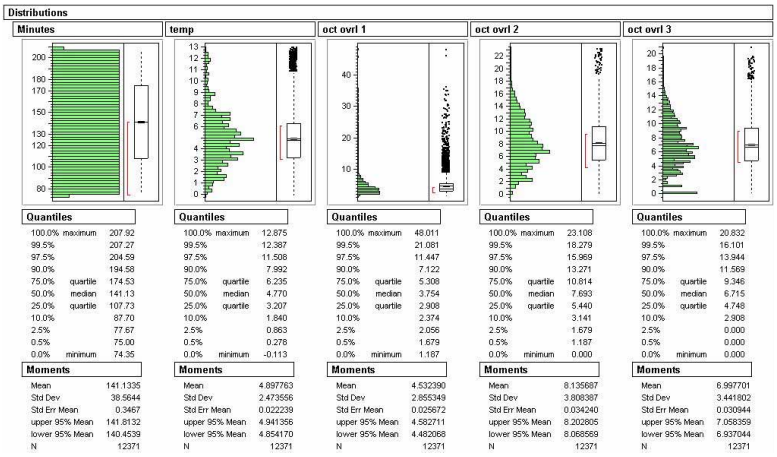

Figure 10. DistributionRN6873-19243

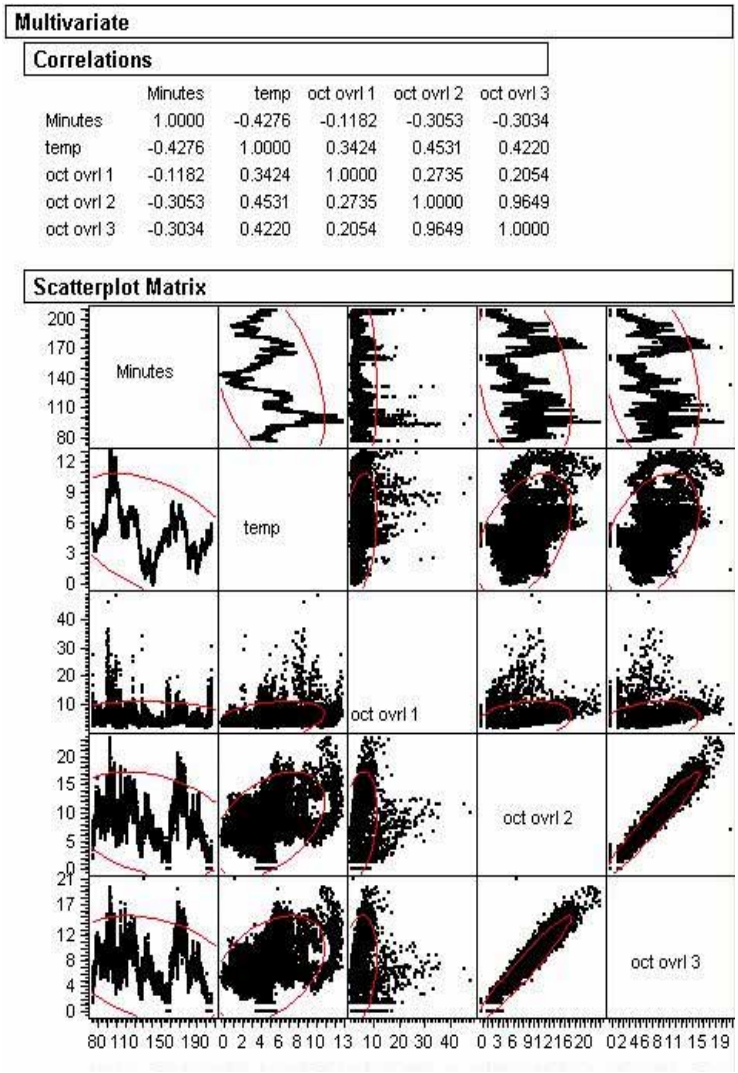

Figure 11. Correlations Between Temperature and Strains

Section 3.4

Initiation and Growth of Cracks in Metallic Plates at Resonant Frequencies

Paper presented at FM2003

FM = Fracture Mechanics
Shanghai, China
August 19-23, 2003

Initiation and growth of cracks in metallic panels at resonant frequencies

David Banaszak [a,*], Mohan M. Ratwani [b]

[a] *Air Force Research Laboratory/VASM, Building 65, Area B, 2790 D Street, WPAFB, Ohio 45433-7402, USA*
[b] *R-Tec, 28441 Highridge Road, Suite 530, Rolling Hills Estate, California 90274-886, USA*

Abstract

A test program was carried out to obtain crack initiation and growth data on aluminium panels under vibratory loads on a shaker. In the shaker test, the test specimens are subjected to fully reversed bending loads (R=-1, where R is ratio of minimum to maximum stress in fatigue). A total of four test series of specimens with two different panel thicknesses (1 mm and 3.2 mm) and panel sizes (85x180 mm, and 170x360 mm) were used. The panels were fatigued at resonant frequencies. It was observed that the resonant frequencies of the panels decreased as cracks initiated and propagated. A Visual Crack Measurement System (VCMS) using temperature sensitive paint was used to monitor cracks in the test panels.

A large scatter in total fatigue lives was observed in each test series specimens. The scatter in test data reduced significantly when crack initiation was excluded. The scatter in test data was large for thick specimen as compared to thin specimen. It was found that in thick specimens cracks on two surfaces of the specimens did not initiate in the same through-the-thickness plane under vibratory loads. In thick specimens cracks initiated as surface cracks in different planes on two surfaces under fully reversed bending loads.

Keywords: cracks; crack initiation; crack growth; fatigue; resonant frequency; vibratory loads; visual crack measurement system.

1. Introduction

Cracks are known to initiate and grow in acoustic environment in aircraft structures. Analytical prediction of fatigue life in acoustic environment has been a problem due to complex nature of stresses, produced by dynamic loading, and high frequencies. A common practice is to rely on test data. The test data is generally obtained on a shaker at resonant frequencies.

Present study was carried out to 1) determine the effect of specimen size and thickness on crack initiation and growth under vibratory loads, 2) evaluate the capability of Visual Crack Measurement System (VCMS) using Temperature Sensitive Paint (TSP), and 3) evaluate capabilities of present analyses to predict crack growth under vibratory loads.

2. Test program

Rectangular test specimen geometry shown in Fig. 1 was selected for tests. Test program was designed to investigate two different specimen thicknesses and specimen sizes as shown in Table 1. The schematic of VCMS used to monitor cracks [1,2] is shown in Fig. 2. TSP was applied to the panels to enhance crack visibility and get temperature profile of cracking panels. As the panels start to crack, stress concentrations at the crack tip are observed as temperature increases or intensity changes.

In fatigue tests, the shaker input was selected so as to get approximately same strain in all specimen series. Input g levels of 6g for test series 1 and 2 and 3g for test series 3 and 4 resulted in almost equal stain values at the root as shown in Table 2. Observed peak displacements of the first bending mode were used for displacement values in static beam equations to estimate the strain levels at the root. The table also shows the strains predicted by dynamic analysis [3]. The agreement between strains computed from observed deflections in tests and dynamic analysis is good. The table also shows the resonant frequencies for each test series before cracks initiated in test specimens.

* Corresponding author.
E-mail address: david.banaszak@wpafb.af.mil (David Banaszak).

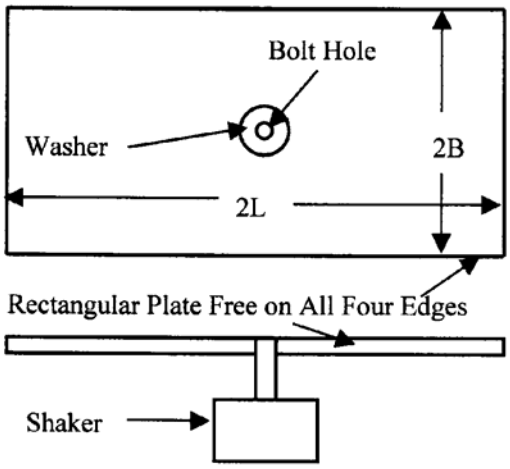

Fig. 1. Test specimen geometry.

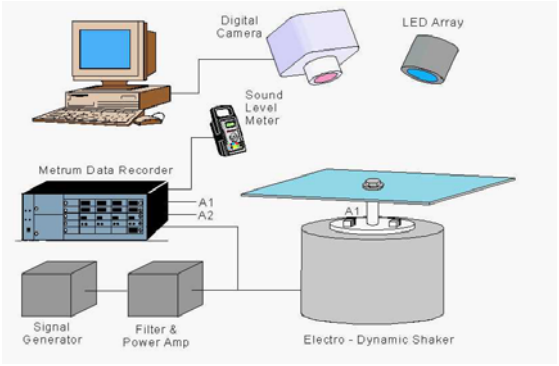

Fig. 2. Schematic of VCMS.

Table 1. Test specimen dimensions

Test Series	Width mm	Length mm	Thickness mm	Input Loading
1	85	180	1	6g
2	85	180	3.2	6g
3	170	360	1	3g
4	170	360	3.2	3g

Table 2. Predicted and test strains

Test Series	Strains (μm/m)		Resonance Frequencies
	Test	Predicted	
1	3187	3088	110-112 Hz
2	3346	3377	330-336 Hz
3	3187	2941	27-28 Hz
4	3226	3101	82-83 Hz

Under the vibratory loading, the fatigue cracks initiated and grew at the edges of the bolthole on either side of the specimen centerline as shown in Fig. 3. Thus, two cracks were growing in each specimen. As the cracks were initiating and growing underneath the bolthole washer, they could not be monitored with VCMS until they were outside the washer. Crack measurements were taken at regular intervals with VCMS. Resonant frequencies of test specimens dropped as cracks grew. Test frequencies were adjusted at regular intervals to correspond to the resonant frequencies. Analytical techniques were developed to predict resonant frequencies of panels with cracks [4]. A comparison of predicted and test resonant frequencies for Test Series 2 panels is shown in Fig. 4.

3. Crack growth including initiation

The fatigue crack growth of Test Series 1 specimens is shown in Fig. 5. The number of fatigue cycles shown in the figure includes initiation cycles. The test data shows a large scatter in number of cycles to first crack detection. The numbers of cycles vary form 40,000 to 120,000 at the first observed crack length of about 10 mm when the crack was visible outside the washer. This scatter in data is not unusual when crack initiation is included in crack growth life.

The fatigue behavior of Test Series 2 specimens is shown in Fig. 6. The test data from this series of specimens show less scatter. Numbers of cycles to first crack detection are not much different for 3 specimens. An interesting thing to note is that growth of one crack in each specimen increases with number of cycles; however, the second crack in each specimen is retarded and shows very little growth.

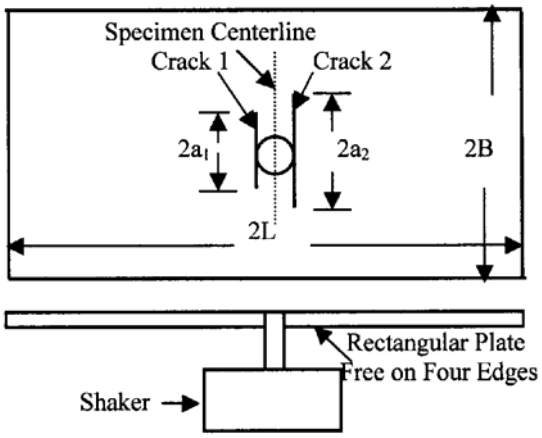

Fig. 3. Crack initiation locations.

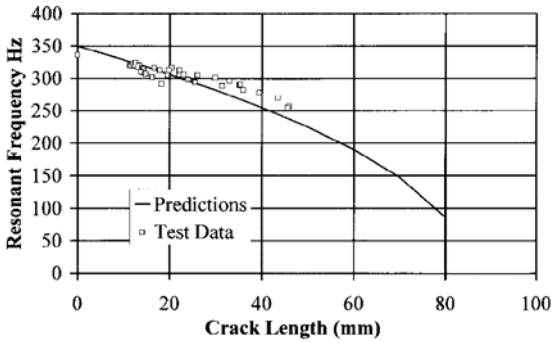

Fig. 4. Comparison of predicted and test resonant frequencies.

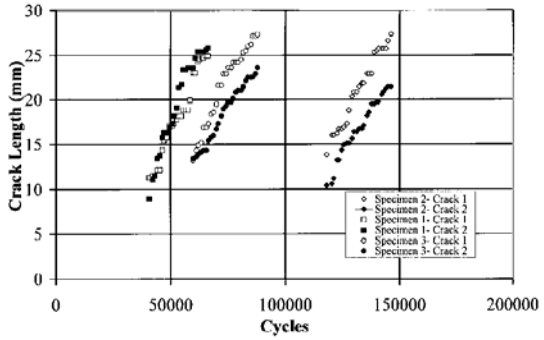

Fig. 5. Crack growth in series 1 specimens (including initiation).

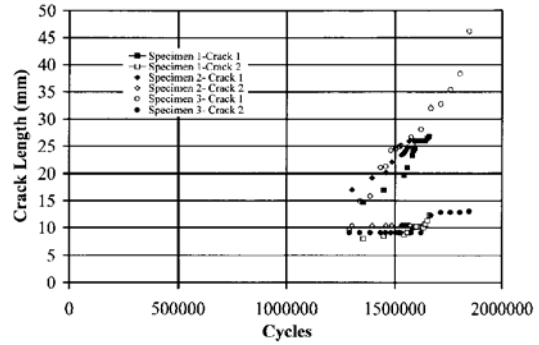

Fig. 6. Crack growth in series 2 specimens (including initiation).

The fatigue behaviour of Series 3 specimens is shown in Fig. 7. The test data show much less scatter. Number of cycles to first crack detection are not much different for 3 specimens. An interesting thing to note is that the fatigue cycles to 10 mm crack in Series 1 specimens are much more as compared to those for Series 3 specimens even though both the specimen series have same thickness and same maximum strain of 3,187 m/m at the root (crack initiation site) as indicated in Table 2. The difference in crack growth life is attributed to dynamic effects. The test resonant frequencies for series 1 specimens are between 110 to 112 Hz and for Series 3 specimens between 27 and 28 as shown in Table 2. Thus, the resonant frequencies for Series 1 specimens are 4 four times those for Series 3 specimens. These results indicate that effect of dynamic loading frequencies has to be considered in any prediction methodology.

The fatigue behavior of Series 4 specimens is shown in Fig. 8. The test data show a large scatter. A comparison of Series 2 (Fig. 6) and Series 4 (Fig. 8) test data shows that cycles to 10- mm crack for Series 4 specimens are less as compared to those for Series 2 specimens even though both the specimen series have same thickness and about the same maximum strain at the root as shown in Table 2. The test resonant frequencies for Series 2 specimens are between 330 to 336 Hz and for Series 4 specimens between 82 to 83.

4. Crack growth behavior after first crack detection

In view of significant scatter in observed fatigue test data that included crack initiation, the test data were analyzed to investigate only crack growth behavior under vibratory loading. For each specimen of data series shown in Table 1, the crack growth was plotted as a function of number of cycles after the first crack was detected in each specimen. Thus, for each specimen the time at which first crack was observed was considered as starting point with zero cycles and cycles were counted from this point onwards for comparing crack growth behavior.

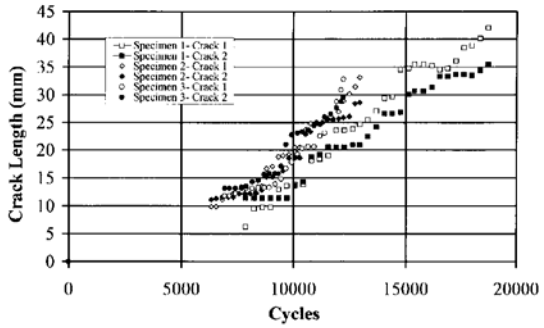

Fig. 7. Crack growth in series 3 specimens (including initiation).

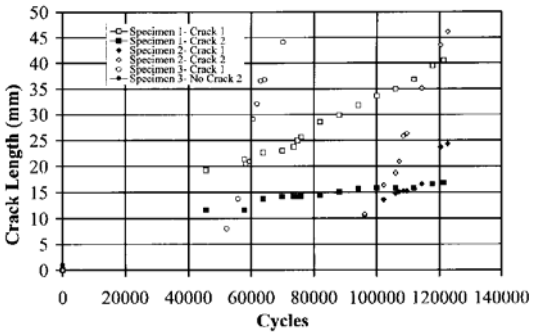

Fig. 8. Crack growth in series 4 specimens (including initiation).

The crack growth behavior of Series 1 specimens after first crack was detected is shown in Fig 9. As seen in the figure, the crack growth data show less scatter as compared to when initiation life was included (Fig. 5). The crack growth rate increases uniformly as crack length increases, however, after about 15,000 cycles, rate of increase in crack growth rate slows down. The slowing down in crack growth rate is attributed to interaction between parallel cracks. As shown in Fig. 3 two cracks initiate in each specimen, on either side of specimen centerline. The parallel cracks shield each other and reduce stress intensity factors, hence, crack growth rate.

The crack growth data for Test Series 2-4 specimens are shown in Figs. 10-12. The crack growth data for specimen Series 2 show a large difference in crack growth rates for crack 1 and crack 2 in each specimen. One crack in each of Series 2 specimens is retarded and is growing at very slow rate.

The test specimens were examined to understand the reason for large scatter in thick specimens. It was found that in the thick specimen cracks on two surfaces of the specimens did not initiate in the same through-the thickness plane under vibratory loads. The specimens were subjected to fully reversed bending loads (R= –1). In the thick specimens, cracks initiate as surface cracks in different planes on two surfaces. Some thick test specimens showed three cracks, two on one side of specimen centerline and one on the other side.

5. Comparison of fatigue crack growth in various specimen series

A comparison of crack growth behavior in Test Series 1 and 2 is shown in Fig. 13. The specimens in the tests are made from same material and have the same size (Length and Width). However, the thickness of Test Series 2 specimens is three times that of Test Series 1. The maximum strains in both the specimen series are almost the same. Hence, crack growth behavior should be similar. However, Fig.12 indicates the crack growth in Test Series 1 to be much faster compared to Test Series 2. The resonant frequency of Test Series 2 specimens (330-336 Hz) is 3 times that for Test Series 1 specimens (110-112 Hz). It is shown in [5] that higher frequency causes reduction in

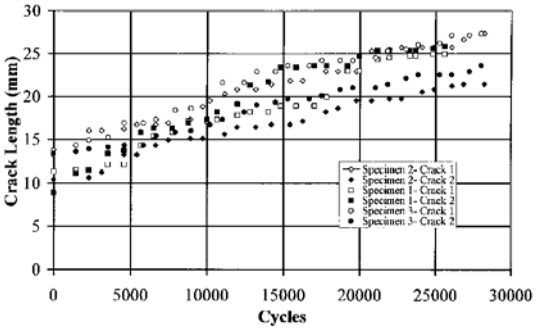

Fig. 9. Crack growth in series 1 specimens (after first crack detection).

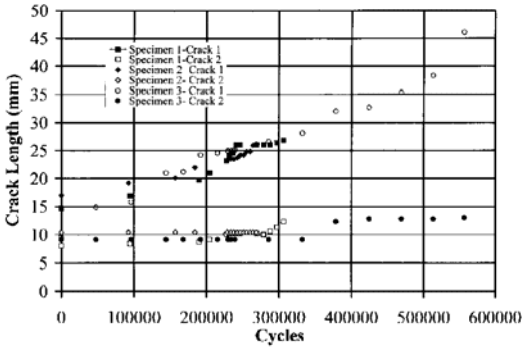

Fig. 10. Crack growth in series 2 specimens (after first crack detection).

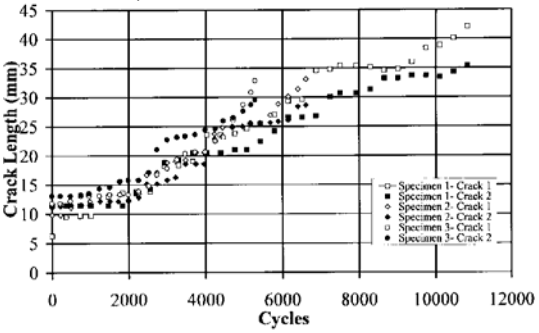

Fig. 11. Crack growth in series 3 specimens (after first crack detection).

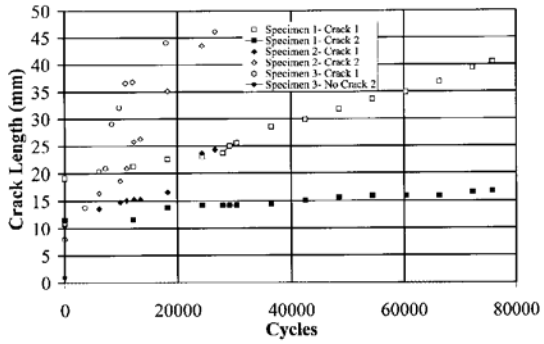

Fig. 12. Crack growth in series 4 specimens (after first crack detection).

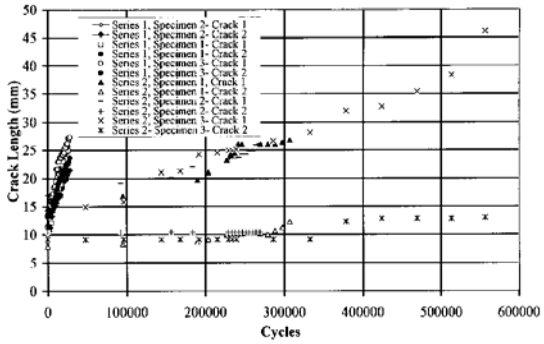

Fig. 13. Comparison of crack growth in test series 1 and 2 specimens.

stress intensity factors, hence, slower crack growth. Also, in thicker specimens under fully reversed bending cracks do not initiate in the same plane. Hence, instead of one crack on each side of specimen centerline there may be two parallel cracks that try to shield each other. This will reduce stress intensity factors and crack growth rate.

A comparison of crack growth in Test Series 1 and 3 is shown in Fig. 14. Test specimen Series 1 and 3 are of same material and thickness with almost same maximum strains as indicated in Table 2. However, size of specimens (length and width) in Test Series 3 is twice that in Test Series 1. In view of similar strains in two specimen series, crack growth behavior is expected to be same. However, Fig. 13 indicates the crack growth in Test Series 3 to be much faster as compared to Test Series 1. This is attributed to different test frequencies (resonant frequencies) of the test series and bending stress intensity factors under bending loads. The resonant frequency of specimens in Test Series 1 (110-112Hz) is 4 times that for Test Series 3 (27-28 Hz).

A comparison of crack growth behavior in Test Series 2 and 4 is shown in Fig. 15. The specimens in these test series are made from same material and have same thickness. However, size of specimens (Length and Width) in Test Series 4 is twice that of Test Series 2. The maximum strain in both the specimen series is almost the same. Hence, crack growth behavior should be similar. However, Fig. 15 indicates the crack growth in Test Series 4 to be much faster as compared to Test Series 2. The test frequencies (resonant frequencies) of two specimen series are different. The resonant frequency of Test Series 2 specimens (330-336 Hz) is 4 times that for Test Series 4 specimens (82-83 Hz).

A comparison of crack growth behavior in Test Series 3 and 4 is shown in Fig. 16. The specimens in these test series are made from same material and have the same size (length and width). However, the thickness of Test Series 4 is three times that of Test Series 3 specimens. The maximum strains in both the specimen series are almost the same. Hence, crack growth behavior should be similar. However, Fig. 16 indicates the crack

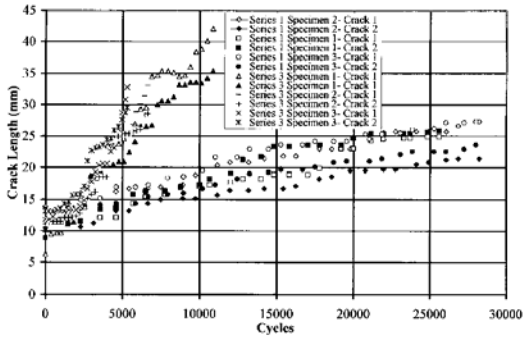

Fig. 14. Comparison of crack growth in test series 1 and 3 specimens.

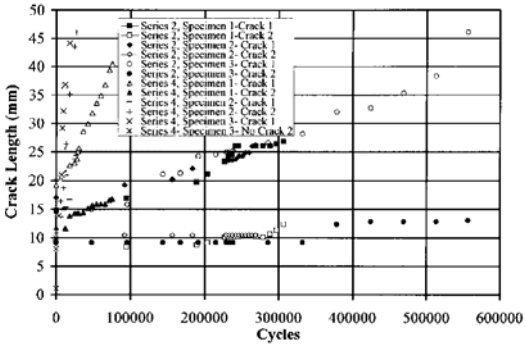

Fig. 15. Comparison of crack growth in test series 2 and 4 specimens.

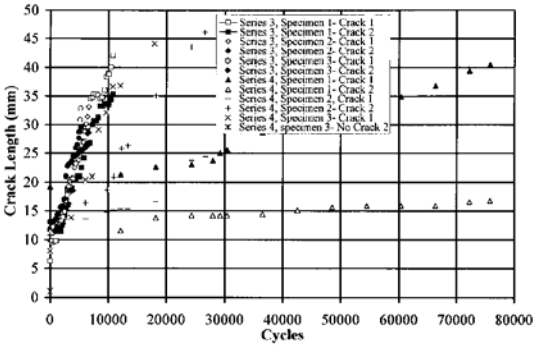

Fig. 16. Comparison of crack growth in test series 3 and 4 specimens.

growth in Test Series 3 to be much faster as compared to Test Series 4. The test frequencies (resonant frequencies) of two specimen series are different. The resonant frequency of Test Series 4 specimens (82-83 Hz) is 3 times that of Test Series 3 specimens (27-28 Hz). Also, in thicker specimens under fully reversed bending the cracks may not initiate in the same through-the-thickness plane. Hence, instead of one crack there may be two parallel cracks on each side of specimen centerline shielding each other. This will significantly reduce crack growth rate.

6. Concluding remarks

Fatigue crack growth data on panels under vibratory environment have been analysed. It is shown that the scatter in data can be significantly reduced if only crack growth data is considered and initiation life is neglected. High resonant frequencies in fatigue can have significant influence on crack growth rate. Higher frequencies seem to reduce crack growth rate.

The resonant frequencies decrease as cracks initiate and propagate in panels. The change in frequencies due to crack propagation can be analytically predicted.

Acknowledgement

The test program using VCMS was carried out at Wright Patterson Air Force Base, Ohio, USA under in-house research development program. The analytical development and test data evaluation was carried out by R-Tec, Rolling Hills Estates, California, USA under Phase I Small Business Innovation Research Contract F33615-01-M-3127.

References

[1] Banaszak, D. Lassiter, J. O. and Baust, H. D. (1999), Thermal-Optical Measurements in Structures with Damped Composite Repairs, The USAF Aircraft Structural Integrity Programs Conference.

[2] Banaszak, D., Dale, G., Watkins, N., and Jordan, J. D. (1999), An Optical Technique for Detecting Fatigue Cracks in Aerospace Structures, 18th International Congress on Instrumentation in Aerospace Simulation, Toulouse, France.

[3] Ratwani, M. (2002), Development of Validated Crack Measurement System for Vibrating Structures, Report AFRL-VA-WP-TR-2002-3005.

[4] Ratwani, M., Jacobson, M., and Banaszak, D. (2002), Resonant Frequencies of Vibrating Panels with Cracks and Bonded Composite Patches, Proceeding of Sixth Joint FAA/DoD/NASA Conference on Aging Aircraft, San Francisco.

[5] Folias E. S. (1968), On the Steady State Transverse Vibrations of a Cracked Plate, *Engineering Fracture Mechanics*.

Section 3.5

Sonic Fatigue Damage Service Environment and Life Improvement from Dosimeter Data

Poster presented at ASIP 2003

ASIP = Aircraft Structural Integrity Program
Savannah, GA
December 2-4, 2003

(NOTE: In the digital version of this report, see original PowerPoint attachment, ASIP2003.ppt)

Sonic Fatigue Damage Service Environment and Life Improvement from Dosimeter Data

Authors:

Dr. Lynn Rogers, AFRL/VASM **David Banaszak, AFRL/VASM**

Capt. David Laird, AFRL/VASM **Dansen Brown, AFRL/VASV**

BASELINE STRUCTURE

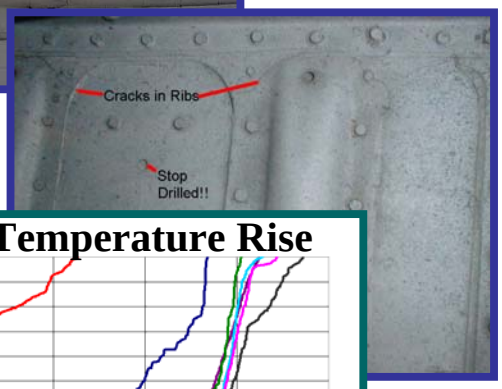

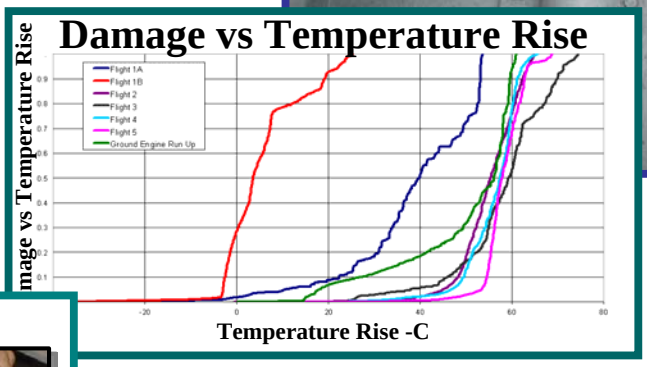

- Dosimeter
- Context – Annoyance High Cycle Fatigue(HCF) Damage of Secondary Structure – Costly Repair
- 3 Dynamic Strain Gages/ 1 Temperature
- Autonomous – no AC power; sleeps; checks strain every min; when exceed threshold; compute 1/3 octave; store 57 rms 1/3 octaves & 1 temperature.

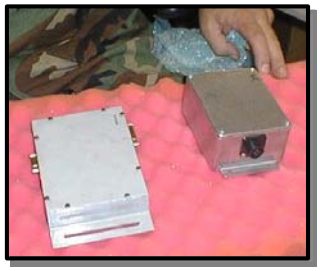

- Analysis
- SN is straight line $S = S_{UHCF} * N^{b}$
- Miner's Law $d = n / N$
- Damage proportional to Strain**5.64

$$n = f_{av} * \Delta t;$$

$$1/N = \left(E * \varepsilon / S_{UHCF}\right)^{-1/b} \propto \left(\varepsilon\right)^{5.64....};$$

$$d \propto \left(\varepsilon / 100\right)^{5.64....}$$

Flight 2 Cumulative Damage Plot

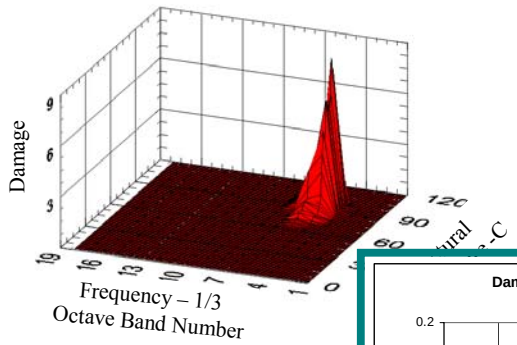

Damping Treatment

Structural Mod

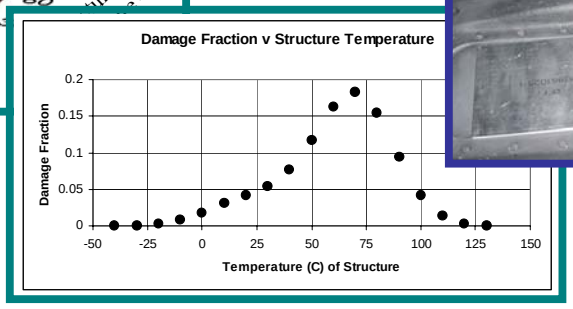

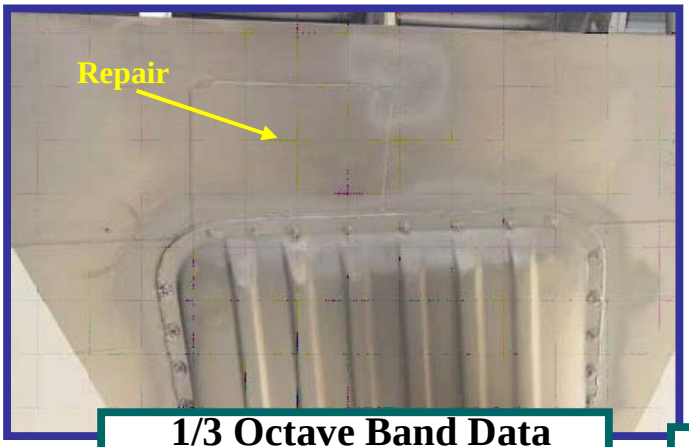

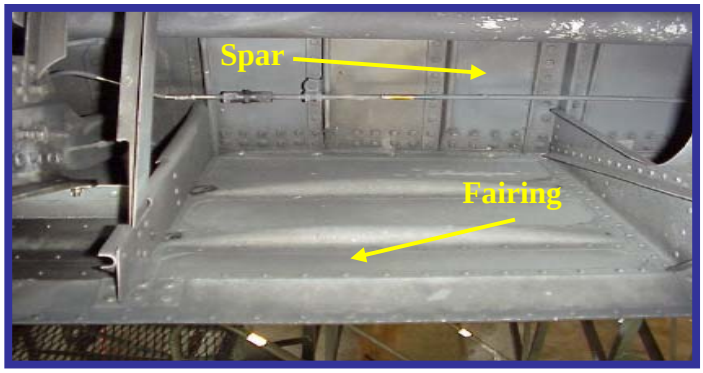

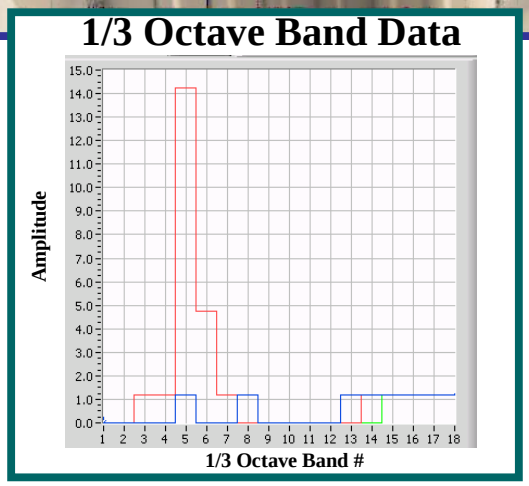

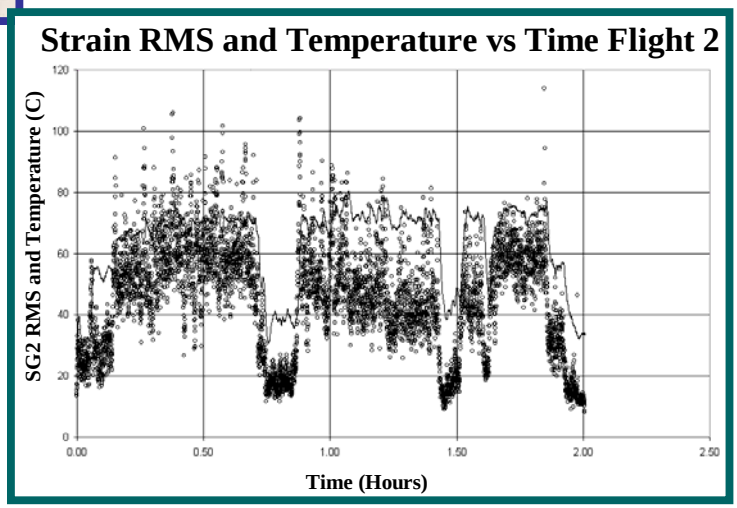

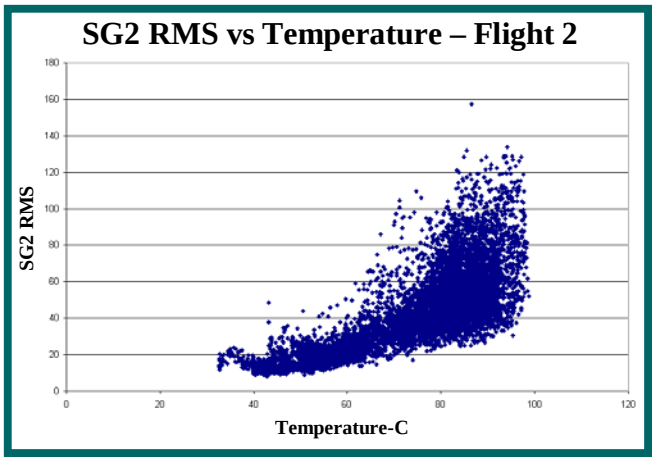

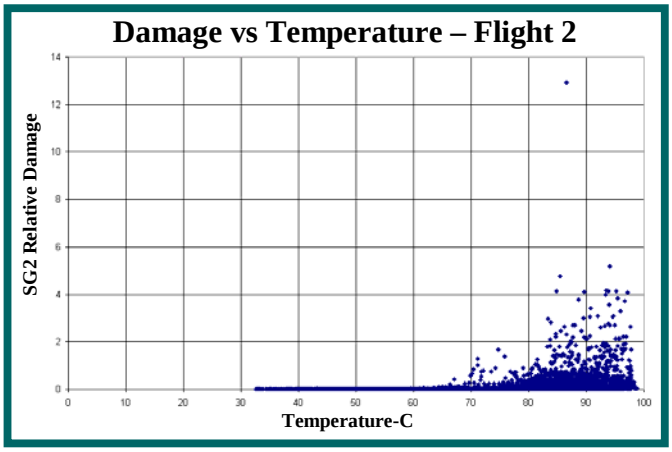

- Conclusions
- Dosimeter confirmed in service
- Identified Option to extend service life; Life Improvement Factor=4.6

Section 3.6

Autonomous Environmental Definition of C-130 Flap Well Skin Panel

IEST Journal Article

ESTECH 2004 Paper Version of the IEST Journal Article

ESTECH = Engineering Science and Technology
Annual meeting of the Institute of Environmental Sciences and Technology (IEST)
Las Vegas NV
April 25-28, 2004

Autonomous Environmental Definition of C-130 Flap Well Skin Panel

David Banaszak, Air Force Research Laboratory (AFRL)
Dansen L. Brown, Air Force Research Laboratory (AFRL)
David J. Laird, Air Force Research Laboratory (AFRL)

Abstract

Air Force C-130 aircraft require numerous aluminum doubler repairs on the wing flap skin aft of the right-hand outboard engine. These repairs are costly and require riveting. Rivets often provide new areas of stress concentration, which causes new cracks to develop elsewhere. Boeing and the Air Force Research Laboratory (AFRL) are measuring the thermal and strain environment behind the right-hand outboard engine of a North Carolina Air National Guard (NCANG) operational C-130 aircraft (TN 93-1456) for use in design of a damped repair patch to prevent the growth of cracks in skin under the wing flap panel. During June 2003, AFRL engineers and technicians acquired data using an autonomous damage dosimeter during five operational C-130 flights. The damage dosimeter measures structural strains and temperatures on in-service aircraft to diagnose structural conditions that are difficult to analyze, such as acoustics and high cycle fatigue (HCF). The first flight was from Charlotte, North Carolina to Warner Robins Air Force Base (AFB), Georgia and returned to Charlotte. The last four flights were assault flights where the C-130 simulated cargo drops. Pilots logged the altitude and indicated airspeed, engine speed, and flap positions for the first four flights. Flap position settings were compared with dosimeter temperature and root mean square (rms) strain measurements.

This paper presents typical third octave plots showing engine speed vibratory frequencies, rms time histories (TH), and correlation data for a flight. This paper also presents typical limited data in TH, probability density function (PDF), power spectral density (PSD), and rain flow formats.

KEYWORDS

Dosimeter, data acquisition, vibration, structures, high cycle fatigue (HCF), strain, third octave, time history (TH), correlations

BACKGROUND

Typical secondary aircraft structural crack damage on a C-130 resulting from a high cycle fatigue (HCF) environment of greater than 10^6 cycles is shown in Figure 1. Turbulent airflow from the prop-wash causes HCF in this region and the damage results in costly inspection and repair. Currently, repair is accomplished by riveting aluminum doubler plates. However, the structure continues to respond in a resonant fashion and new cracks form due to stress intensities at the new fastener locations. A better solution is to apply a specifically designed damped bonded repair patch.[1] The design of composite durability repair patches requires environmental information characterizing temperature, resonant response frequency, and strain levels.

The Air Force Research Laboratory (AFRL) acquires this environmental information by measuring the operating environment of the structure with a compact, stand-alone electronic device called a damage dosimeter. The damage dosimeter was designed to measure structural strains and temperatures on in-service aircraft. The dosimeter, strain gages, and temperature sensor are installed in the C-130 wing flap well behind the outboard engine (Figure 1).[2]

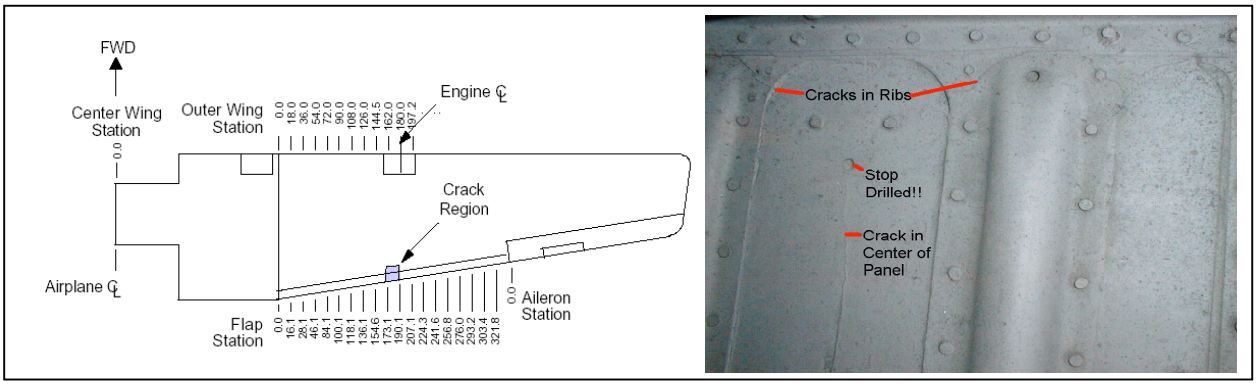

Figure 1. Crack location on C-130 secondary structure.

The AFRL is completing work on the C-130 that includes five data-gathering flights on the C-130, an application of a repair, and six more dosimeter flights. The dosimeter records the strain and temperature environment on the edge of the flap well of a C-130 aircraft that has experienced cracking.

REVIEW OF DOSIMETER OPERATION

The damage dosimeter provides autonomous threshold operation or continuous operation, on-board fast Fourier transform (FFT) computation, and storage of third octave frequency spectra; i.e., the dosimeter can record third octave data continuously or be programmed to record data autonomously when a strain threshold is exceeded.[3] An Anderson Current Loop (ACL) conditions strain gage signals to minimize the power required to excite the dynamic gages and to eliminate the need to account for wire-length effects.[4]

The dosimeter is a rugged, small, battery-powered, lightweight (weighs less than .69 kg [1.5 lb] without battery) data acquisition system that measures three channels of strain at rates of 7600 samples per second and a single channel of temperature at a rate of 1.3 samples per second. The autonomous dosimeter is programmed to acquire only data above a root mean square (rms) strain threshold. The strain data for each of the three gages is processed through a FFT analyzer to generate a power spectral density (PSD). The PSD is then converted to 18 third octave frequency bands.[5] The dosimeter is programmed to store 42 records of time history (TH) data each 0.3 seconds long, and records and stores third octave records until the 4-megabyte memory is filled.

The AFRL used the dosimeter to gather data because it is small and able to operate with minimum support requirements from aircraft operational personnel. Because the dosimeter operates on batteries, the instrumentation did not require aircraft power and could be located close to the measurement area, thus eliminating the need to route long cables. The dosimeter programmed frequency range covered the expected vibratory range of DC-2000 Hz, which required a minimum sampling rate of 4000 samples per second plus on-board anti-aliasing filters. Since on-board time for data processing and memory were limited, only one 2048 sample block was used to compute the PSD. Future versions of hardware and software for the dosimeter should incorporate provisions for multiple blocks so average PSDs can be computed.

Previous studies investigated techniques to perform system and physical (mechanical) end-to-end calibration of bonded strain gages.[6,7] No uncertainty analysis was performed on the dosimeter measurements. However, based on end-to-end system checks with a portable vibration pager, the dosimeter appeared to be able to resolve 1 micro strain (με) rms inside the third octave band containing 150 Hz. Techniques include inserting shunt calibration resistors in line for a system calibration and exciting the strain gages with a remote control structural exciter for a physical end-to-end calibration.[8] Banaszak and Brown have described in detail dosimeter data collection, processing, and recording[6] and provided a preliminary look at data recorded continuously on an F-15 aircraft.[9]

PAST C-130 EFFORTS AND AFRL FLIGHTS DURING JUNE 2002 AND SEPTEMBER 2002

The dosimeter was used to collect dynamics data on several C-130 flight tests before completion of the durability patch contract in June 2001.[2] The dosimeter was located in the wing flap well between wing stations 100.1 and 118.1. The strain gages and temperature sensor were located between fuselage stations (F.S.) 173.1 and 190.1. AFRL engineers continued collecting dosimeter data on C-130 Tail Number 93-1456 at the North Carolina Air National Guard (NCANG) base in Charlotte, North Carolina. From February 2001 to June 2002, the C-130 was inoperable while awaiting parts for repair of wheel well flap damage from a flat tire. In June 2002, an AFRL engineer traveled to the NCANG base to conduct data acquisition and found strain gage (SG) 1 open. NCANG personnel bypassed the gage with a dummy 350-ohm resistor so the series strain gage configuration would operate. SG1 was now a dummy check channel. The NCANG flew two flights during June 2002 where the dosimeter collected only 17 records on the first flight and 1 record on the second flight while operating in the autonomous threshold mode. The engineer thought these results might have been due to low strain levels not exceeding the threshold values. Based on data from an earlier study on the C-130, SG1 was the most active strain gage. SG2 and SG3 may not have had high enough strain levels to activate dosimeter data collection.[2] The engineer reprogrammed the dosimeter for continuous collection of rms third octave data for the next two NCANG dosimeter flights during September 2002. The dosimeter collected data continuously for approximately five hours per flight as expected. The data collected appeared to be invalid after aircraft takeoff; however, after aircraft landing, the data appeared to be valid. A possible explanation for this discrepancy is that one of the gage circuits opened as the wing flexed (i.e., a change in the wing static loading after the aircraft is airborne) during aircraft takeoff and closed again as the wing flexed back to its ground position.

Laboratory experiments after the flights indicated that a similar effect occurs when one of the strain gage circuits opens while the dosimeter is collecting data continuously from dynamic strain gages on a plate excited by an electrodynamics shaker. The AFRL assumed that the gages were opening during takeoff and closing when the aircraft was on the ground. Unable to fix the current strain gage installation, the AFRL decided to install new strain gages, temperature sensors, and cabling. By June 2003, AFRL engineers and technicians and NCANG personnel and schedules were coordinated so the AFRL could reinstall the strain gages.

STRAIN GAGE AND TEMPERATURE SENSOR REINSTALLATION

In December 2002 and March 2003, AFRL engineers revisited the NCANG base to plan removal and reinstallation of the strain gages. During discussion with a sheet metal worker, the AFRL engineers learned that the cracks always started in the hat riser area; therefore, the gage locations were changed from the previous flights. In June 2003, an AFRL engineer and technician reinstalled the strain gages (Figure 2).

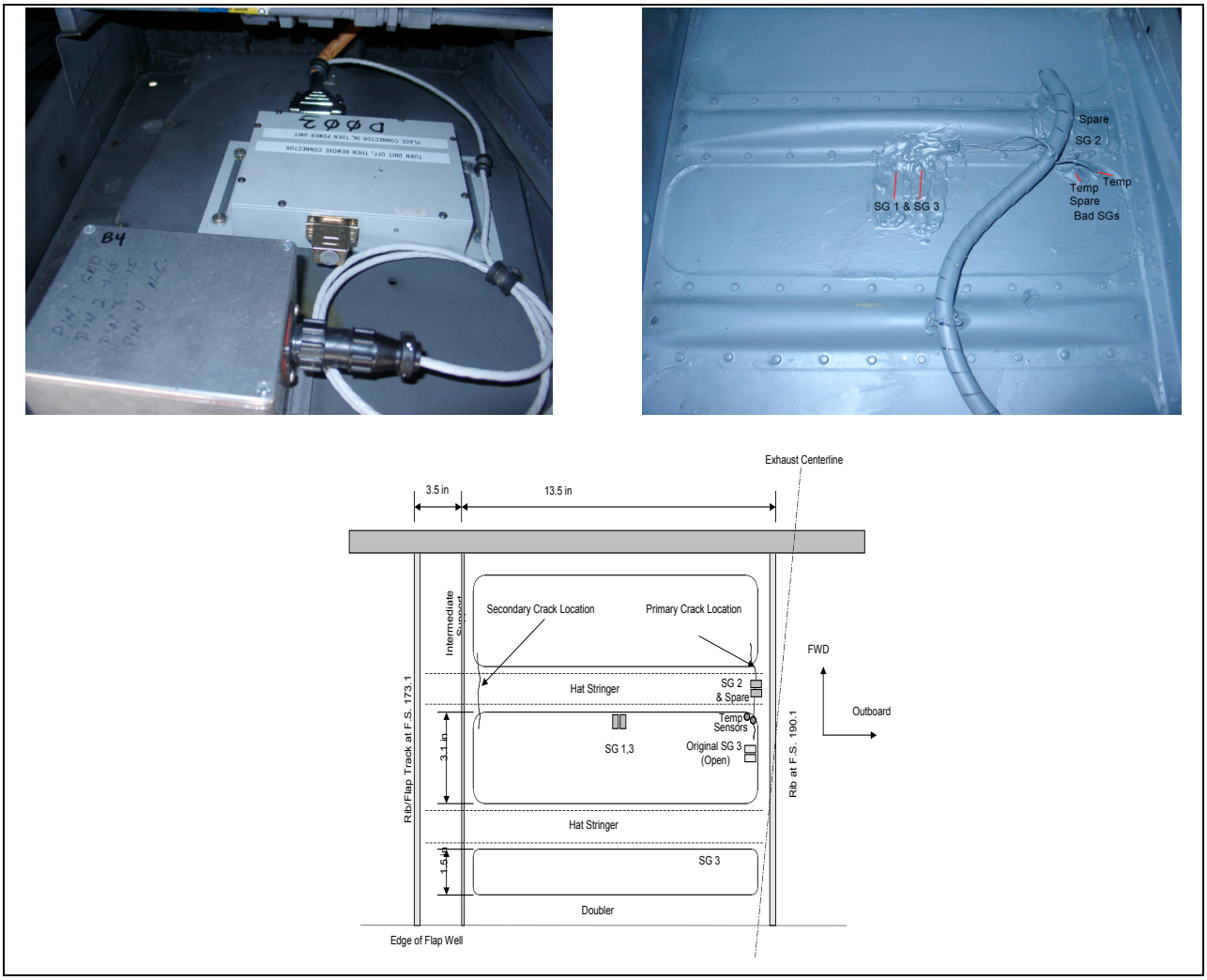

Figure 2. New damage dosimeter installation in C-130 during June 2003.

First, the old room-temperature vulcanized (RTV) silicone was removed with a silicone cleaner and surface preparation solvent and phenolic scrapers. The temperature sensor was located near the hat riser. An AFRL technician and engineer installed six strain gages using a fast curing adhesive. The gages were covered with polytetrafluoroethylene (PTFE) tape and coated with a two-part polysulfide liquid polymer compound, since the temperature was expected to be approximately 100 °C. The technician and engineer also installed two two-terminal temperature transducers. Spare gages and temperature transducers were installed in the event any of the sensors developed problems. After bonding of the transducer and cable routing, the installers found that the two gages on the right side were not operating properly. For the final configuration, SG2 was located on the hat riser and SG1 and SG3 were adjacent to each other at the center of the panel.

FLIGHTS FLOWN DURING JUNE 2003

During June 10–12, 2003, an AFRL engineer assisted NCANG personnel in acquiring dosimeter data from five flights (Table 1). The C-130 was then ready for installation of the repair, but the constrained layer-damping (CLD) repair was postponed until October 2003 because the NCANG unit was being deployed. After repair installation, more dosimeter data flights were flown. Repair data was still being processed at the time of this study. This paper reports the data collected during June 2003.

For five flights flown during June 2003 (Table 1), the flight crew completed flight logs containing flight activity, time, flap setting, altitude, engine 4 total inlet temperature, airspeed in knots, and engine revolutions per minute. Flight 1, designated a local flight by NCANG personnel, consisted of the C-130 flying to Warner Robins Air Force Base (AFB) Air Logistics Center (ALC), Georgia, (1A) unloading cargo, and returning to the NCANG base (1B). Dosimeter clock, temperature, and strain data were erratic during the end of flight 1A and the beginning of flight 1B, requiring that much of the downloaded data be hand edited. Two possible explanations for this erratic data are that either the dosimeter became erratic at higher altitude or there was a problem with dosimeter serial number 1 (SN1). On all five flights, the dosimeter powered on at engine run-up and powered down after engine shutdown after landing, thus successfully implementing the autonomous threshold mode of operation. Flights 2 through 5 consisted mostly of cargo drops; hence, flap position was changed several times during these flights. On only the flight logs for flights 2 and 3 could the crew document the flap positions during the flight. Data on flights 2 through 5 used dosimeter SN3. When possible, the engineer performed a strain gage shunt calibration before the flight.

Table 1. C-130 flights flown during June 2003.

Flight	Date	Type	Description	Hours	Dos SN	Record #
1-1A	June 10	Local	NCANG to WR-ALC	0.90	1	499-5529
1-1B	June 10	Local	WR-ALC to NCANG	0.92	1	5834-10651
2	June 11	Tactical mission	Air drops at Pope AFB	3.01	3	1-8286
None	June 11	Ground	Ground engine run	0.49	3	8287-9636
3	June 11	Local-Asslt	Multiple landings	2.35	3	9641-16126
4	June 12	Tactical mission	Air drops	1.79	3	15-4651
5	June 12	Tactical mission	Air drops	2.64	3	4652-11808

DESCRIPTION OF LATEST DOSIMETER VIEWER SOFTWARE AND EXAMPLES

The AFRL is continuously improving the dosimeter viewer software to meet various user needs. The dosimeter stores two types of records—TH and third octave standard data record (SDR). The AFRL developed software using graphical programming with virtual instruments (VIs) to enable engineers to quickly look at downloaded binary dosimeter data in the laboratory or in the field. The VI shows the desired TH or SDRs by displaying data from the raw dosimeter data file and allows the user to create spreadsheet files.

Since the initial reports, the VIs have undergone significant changes and enhancements. A display of the first record of data downloaded for flight 2 is shown in Figure 3. On the left side of the plot is the temperature, month, day, minute, hours, seconds, TH peak strains, and third octave bands as recorded in the dosimeter memory. Third octave band start and end frequencies are listed in Table 2. Due to the age of the internal clock battery, dosimeter time was several hours behind real time. Figure 3 also shows the record number and third octave overall rms computed (described later in this paper). The right side of Figure 3 shows the TH for the first 42 records and values of mean, rms, and standard deviations computed from the displayed TH. The ‘SD record #’ button on the left side of the plot allows the selection of a record number to display third octave data. The ‘enable quickview’ button sequences through all records.

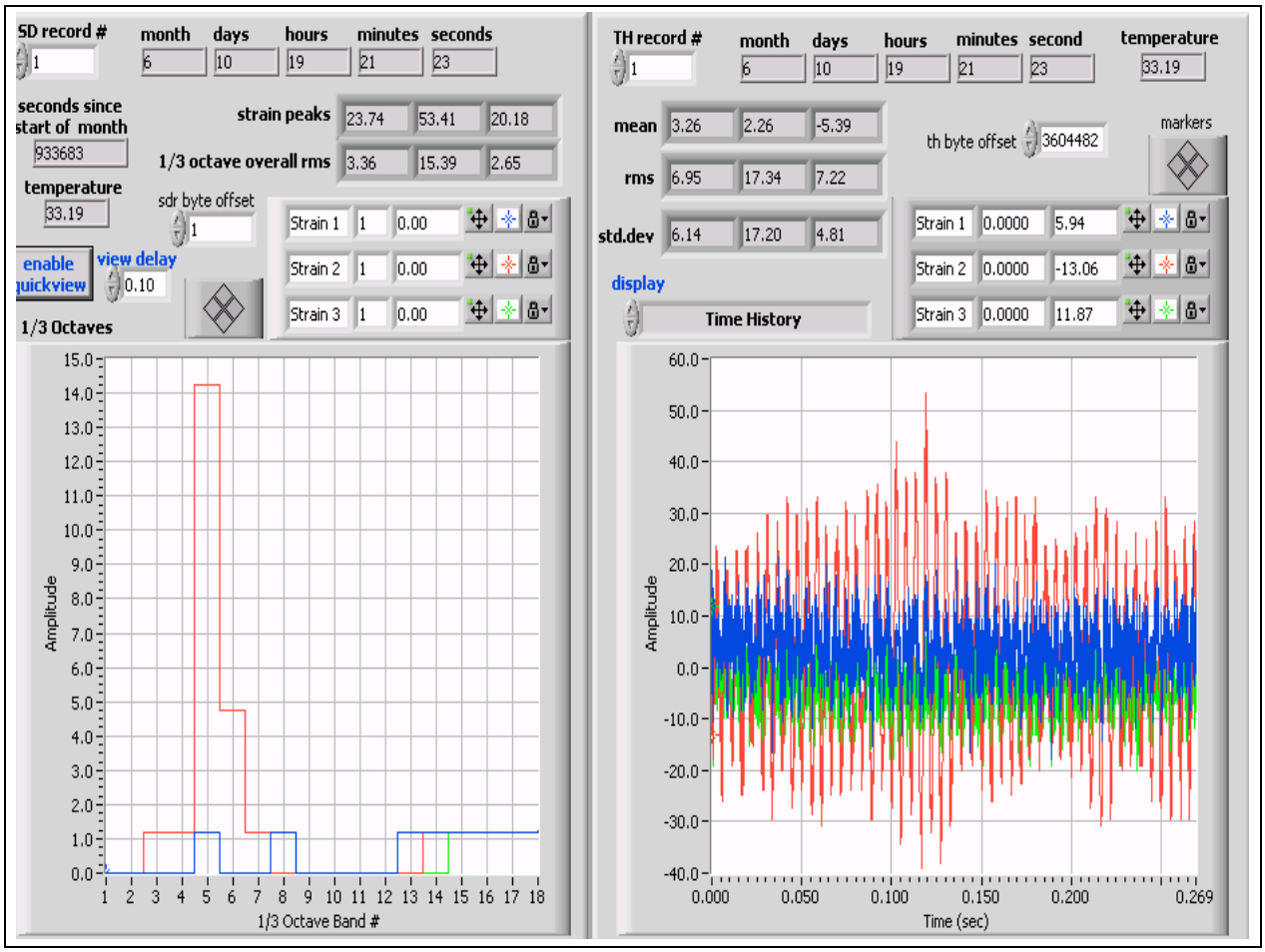

Figure 3. Third octave and TH from flight 2, record 1.

Table 2. Frequency (F) versus third octave bands.

Band #	Fstart (Hz)	Fcenter (Hz)	Fend (Hz)	Band #	Fstart (Hz)	Fcenter (Hz)	Fend (Hz)
1	61.2	67.8	76.1	10	454.5	507.4	569.5
2	76.1	84.3	94.6	11	569.5	639.6	717.9
3	94.6	104.1	116.9	12	717.9	804.8	903.4
4	116.9	130.6	146.5	13	903.4	1013.1	1137.1
5	146.5	163.6	183.6	14	1137.1	1274.2	1430.2
6	183.6	203.3	228.2	15	1430.2	1604.7	1801.2
7	228.2	256.2	287.5	16	1801.2	2021.2	2268.7
8	287.5	322.3	361.7	17	2268.7	2546.7	2858.6
9	361.7	404.9	454.5	18	2858.6	3207.7	3600.6

From this first record from both the 1/3 octave and TH plots, SG2 is seeing the most activity. In Figure 3, the third octave shows a cyclic component in bands 5 and 6, equivalent to 146.5 Hz to 183.6 Hz for band 5 and 183.6 Hz to 228.2 Hz for band 6. The TH for SG2 shows a cyclic component with a period of approximately 5.55 milliseconds or a frequency of 180 Hz. From the pilot log, the engine speed is 72.5% at engine startup for a frequency of 230.33 Hz × .725 Hz = 166.98 Hz. Accordingly, the engine cyclic frequency is measured as vibration on the hat riser, which is the location of SG2. This gives the experimenter more confidence in the validity of the measured strain. Computation of rms values from third octave data is described later in this paper.

The 'STORE DATA' button on the VI allows the engineer to save all data as a spreadsheet file for further analysis. Stored spreadsheet data includes all recorded dosimeter data (temperature, peak strain, and clock time), rms values computed from third octave records, and computed TH statistics (mean, standard deviation, and rms). In addition to 2048-point TH displays, the right-hand display can view the autocorrelation function, probability density function (PDF), and amplitude frequency spectrum computed from the TH to certify data validity.[10] In addition, a rain flow display is provided using the full cycle lookup American Standard Test Method (ASTM).[11] The autocorrelation function, PDF, PSD, and rain flow displays for record 1 of flight 2 are shown in Figure 4. As occurred in the 1/3 octave data in Figure 3, the amplitude peaked at about 180 Hz as recorded in the PSD shown in Figure 5. The PDF confirms that there are no extraneous spikes or other unusual occurrences in the TH.

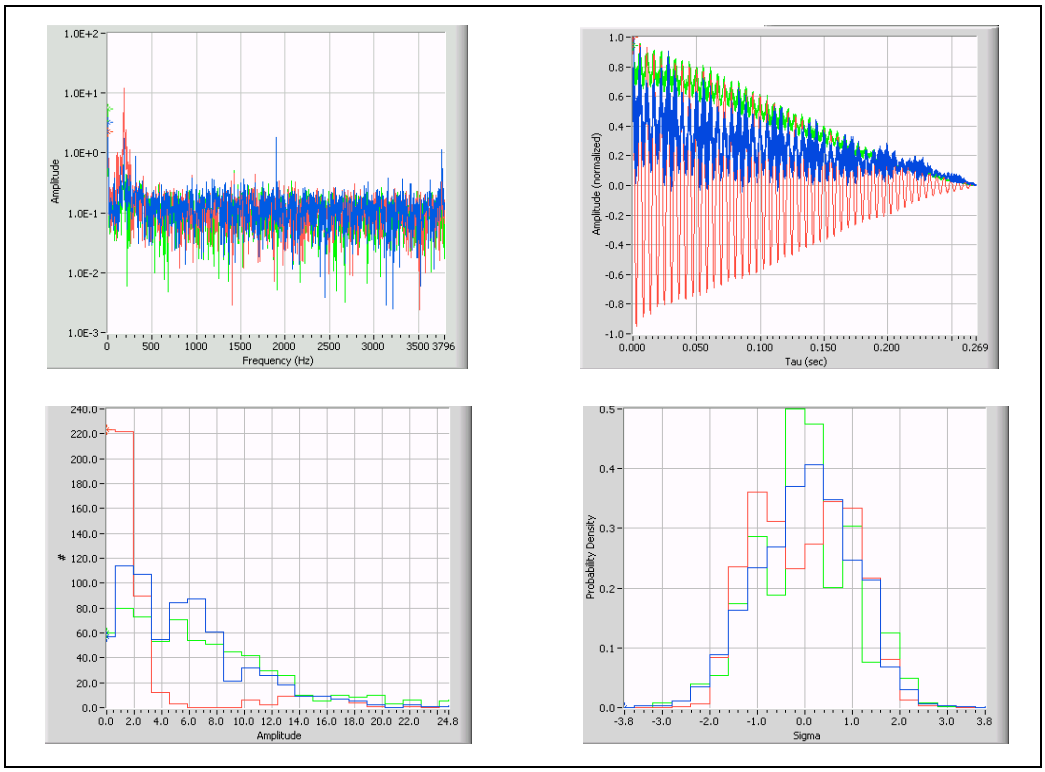

Figure 4. Flight 2, record 1 autocorrelation function (top right plot), PDF (lower right plot), PSD (top left plot), and rain flow display (lower left plot).

Computation of rms TH from Third Octave Data

One-third octave bands are stored in a maximum of 29,455 SDRs. The starting point of the third octave band distribution is programmable. The dosimeter records third octave band rms values for each strain gage. The three steps used to compute the third octave overall rms were: 1) square each band rms to get the mean square, 2) sum all resultant band rms^2, 3) take the square root of that result to produce the overall rms, which can be expressed as:

$$\text{overall } rms^2 = \sum_{i=1}^{18} rms(i)^2 \qquad (1)$$

where i is the band number. Equation 1 shows that bin center frequency knowledge is not required to compute the overall rms.

The AFRL data analysis process consisted of the following steps: 1) The VI was used to save a maximum of 22,548 records as a spreadsheet file; 2) Line 1 of the file was deleted and the new data was saved as a worksheet file; 3) The TH information and inactive data records were removed from the files

so only flight data remained (i.e., data record numbers); 4) Temperature and SG2 rms TH files were created in the spreadsheet program for each flight; 5) The worksheet data file was imported into statistical analysis software using multivariate analysis to provide correlation plots.[12,13]

DISCUSSION OF RESULTS

Temperature Plots with Marks for Flap Position

One theory for changing levels in the plots is that the flap position impacts the strain levels and the temperatures of the wing flap skin. Temperature TH data for flight 1 were hand edited in the software program to remove intermittent data during the middle of data collection. The only editing required for the data for the other four flights and engine ground runs was to determine the start and stop of flights. Figure 5 shows the temperature versus flight time for flights 1 through 5 as well as a ground run between flights 2 and 3. As seen in the plots, the highest temperature seen in the wing flap well was approximately 104 °C during flight 3. For flight 1, edited data are shown in Figure 5. For flights 2 and 3, an indication of flap position was also included on the plot by adding a column on the spreadsheet for flap position and estimating as closely as possible the time and flap position from the flight logs. A flap position of 50% or greater (i.e., the flap is extended or lowered more than 50%) usually indicated a temperature decrease. The flight crew may have forgotten to record one flap position change on flight 2. Flight 1 was basically a takeoff and cruise to Warner Robins AFB and return to the NCANG base. Flight 1 flew at higher altitudes than the other flights, had no flap position changes except at takeoff and landings, and had the lowest temperature (approximately 10 °C) of the five flights. Since there was little flap position information on the flight log for flights 4 and 5, a mark for flap position could not be included. Looking at the temperature TH for these flights and taking into consideration that these were flights with multiple cargo drops and landings, the flap position may have been 50% or greater (i.e., the flap is extended or lowered more than 50%) at the temperature dips in the two flights.

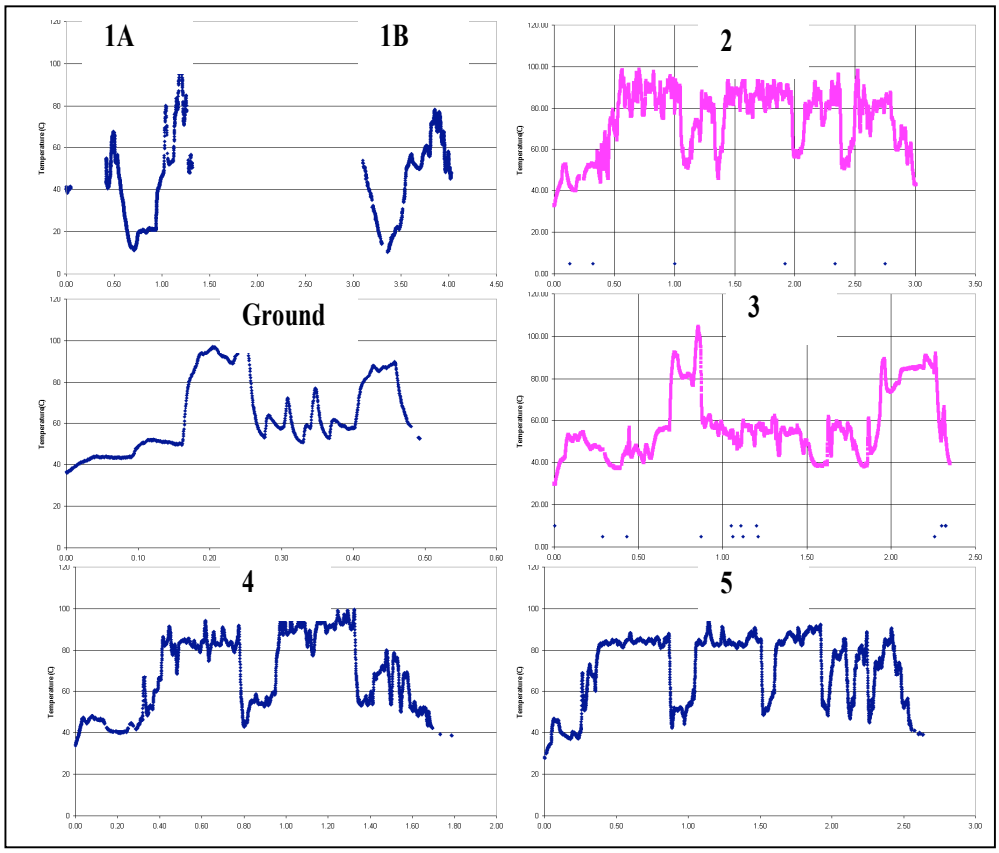

Figure 5. Temperature (°C) versus time (hours) for each flight.

SG2 rms TH FROM THIRD OCTAVE DATA

Figure 6 shows TH plots for the rms values of SG2 versus time using the rms third octave values. SG2 data is presented since it had the highest strain readings. Figure 6 shows rms TH for flights 1 through 5 as well as the ground run between flights 2 and 3. These rms values included only the dynamic component of the strain signal.[12] The highest rms strain level recorded in the plots in Figure 6 was approximately 160 με rms. This level was reached during flights 1, 2, and 3 during very short time periods. Most of the time the strain levels were less than 140 με rms.

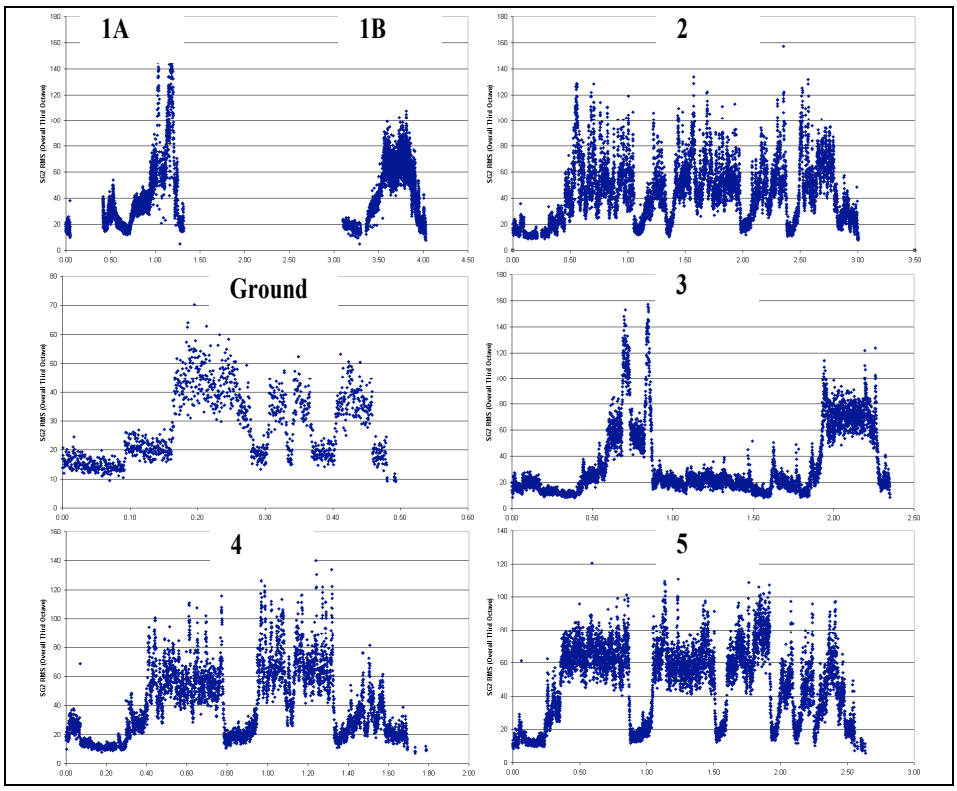

Figure 6. SG2 (με rms) versus time (hours) for each flight.

Correlation Between Temperature, Strain, and Damage Plots for Durability Patch Design

One consideration in the design of durability patches is the correlation between different strain gages and temperature. Using multivariate analysis, the AFRL generated the correlations and scatter plot shown in Figure 7 for flight 2.[13] In the plots in Figure 7, the label 'oct ovrl1' is used to identify the overall rms level computed from the third octave data for SG1. The labels 'oct ovrl2' and 'oct ovrl3' identify the overall rms level computed from the third octave data from SG2 and SG3, respectively. In the plots, there is significant correlation between most of the combinations of the parameters; in particular the correlation between SG1 and SG3 is very high (i.e., > .99), because SG1 and SG3 are next to each other. This correlation is demonstrated in the scatter plots between SG1 and SG3, which show a tightly packed pattern on nearly a straight line. The scatter plots also confirm that SG2 appears to have the highest strain level. The plots of temperature versus strain have more scatter than the other plots.

The measurements in Figures 5 and 6 and the correlation plots in Figure 7 show a correlation between the skin strain and temperature. A reasonable explanation for this correlation might be that the higher vibratory levels exist near the ground for cargo drops and touch-and-go landings, since the ambient temperature is expected to be lower at altitude and the vibration levels are expected to be higher near ground conditions.

The AFRL generated cumulative damage plots for the C-130 before repair as shown by a typical example for flight 2 (Figure 8). The methodology and calculation of cumulative damage versus frequency and temperature are further explained in a separate study.[14] This damage plot appears to indicate that most of the cumulative damage is at approximately 75 °C to 100 °C and in frequency bands 5 to 6 (146.5 Hz to 228.2 Hz) during flight 2.

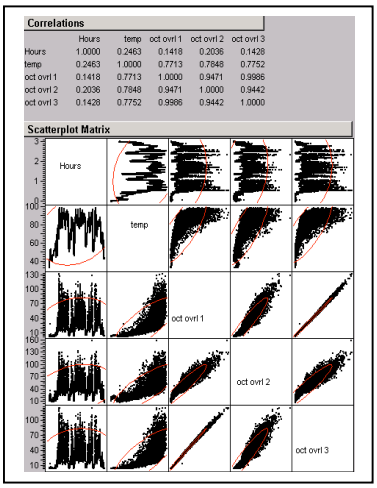

Figure 7. Flight 2 correlations between temperature and strains.

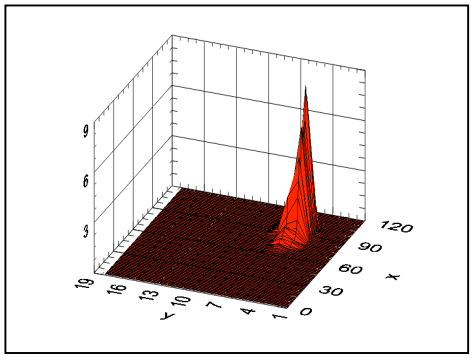

Figure 8. Normalized cumulative damage plot for SG2 versus frequency 1/3 octave band number (Y) versus temperature °C (X).

SUMMARY AND CONCLUSIONS

The damage dosimeter is a useful tool to produce quick-response definition of thermal and dynamic strain frequencies on military and commercial aircraft. The TH of temperature versus flight time and rms values of third octaves versus flight time were presented in this paper. The highest temperature for the five flights analyzed appears to be 104 °C. The lowest temperature appears to be on flight 1 where the C-130 was cruising at altitude most of the time. When the flap position is 50% or greater (i.e., the flap is extended or lowered more than 50%), the temperature appears to decrease. Better flap position data for flights 4 and 5 would have helped to confirm this conclusion. SG2 appeared to have the highest strain levels. Usually the levels for SG2 were less than 140 με rms, but there were several peaks close to 160 με rms. There is high correlation between the rms values of SG1 and SG3 as expected since they are located next to each other. SG2 rms values are higher than SG1 and SG3. SG2 is located on the corner of the hat riser where the cracks usually originate. Figure 8 shows that the third octave rms data and temperature data can be used for an estimation of structural damage versus frequency and temperature. This data is needed for design of damped composite repairs to slow and prevent HCF cracks. After the C-130 returned from overseas missions and a repair was applied, the NCANG flew more dosimeter measurement flights to ascertain the environmental changes and the effectiveness of the repair.

There is a positive correlation between temperature and vibratory strain levels measured in the C-130 flap well skin panels. Relationships between temperature vibratory strain levels are important in the design of damped repairs required to increase the lifetime of the flap well skin panels. This paper presented data collected by the AFRL on the C-130 for five flights during September 2003. After application of a repair was made, the AFRL successfully collected data on seven additional flights of the C-130 during October 2003. The AFRL plans to present vibratory and temperature data collected after repair installation in a future report. The future data report should determine the impact of the repair on increasing the lifetime of the panel.

ACKNOWLEDGMENTS

The authors thank David Smith of Integrity Design Engineering, Karl Anderson of Valid Measurements™, and Lyle Wells of Trig-Tek, Inc. for helping AFRL engineers to fully understand the damage dosimeter. Also, special thanks to Chief Master Sergeant Michael Bigger and Master Sergeant Tim Roberts of the 145th Air Wing (145AW/LG) at the NCANG base, who supported AFRL efforts to collect data on the C-130. Captain Michael Myers managed the dosimeter delivery to completion on AFRL contract F33615-95-D-3203 and Mark Baker installed the strain gages and temperature sensors.

REFERENCES

1. Roach, Dennis P. April 1998. Bonded Composite Doublers for Commercial Aviation Use. *Aerospace Engineering*, 37-39.
2. Ikegami, R., E. Haugse, A. Trego, L. Rogers, and J. Maly. 2001. Structural Technology and Analysis Program (STAP) Delivery Order Number: 004 Durability Patch, AFRL-VA-WP-TR-2001-3037, ADA408003, Air Force Research Laboratory, Wright Patterson Air Force Base, OH.
3. Smith, D. and I. Searle. February 1998. Damage Dosimeter: A Portable Battery Powered Data Acquisition Computer. *Western Regional Strain Gage Committee Paper*. http://www.vm-usa.com.
4. Anderson, K. F. January 1995. Practical Applications of Current Loop Signal Conditioning. *Technical Memorandum: NASA-TM-4636*. Edwards, CA: NASA Dryden Flight Research Facility.
5. Banaszak, D., D. L. Brown, and A. Trego. 2002. A Quick Look at Flight Data from a Digital Damage Dosimeter. *ESTECH 2002 Proceedings*. Rolling Meadows, IL: IEST.
6. Banaszak, D. and D. Brown. 2003. Challenges in Validating Strain Gage Flight Data from a Digital Damage Dosimeter. *ESTECH 2003 Proceedings*. Rolling Meadows, IL: IEST.
7. Banaszak, D. 2002. End-to-End Mechanical Calibration of Strain Channels in Dynamic Health Monitoring Systems. *Journal of the IEST* 45:113-120.
8. Himelblau, H., A. G. Piersol, J. H. Wise, and M. R. Grundwig. 1990. *IEST-RP-DTE012.1*. 1993. *Handbook for Dynamic Data Acquisition and Analysis*. Rolling Meadows, IL: Institute of Environment Sciences and Technology 148-152.
9. Banaszak, D. and D. Brown. August 2003. A Statistical Look at Damage Dosimeter Data from a Fighter Aircraft. *American Statistical Association 2003 Proceedings of the Section on Physical and Engineering Sciences*. Alexandria, VA: American Statistical Association 3-7.
10. Bendat, J. S. and Alan G. Piersol. 2000. *Random Data Analysis and Measurement Procedures*, 14. New York: John Wiley & Sons.
11. Bannantine, J. A., J. J. Comer, and J. L. Handrock. 1990. *Fundamentals of Metal Fatigue Analysis*. New Jersey: Prentice-Hall, Inc.
12. Banaszak, D., D. L. Brown, and A. Trego. August 2002. Damage Dosimeter Third Octave and RMS Time History Values. *American Statistical Association 2002 Proceedings*, *Joint Statistical Meeting in New York*. Alexandria, VA: American Statistical Association.
13. SAS® Institute Inc. 2000. *JMP® Introductory Guide Version 4*. Gary, NC.
14. Rogers, L., D. Banaszak, D. Laird, and D. Brown. December 2003. Sonic Fatigue Damage Service Environment and Life Improvement From Dosimeter Data. Savannah, GA: Aircraft Structural Integrity Program (ASIP) 2003 Poster.

ABOUT THE AUTHORS

David Banaszak received a BS in electrical engineering from the University of Wisconsin and a MS in applied statistics from Wright State University. Banaszak works for the Air Vehicles Directorate of the AFRL and performs acoustic, vibration, and loads measurements for numerous laboratory and field test programs. He is a member of the American Institute of Aeronautics and Astronautics, American Statistical Association, and Vehicular Instrumentation/Transducer Subcommittee of the Range Commander's Council Telemetry Group. He is an IEST Fellow, an IEST Vice President, and president of the IEST Greater Ohio Chapter.

Dansen Brown has over 30 years of experience in processing and analyzing dynamics data. He received bachelor's and master's degrees in mathematics from Miami University, Oxford, Ohio. He has worked for the AFRL since 1972, where he develops and maintains an advanced capability for the processing and analysis of dynamics data recorded during flight and ground tests conducted by the Experimental Validation Branch of the Structures Division. He also frequently develops computer programs to recover, process, and analyze data recorded from other Air Force programs.

Captain David J. Laird received a BS degree in aeronautical and astronautical engineering from the University of Illinois. He studied at Iowa State University as a teaching assistant and research assistant, receiving a MS degree in aerospace engineering. Laird received a commission into the US Air Force in 1996. He served at Los Angeles AFB as the payload design engineer for the MILSATCOM Advanced Systems Directorate. He received a PhD from the School of Engineering at the Air Force Institute of Technology while specializing in solid mechanics and studied hypervelocity impacts. He is the former deputy chief of the Structural Mechanics Branch in the Air Vehicles Directorate of the AFRL.

AUTONOMOUS ENVIRONMENTAL DEFINITION OF C-130 FLAP WELL SKIN PANEL

David Banaszak, Air Force Research Laboratory (AFRL)
Dansen L. Brown, Air Force Research Laboratory (AFRL)
David J. Laird, Air Force Research Laboratory (AFRL)

Biography

David Banaszak received a Bachelor of Science (BS) in Electrical Engineering from the University of Wisconsin and a Master of Science (MS) in Applied Statistics from Wright State University. Dave works for the Air Vehicles Directorate of the Air Force Research Laboratory and does acoustic, vibration and loads measurements for numerous laboratory and field test programs. Dave is a member of the American Institute of Aeronautics and Astronautics, American Statistical Association and Vehicular Instrumentation/Transducer Subcommittee of the Range Commander's Council Telemetry Group. He is President of the Greater Ohio Chapter of the Institute of Environmental Sciences and Technology.

Dansen Brown has over 30 years experience in processing and analyzing dynamics data. He received Bachelor's and Master's degrees in Mathematics from Miami University (Oxford, Ohio) in the late '60s. He has worked for AFRL since 1972, where he develops and maintains an advanced capability for the processing and analysis of dynamics data recorded during flight and ground tests conducted by the Experimental Validation Branch of the Structures Division. He also frequently develops computer programs to recover, process, and analyze data recorded from other Air Force programs.

Captain David J. Laird received a BS degree in Aeronautical and Astronautical Engineering from the University of Illinois. He studied at Iowa State University as a teaching assistant and a research assistant, receiving a MS Degree in Aerospace Engineering. Dave received a commission into the US Air Force in 1996. He served at Los Angeles AFB as the payload design engineer for the MILSATCOM Advanced Systems Directorate. Dave received a PhD from the School of Engineering at the Air Force Institute of Technology while specializing in solid mechanics and studied hypervelocity impacts. He is deputy chief of the Structural Mechanics Branch in the Air Vehicles Directorate of AFRL.

Abstract

Air Force C-130 aircraft require numerous aluminum doubler repairs on the wing flap skin aft of the right hand outboard engine. These repairs are costly and require riveting. Rivets often provide new areas of stress concentration causing new cracks to develop elsewhere. Boeing and the AFRL are measuring the thermal and strain environment behind the right hand outboard engine of a North Carolina Air National Guard (NCANG) operational C-130 aircraft (TN 93-1456) for use in design of a damped repair patch to prevent the growth of cracks in skin under the wing flap panel. During June 2003, AFRL engineers and technicians acquired data using an autonomous damage dosimeter during 5 operational flights. The Boeing-designed damage dosimeter measures structural strains and temperatures on in-service aircraft to diagnose difficult-to-analyze structural conditions, such as acoustics and high-cycle fatigue. On the first flight, the C-130 flew from Charlotte, NC to Warner Robbins AFB and returned to Charlotte. The last four flights were assault flights where the C-130 did simulated cargo drops. Pilots logged the altitude, indicated airspeed, engine speed and flap positions for the first 4 flights. Flap position settings were compared with dosimeter temperature and root mean square (rms) strain measurements. The paper presents typical third octave plots showing engine speed vibratory frequencies, rms time histories and correlation data for a flight. This paper also presents typical limited data in time history, probability density, power spectral density and rain flow formats.

Keywords

Dosimeter, Data Acquisition, Vibration, Structures, High Cycle Fatigue, Strain, Third Octave, Time History, Correlations

Background

Typical secondary aircraft structural crack damage on a C-130 resulting from a high cycle fatigue (HCF) environment of greater than 10^6 cycles is shown in figure 1. Turbulent airflow from the prop-wash causes high cycle fatigue in this region. This damage results in costly inspection and repair. Current repair is accomplished by riveting aluminum doubler plates, but the structure continues to respond in a resonant fashion and new cracks form due to stress intensities at the new fastener locations. A better solution is applying a specifically designed damped bonded repair patch. Design of

composite durability repair patches requires environmental information characterizing temperature, resonant response frequency and strain levels. Roach [1998] shows an example of a composite bonded patch.

AFRL finds this information by measuring the structure's operating environment with a compact, stand-alone, electronic device called a damage dosimeter. The Boeing Company designed the damage dosimeter to measure structural strains and temperatures on in-service aircraft. The dosimeter, strain gages and temperature sensor are installed in the C-130 wing flap well behind the outboard engine as shown in figure 1. Work completed on an AFRL contract with Boeing is documented by Ikegama, Haugse, Trego, Rogers and Maly [2001]. AFRL is finishing work on the C-130 that included five

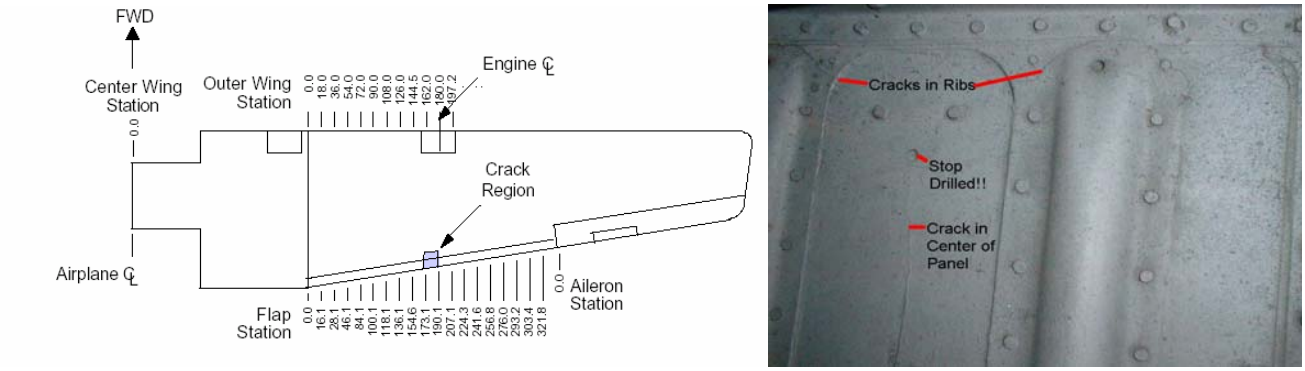

Figure 1. Crack Location on C-130 Secondary Structure

data-gathering flights on the C-130, an application of a repair and then six more dosimeter flights.

Review of Dosimeter Operation

The damage dosimeter features include autonomous threshold operation or continuous operation, on-board Fast Fourier Transform (FFT) computation and storage of third octave frequency spectra. That is, the dosimeter can record third octave data continuously or be programmed to autonomously record data when a strain threshold is exceeded. An Anderson Current Loop (ACL) conditions strain gage signals to minimize the power required to excite the dynamic gages and to eliminate the need to account for wire-length effects as described by Anderson [1995]. Smith and Searle [1998] give a complete description of the dosimeter.

The dosimeter is a rugged, small (fits in palm of hand), battery powered, lightweight (weighs less than 1.5 lb. (.69kg) without battery), data acquisition system that measures 3 channels of strain at rates of 7600 samples per second and a single channel of temperature at a rate of 1.3 samples per second. The autonomous dosimeter is programmed to only acquire data above a rms strain threshold. The strain data for each of the three gages is processed through a Fast Fourier Transform (FFT) analyzer to generate a Power Spectral Density (PSD). The PSD is then converted to 18 third octave frequency bands described more fully in Banaszak, Brown and Trego [2002-ESTECH]. The dosimeter is programmed to store 42 records of time history data each 0.3 seconds long and records and stores third octave records until its 4-Megabyte memory is filled.

Banaszak and Brown [2003-ESTECH] and Banaszak [2002] investigated techniques to perform system and physical (mechanical) end-to-end calibration of bonded strain gages. Techniques include inserting shunt calibration resistors in line for a system calibration and exciting the strain gages with a remote control structural exciter for a physical end-to-end calibration in accordance with the Institute of Environmental Science and Technology (IEST) Recommended Practice by Himelblau, Piersol, Wise and Grundwig [1990]. Banaszak and Brown [2003-ESTECH] also describe in detail dosimeter data collection, processing and recording. Banaszak and Brown [2003-ASA] provide a preliminary look at data recorded continuously by Boeing on an F-15 aircraft.

Past C-130 Efforts and AFRL Flights During June 2002 and September 2002

The Boeing Company used the dosimeter to collect dynamics data on some C-130 flight tests before completion of the durability patch contract during June 2001. Detailed descriptions of flight-test installation and data measured using the damage dosimeter are in Ikegami, Haugse, Trego, Rogers, and Maly [2001]. The dosimeter was located in the wing flap well between wing station 100.1 and 118.1, and the strain gages and temperature sensor were located between F.S. 173.1 and F.S. 190.1. AFRL engineers continued collecting dosimeter data on C-130 Tail Number 93-1456 at the North Caroline Air National Guard (NCANG) Base in Charlotte. From February 2001 to June 2002 the C-130 was inoperable while awaiting parts for repair of wheel well flap damage from a flat tire. During June 2002, an AFRL engineer traveled to the NCANG to conduct data acquisition. The engineer found strain gage 1 (SG1) open and NCANG personnel bypassed the gage with a dummy 350-ohm resistor so that the series strain gage configuration would operate. Now strain gage 1 was a dummy check

channel. The NCANG flew two flights during June 2002. The dosimeter only collected 17 and 1 records respectively on the first and second flights while operating in the autonomous threshold mode. The engineer thought this might be due to low strain levels not exceeding the threshold values. Based on data found in Ikegami, et.el. [2001] for the C-130, SG1 was the most active strain gage and strain gages 2 and 3 may not have had high enough strain levels to activate dosimeter data collection. The engineer reprogrammed the dosimeter for continuous collection of rms third octave data for the next NCANG dosimeter flights. The NCANG gathered data on two flights during September 2002. These flights indicated that the dosimeter collected data continuously for about 5 hours per flight as expected. Unfortunately, it appeared that the data were invalid after aircraft takeoff. After aircraft landing the data again appeared to be valid. One possible explanation is that one of the gage circuits opened as the wing flexed (i.e. a change in the wing static loading after the aircraft is airborne) during aircraft takeoff and closed again as the wing flexed back to its ground position.

Laboratory experiments after the flights indicated that a similar effect happens when one of the strain gage circuits open while the dosimeter is collecting data continuously from dynamic strain gages on a plate excited by an electrodynamics shaker. The assumption was made that somehow the gages were opening during takeoff and closing when the aircraft was on the ground. Unable to fix the current strain gage installation, AFRL decided to install new strain gages, temperature sensors and cabling. By June 2003, AFRL engineers and technicians and the NCANG personnel and schedules were coordinated so that AFRL could reinstall the strain gages.

Strain Gage and Temperature Sensor Reinstallation

During December 2002 and March 2003, AFRL engineers revisited the NCANG to plan removal and reinstallation of the strain gages. During discussion with a sheet metal worker, AFRL learned that the cracks always start in the hat riser area. Therefore the gage locations were changed from the previous flights.

During June 2003, an AFRL engineer and technician reinstalled the strain gages as shown in figure 2. First they

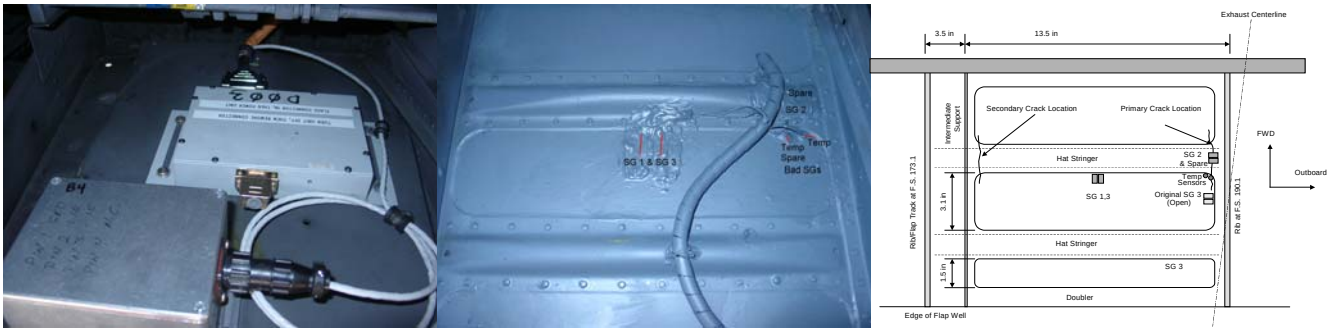

Figure 2. New Damage Dosimeter Installation in C-130 during June 2003

removed the old RTV with Dow Corning OS-2 solvent and phenolic scrapers. The temperature sensor is now located near the hat riser. An AFRL technician and engineer installed 6 Measurement Group type WK-13-250BG-250 Option W strain gages using M-Bond 600. The gages were covered with Teflon tape then coated with M Coat J since temperature expectations were about 100 degrees Centigrade (°C). They also installed 2 Analog Devices two-terminal IC AD590 temperature transducers. Spare gages and temperature transducers were installed in case any of the sensors developed problems. After bonding of the transducer and cable routing, the installers found the two gages on the right side were bad. For the final configuration, strain gage 2 is now located on the hat riser and strain gage 1 and 3 are adjacent to each other at the center of the panel.

Table 1. C-130 Flights Flown June 2003

Flight	Date	Type	Description	Hours	DosSN	Record#
1-1A	June 10 2003	Local	NCANG to WR-ALC	0.90	1	499-5529
1-1B	June 10 2003	Local	WR-ALC to NCANG	0.92	1	5834-10651
2	June 11 2003	TAC	Air Drops at POPE	3.01	3	1-8286
None	June 11 2003	Ground	Ground Engine Run	0.49	3	8287-9636
3	June 11 2003	Local-Asslt	Multiple Landings	2.35	3	9641-16126
4	June 12 2003	TAC	Air Drops	1.79	3	15-4651
5	June 12 2003	TAC	Air Drops	2.64	3	4652-11808

Flights Flown during June 2003

During the period of June 10-12, 2003, an AFRL engineer assisted NCANG personnel in acquiring dosimeter data from 5 flights. The C-130 was now ready for installation of the repair, but since the NCANG unit was being deployed, the constrained layer-damping (CLD) repair by Damping Technologies, Inc., was postponed until October 2003. After repair installation, more dosimeter data flights were flown. Repair data is still being processed. This paper reports the data collected during June 2003.

NCANG personnel flew five flights where dosimeter data were acquired as shown in Table I. The flight crew completed flight logs containing flight activity, time, flap setting, altitude, engine 4 total inlet temperature, knots indicated airspeed and indicated engine revolutions per minute. Flight 1, designated a local flight by NCANG personnel, consisted of the C-130 flying to Warner Robbins AFB (1A), unloading cargo and then returning to the NCANG base (1B). Dosimeter clock, temperature and strain data were erratic during the end of flight 1A and beginning of flight 1B and much of the downloaded data had to be edited by hand. Two possible explanations are that either the dosimeter went erratic at higher altitude or there is some problem with dosimeter serial number 1 (SN1). On all five flights the dosimeter powered on at engine run up and powered down after engine shutdown after landing, thus successfully implementing the autonomous threshold mode of operation. Flights 2 through 5 consisted mostly of cargo drops and hence flap position was changed a number of times during these flights. On only the flight logs for flight 2 and 3 were the crew able to document the flap positions during the flight. Data on flights 2-5 used dosimeter SN 3 as noted in Table 1. When possible, the engineer preformed a strain gage shunt calibration before the flight.

Description of Latest Dosimeter Viewer Software and Examples

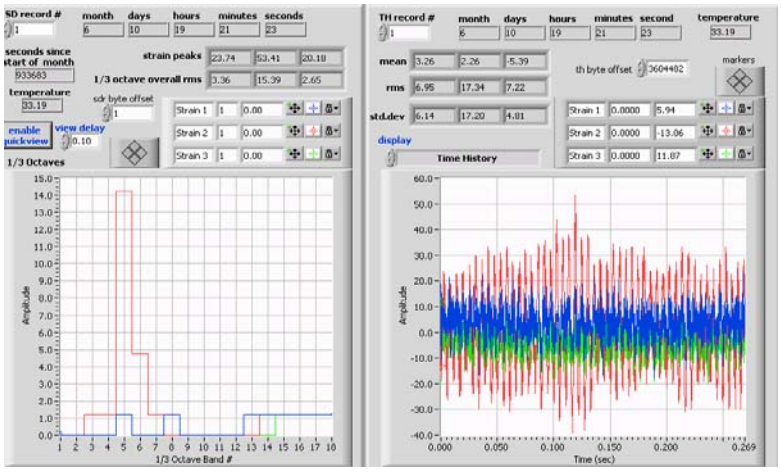

Figure 3. Third Octave and Time History (TH) from Flight 2 Record 1

AFRL is continuously improving the software to meet various user needs. The dosimeter stores two types of records, time history (TH) and third octave (SDR). AFRL developed software using LabVIEW™ virtual instruments (VIs) to provide engineers with the capability to quickly look at downloaded binary dosimeter data in the laboratory or in the field. The VI shows the desired TH or SDR records by displaying data from the raw dosimeter data file. The VI also allows the user to create spreadsheet files.

Since the initial reports, the LabView virtual instruments have undergone significant changes and enhancement. A display of the first record of data downloaded for flight 2 is shown in figure 3. On the left side of the plot is the temperature, month, day, minute, hours, seconds, time history peak strains, and third octave bands as recorded in the dosimeter memory. Due to age of the internal clock battery, dosimeter time was several hours behind real time. Also shown is the record number and third octave overall rms computed as described later. The right hand side of the display shows the time history for the first 42 records and values of mean, rms and standard deviations computed from the displayed time history. On the left side there is a button to select record number to display third octave data and an 'enable quickview' button quickly sequences through all records.

From this first record, we see that SG2 is seeing the most activity. As seen in figure 3, the third octave shows a cyclic component in bands 5 and 6, which is equivalent to 146.5 to 183.6 hertz for band 5 and 183.6 to 228.2 hertz for band 6. Looking at the time history for SG2 we see a cyclic component with a period of about 5.55 milliseconds or a frequency of 180 hertz. From the pilots log, the engines speed is 72.5% at engine startup for a frequency of 230.33 Hz x .725 = 166.98 hertz. It seems reasonable that engine cyclic frequency is measured as vibration on the hat riser, which is the location of SG2. This gives the experimenter more confidence in the validity of the measured strain. Computation of rms values from third octave data will be described later.

There is a STORE DATA button on the VI that allows the engineer to save all data as a spreadsheet file for further analysis. Stored spreadsheet data includes all recorded dosimeter data (temperature, peak strain, and clock time), rms values computed from third octave records, and computed time history statistics (mean, standard deviation and rms). In addition to 2048-point time history displays, the right hand display can view the autocorrelation function, probability density function and amplitude frequency spectrum computed from the time history as recommended by Bendat and Piersol [2000] to certify

data validity. In addition a rain flow display is provided using the full cycle look up ASTM method described in Bannantine [1990]. These 4 additional plots are showed in figure 4 for record 1 of flight 2. Again the peak in the amplitude at about 180 hertz can be seen in the amplitute frequency spectrum. The PDF confirms that there are no extraneous spikes or other unusual occurrences in the time history.

Computation of RMS time Histories from Third Octave Data

One-third octave bands are stored in up to 29,455 SDR records. The starting point of the third octave band distribution is programmable. The dosimeter records third octave band rms values for each strain gage. The three steps to compute the third octave overall rms are (1) square each band rms to get the mean square, (2) sum all resultant band rms^{2}s and (3) take the square root of that result to get to the overall rms. That is

$$\text{overall } rms^2 = \sum_{i=1}^{18} rms(i)^2 \quad (1)$$

where i is the band number. Equation (1) shows that bin center frequency knowledge is not required to compute the overall rms.

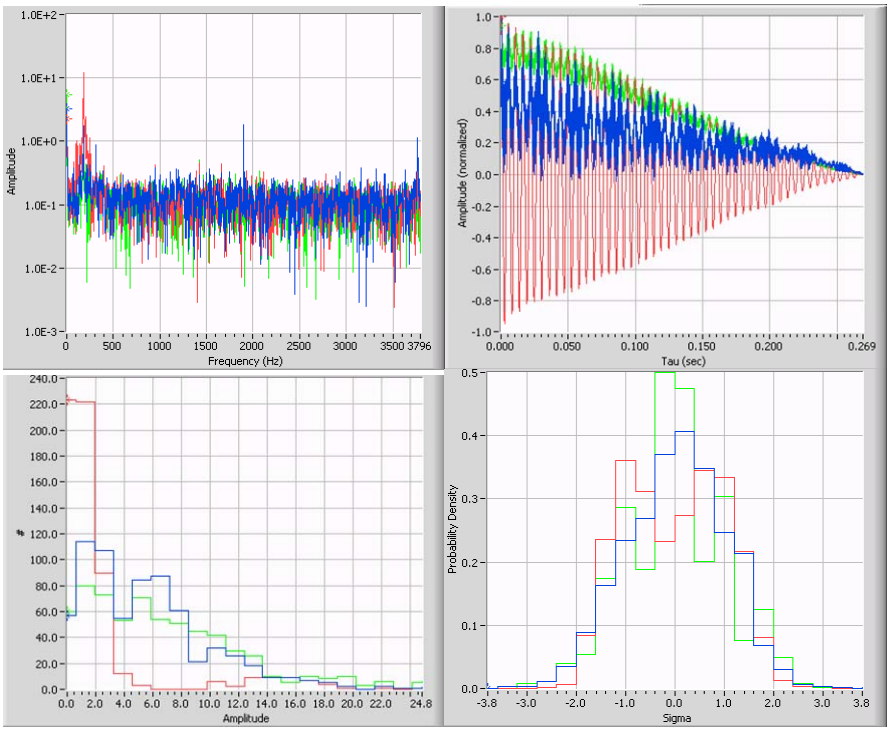

Figure 4. Flight 2 Record 1 Amplitude Spectrum (PSD), Autocorrelation, Rain Flow and Probability Distribution Function (PDF)

AFRL data analysis process consisted of the following steps. 1) The LabVIEW™ VI described by Banaszak, Brown, Trego [2002-ASA] was used to save up to 22,548 records as a spreadsheet file, 2) Microsoft® Excel was used to read the spreadsheet file. Line 1 of the file was deleted and the new data saved as an Excel worksheet file. 3) Next the time history information and inactive data records were removed from the excel files so that only data during flight remains (i.e. data record numbers), 4) Microsoft® Excel was then used to create temperature and SG2 rms time histories files for each flight and 5) the worksheet data file was imported into SAS® JMP® [2000] which was used to get correlation plots.

Discussion of Results

Temperature Plots with Marks for Flap Position

One theory is that the flap position impacts the strain levels and temperatures of the wing flap skin. Temperature time history data for flight 1 were hand edited in Excel to remove intermittent data during the middle of data collection. The other 4 flights and engine ground runs required no data editing other than determining the start and stop of flights. Figure 5 shows the temperature versus flight time for flights 1 through 5 and a ground run between flights 2 and 3. As seen in the plots, the highest temperature seen in the wing flap well is about 104 °C during flight 3. For flight 1 edited data are shown in figure 5. In addition, for flight 2 and 3 an indication of flap position were included on the plot by adding a column for flap position on the spreadsheet and estimating as good as possible the time and flap position from the flight logs. It appears that a flap position of 50% or greater was usually an indication of a temperature decrease. In fact it appears that the flight crew may have forgotten to record one flap position change on flight 2. Flight 1 was basically a takeoff and cruise to Warner Robins AFB and return to the NCANC Base. Flight 1 was flown at higher altitudes, had no flap position changes other than take off and landings and had the lowest temperature (approximately 10 °C) of the 5 flights. Since there was little flap position information on the flight log for flights 4 & 5, a mark for flap position could not be included. Looking at the temperature time histories for these flights and the fact these were also flights with multiple cargo drops and landings, it may be the flap position was 50% or greater at the temperature dips in the two flights.

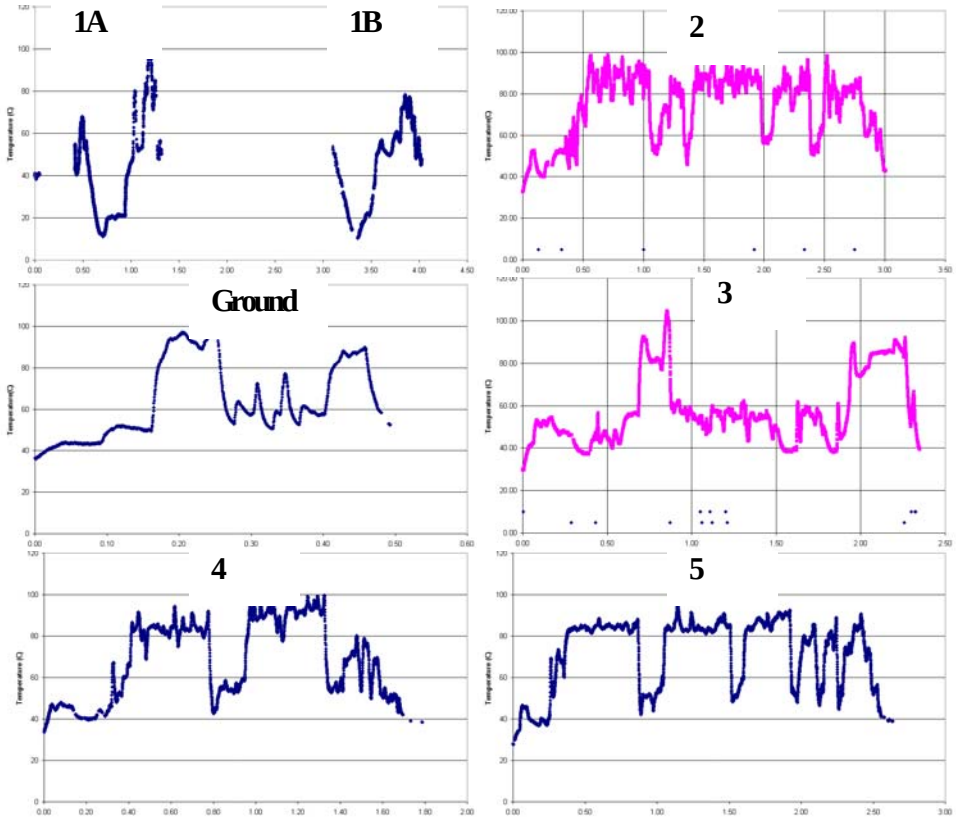

Figure 5. Temperature (°C) versus Time (Hours) for Each Flight

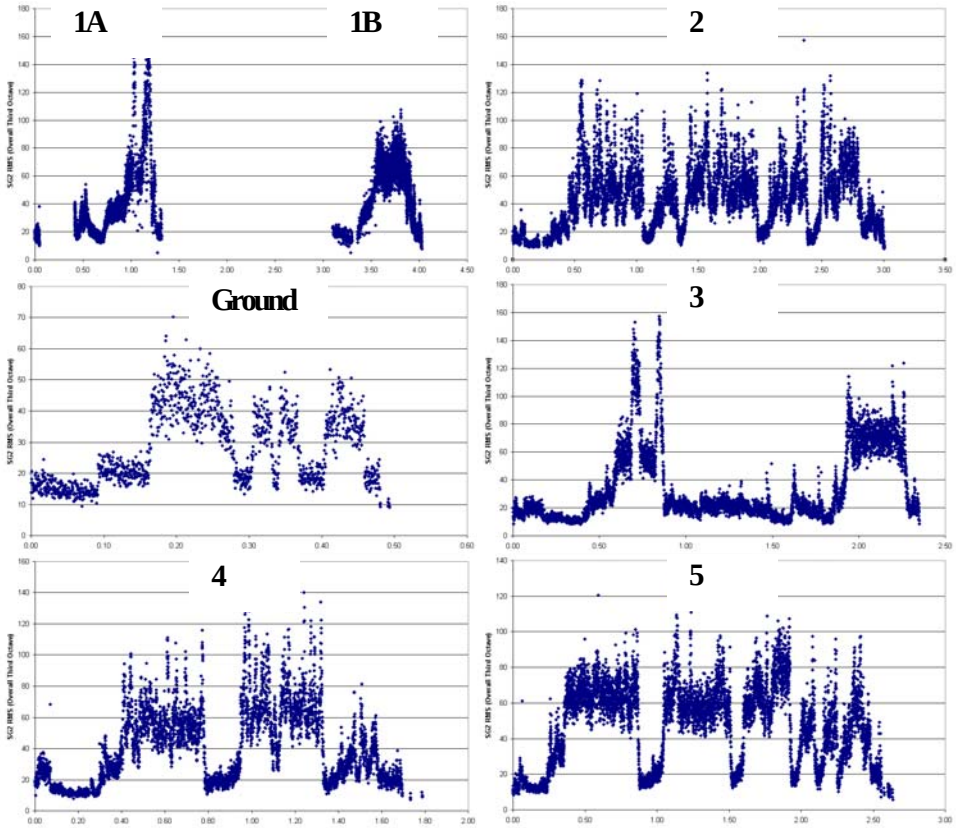

Figure 6. Strain Gage 2 (με) versus Time (Hours) for Each Flight

SG2 RMS Time Histories from Third Octave Data

Figure 6 shows time history plots for the rms values of SG2 versus time using the rms third octave values. Basically, figure 6 shows rms time histories for flights 1 through 5 and the ground run between flights 2 and 3. SG2 is presented since it had the highest strain readings. As mentioned in Banaszak, Brown and Trego [2002], these rms values included only the dynamic component of the strain signal. From the plots in figure 6, it appears that the highest rms strain level is about 160 micro strain (με) rms. This level was reached during flight 1, flight 2 and flight 3 during very short time periods. Most of the time the strain levels were less than 140 με rms.

Correlation Plots Between Temperature and Strain and Damage Plots for Durability Patch Design

One consideration in the design of durability patches is the correlation between different strain gages and temperature. Using SAS® JMP® multivariate analysis, AFRL generated the correlations and scatter plot shown in figure 7 for flight 2. In the plots in figure 7, the label octovlr1 means the overall rms level computed from the third octave data for strain gage 1. Likewise octovrl2 and octovrl3 means the overall rms level computed from the third octave data from strain gage 2 and 3 respectfully. In the plots there is significant correlation between most combinations of the parameters. In particular, the correlation between SG1 and SG3 is very high (i.e. > .99) since SG1 and SG3 are next to each other. This is shown in the scatter plots between SG1 and SG3, which show a tightly packed pattern on nearly a straight line. The scatter plots also confirm that SG2 appears to have the highest strain level. The plots of temperature versus strain have more scatter than the other plots.

AFRL generated cumulative damage plots for the C-130 before repair as shown by a typical example for flight 2 in figure 8. See Rogers, Banaszak, Laird and Brown [2003] for details on methodology and calculation of cumulative damage versus frequency and temperature shown in the figure. This damage plot seems to indicate that most of the cumulative damage is at approximately 75-100 °C and in frequency bands 5 to 6 (146.5 Hz to 228.2 Hz) during flight number 2.

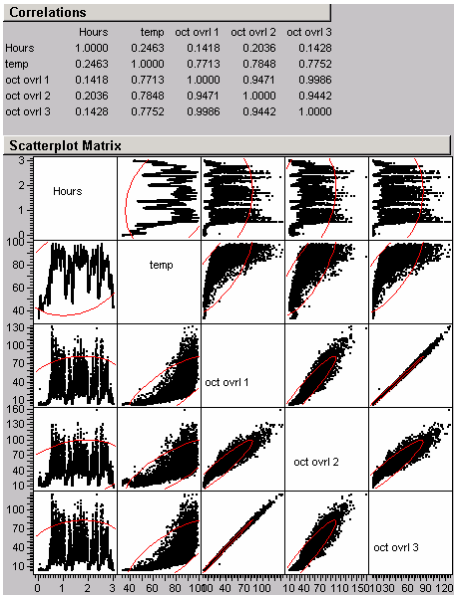

Figure 7. Flight 2 Correlations Between Temperature and Strains

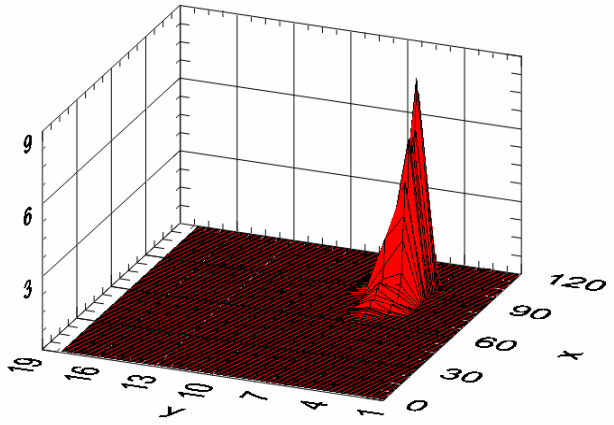

Figure 8. Normalized Cumulative Damage Plot for SG2 versus Frequency 1/3 Octave Band Number (Y) versus

Summary and Conclusions

The damage dosimeter is a tool to get quick response definition of thermal and dynamic strain frequencies on military and commercial aircraft. Time histories of temperature versus flight time and rms values of third octaves versus flight time were presented. The highest temperature for the 5 flights appears to be 104 °C. The lowest temperature appears to be on flight 1 where the C-130 was mostly cruising at altitude. When the flap position is 50% or greater, the temperature appears to decrease. Better flap position data for flights 4 and 5 would help to confirm this conclusion. SG2 appeared to have the highest strain levels. Most of the time the levels for SG2 were less than 140 με but there were several peaks close to 160με rms. There is high correlation between the rms values of SG1 and SG3 as expected since they are located next to each other. SG2 rms values are higher than SG1 and SG3. SG2 is located on the corner of the hat riser where the cracks usually

originate. The main conclusion is that the third octave rms data and temperature data can be used for structural estimation of damage versus frequency and temperature. This information is needed for design of damped composite repairs to slow and prevent high cycle fatigue cracks. After the C-130 returned from overseas missions, the NCANG flew more dosimeter measurement flights after application of a repair to ascertain the environmental changes and the effectiveness of the repair.

Acknowledgments

The authors thank David Smith of Integrity Design Engineering, Karl Anderson of Valid Measurements™ and Lyle Wells of Trig-Tek, Inc. in helping AFRL engineers to fully understand the damage dosimeter. Also, special thanks to Chief Master Sergeant Michael Bigger and Master Sergeant Tim Roberts of the 145th Air Wing (145AW/LG) at the NCANG Base, who supported AFRL efforts to collect data on the C-130. Captain Michael Myers managed the dosimeter delivery to completion on AFRL contract F33615-95-D-3203 and Mark Baker installed the strain gages and temperature sensors.

References

1. Anderson, K. F. (1995), "Practical Applications of Current Loop Signal Conditioning", Technical Memorandum: NASA-TM-4636, January, NASA Dryden Flight Research Facility, Edwards CA.
2. Bannantine, J.A., and Comer, J.J. and Handrock J. L. (1990), Fundamentals of Metal Fatigue Analysis. New Jersey: Prentice-Hall, Inc.
3. Banaszak, D. and Brown, D. (2003), "A Statistical Look at Damage Dosimeter Data from a Fighter Aircraft", ASA 2003 Proceedings of the Section on Physical and Engineering Sciences, San Francisco, CA 3-7 Aug 2003.
4. Banaszak, D., and Brown, D. (2003), "Challenges in Validating Strain Gage Flight Data from a Digital Damage Dosimeter", Institute of Environmental Sciences and Technology (IEST) 2003 Proceedings Design, Test, and Evaluation Product Reliability, ESTECH 2003 the 49th ATM, Phoenix, AZ, 18-21 May.
5. Banaszak, D. (2002), "End-to-End Mechanical Calibration of Strain Channels in Dynamic Health Monitoring Systems", Journal of the IEST Volume 45 2002 Annual Edition, pp 1134-120, Rolling Meadows, IL.
6. Banaszak, D., Brown, D.L. and Trego, A. (2002), "Damage Dosimeter Third Octave and RMS Time History Values", American Statistical Association 2002 Proceedings, Joint Statistical Meeting in NY, August, ASA, Alexandria, VA.
7. Banaszak, D., Brown, D.L. and Trego, A. (2002), "A Quick Look at Flight Data from a Digital Damage Dosimeter", ESTECH 2002 Proceedings, Apr 28-May 1, Anaheim, CA.
8. Bendat, J.S. and Piersol, Alan G. (2000), Random Data Analysis and Measurement Procedures, John Wiley & Sons, NY, page 14.
9. Himelblau, H., Piersol, A. G., Wise, J. H., and Grundwig, M. R. (1990), Handbook for Dynamic Data Acquisition and Analysis, Institute of Environment Sciences and Technology (IEST) Recommended Practice DTE012.1, 148-152, Mount Prospect, IL.
10. Ikegami, R., Haugse, E., Trego, A., Rogers, L, and Maly, J. (2001), Structural Technology and Analysis Program (STAP) Delivery Order Number: 004 Durability Patch, AFRL-VA-WP-TR-2001-3037, ADA408003, Air Force Research Laboratory, Wright Patterson AFB, OH.
11. Roach, Dennis P. (1998), "Bonded Composite Doublers for Commercial Aviation Use", *Aerospace Engineering*, pages 37-39, April.
12. Rogers, L., Banaszak, D., Laird, D., Brown, D. (2003), "Sonic Fatigue Damage Service Environment and Life Improvement From Dosimeter Data", ASIP 2003 Poster, Dec., Savannah, GA.
13. SAS® Institute Inc. (2000), JMP® Introductory Guide Version 4, Gary, NC.
14. Smith, D. and Searle, I. (1998), "Damage Dosimeter: A portable Battery Powered Data Acquisition Computer." Western Regional Strain Gage Committee Paper, Dave Smith and Ian Searle, February 1998. (http://www.vm-usa.com)

Section 3.7

Lab Evaluation of Fiber Optic EFPI Sensors for Extreme Environment Tests

Paper presented at JSM2005

JSM = Joint Statistical Meetings
Minneapolis MN
August 7-11, 2005

Lab Evaluation of Fiber Optic EFPI Sensors for Extreme Environment Tests

David Banaszak and Larry Kretz
Air Force Flight Research Laboratory
Air Vehicles Directorate

KEY WORDS: Fiber, Sensor, Strain, Measurement, Temperature, Correlation

Abstract

AFRL engineers are evaluating Extrinsic Fiber Fabry-Perot Interferometer (EFPI) sensors' ability to measure strain on structures experiencing both applied mechanical loads and temperatures up to 2000ºF (1093.3ºC), which cause conventional strain gages to fail. This extreme thermal environment is similar to that experienced by air vehicles during reentry and high performance aircraft structures exposed to hot engine exhaust. Through in-house experimentation, AFRL engineers are evaluating the control variables affecting EFPI output and uncertainty and investigating the EFPI's potential to replace conventional strain gages in high temperature tests. This paper presents the plans, efforts, and results for this investigation.

Introduction

EFPIs consist of a fiber reflector and an incoming fiber, which are threaded through a quartz tube and bonded to the test specimen using a high temperature adhesive or flame spray technique. The distance between the fiber attachment points on the test specimen is known as gage length (GL). The fibers within the tube are separated by a nominal gap of 50µm (1.97 mil). As the operator sends a light source down the incoming fiber, multiple light-waves reflect between the incoming and reflector fibers. The result is an interference pattern that can be used to measure the gap length (L), which varies between 30-80 µm (1.18-3.15 mil) as the test specimen expands or contracts due to stress and thermal loads. EFPI signal conditioner output is an analog voltage proportional to the strain ($\Delta L/GL$, where ΔL is the change in gap length). Strain is a unit-less quantity that is usually expressed in terms of microstrain, (i.e. microstrain = $\mu\varepsilon = (\Delta L/GL) \times 10^{-6}$). Yu and Yin (2000) provide explanations of interferometer measurement techniques. Beyond the basic theory, there are many variables involved. Some of these variables are the type of fiber material, installation techniques, and adhesives. Control variables include test type, specimen material, specimen shape or size, attachment techniques, fiber and strain gage location, specimen side, test temperature, maximum test strain, and atmosphere.

Shull and Wright (2002) discuss the use of conventional strain gages designed for dynamic strain measurements for extreme environments. Poland (2002) discusses fiber optic strain gage techniques and applications. Luna Innovations (2001) discussed the theory of commercial extensometer EFPI strain sensor operation. This commercial sensor operates at temperatures up to 350ºC (662ºF). However, extreme aerospace thermal environments often require operations at temperatures up to 2000ºF to 3000˚F (1093.3ºC to 1648.9ºC). Therefore, Piazza (2004), Moore (1997), Moore and Hart (2002), and Hart and Moore (2000) attempted to extend the temperature range of commercial EFPIs during numerous experiments at the National Aeronautics and Space Administration (NASA) Langley Research Center (LARC) and NASA Dryden Flight Research Center (DFRC). They manually fabricated EFPI extensometers using Luna-manufactured gold plated optical fibers with a Nextel jacket, quartz tubes, and new attachment techniques. For temperatures above 1800ºF (i.e. gold's melting point) Bhatia, V, Green, J., et. al. (1996) experimented with sapphire fibers. Bhatia, V., Greene, J., et. al. (2000) outlined the theory behind an EFPI extensometer and described the techniques and equations to determine the gap between the two fiber pieces. In addition, EFPI sensor manufactures, such as Luna, Blue Road, and Fiso, provided technical details

Building upon this work, AFRL engineers are examining EFPI sensors' potential to measure strain on aerospace structures at temperatures up to 2000ºF (1093.3ºC).

Preliminary Thermocouple Tests

A prerequisite for full EFPI evaluation is finding reliable methods of bonding the EFPI sensor to the test structure at high temperatures. During preliminary experiments in July 2004, AFRL engineers used the ceramic adhesive Zircon Potting Cement No. 13 (made by Sauereisen and known as Sauereisen 13) to bond several K-type thermocouples to Carbon-Carbon (CC) material flame sprayed with a base coat by Roth (2004). Next, they subjected the attachments to temperatures up to 2000ºF (1093.3ºC). The temperature profile increased to 2000ºF (1093.3ºC) in approximately 40,000 seconds (about 11.1 hours). Sauereisen 13 also successfully bonded approximately 40 thermocouples simultaneously to a CC test article during August 2004.

Overview of EFPI Strain Sensor Mounting and Installation Techniques

Engineers are exploring two methods of bonding EFPI sensors to test materials: flame spray techniques and high temperature adhesives. AFRL is still developing flame spray capabilities. Engineers are developing and installing an in-house flame spray capability facility, which is scheduled to be operational in September 2005. Meanwhile, they are experimenting with using ceramic adhesives, like Sauereisen 13, to attach the EFPI sensors.

For their initial attempts, AFRL engineers bonded EFPI sensors to Aluminum and CC using Sauereisen 13. Figures 1 and 2 shows the initial attempts to mount the EFPI sensors.

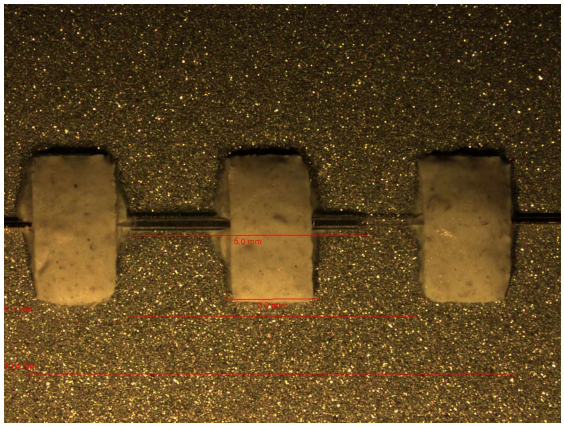

Figure 1: Sample Adhesive Mount of EFPI Sensor on Test Item 1 (Aluminum)

The sensor in Figure 1 is mounted directly to the aluminum. It was used only for practice at room temperature because the adhesive does not adhere to aluminum at higher temperatures. Engineers estimated GL by using the formula GL= (2*inner+outer)/3, where "inner" and "outer" are the inner and outer distances in millimeters (mm) of the end attachment bonds. Luna (2001) recommends this formula when bond widths at the end points are not an infinitesimal point. In Figure 2, the GL = (2*6.5+10.0)/3 = 23/3 = 7.67 mm (.302 inches), where the inner distance is 6.5 mm (.256 inches), and the outer distance is 10.0 mm (.394 inches).

AFRL Test Requirements and Past Results

Engineers expect temperatures exceeding 1832ºF (1000ºC) on structures experiencing extreme thermal environments and high vibratory strain and loads. For example, a conventional foil strain gage will be incinerated when heated to 1600ºF (871.1ºC). A conventional foil strain gage is limited to 550ºF (287.8ºC) continuous, 700ºF (371.1ºC) for short term such as seconds. Figure 3 illustrates the output of a high temperature free filament strain gages. The data presented shows the output of each leg of the strain gage, active and compensating as well as the combined results. Note, the extremely large output of the active gage, and yet when combined with the compensating gage, there is

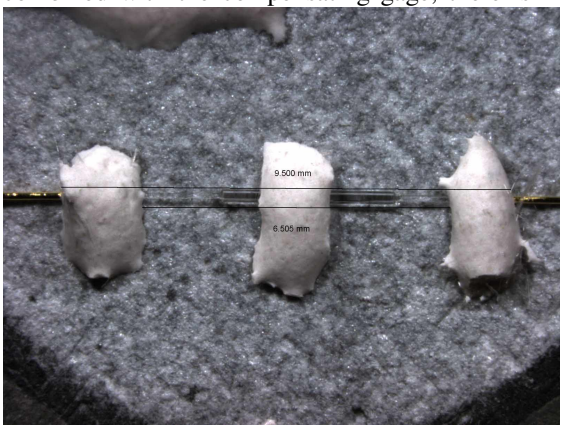

Figure 2: Sample Adhesive Mount of EFPI Sensor on Test Item 4 (CC) Fiber 3

still significant apparent strain signal that has to be corrected. High temperature, free filament gages can be heated and corrected to 1600ºF (871.1ºC), however as illustrated in figure 3, a practical valid strain measurement for compensated gages should be limited to 1250ºF (676.7ºC). Apparent strain is expressed as $\Delta R/R$

and is converted to strain by using the appropriate strain gage factor (GF) used for conventional resistance gages.

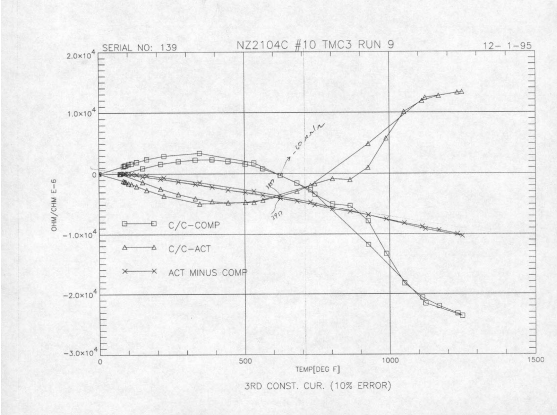

Figure 3: Apparent Strain Results using Conventional Strain Gages (1 Dec 95)

Lab Test Measurement System

The quick response measurement system in these tests used a personal computer USB data acquisition board, designed by AFRL personnel, that measured outputs from the fiber optic signal conditioners, strain gage conditioners, and thermocouples in a timely manner. AFRL engineers acquired the test data using a read data virtual instrument (VI), which sampled each channel 10 times per second. They then used a VI titled "overlayer" to create an ASCII and Microsoft® Excel readable file. Finally, they imported all the data into an Excel workbook to generate time history and apparent strain plots. Engineers did not use anti-aliasing filters; however, these filters are highly recommended for a sampling based data acquisition system. For the oven portion of this test, engineers used a VAX based data acquisition system to record data from the thermocouples and strain sensor signal conditioners once per second.

Preliminary Design of Experiments (DOE)

Engineers needed experiments that validated the correlation between conventional strain gages and EFPI sensors at room temperature, high temperatures, and under in-plane and out-of-plane mechanical loading (bending). A Design of Experiments (DOE) was the ideal solution because many control variables were required to account for all possible strain output signal variations. Ideally, engineers should use a checklist like the one recommended by Dean and Voss (1999) to determine objectives, sources of variation, rules for assigning experimental units to treatments, measurements to be made, experimental procedure, pilot experiments, a statistical model, type of analysis, and other important experimental considerations. When evaluating EFPI sensors for high temperature strain measurements, determining which control variables and response variables to measure was a challenge. Experimental outputs for this paper included strain correlation and apparent strain measurements on Test Item 1 (a rectangular piece of Aluminum 2024 measuring 1.5 inches by 8.25 inches (38.1mm by 209.6mm)), Test Item 2 (a rectangular piece of CC-1 measuring 1.25 inches by 4 inches (31.8mm by 101.4mm)), and Test Item 4 (a round piece of CC 69.8mm in diameter) in a large test matrix. The experiments run to date are considered pilot experiments in an attempt to complete this test matrix with different test types, materials, sizes, attachments, locations, ages, atmospheric environments, oven types, temperatures, and strains.

1. Correlation between EFPI and Strain Gages at Room Temperature

Engineers correlated EFPI sensors and standard strain gages using bending and axial loading at room temperature. AFRL technicians took this opportunity to practice mounting EFPI sensors and foil strain gages on known materials, such as aluminum, steel, and CC with a flame sprayed base coat. Piazza (2004) provided AFRL the NASA-DFRC recommended installation instructions for flame spraying EFPI sensors onto test items. In the fiber optic laboratory, engineers measured the strain outputs for bending loads to determine the strain correlation.

2. Apparent Strain Curves

AFRL engineers conducted limited testing to measure apparent strain curves up to 1600°F (871.1°C) for fiber optic EFPI sensors attached to sample CC materials with a flamed sprayed base coat provided by NASA-LARC. Figure 4 shows the layout for the sensors on Test Item 2 (CC rectangular coupon), where there are two EFPI Sensors(Fn-42 and Fn-37) and one thermocouple (TC) mounted with Sauereisen 13 and a convention strain gage mounted using M-Bond 600 adhesive. To measure apparent strain, engineers heated these specimens but did not

strain them in two types of heat tests. First, they clamped the test specimen to the laboratory bench and heated it to about 500ºF (260ºC) using a heat gun. Next, they placed it in an oven for measuring apparent strain curves at temperatures up to 2000°F (1093.3ºC). Engineers purged the chamber with nitrogen to prevent subjecting the test article to an oxidizing environment, which would have destroyed it at temperatures above 800°F (426.7ºC).

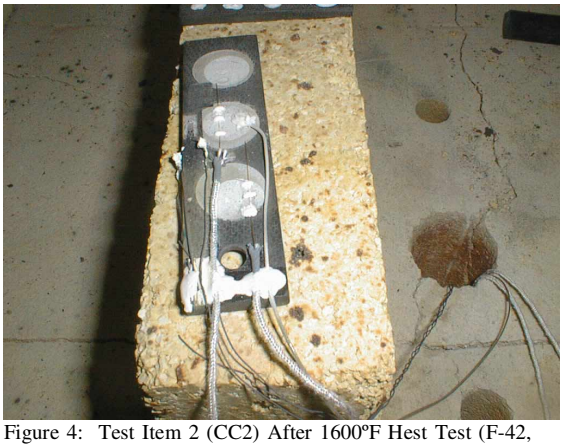

Figure 4: Test Item 2 (CC2) After 1600ºF Hest Test (F-42, TC, SG-Center & F-37-Hole) (7Jan05)

3. Combined Strain Correlation and Apparent Strain at High Temperatures

AFRL is currently building a combined temperature and mechanical loading test chamber, which will enable correlation between the EFPI sensor and strain gages at low, medium and high temperatures. It will be capable of subjecting specimens to 2100°F (1148.9ºC) and 1000 με of in-plane or out-of-plane loading. The chamber will have nitrogen purge capabilities and attain a set temperature in less than 1 hour, which will simulate thermal transient environments. The chamber will enclose a high temperature quartz lamp bank.

Test Results to Date on CC and Aluminum

1. Test Item 1 Laboratory Bending and Heat Tests

Using the layout shown in Figure 5, engineers conducted several quick look tests at room temperature. For the simple bending test, they achieved approximately equal bending strain on both the strain gage and EFPI sensors by clamping the aluminum beam to a laboratory work bench. As the beam was bent to stimulate tension and compression, engineers compared the strain gage and EFPI sensor outputs. These values were slightly different. After small corrections for Test Item 2's GL, the EPFI sensor and strain gage outputs correlated at room temperature.

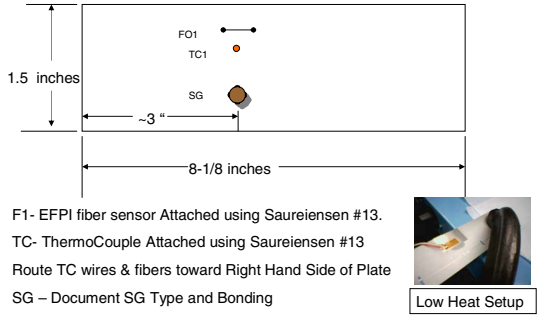

Figure 5: Test Item 1(2024-T3 Al) Layout

This correlation was similar to the results for more extensive experiments conducted by Hare and Moore (2000). The correction most likely involved gage length measurement uncertainty since the bond area is not infinitesimal small.

Engineers heated the aluminum specimens to approximately 500˚F using a heat gun. As predicted by the adhesive manufacture, the ceramic Sauereisen 13 adhesive detached from the aluminum during heating.

2. Test Item 2(CC) Laboratory Bending, Heat Gun and Oven Heat Tests.

Test Item 2 was a rectangular piece of CC material designed to withstand temperatures up to 2000ºF (1093.3ºC). Figure 4 shows the sensors on Test Item 2. The circular spots on the CC were flame sprayed by Roth (2004) so that ceramic adhesives would bond to Test Item 2 at high temperatures. As shown in the figure, engineers used Sauereisen 13 to install an EFPI sensor (F-37) on the flame spray spot near the hole and an EFPI fiber sensor (F-42) and thermocouple (TC) on the center spot. They then mounted a conventional strain gage (SG) along side the flame sprayed spot using M-Bond 610 adhesive for comparison at temperatures up to 500ºF (260ºC).

F-42 was reattached following the initial bending test and the first heat gun test because the reflector end of F42 detached. Unfortunately, GL was not re-measured following this adjustment, so engineers used the nominal value,

GL=10.0, for F42 for later tests. For F37, the gage length was 8.921. The GL for F42 was 9.824 mm before it was reattached.

First, engineers clamped the beam to a laboratory work bench to form a cantilever beam that could be bent manually to induce tension and compression of roughly equal magnitudes into each of the strain sensors. Figure 6 shows the outputs for fiber ID Fn-42 and the strain gage in the center of the beam and fiber ID Fn-37 located at the end of the beam. Although fiber Fn-42 and the strain gage output appear to be correlated, they have significant different readings.

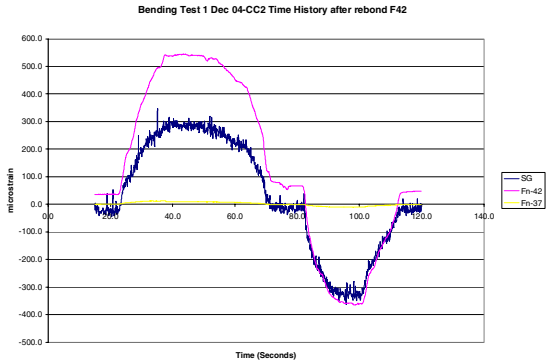

Figure 6: Test Item 2 (CC) Lab Bending Fiber F-42 and Strain Gage - no Correction (1 Dec 04)

The plot of the output of fiber Fn-42 versus the strain gage in Figure 7 confirms this high

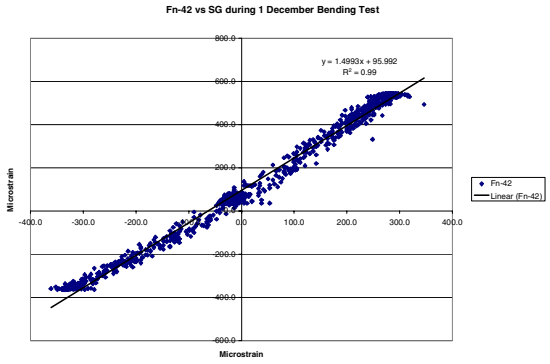

Figure 7: Test Item 2 (CC) Lab Bending fiber F42 versus Strain Gage (1 Dec 04)

correlation. Using regression for the best fit straight line (BFSL), engineers obtained the equation (y=1.4993x+95.962 with a correlation R^2 = .99) relating the fiber output to the strain gage output. Ideally, the BFSL readings for the strain gage and EFPI sensor should be equal. Thus, we can correct the fiber output by dividing GL by the slope (1.4993) of the BFSL shown in Figure 7.

Figure 8 shows the original fiber Fn-42 output, strain gage output, and corrected fiber Fn-42. The correction resulted in much closer agreement, even without applying the offset term. This same technique worked well for the bending tests on Test Item 1. Note that the output of fiber F-37 near the end of the beam was much lower; engineers expected this result because fiber F-37 was further away from the clamped edge of the beam at the flame spayed circle farthest from the hole.

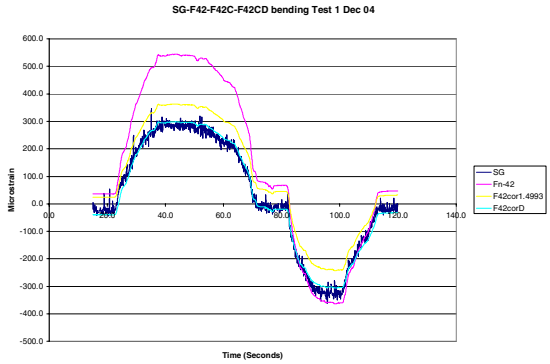

Figure 8: Test Item 2 (CC) Lab Bending fiber F-42 (Corrected) and Strain Gage (1 Dec 04)

Next, engineers heated Test Item 2 up to approximately 500ºF (260ºC) using a heat gun. The apparent strain curve in Figure 9, shows a plot of the EFPI sensors F42 and F37 and Strain Gage versus temperature. F42 did not return exactly to zero microstrain, and F37 had very small response. Also, the standard strain gage had a noisy signal. These mixed results caused AFRL engineers to continue to heat the specimen in an oven to search for new insights.

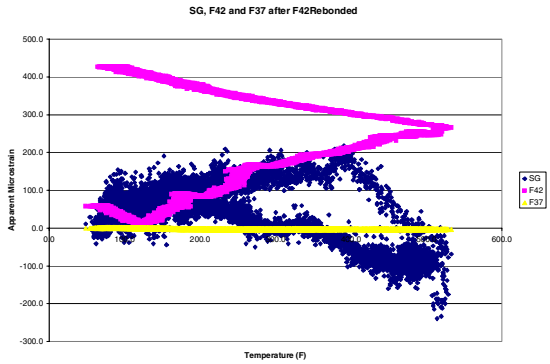

Figure 9: Test Item 2 (CC2) after Heat Gun Test to 500ºF Dec 1 05(F42, TC, SG-Center&F37 Hole)

First, AFRL engineers conducted oven tests using thermal profiles with a maximum of 500ºF (260ºC) and 600ºF (315.6ºC) before proceeding to the profile with a maximum temperature of 1600ºF (871.1ºC). Figure 4 shows Test Item 2 after it was heated to 1600ºF (871.1ºC). Successful completion of this test required over 40 hours, a much longer time than originally planned. Engineers set the oven controller for a half hour ramp and a two hour soak at 1600ºF (871.1ºC). However, the actual ramp time was about four hours; the soak time was two hours, and the cool down time was almost 40 hours. At 24 hours, engineers opened the oven door to decrease cool down time. Figure 10 shows the result of plotting apparent strain versus temperature for fiber F42, and Figure 11 shows the result of plotting apparent strain versus temperature for fiber F37. Note that fiber 42 has large step changes in jumps and that fiber 37 has much lower apparent strain reading. The conventional strain gage output started to fail at about 800ºF (426.7ºC).

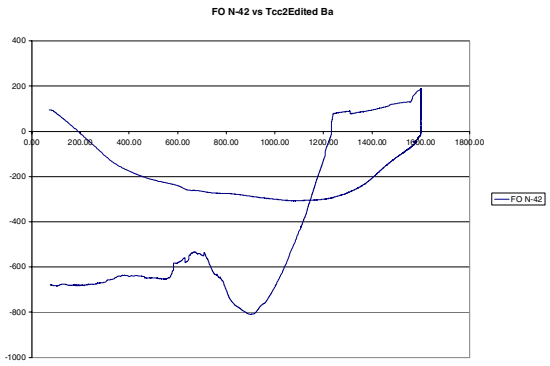

Figure 10: Test Item 2 (CC2) F42 versus Temperature for 2 hour soak at 1600F (5 Jan 05)

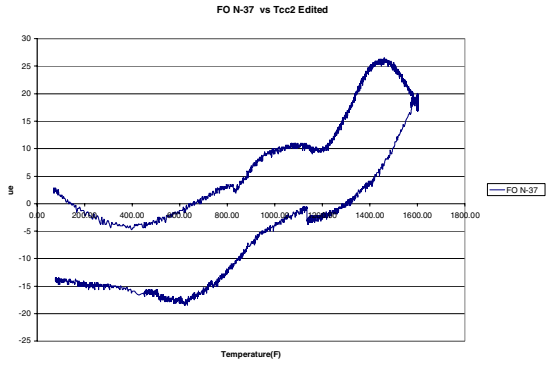

Figure 11: Test Item 2 (CC2) F37 versus Temperature for 2 hour soak at 1600F (5 Jan 05)

3. Test Item 4 (Round CC) Laboratory Bending and Heat Gun Tests

The following preliminary data are from laboratory testing of Test Item 4, shown in Figure 12. Test Item 4 was a round coated CC coupon with a strain gage and commercial EFPI strain sensor (Serial number K010125), both mounted with M-Bond 610 adhesive. Engineers mounted three additional EFPI sensors (F3 for serial number F52, F2 for serial number F47, and F1--a sensor with no serial number), and a thermocouple with Sauereisen 13.

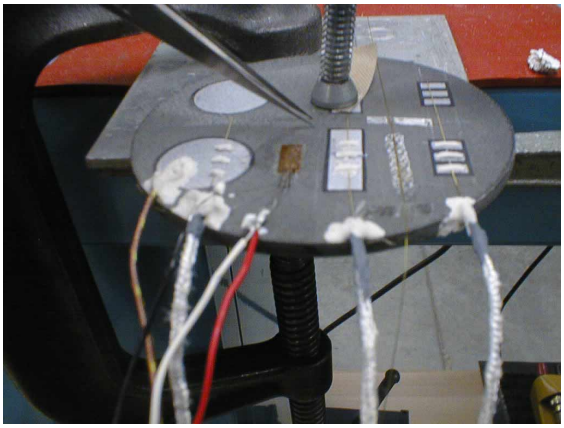

Figure 12: Test Item 4 Laboratory -Bending & Heat Gun Test (Sensors: L-R) (3 Feb 05)
TC, F3-52, SG, F2-47, COTS-K01025, F1-No ID

Figure 13 shows apparent strain for temperatures up to 450ºF using the heat gun. For EFPI sensor F3, the optical signal conditioning displayed "CHECK SENSOR," and optical tests indicate that the connector most likely failed. As expected, he round specimen did not produce equal strain during the bending test. A point load was applied to the end of the round test item 4 to generate a bending load. This was only applied to generate some output from each of the strain gages. To analyze the exact strain field would be extremely difficult plus note that in figure 12, there was a single point reaction by the C-clamp which further complicates the strain field. The apparent strain showed the commercial sensor did not return to zero after heat gun removal. The large shift in commercial EFPI strain sensor (K01025) may have indicated improper curing time for the M-Bond 610 adhesive. A post inspection of this sensor showed it became unbonded at one end. EFPI fiber F1 and F2 show similar apparent strain characteristics with apparent strains less than 120 με at temperatures up to 440ºF (226.7ºC). F2 had a much lower response than F1. The zero

shifts for F2 and F3 began after bending test completion. Additional evaluations are needed to determine the validity of these results. The next step will be to quickly heat Test Item 4 to temperatures as high as 2000ºF (1093.3ºC) in AFRL's future high temperature chamber.

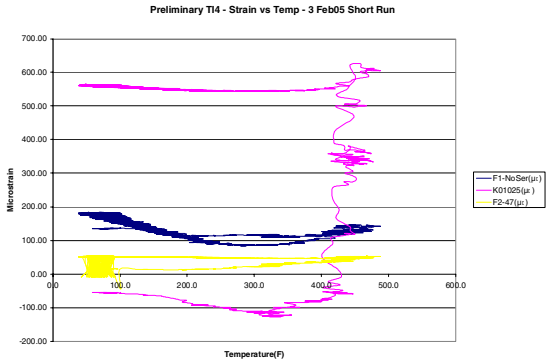

Figure 13: Test Item 4 Apparent Strain versus Temperature during Heat Gun Test (3 Feb 05)

Conclusions

In limited testing to date, the EFPI sensors successfully operated throughout a thermal heating cycle up to 1600ºF (871.1ºC). However, a number of questions about apparent strain and correlation between EFPI sensors and conventional gages require resolution.

Room temperature test comparisons between the EFPI sensor and conventional strain cage indicated that in order to achieve good correlation, the gage length (GL) requires correction in a manner similar to that shown by Hare and Moore (2000).

Figure 14: Future Tests Will Use Flame Spray Attachment Technique

As predicted by its manufacturer, Sauereisen 13 adhesive did not bond well to a heated Aluminum specimen. However, further evaluation is needed to understand the physics involved with using Sauereisen 13 adhesive with the CC specimens. AFRL plans to conduct more evaluations by attaching EFPI sensors using the flame spray techniques shown in Figure 14.

A very large number of control variables are involved. Preliminary control factors should be expanded and reviewed to include additional control variables of interest. Because this type of testing is slow and tedious, efficiency is very important. An EFPI sensor test matrix will be expanded as new material test requirements evolve.

AFRL engineers are determined to find a method to measure strain on aerospace structures at temperatures up to 2000ºF (1093.3ºC). They are confident that the EFPI fiber strain sensors will successfully take strain measurements in extreme thermal environments where many previous sensors failed. Preliminary experiments with mounting sensors using ceramic adhesives are not conclusive. The sensors appear to survive and give outputs at temperatures up to 1600ºF (871.1ºC) whereas conventional strain gages incinerate at temperatures exceeding 700ºF (371.1ºC). AFRL engineers assume that attaching the sensors by using flame spray or plasma spray techniques pioneered by NASA-LARC and NASA-DFRC will enable accurate apparent strain curves. However, this effort will require additional practice and experimental iteration.

In addition to developing a flame spray capability, AFRL is developing an oven to evaluate high temperature strain measurement techniques in a timely and realistic manner. The oven will heat a test specimen to 2000ºF (1093.3ºC) is less than a half hour and cool the specimen down in less than a half hour. Currently, the heat gun can raise the specimen to about 500ºF (260ºC) in a couple of minutes, and then, the air cools the specimen quite rapidly.

Acknowledgements

The authors thank the personnel at NASA-LARC (Trent Kite, Tom Moore, Mark Roth, and David Hare) and at NASA-DFRC (Anthony Piazza) for their help during numerous conversations regarding the use of EFPI fiber optic sensors. In

addition, Trevor Rice and Larry Vicari at Luna Innovations were very helpful in initiating AFRL personnel to EFPI sensor technology in high temperature environments. Most importantly, many AFRL structural test facility experts provided an abundance of labor and helpful advice. They include Ken Leger, Ray Fisher and Mathew Leonard of the experimental validation branch; Roderick Moore, Mark Clapper, Mike Marando, Dale Gerken, Paul Brown and Jim Taylor, the on-site contractors from SelectTech Inc.; and Gerry Ewing and Ken Koverman of AdTech. Most importantly, special thanks are extended to Melissa Withrow for providing technical editing expertise.

References

Bhatia,V., Murphy, K.A., May, R.G.,Claus,R.O.,Tran,T.A.,Greene,J.A. and Coate, J.E. (1996), "High Temperature Sapphire Optical Fiber Interferometric Strain Sensor", High Temperature and Materials Science, Vol.35, pp 31-41, Humana Press Inc., Totowa, NJ.

Dean, A.and Voss, D. (1999), Design and Analysis of Experiments,Springer-Verlag, NY,NY.

Hare, D.A. and Moore, T.C., (2000), Characteristics of Extrinsic Fabry-Perot Interferometric (EFPI) Fiber-Optic Strain Gages, NASA/TP-2000-210639, December, Langley Research Center, Hampton, VA.

Luna Innovations, (2001), Application Notes "Extensometer EFPI Strain Gages", Blacksburg, VA.

Moore, T.C., (1997) Recommended Strain Gage Application Procedures for Various Langley Research Center Balances and Test Articles', NASA Technical Memorandum 110327, March, NASA Langley Research Center.

Moore, T.C. and Hart, D.A., (2002) "Performance Evaluation of Commercially Available High-Temperature Fiber-Optic Extensometer on Inconel 100 Test Beams at Elevated Temperatures" Western Regional Strain Gage Committee-2002 Winter Meetings, Society Experimental Mechanics, Bethel, CT.

Poland, Steve (2002), "Luna Fiber Optic Strain Gages and their Applications" Western Regional Strain Gage Committee-2002 Winter Meetings, Society Experimental Mechanics, Bethel, CT.

Piazza, Anthony, (2004), Conversions, NASA-Dryden Flight Research Center, CA.

Roth, Mark, (2004), Conversions, Modern Machines & Tool Co., Inc., Newport News, VA.

Shull, L.C. and Wright, C.P., (2002) "Strain Gages for Extreme Temperatures", Experimental Techniques, January/February, pp39-41.

Yu, Francis T. and Yin Scizhue Editors (2002), Fiber Optic Sensors, Marcel Dekker, inc., New York.

Section 3.8

Autonomous Environmental Definition of C-130 Flap Well Skin Panel After Constraint Layer Damping Repair

ESTECH 2006 Paper

ESTECH = Engineering Science and Technology
Annual meeting of the Institute of Environmental Sciences and Technology (IEST)
Phoenix, AZ
May 8, 2006

(NOTE: In the digital version of this report, see original PowerPoint attachment, ESTECH2006.ppt)

Autonomous Environmental Definition of C-130 Flap Well Skin Panel After Constraint Layer Damping Repair

Air Force Research Laboratory
Air Vehicles Directorate-Structures Division
Wright Patterson AFB, OH
David.Banaszak@wpafb.af.mil
Damping Technology, Inc. - Mishawaka, IN
Michael L. Parin mikep@damping.com

Monday-May 8, 2006

This is the opening title chart. Co-author Mike Parin's help and support is very much appreciated.

Talk Overview

- Recent References
  - ESTECH04 and IEST Journal Vol. 48. No. 1
  - June 2005 Issue of AFRL Technology Horizons
- Instrumentation Location and Installation
- No Repair Flight Data - June 2003
- Constrained Layer Damping Repair - October 2003
- Repair Flight Data - October 2003
- Repair Removed - April 2004
- Conclusions

Abstract

Air Force C-130 aircraft require numerous aluminum doubler repairs on the wing flap skin aft of the right hand outboard engine. These repairs are costly and require riveting. Rivets often provide new areas of stress concentration causing new cracks to develop elsewhere. AFRL measured the thermal and strain environment behind the right hand outboard engine of a North Carolina Air National Guard (NCANG) operational C-130 aircraft (TN 93-1456) before and after installation of a constrained layer damping (CLD) repair to prevent the growth of cracks in skin under the wing flap panel. During June 2003, AFRL engineers and technicians acquired data using an autonomous damage dosimeter during 5 operational flights without a repair installed. After the June Flights, Damping Technologies, Inc. installed a CLD repair to see if the vibration levels could be lowered. During October 2003, the C-130 flew 7 more flights with a CLD repair installed. When possible, pilots logged the altitude, indicated airspeed, engine speed and flap positions for the flights. A Boeing-designed damage dosimeter measured structural strains and temperatures on the C-130 to help diagnose the difficult-to-analyze structural environment on the wing flap skin such as acoustics and high-cycle fatigue. Data from the June 2003 flights were presented at ESTECH 2004 and presented flap position settings compared with dosimeter temperature and root mean square (rms) strain measurements. This paper will review data from no repair flights during June 2003 and present data for the seven flights with the repair installed during October 2003.

Background
Cracks in Secondary Structures & Repairs

- Cause of Cracks
  - Acoustic High Cycle Fatigue
  - Vibratory High Cycle Fatigue
  - Where High Cycle Fatigue > 10^6 Cycles
  - i.e. Resonant Vibration Out-of-Plane Excitation
- Costly to Inspect and Repair
- Repair Patch Design Requires
  - Vibratory Frequencies
  - Temperature

Turbulent airflow from the prop-wash causes high cycle fatigue in this region. This damage results in costly inspection and repair. Current repair is accomplished by riveting aluminum doubler plates, but the structure continues to respond in a resonant fashion and new cracks form due to stress intensities at the new fastener locations. A better solution is applying a specifically designed damped bonded repair patch. Design of composite durability repair patches require environmental information characterizing temperature, resonant response frequency and strain levels.

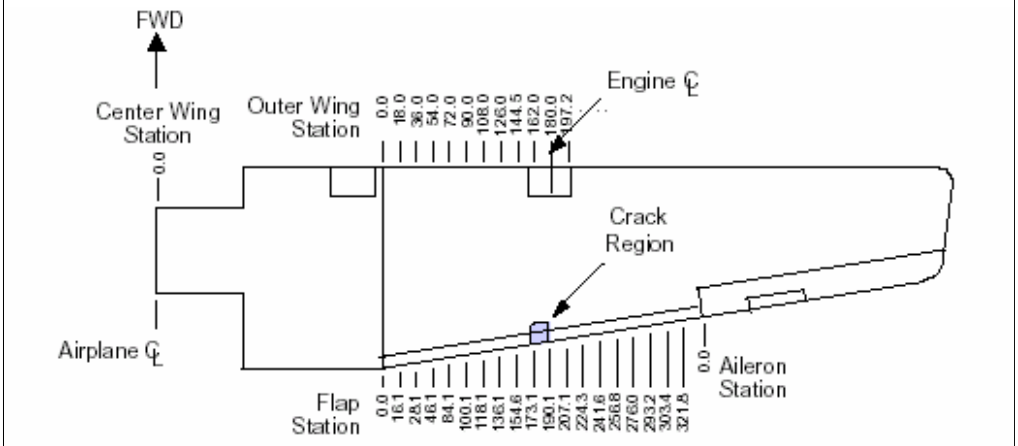

Figure 65. Cracking Region on C-130 Flap Well Skin Panel

The crack location on C-130 secondary structure is shown in this chart. AFRL finds this information by measuring the structure's operating environment with a compact, stand-alone, electronic device called a damage dosimeter. AFRL conducted five data-gathering flights with the dosimeter on the C-130 without a repair during June 2003 and seven more flights with a repair applied during October 2003.

Background

Cracks in Secondary Structures & Repairs

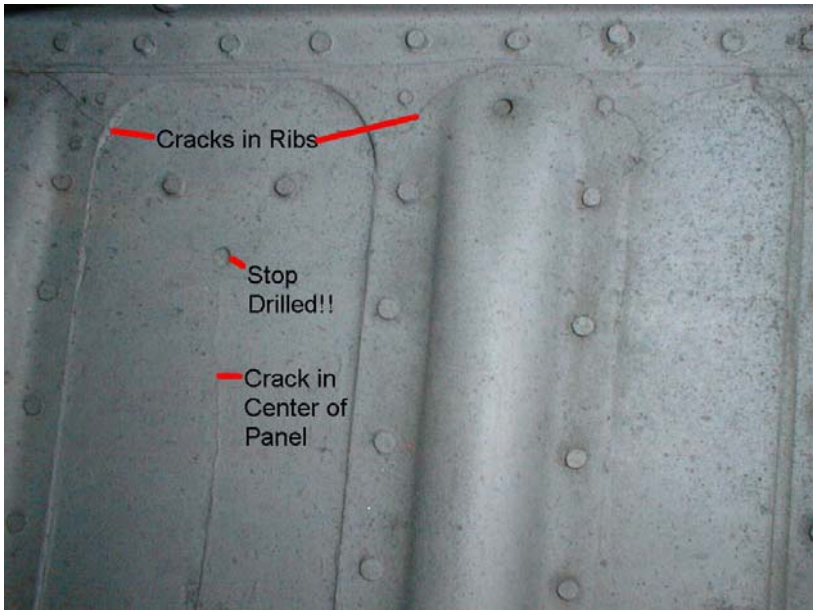

Typical secondary aircraft structural crack damage on a C-130 resulting from a high cycle fatigue (HCF) environment of greater than 10^6 cycles is shown in this chart. The chart shows the inside of the flap well skin panel. A stop drilled hole din not arrest crack growth. Cracks in the hat riser (ribs) are where the initial cracks occur.

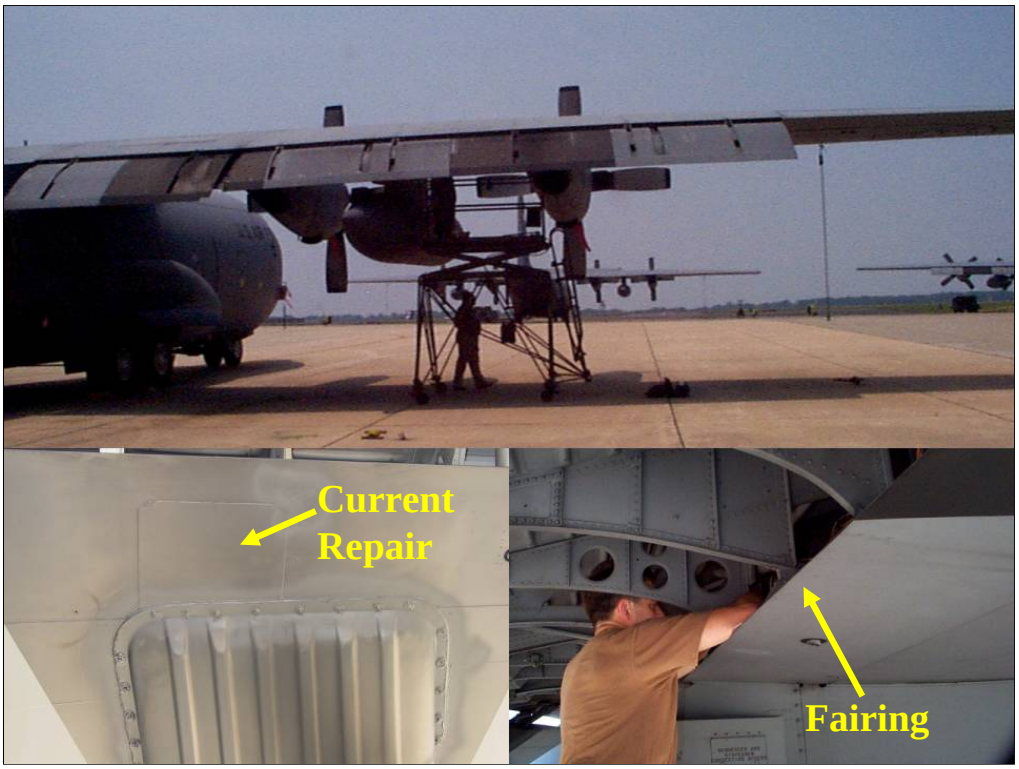

The Boeing Company designed the damage dosimeter to measure structural strains and temperatures on in-service aircraft. The dosimeter, strain gages and temperature sensor are installed in the C-130 wing flap well behind the outboard engine in the area in the photo where the technician is working over the fairing. Current repairs consists of aluminum doublers.

Dosimeter Operation

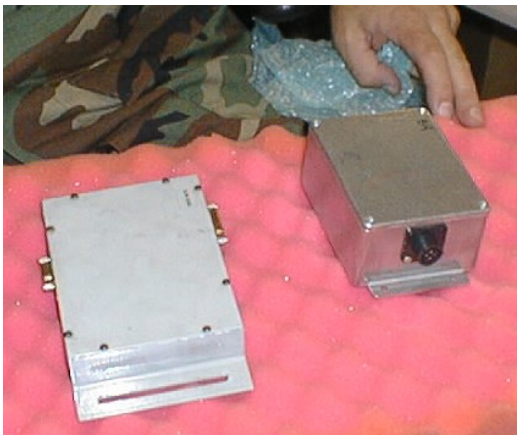

Data Collection
Autonomous or Continuous
Battery Powered & Light Weight
1 Temperature & 3 Dynamic Strains
Uses Anderson Current Loop (ACL)
Programmable
4 Megabyte Non-volatile memory
ADC = Analog to Digital Converter
DSP = Digital Signal Processor
Records Third Octaves(18 Bands)

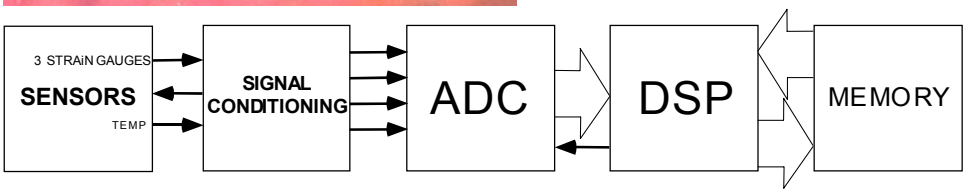

The damage dosimeter features include autonomous threshold operation or continuous operation, on-board Fast Fourier Transform (FFT) computation and storage of third octave frequency spectra. That is, the dosimeter can record third octave data continuously or be programmed to autonomously record data when a strain threshold is exceeded.

The dosimeter is a rugged, small (fits in palm of hand), battery powered, lightweight (weighs less than 1.5 lb. (.69kg) without battery), data acquisition system that measures 3 channels of strain at rates of 7600 samples per second and a single channel of temperature at a rate of 1.3 samples per second.

Data Collection, Processing & Recording

- First Time Threshold Calculation
  Determine Background Noise for Setting RMS Threshold
- Data Collection
  While off- power up every 99 seconds to determine current activity
  Temperature-1.3 Samples/Second
  Acquire Data for 2048 samples at 7600 samples/second(about .27 seconds)
  Process data for rest of next second.
- Data Processing
  Compute FFT, Peak Value and Third Octave
- Threshold Comparison
  Process Data above RMS Threshold
- Data Recording
  Store first 42 Time Histories and up to 29,544 Third Octaves

The autonomous dosimeter is programmed to only acquire data above a rms strain threshold. The strain data for each of the three gages is processed through a Fast Fourier Transform (FFT) analyzer to generate a Power Spectral Density (PSD). The PSD is then converted to 18 third octave frequency bands. The dosimeter is programmed to store 42 records of time history data each 0.3 seconds long and records and stores third octave records until its 4-Megabyte memory is filled.

Techniques to perform system and physical (mechanical) end-to-end calibration of bonded strain gages include inserting shunt calibration resistors in line for a system calibration and exciting the strain gages with a remote control structural exciter for a physical end-to-end calibration in accordance with the Institute of Environmental Science and Technology (IEST) Recommended Practices.

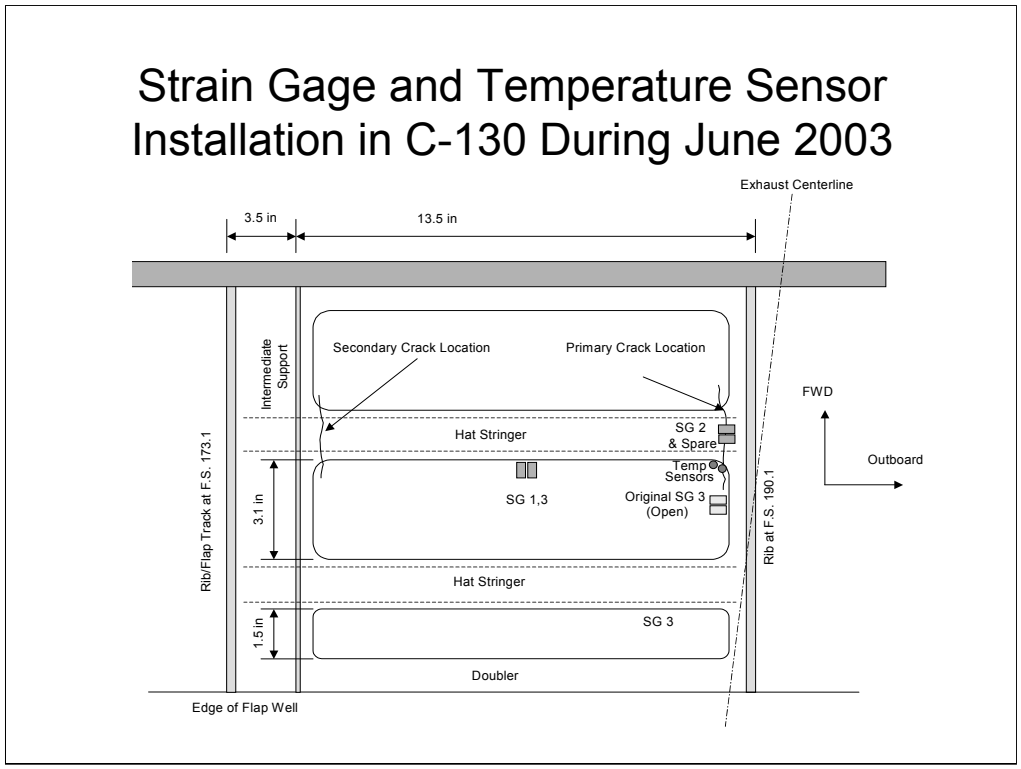

The dosimeter was located in the wing flap well between wing station 100.1 and 118.1 and the strain gages and temperature sensor were located between F.S. 173.1 and F.S. 190.1. During June 2003, AFRL engineers and technicians and North Carolina Air National Guard (NCANG) personnel installed strain gages and temperature sensors as shown in the chart.

Strain Gage and Temperature Sensor Installation in C-130 During June 2003

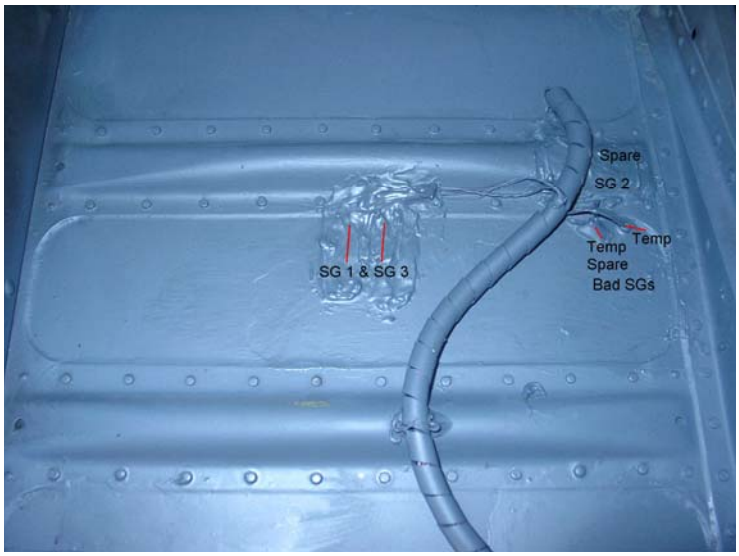

An AFRL engineer and technician installed the strain gages and temperature sensor as shown in the chart. First they removed old RTV with Dow Corning OS-2 solvent and phenolic scrapers. The temperature sensor is located near the hat riser. AFRL installed 6 Measurement Group type WK-13-250BG-250 Option W strain gages using M-Bond 600. The gages were covered with Teflon tape then coated with M Coat J since temperature expectations were about 100 degrees Centigrade (°C). They also installed 2 Analog Devices two -terminal IC AD590 temperature transducers. Spare gages and temperature transducers were installed as shown. After bonding of the transducer and cable routing, the installers found the two gages on the right side were bad. For the final configuration, strain gage 2 is located on the hat riser and strain gage 1 and 3 are adjacent to each other at the center of the panel.

Flights Flown during June 2003

- Five Flights Flown
- Repair Scheduled for Oct 2003
- Flight 1 – Local – Not as many Flap Changes
  - Flight 1 – Had to delete mid flight spikes during data analysis
- Flight 2-5 Multiple Flap Changes
  - Flap Changes only noted on Flights 2 & 3
- SG Shunt Cal before flight when possible

During the period of June 10-12, 2003, AFRL assisted NCANG personnel in acquiring dosimeter data from 5 flights. The C-130 was now ready for installation of the repair, but since the NCANG unit was being deployed, the constrained layer-damping (CLD) repair by Damping Technologies, Inc. was postponed until October 2003. After repair installation, more dosimeter data flights were flown during October 2003.

Table 1. C-130 Flights Flown June 2003

Table 1. C-130 Flights Flown June 2003

Flight	Date	Type	Description	Hours	DosSN	Record#
1-1A	June 10 2003	Local	NCANG to WR-ALC	0.90	1	499-5529
1-1B	June 10 2003	Local	WR-ALC to NCANG	0.92	1	5834-10651
2	June 11 2003	TAC	Air Drops at POPE	3.01	3	1-8286
None	June 11 2003	Ground	Ground Engine Run	0.49	3	8287-9636
3	June 11 2003	Local-Asslt	Multiple Landings	2.35	3	9641-16126
4	June 12 2003	TAC	Air Drops	1.79	3	15-4651
5	June 12 2003	TAC	Air Drops	2.64	3	4652-11808

NCANG personnel flew five flights where dosimeter data were acquired as shown in Table I. The flight crew completed flight logs containing flight activity, time, flap setting, altitude, engine 4 total inlet temperature, knots indicated airspeed and indicated engine revolutions per minute. Flight 1, designated a local flight by NCANG personnel, consisted of the C-130 flying to Warner Robbins AFB (1A), unloading cargo and then returning to the NCANG base (1B). Dosimeter clock, temperature and strain data were erratic during the end of flight 1A and beginning of flight 1B and much of the downloaded data had to be edited by hand. Two possible explanations are that either the dosimeter went erratic at higher altitude or there is some problem with dosimeter serial number 1 (SN1). On all five flights the dosimeter powered on at engine run up and powered down after engine shutdown after landing, thus successfully implementing the autonomous threshold mode of operation. Flights 2 through 5 consisted mostly of cargo drops and hence flap position was changed a number of times during these flights. On only the flight logs for flight 2 and 3 were the crew able to document the flap positions during the flight. Data on flights 2-5 used dosimeter SN 3 as noted in Table 1. When possible, the engineer preformed a strain gage shunt calibration before the flight.

Dosimeter Viewer Examples
Reference *Journal of IEST* Vol. 48 No. 1

- Developed Using LabVIEW™ VIs
- Third Octave & Time History Main Quick Look
  - Shows Temperature, Date, Time History Peak Strain and RMS values in 18 third octave bands
- Can Select Record Numbers Quickly
- Stores selected records in Spreadsheet File
- Peaks in Third Octaves Correlate with Engine Frequency at Engine Start Up
- View Autocorrelation, PDF,Frequency Spectrum or Rain Flow

AFRL is continuously improving the software to meet various user needs. The dosimeter stores two types of records, time history (TH) and third octave (SDR). AFRL developed software to provides engineers with the capability to quickly look at downloaded binary dosimeter data in the laboratory or in the field. The VI shows the desired TH or SDR records and allows the user to create spreadsheet files. Enhancements by Dansen Brown to the LabView Vis were reported at ESTECH 2004. Displays include the temperature, month, day, minute, hours, seconds, time history peak strains, and third octave bands as recorded in the dosimeter memory. Also shown is the record number, third octave overall rms, and the time history for the first 42 records and computed values of mean, rms and standard deviations computed from the displayed time history.

From the 5 flights, SG2 saw the most activity and that third octaves shows a cyclic component is equivalent to 146.5 to 228.2 hertz. The time history for SG2 shows a cyclic component with a period of about of 180 hertz. From the pilots log, the engines speed is 72.5% at engine startup for a frequency of 230.33 Hz x .725 = 166.98 hertz. It seems reasonable that engine cyclic frequency is measured as vibration.

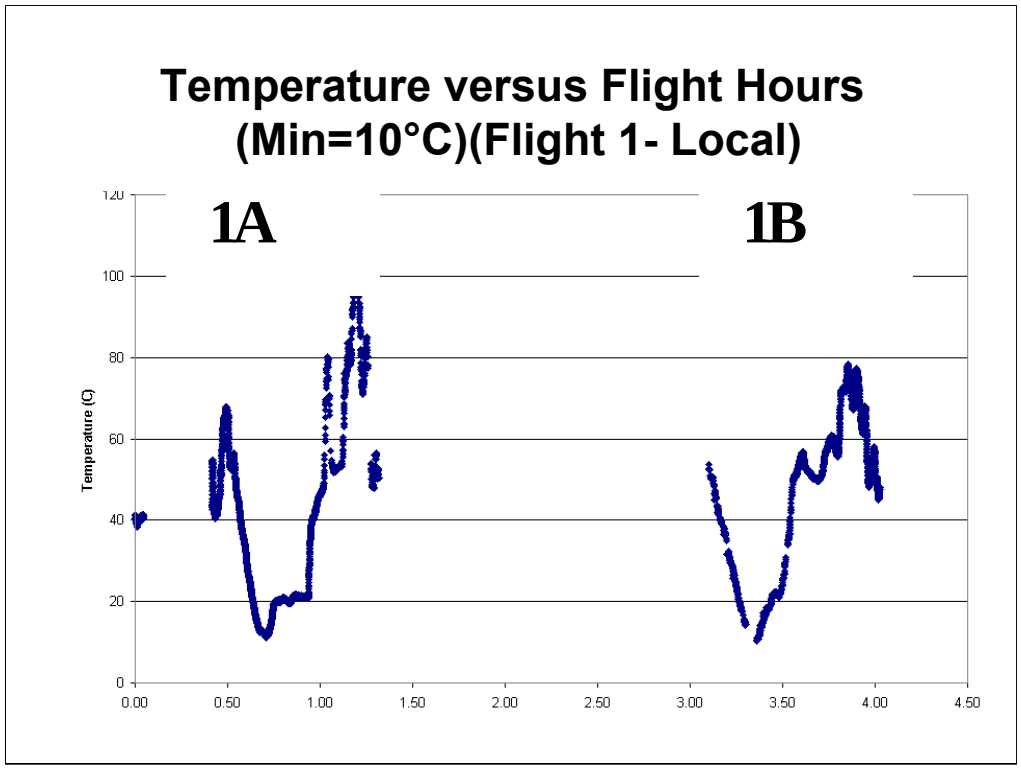

The next charts shows the temperature versus flight time for flights 1 through 5 and a ground run between flights 2 and 3. First we will look at plots of temperature versus time. During Flight 1 we see that the Minimum Temperature is about 10C. Temperature time history data for flight 1 were hand edited in Excel to remove intermittent data during the middle of data collection. Flight 1 was a basically a takeoff and cruise to Warner Robins AFB and return to the NCANC Base.

Flight 1 was flown at higher altitudes, had no flap position changes other than take off and landings and had the lowest temperature (approximately 10 °C) of the 5 flights.

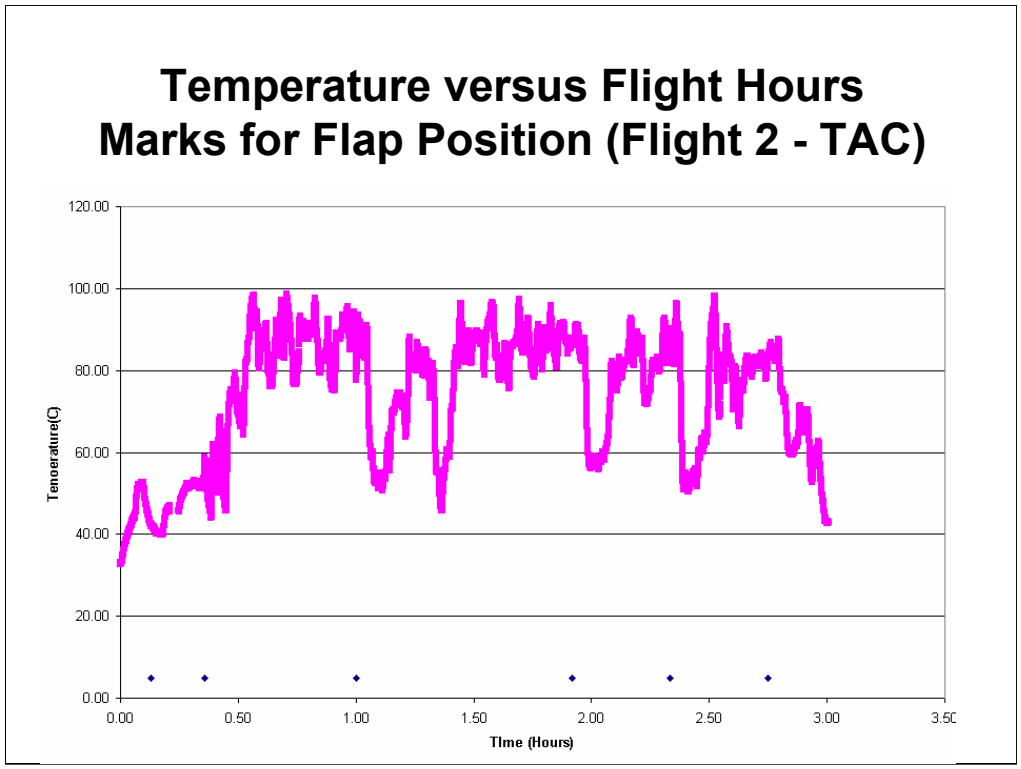

The temperature time history is shown in this data for flight 2. One theory is that the flap position impacts the strain levels and temperatures of the wing flap skin Thus marks for Flap Position were added manually. Maximum temperature on this flight is about 100 C and the lowest temperature is about 32 C.

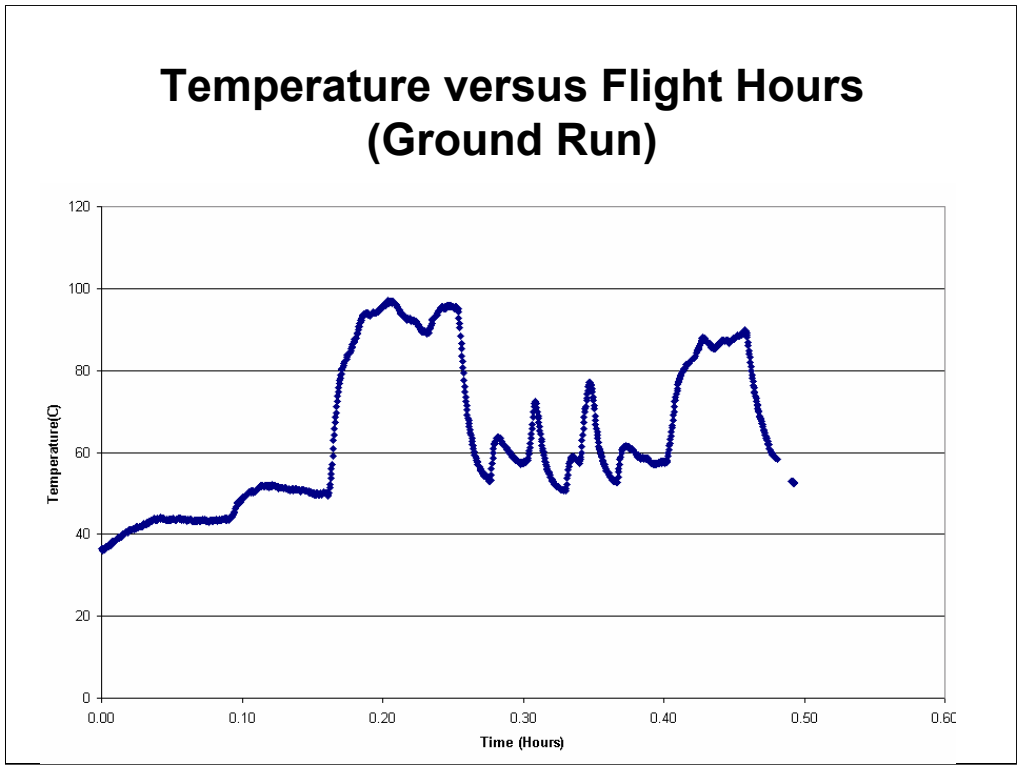

The temperature time history is shown in this plot for a short engine ground run up. The highest temperature is about 98 C and the lowest is about 38C.

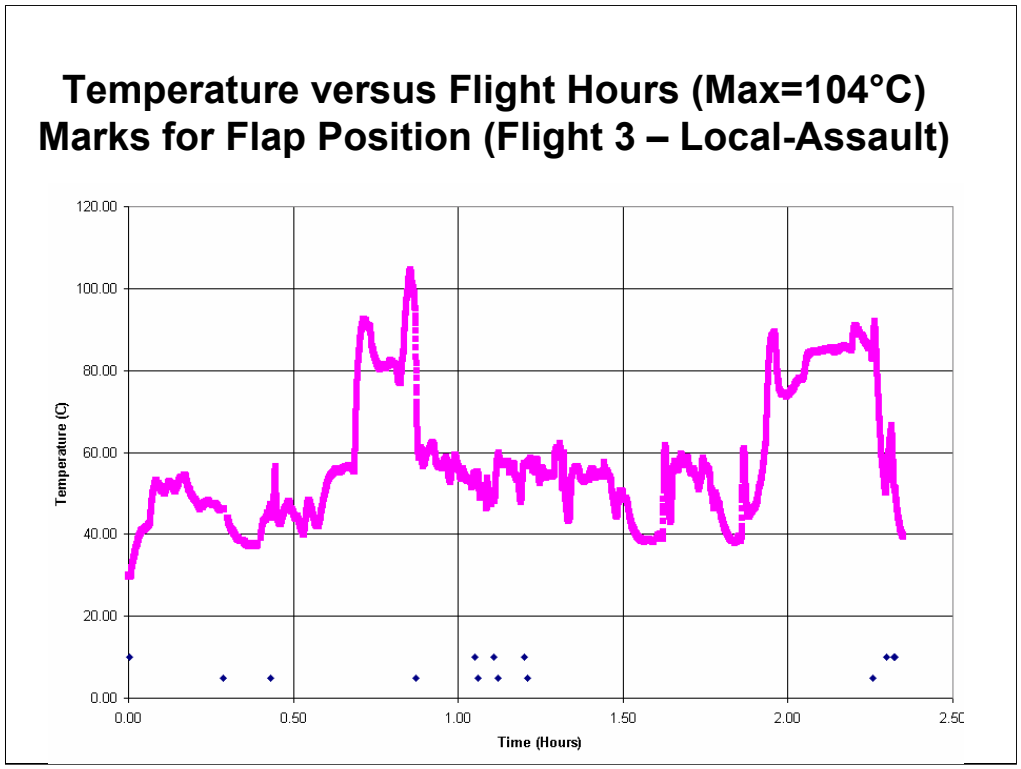

The temperature time history is shown in this data for flight 3. Marks for Flap Position were added manually. As seen in the plots, the highest temperature seen in the wing flap well is about 104 °C during this flight.

The lowest temperature is about 30 C.

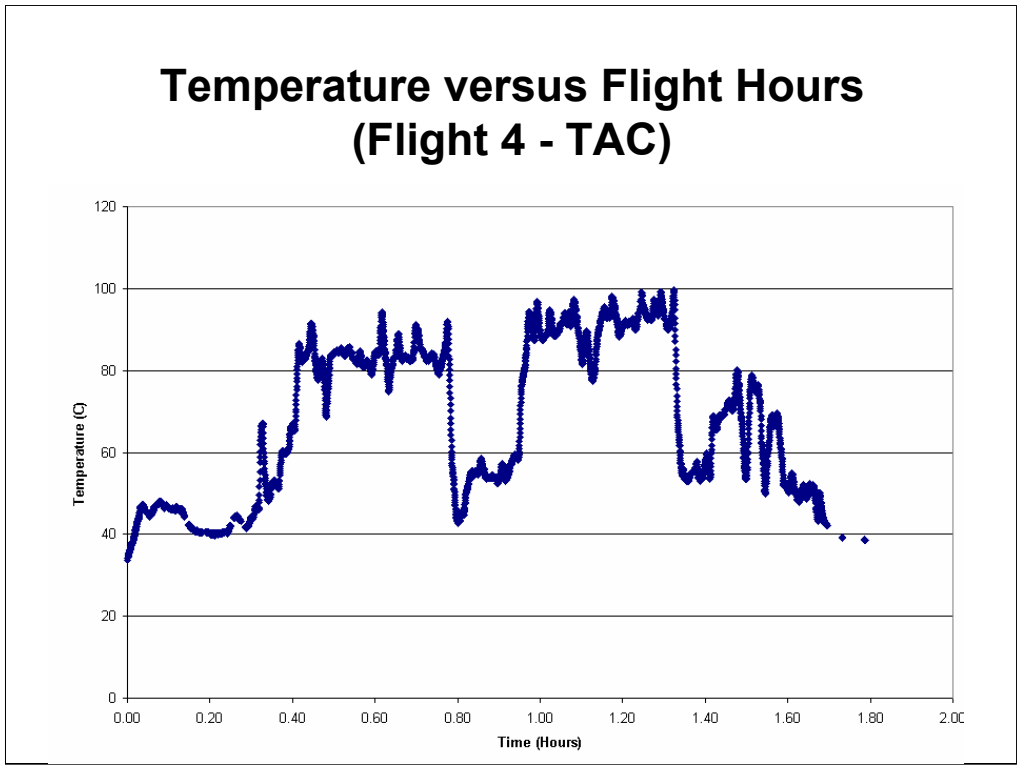

The temperature time history is shown in this data for flight 4. Marks for Flap Position were added manually. Since there was little flap position information on the flight log for flights 4 & 5, a mark for flap position could not be included. Here the highest temperature is about 100 C and the lowest is about 34C.

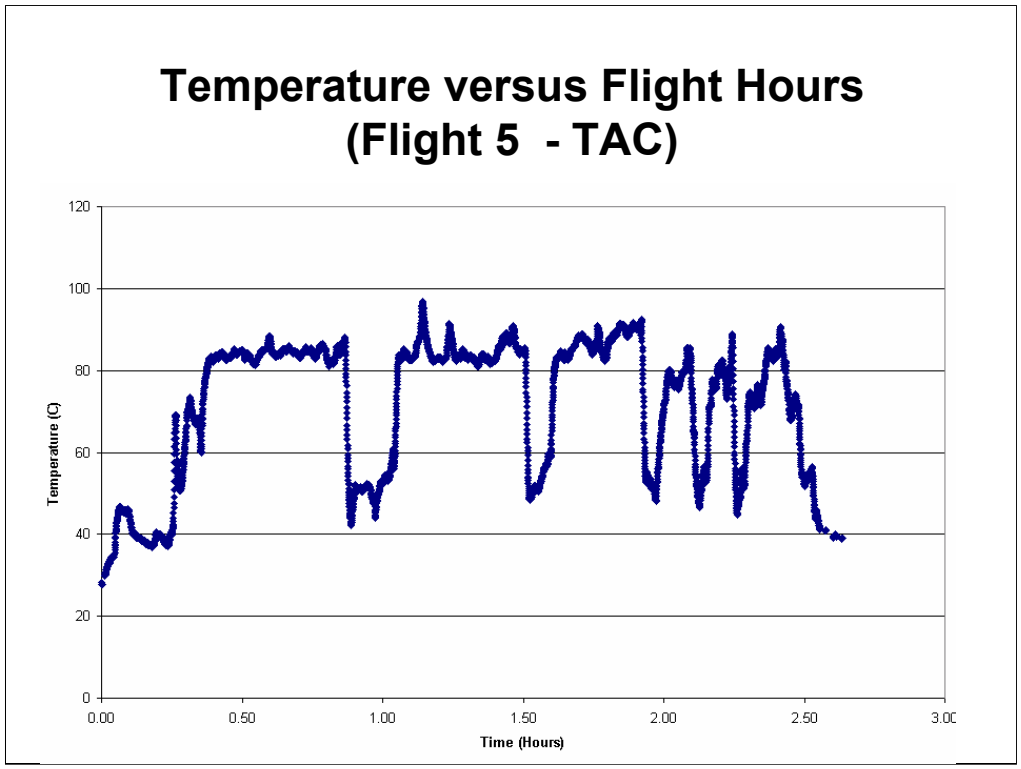

The temperature time history is shown in this data for flight 5 Marks for Flap Position were not added manually due to uncertainty in the flight logs. Here the highest temperatures is about 98 C and the lowest is about 28 C.

As seen in the plots, the highest temperature seen in the wing flap well is about 104 °C during flight 3. In addition, for flight 2 and 3 an indication of flap position were included on the plot by adding a column for flap position on the spreadsheet and estimating as good as possible the time and flap position from the flight logs. It appears that usually that a flap position of 50% or greater was usually an indication of a temperature decrease. In fact it appears that the flight crew may have forgotten to record one flap position change on flight 2. Looking at the temperature time histories for these flights and the fact these were also flights with multiple cargo drops and landings, it may be the flap position was 50% or greater at the temperature dips in the two flights.

RMS Time Histories from Third Octave Data

- 3 steps to compute third octave overall rms
  - (1) square each band rms to get the mean square
  - (2) sum all resultant band rms^{2}s
  - (3) take the square root of result to get to the overall rms.
    - i.e. $\text{overall } rms^2 = \sum_{i=1}^{18} rms(i)^2$
- Save Third Octave Bands to Spreadsheet
- Use Microsoft® Excel to read Spreadsheet
- Most Ground Data Deleted
- Bad Data Deleted from Flight 1
- Excel - plot temperature&strains RMS με vs time
- Excel - plot temperature versus SG2

There is a STORE DATA button on the VI that allows the engineer to save all data as a spreadsheet file for further analysis. Stored spreadsheet data includes all recorded dosimeter data (temperature, peak strain, and clock time), rms values computed from third octaves records, and computed time history statistics (mean, standard deviation and rms). Third octave bands are stored in up to 29,455 SDR records. The dosimeter records third octave band rms values for each strain gage. The three steps to compute the third octave overall rms are (1) square each band rms to get the mean square, (2) sum all resultant band rms^{2}s and (3) take the square root of that result to get to the overall rms. AFRL data analysis process consisted of the steps outlined in the chart.

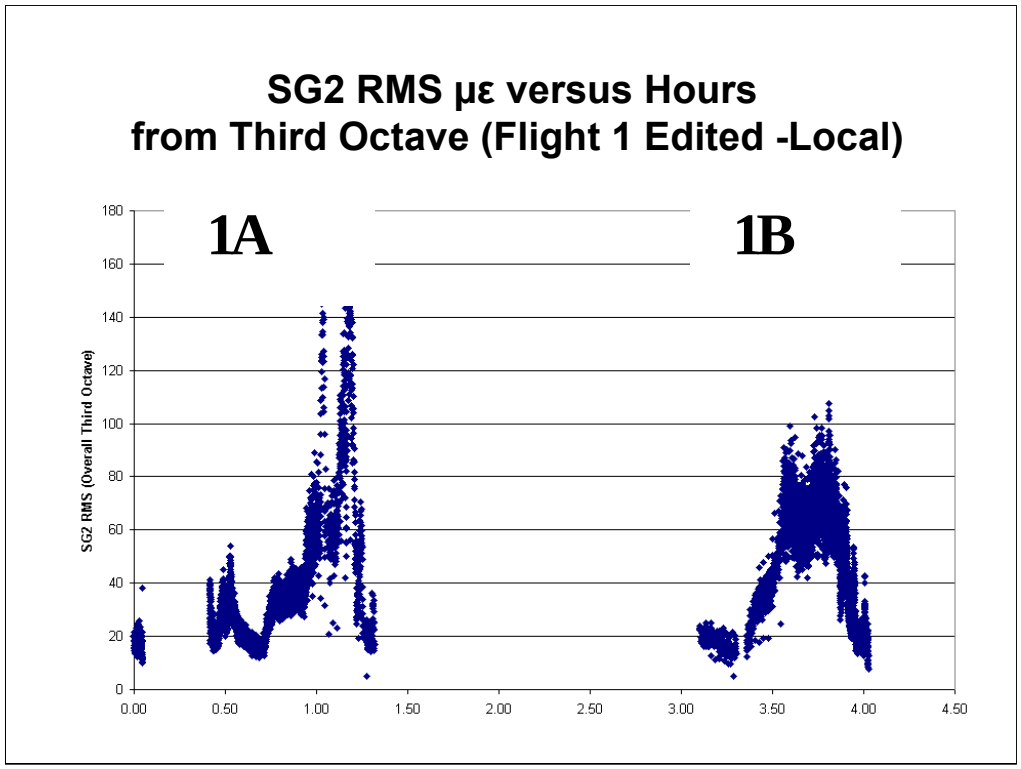

The next charts shows time history plots for the rms values of SG2 versus time using the rms third octave values. SG2 is presented since it had the highest strain readings. Most of the time, the strain levels were less than 140 με rms. For this flight the maximum strain is about 145 microstrain.

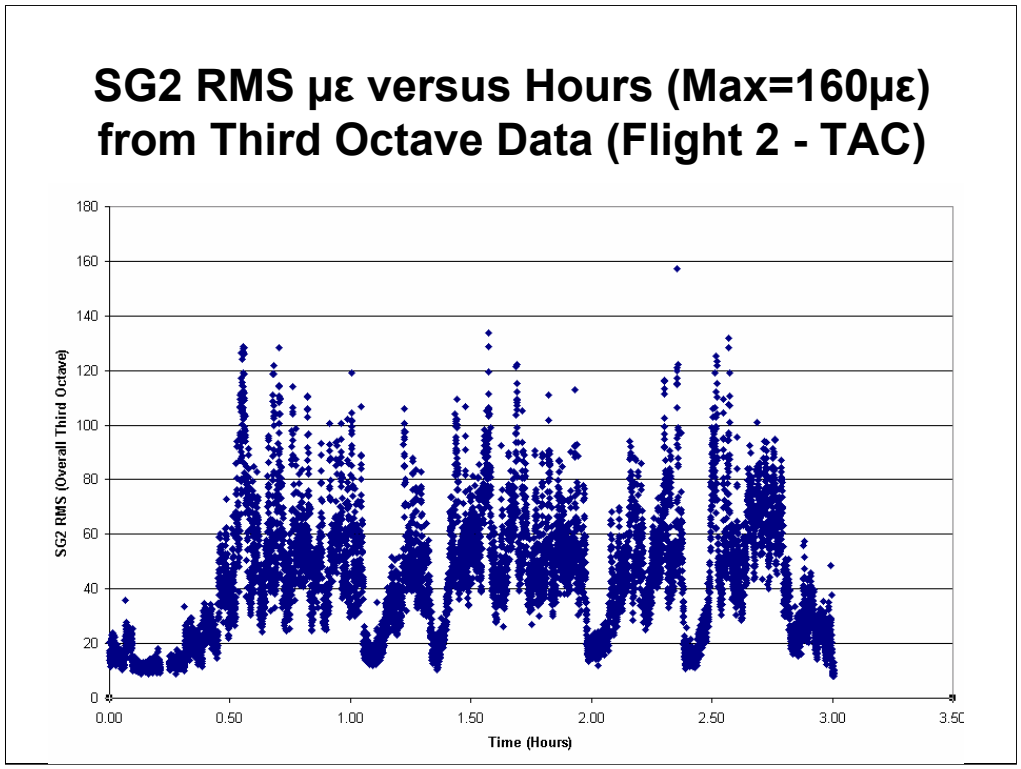

Above is the RMS time history of strain for flight 2 where the highest RMS level is about 158 microstrain.

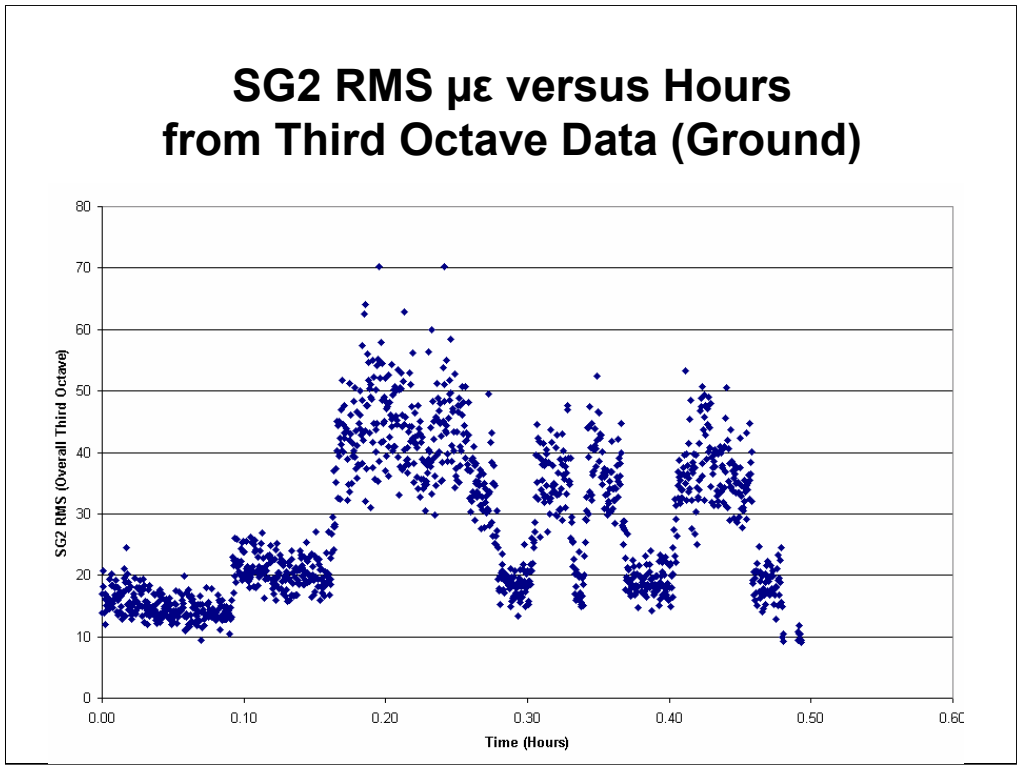

Above is the RMS time history of strain for a ground engine run up between flight 2 and 3 where the highest RMS level is about 70 microstrain.

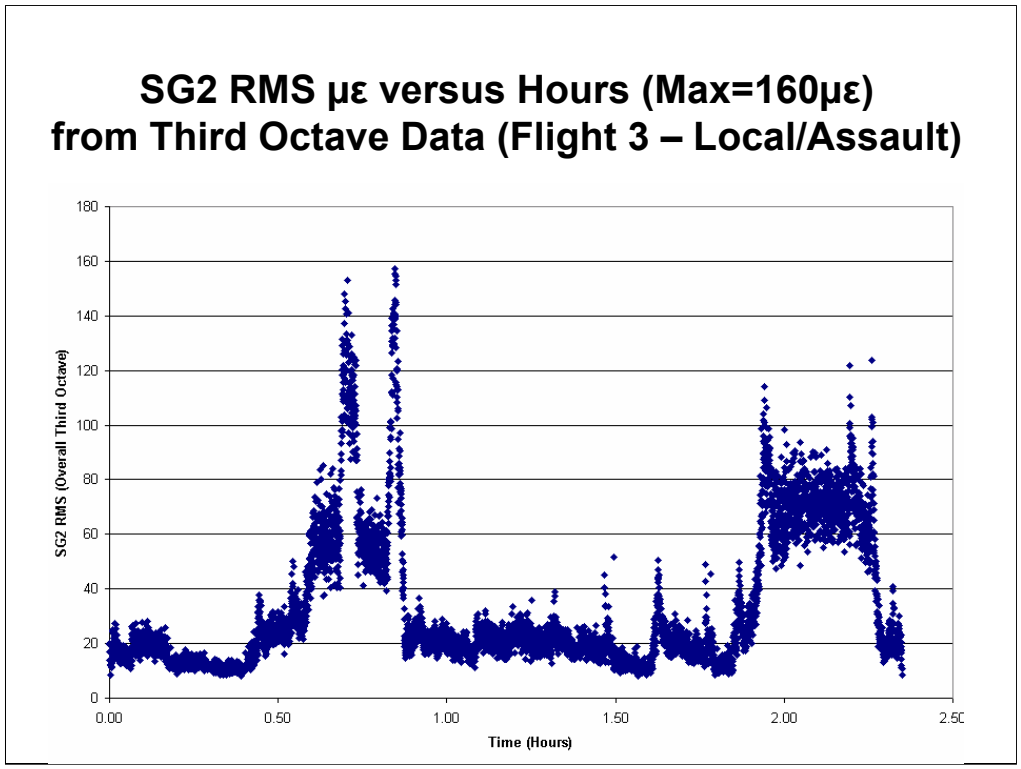

Above is the RMS time history of strain for flight 2 where the highest RMS level is about 160 microstrain.

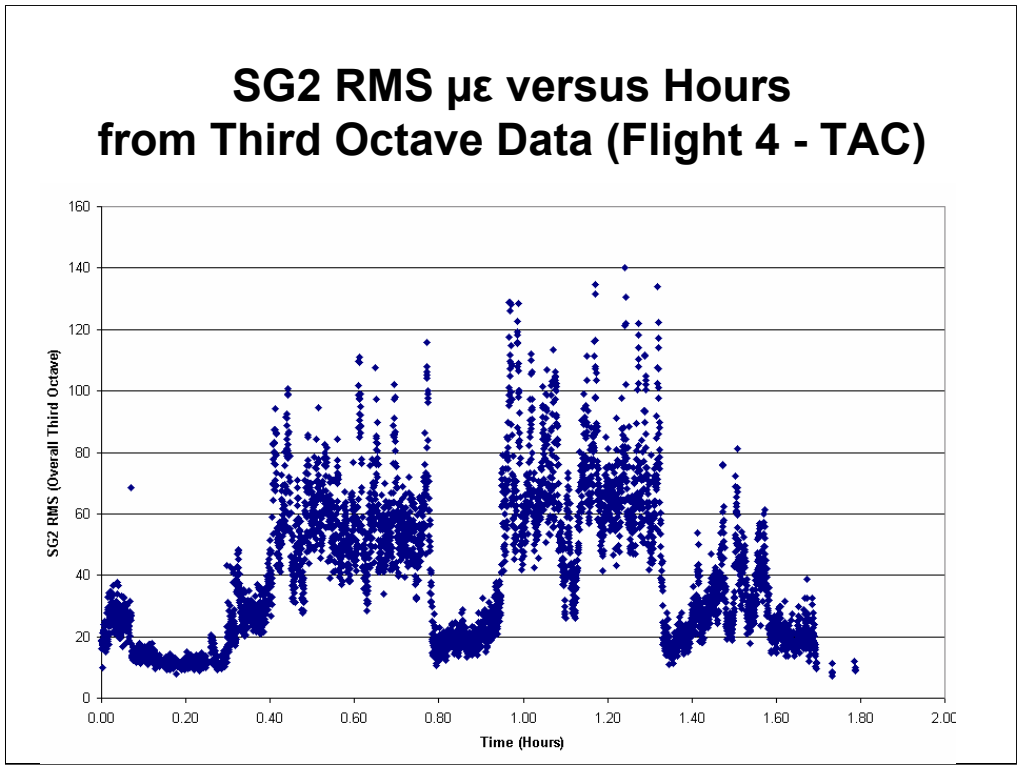

Above is the RMS time history of strain for flight 4 where the highest RMS level is about 140 microstrain.

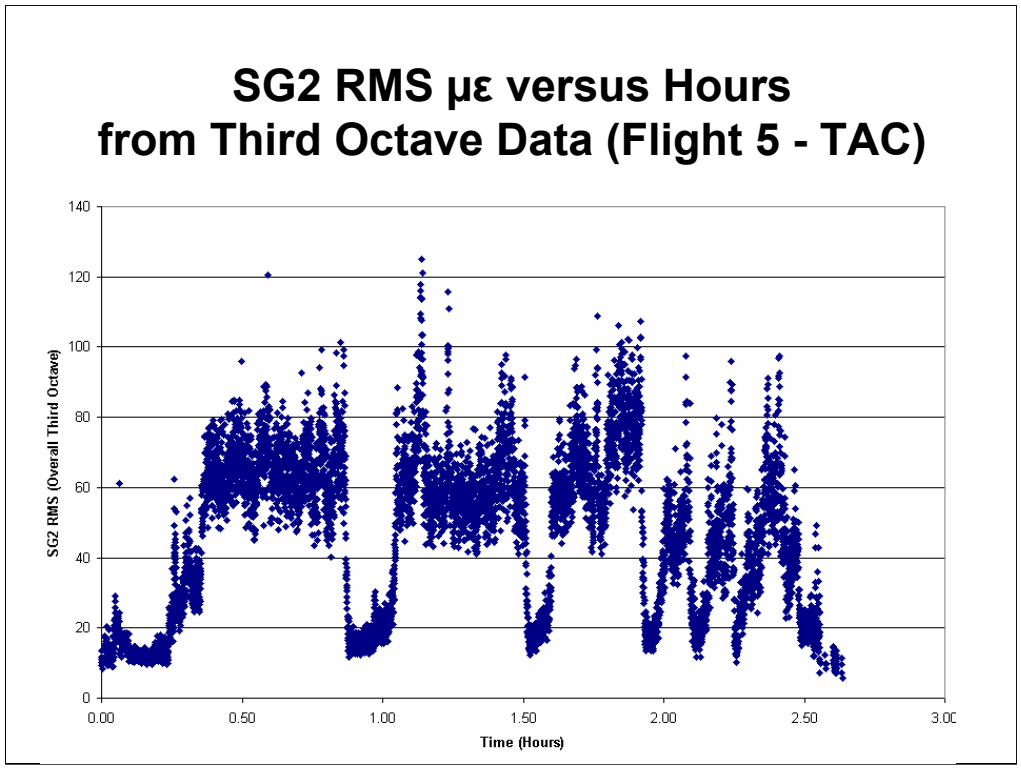

Above is the RMS time history of strain for flight 5 where the hightes RMS level is about 127 microstrain. For these 5 no repair flights, the highest rms strain level is about 160 micro strain ($\mu\varepsilon$) rms. This level was reached during flight 2 and flight 3 during very short time periods

Patch Installation Procedures

- Installed by Mike Parin during October 2003
  - **President - Damping Technology, Inc.**
- Applied 5 Pieces Total
  - **12” x 3” One Piece Forward Bay**
  - **10” x 2” One Piece Aft Bay**
  - **2.5” x 1” One Piece behind Strain Gages in Middle Bay**
  - **4" x 3" Two Pieces Sides of Middle Bay**
- Thickness Approximately 0.08"

During October 2003 Mike Parin of Damping Technologies Inc., traveled to the NCANG to install the patch in accordance with the following procedure.

First Mr. Parin reviewed and inspected the damping system and explained how the system adheres to the panel. Upon inspecting the instrumented panels it was decided to apply the damping system to the instrumentation side and eliminate the edge sealant.

At the Aircraft, Mr. Parin prepared the surface. A dry wipe was performed to remove as much lose dirt as possible. This was followed by repeated solvent wipes with isopropyl alcohol until there as no visible dirt picked up on the cloth. An abrasive pad was used on the panel surface followed by a repeat of the solvent wipe process. A portable heater was used to bring the panel temperature up to a point where it was just warm to the touch. This was accomplished by positioning the heater duct on the underside of the panel and allowing it to dwell there for upwards of five minutes.

Constrained Layer Damping (CLD) Repair

Installed by Damping Technologies Incorporated in 1 Hour (October 2003).

The final Constrained Layer Damping Repair in the forward and middle bays is shown in the photo. A P/N NPE981025-1 damping system measuring approximately 12" x 3“ was applied to the forward most bay by removing the protective release liner, eye balled the alignment, pressed it in place, and applied additional pressure using a squeegee. This process was repeated for the aft most bay where a P/N NPE981025-1 part measuring approximately 2" x 10“ was applied Care was taken to lift the instrumentation wiring and position the damping system under it.

Instrumentation on the center bay prevented a single piece part from being applied, so , two parts measuring approximately 4" x 3“ each were positioned on either side of the center strain gage. An additional piece measuring approximately 2.5" x 1" was also applied to the panel aft of the strain gage. Again care was taker when lifting the instrumentation cable to insert the damping system under it. After all parts were applied, heat was then again applied to the under side of the panel.

NCANG personnel inspected the installation and tried to remove the damping system by hand. The Parts were well secured and they did not expect any adhesion issues.

NPE 981025-1 CONSISTS OF:

.005" 1145-0 AL .002" 8085 VEM .005" 1145-0 AL.002" 8085 VEM .060" KLW SPACER .006" 8085 VEM

REMOVABLE LINER.

Seven Flights With Repair

October 2003

During October 2003, NCANG pilots flew 7 flights with the Repair installed as summarized in the table on the next Chart.

C-130 Flights with Repair - Oct 2003

Table 2. C-130 Flights with Repair During October 2003

Flight	Date	Type	Description	Hours	DosSN	Record#
1P	Oct 09 2003	Local	6 Assault Landings	2.52	2	3515-19464
2P	Oct 18 2003	Tactics	2-Air Drops & Low Level	2.01	15	1167-6770
3P	Oct 21 2003	Local	3 Touch & Gos & 5 Assault Landings	2.30	15	6775-12565
4P	Oct 21 2003	Tactics	Low Level & 2 Air Drops	2.22	15	13110-18273
5P	Oct 22 2003	Local	Sparse Data Log	1.81	1	1-8284
	Oct 23 2003	Ground	Ground Engine Run	0.94	1	8305-12859
6P	Oct 23 2003	Local	4 Touch & Gos	1.69	1	12860-20700
7P	Oct 23 2003	Local	1 Touch & Go Mission Aborted	1.21	1	20701-27249

This table describes the information gathered from the flight logs and the data recorded on the dosimeter during 7 flights flown by NCANG pilots during the period on Oct 9 to Oct 23, 2005.

For the seven flight flown with the repair, rms time histories for all 3 strain gages and temperature will be presented. In addition a scatter plot showing correlation between strain gage 2 and temperature will be shown. Where possible, the highest strain and the temperature for each flight will be presented.

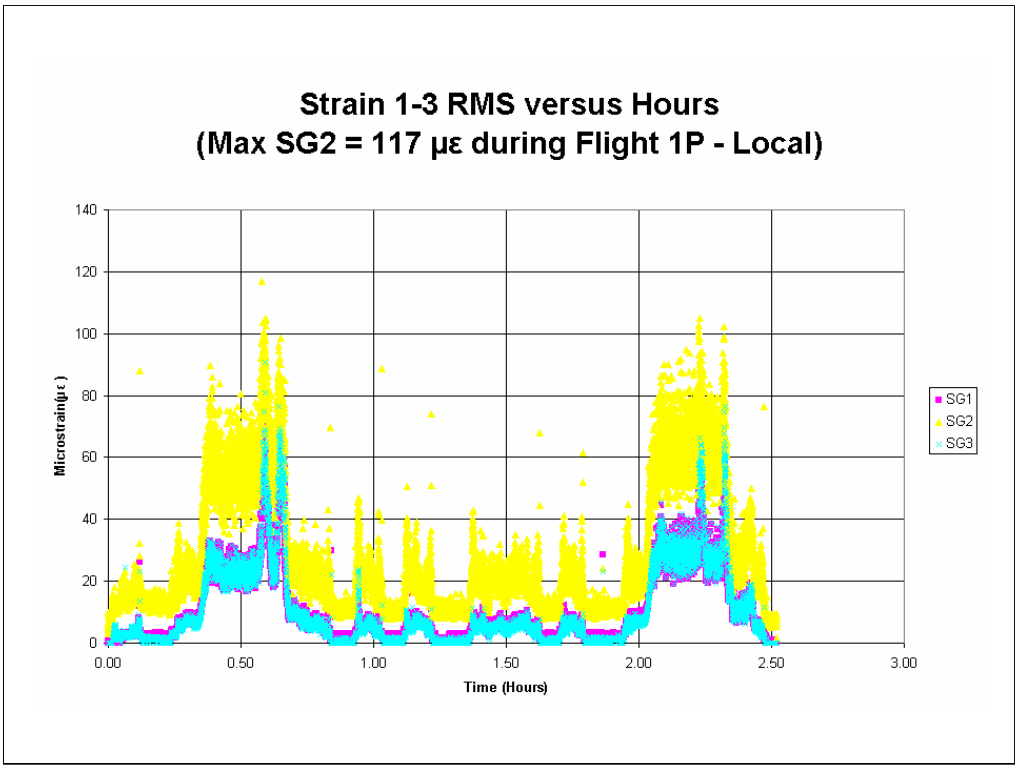

For flight 1P only the strain data is presented since the temperature sensor was not operating properly during this flight. As shown in the chart the maximum strain was about 117 microstrain during this flight.

This is the highest strain recorded on the flights flown with a repair patch.

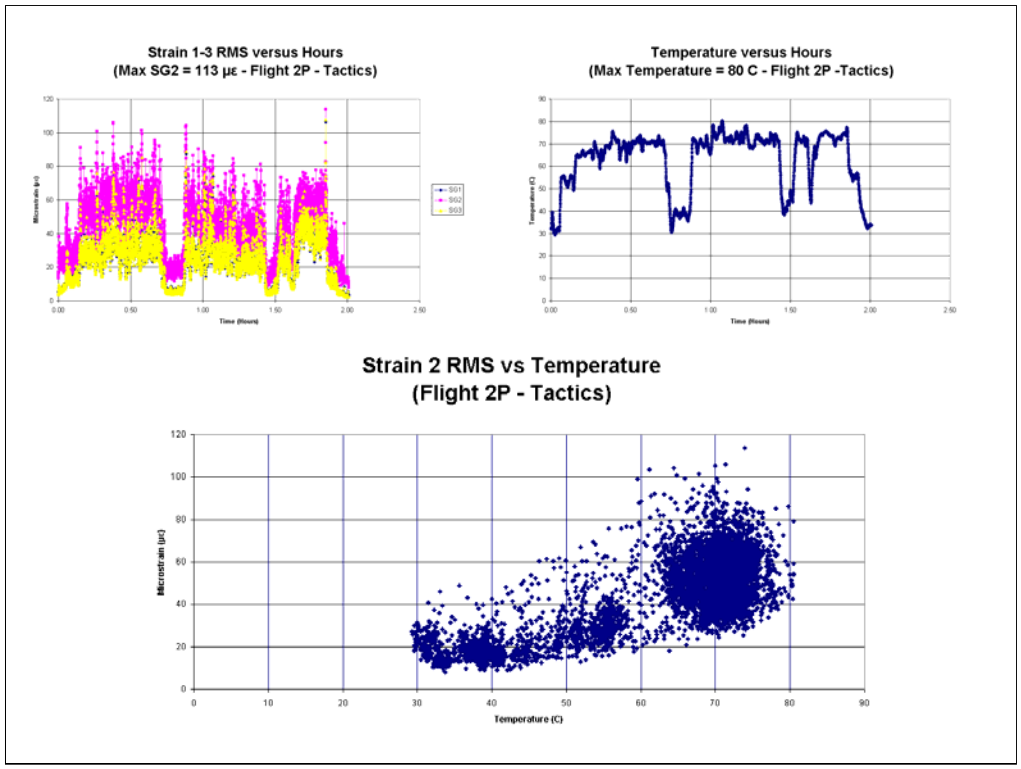

For flight 2 temperature and strain data versus flight time is shown. Also a scatter plot of strain for gage 2 versus temperature is shown. As shown in the chart the maximum strain is about 113 microstrain during flight 2P. The maximum temperature is about 80 C and the minimum temperature is about 30 C.

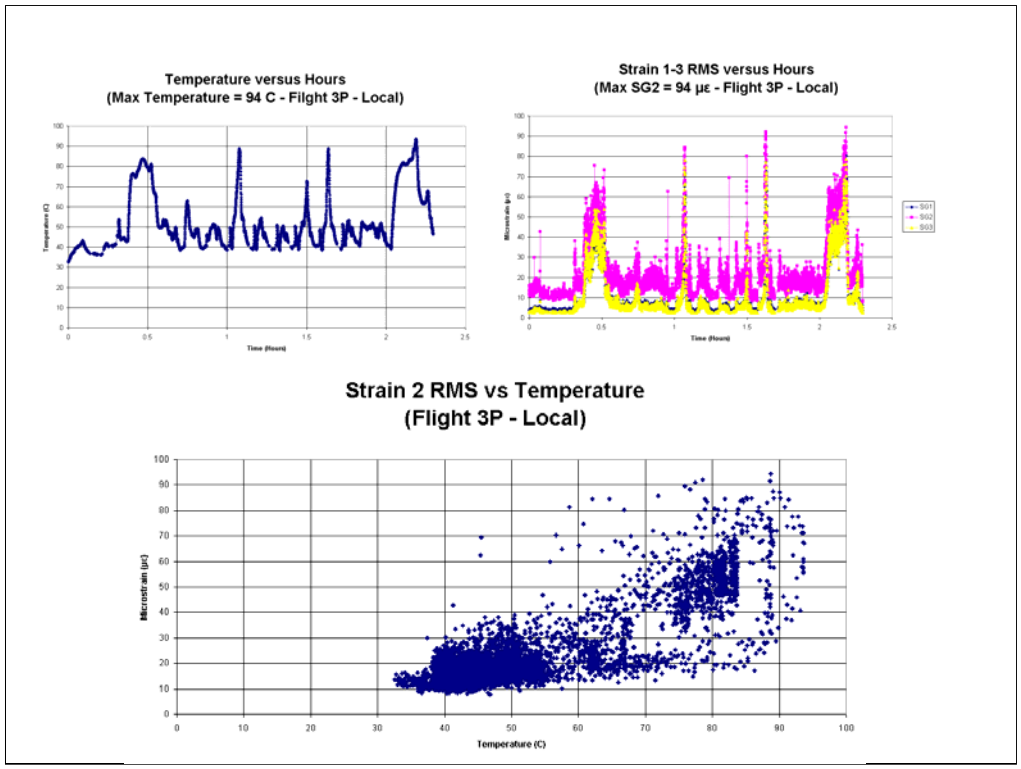

For flight 3P temperature and strain data versus flight time is presented. Also a scatter plot of strain for gage 2 versus temperature is shown. As shown in the chart the maximum strain was about 94 microstrain during flight 3P. The maximum temperature is about 94 C and the minimum temperature is about 33 C.

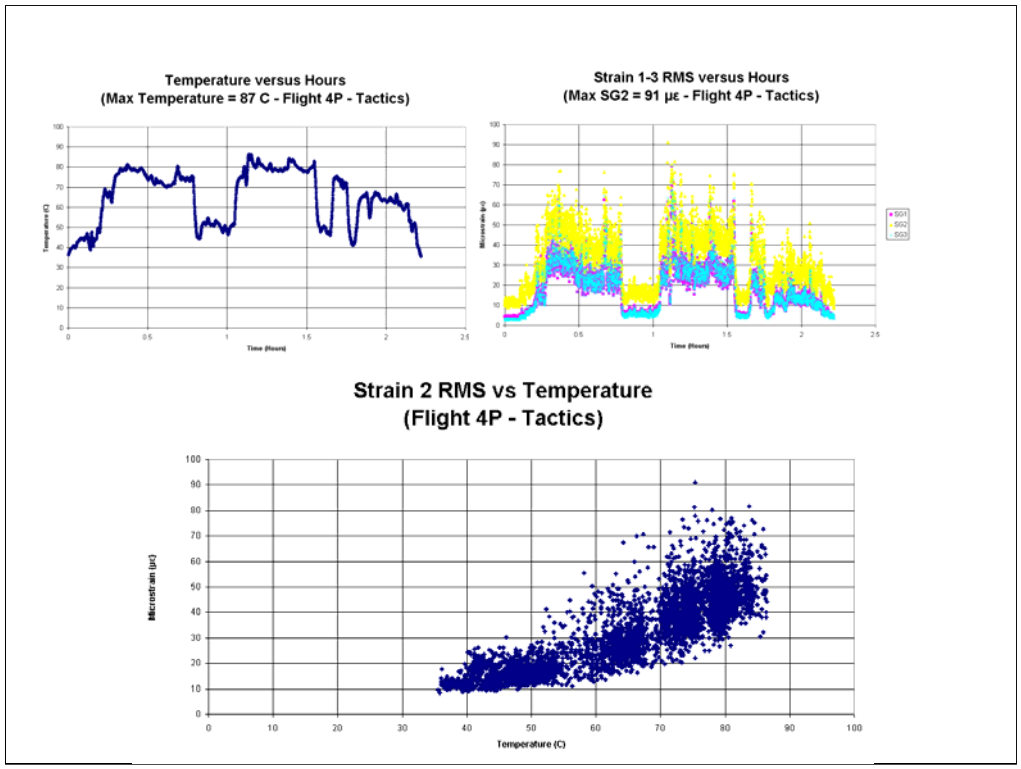

For flight 4P temperature and strain data versus flight time is presented. Also a scatter plot of strain for gage 2 versus temperature is shown. As shown in the chart the maximum strain was about 91 microstrain during flight 4P. The maximum temperature is about 87 C and the minimum temperature is about 34 C.

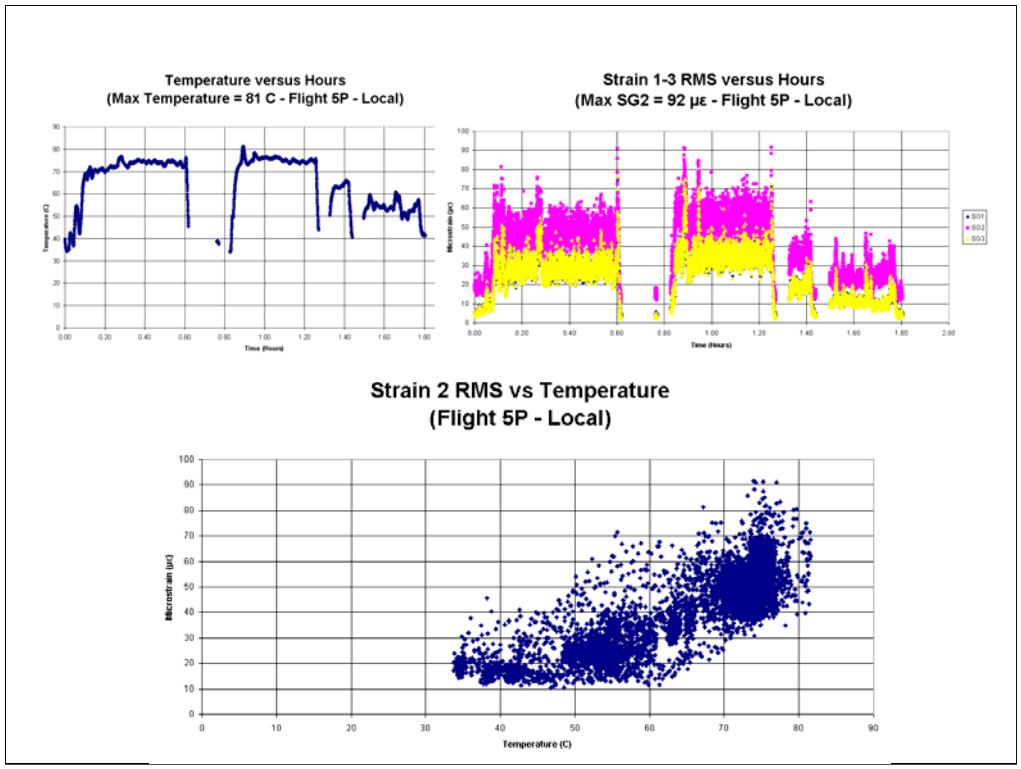

For flight 5P temperature and strain data versus flight time is presented. Also a scatter plot of strain for gage 2 versus temperature is shown. As shown in the chart the maximum strain was about 92 microstrain during flight 5P. The maximum temperature is about 81 C and the minimum temperature is about 33 C.

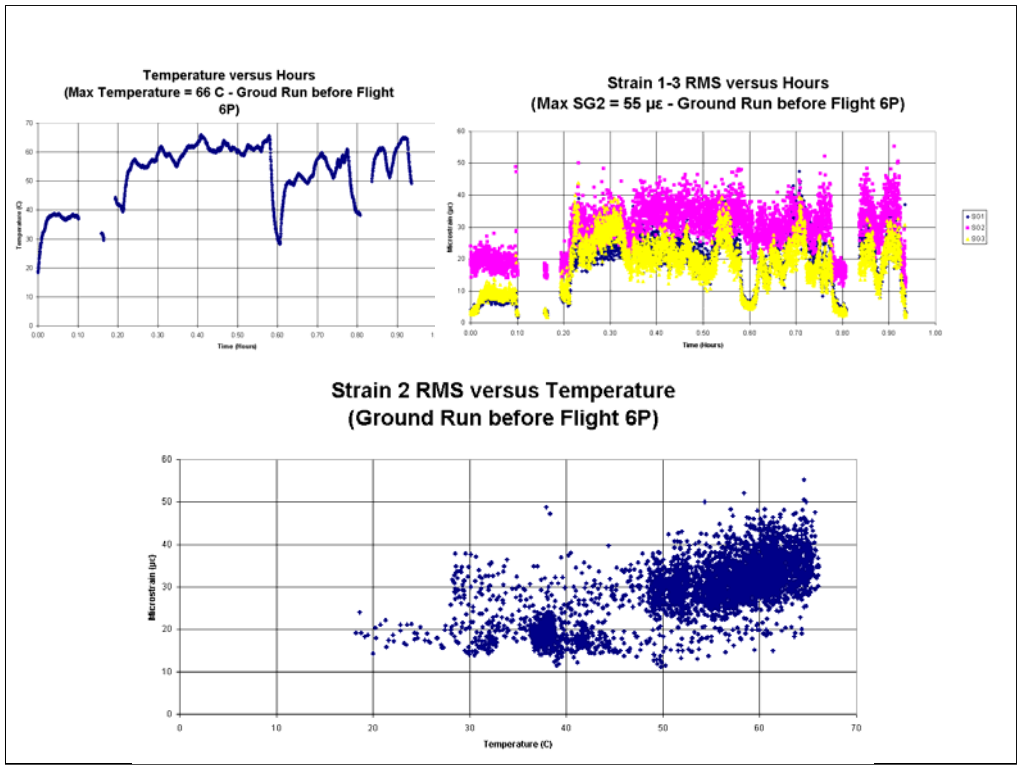

For a engine ground run before flight 6P temperature and strain data versus flight time is presented. Also a scatter plot of strain for gage 2 versus temperature is shown. As shown in the chart the maximum strain was about 55 microstrain during the engine ground round before flight 6P. The maximum temperature is about 66 C and the minimum temperature is about 18 C.

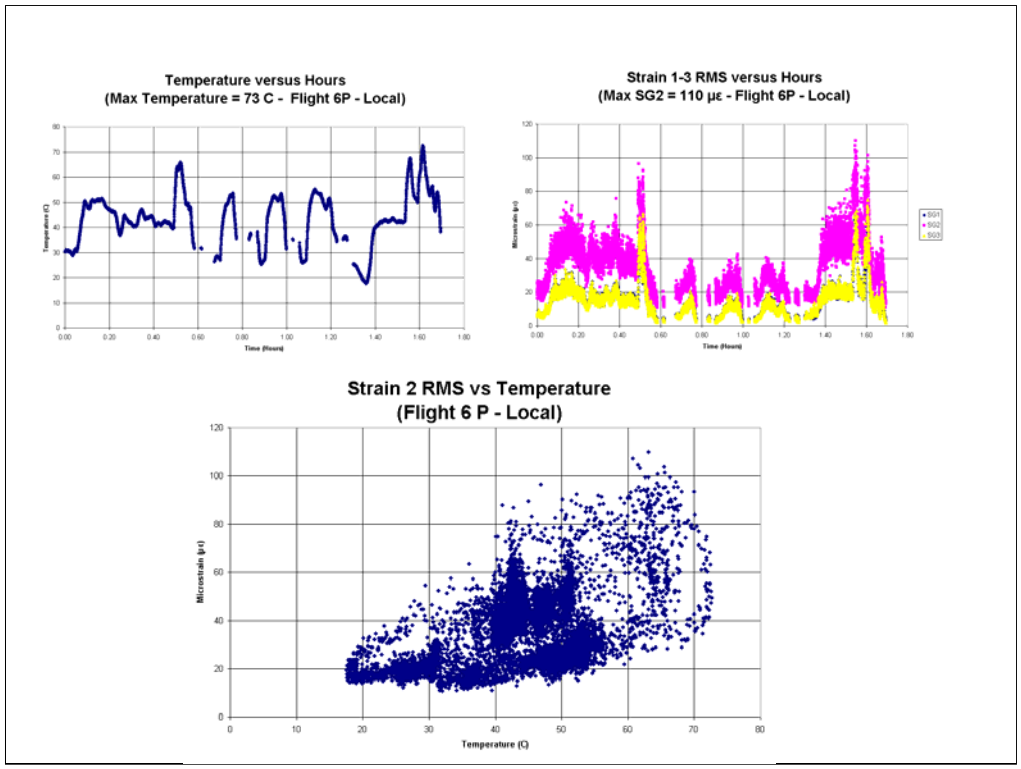

For flight 6P temperature and strain data versus flight time is presented. Also a scatter plot of strain for gage 2 versus temperature is shown. As shown in the chart the maximum strain was about 110 microstrain during flight 5P. The maximum temperature is about 73 C and the minimum temperature is about 18 C.

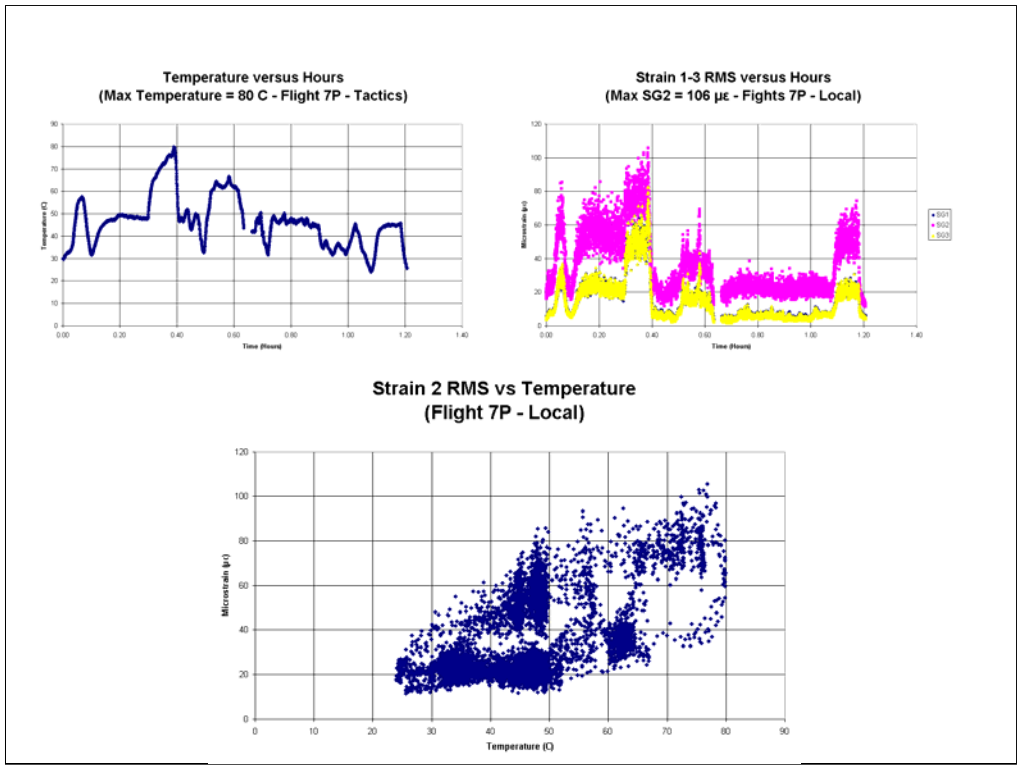

For flight 7P temperature and strain data versus flight time is presented. Also a scatter plot of strain for gage 2 versus temperature is shown. As shown in the chart the maximum strain was about 106 microstrain during flight 7P. The maximum temperature is about 80 C and the minimum temperature is about 24 C.

C-130 Flights with Repair Summary

Table 3. C-130 Flights Max and Min Temperatures and Strains October 2003

Flight	Type	Description	Hours	Max (°C)	Min (°C)	Max(με)
1P	Local	6 Assault Landings	2.52	N/A	N/A	117
2P	Tactics	2-Air Drops & Low Level	2.01	80	30	113
3P	Local	3 Touch & Gos & 5 Assault Landings	2.30	94	33	94
4P	Tactics	Low Level & 2 Air Drops	2.22	87	34	91
5P	Local	Sparse Data Log	1.81	81	33	92
	Ground	Ground Engine Run	0.94	66	18	55
6P	Local	4 Touch & Gos	1.69	73	18	110
7P	Local	1 Touch & Go Mission Aborted	1.21	80	24	106

Table 3 in the chart summarizes the temperature and strain environment of the wing flap during flight with the repair installed. It appears that there was a lower level of strain than during the June flights without the repair installed. Most importantly, this data is needed to optimize the repair of any future C-130s.

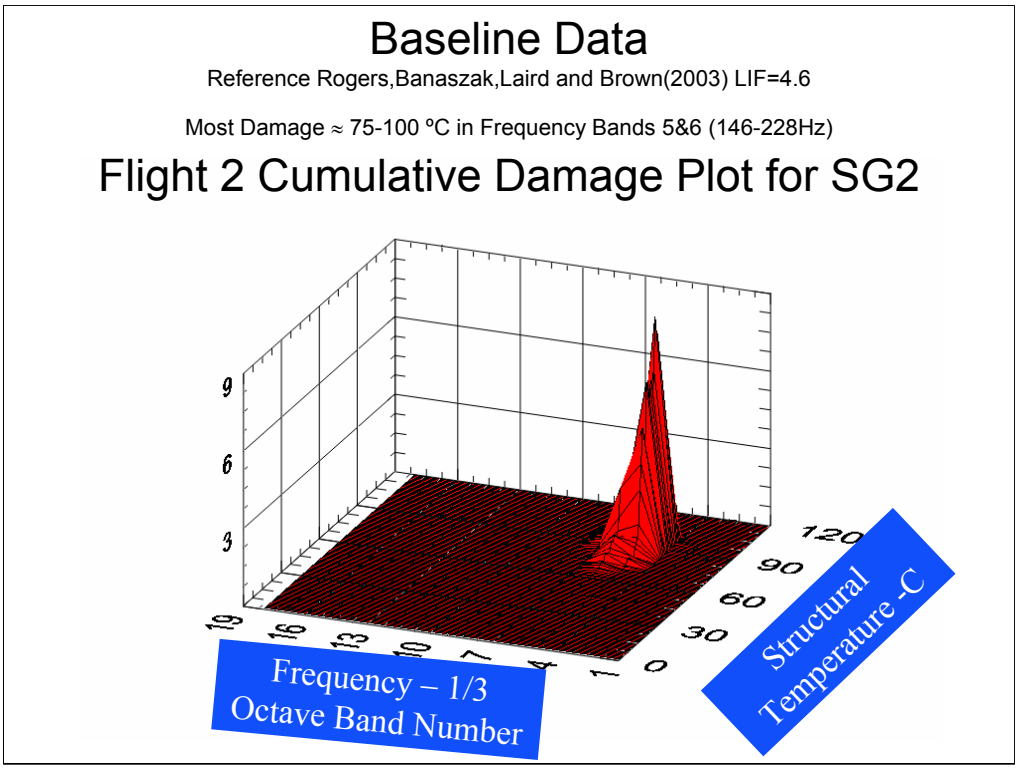

A cumulative damage plot can be prepared as done previously for a flight with no repair during June 2003. This analysis is being continued by an emeritus engineer at AFRL. Preliminary indications are that there is a life improvement factor (LIF) of about 5.

Summary and Conclusions

- Thermal & Strain Environment Before Repair
  - Temperature and Time History for 5 Flights
  - Highest Temperature 104 °C Flight 2 - Lowest 10 °C Flight 1
  - Most SG 2 levels < 140 με RMS - Max of 160 με RMS
  - High Correlation between SG1&SG3 as Expected
  - SG 2 Levels > SG1&SG 3 – SG 2 at site of crack initiation
  - Usually Flap Position ≥ 50% ➔Temperature Drop
- Thermal & Strain Environment After Oct 2003 Repair
  - RMS με & Temperature Help Predict Structural Life
  - Complete Technical Report in Progress
  - Preliminary Indications are LIF = 5.6 per ASIP 2003 Poster Paper
  - Highest Temperature 94 C during flight 2P – No temperature on Flight 1P
  - Highest strain still at Strain Location 2
  - Maximum Strain on SG2 = 117 με RMS during Flight 1P
  - Definition of stress and strain environment need for repair patch design.
- Overall Strains Lower on Flights with Repair Installed
- Need to Design and Update to Dosimeter II

First, time histories were presented for the 5 flights without a repair. The highest temperature was 104 °C during Flight 2 and the lowest 10 °C on Flight 1. Most strain gage 2 (SG2) levels were < 140 με RMS with a maximum of 160 με RMS. There is a high correlation between SG1&SG3 since they are in close physical locations. SG2 levels are > SG1&SG 3 which makes sense since SG 2 is at site of crack initiation. Usually Flap Position ≥ 50% ➔Temperature Drop

The strain levels during the October 2003 flights with the repairs were lower. The RMS με & temperature help to predict Structural Life. Preliminary Indications are LIF = 5.6 per ASIP 2003 Poster Paper. Highest temperature is 94 C during flight 2P, but the temperature sensor did not work on Flight 1P. Again the highest strain is at strain Location 2. The maximum strain on SG2 = 117 με RMS during Flight 1P. The thermal and strain environment are very necessary for repair patch design. Overall strains levels were lower on flights with the repair installed.

Lastly, the dosimeter is a great tool to obtain thermal and mechanical design data. The Air Force needs to design and updat to a Dosimeter II to take advantage of improvement in the state-of-the art in memory storage data acquisition systems since the design of the original dosimeter.

Dosimeter References

- Banaszak, D., Brown, D., Laird, D., (2005), "*Autonomous Environmental Definition of C-130 Flap Well Skin Panel ",* Journal of the IEST Volume 48 No1 pp 50-61. Rolling Meadows, IL.
- Banaszak, D., Brown, D. , Laird, D., (2004) "*Autonomous Environmental Definition of C-130 Flap Well Skin Panel ",* Institute of Environmental Sciences and Technology (IEST) 2004 Proceedings Design, Test, and Evaluation Product Reliability, ESTECH 2004 the 50th ATM, Las Vegas, NV.
- Banaszak, D. (2002), "End-to-End Mechanical Calibration of Strain Channels in Dynamic Health Monitoring Systems", Journal of the IEST Volume 45 2002 Annual Edition, pp 1134-120, Rolling Meadows, IL.
- Himelblau, H., Piersol, A. G., Wise, J. H., and Grundwig, M. R. (1990), Handbook for Dynamic Data Acquisition and Analysis, Institute of Environment Sciences and Technology (IEST) Recommended Practice DTE012.1, 148-152, Mount Prospect, IL.
- Ikegami, R., Haugse, E., Trego, A., Rogers, L, and Maly, J. (2001), Structural Technology and Analysis Program (STAP) Delivery Order Number: 004 Durability Patch, AFRL-VA-WP-TR-2001-3037, ADA408003, Air Force Research Laboratory, Wright Patterson AFB, OH.
- Withrow, Mellissa, (2005) "C-130 Durable Repair Patch: Engineers demonstrate a new repair Patch that dissipates panel vibration.", *Air Force Research Laboratory Technology Horizon*, Vol. 6. , No. 3, June 2005, page 41.
- See Banaszak, Brown and Laird (2005) for more References.

The main reference is the recent IEST Journal article which contains numerous references to other papers describing use and applications of the dosimeter.

The authors thank David Smith of Integrity Design Engineering, Karl Anderson of Valid Measurements™ and Lyle Wells of Trig-Tek, Inc. in helping AFRL engineers to fully understand the damage dosimeter. Also, special thanks to Chief Master Sergeant Michael Bigger and Master Sergeant Tim Roberts of the 145th Air Wing (145AW/LG) at the NCANG Base, who supported AFRL efforts to collect data on the C-130. Captain Michael Myers managed the dosimeter delivery to completion on AFRL contract F33615-95-D-3203 and Mark Baker installed the strain gages and temperature sensors. Also thanks to Capt. David Laird who helped Mark and the NCANG in completing this program.

This should not be the end. This should be the beginning.

Section 3.9

Exploring Fiber Optic Strain Sensors for Testing Future Aerospace Structures

Presentation at 22nd Transducer Workshop

TWS = Transducer Work Shop
Sponsored by Range Commanders Council (RCC)/ Telemetry Group(TG)
At Texas Christian University, Fort Worth TX
June 20, 2006

(NOTE: In the digital version of this report, see original PowerPoint attachment, 22TWS.ppt)

Evaluation of a Distributed Sensing System with Simple Bending Beams

Enrique.Medina@wpafb.af.mil
Radiance Technologies and Ohio University
Dayton, OH 45430 937-255-2236

David.Banaszak@wpafb.af.mil,
Air Force Research Laboratory
AFRL/VASV, WPAFB, OH 45433, 937-904-6859

1

This Report documents a cooperative effort between the Materials Directorate (ML) and Air Vehicles Directorate (VA) in evaluating a LUNA Distributed Sensing System (DSS) developed on a SBIR contract for ML.

VA needs new instrumentation systems to measure multiple strains at different locatations in a timely and efficient manner.

This report shows evaluation results conducted by VAS for MLL.

Introduction

- 17 Aug 05-MLL support request to VAS
- 28 Oct 05-VAS agrees to support
- 20 Jan 06-MLL provides DSS System to VAS
- Feb 06 VASV conducts Beam Lab Experiments
- Mar-Jun 06 MLLP and VASV Joint Effort
  - VASV Analyzes Data using Excel
  - MLLP writes MATLAB® Analysis Routines
- VASV Prepares Beam Experiment Report

2

In a letter dated 17 August, 2005, MLL requested the support of VAS in testing the Luna Distributed Sensing System (DSS) deliverable under SBIR Topic AF# SD01-CBM04. AFRL/VAS agreed to provide this support in a memorandum dated 28 October 2005. The DSS hardware fits well into current VASV research plans. The payoff of this support included a new structural test measurement capability for efficient onboard sensing of multiple stain locations with a single fiber as well as enabling capability for Vehicle Health Monitoring in locations that are inaccessible to current NDE methods.

ML & VAS Start Evaluation of DSS System (26 Jan 06)

ML Presenting Test Beam to VASV

Luna DSS System

3

On 20 January 2006, AFRL/MLLP(Lt. Bill Freemantle) delivered the DSS system (shown above right) to AFRL/VASV (Mr. David Banaszak). On 26 January 06, AFRL/MLLP delivered 3 instrumented test beams for evaluation by VASV. The DSS system measures strain using Fiber Bragg Grating (FBG) optical sensors.

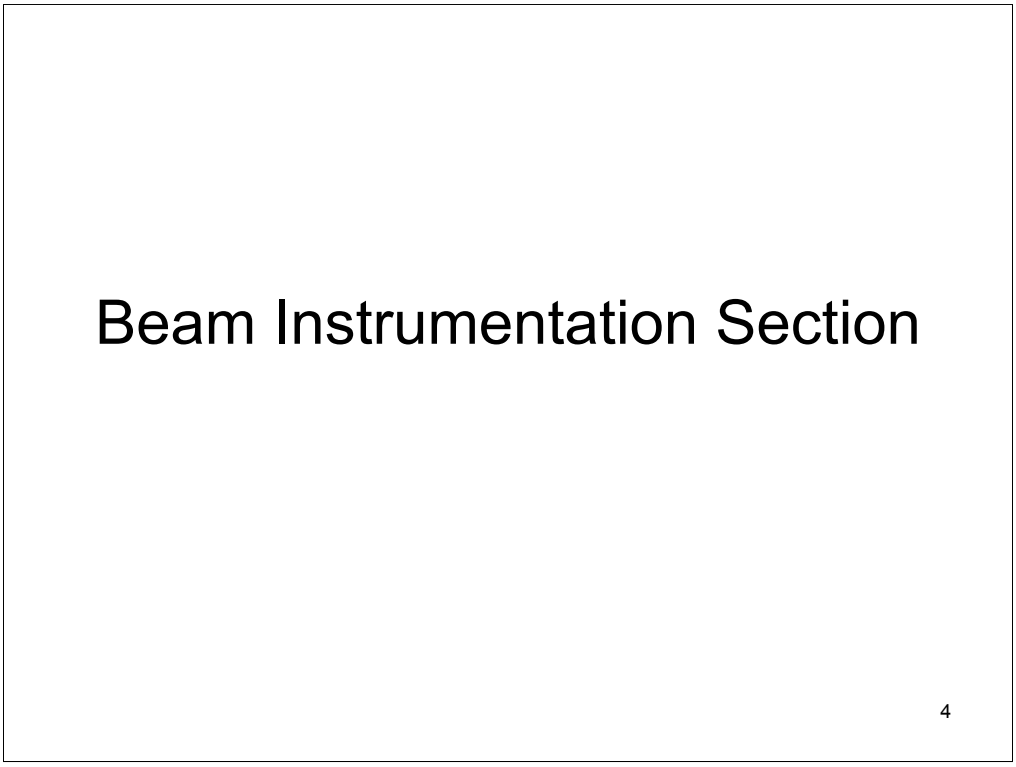

Per the AFRL/MLL request, VASV tested three 18” (457.2mm) x 1” (25.4 mm) x 1/8” (3.175mm) beams with FBG sensors attached by Luna personnel (Mike Nuckels) using recommended LUNA installation instructions and GA-2 adhesive.

Fiber Braggs Grating and SGs on 3 Beams (26 Jan 06)

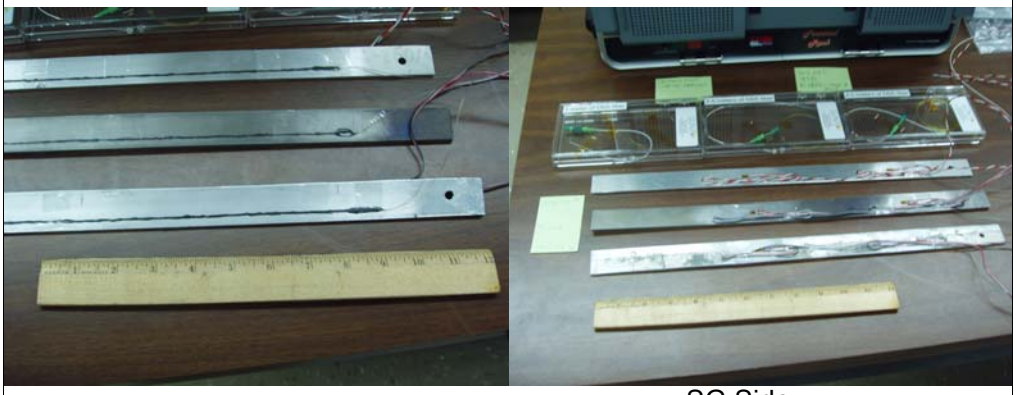

FBG Side

SG Side

5

AFRL/MLL (Enrique Medina) attached strain gages on the opposite side of the beams for comparisons during simple bending test as shown. The three materials were 2024-T3 aluminum, 7075-T6 aluminum and Ti-6-4-2-4. For each beam, one 650 nanometer (nm) wavelength fiber containing Bragg gratings were installed on one side of the beam. Assuming 1 strain measurement every centimeter (cm), this allowed the DSS system to make about 35 strain measurements per beam.

Two conventional electrical strain gages were attached on the opposite side of the beam as shown above. The data from FBG sensors were recorded directly into the DSS computer. Data from the strain gages and a room temperature thermocouple were recorded on a laptop PC using P3500 and P3 Measurement Group signal conditioners connected to Data Translation DT9805 and 9806 USB data acquisition boards.

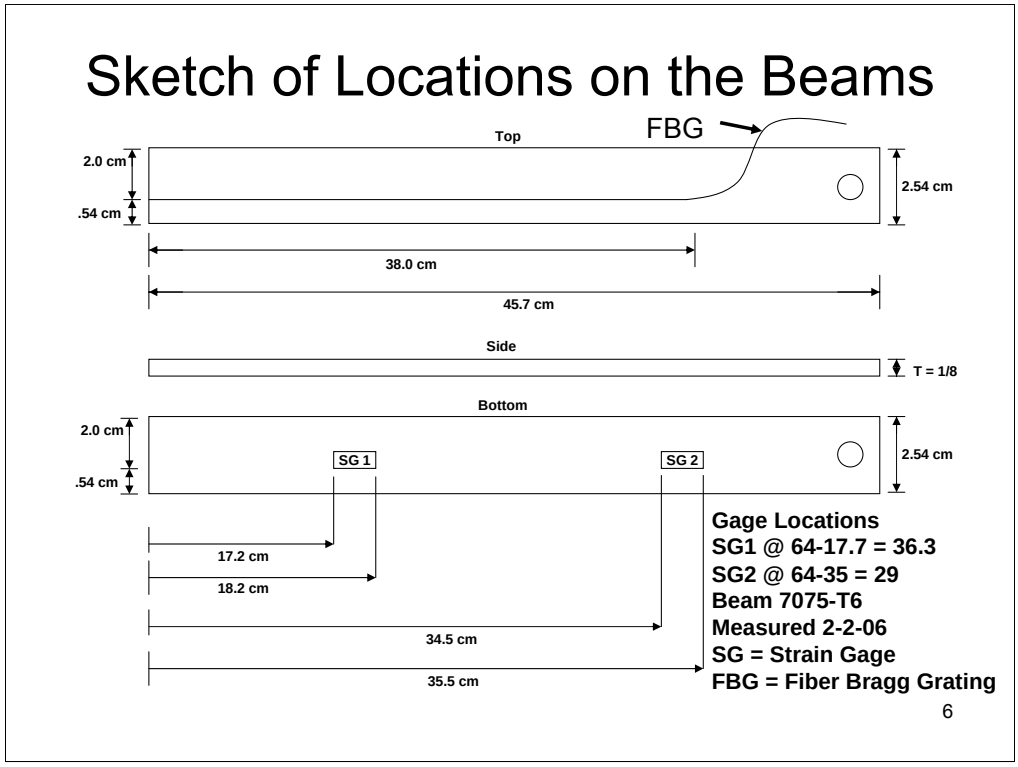

A sketch of the strain gages (SGs) and FBG sensor is shown above. The last FBG location is at about 65 cm on the left end of the beam. As show by the drawing, the strain gage 1(SG1) is at about fiber bragg grating location 37 and strain gage 2(SG2) is at about FBG location 29. Location 1-28 did not show strain during beam deflection since the FBG sensor was not attached for about the first 28 centimeters of the fiber.

Installation of SGs and FBG Fibers on the Three Test Beams

- FBG Installation
  - Installed by LUNA (Mike Nuckels)
  - Current fibers good for maximum of 1500 με
  - Used GA-2 adhesive to mount
- Strain Gage Installation
  - Accomplished by MLLP (Enrique Medina)
  - Type CEA-06-125UN-350 on Ti-6242
  - Type CEA-13-125UN-350 on Aluminum
  - Use M-BOND 200 Adhesive to Mount

7

As noted earlier, the FBG sensors were installed on the beam by Luna Innovations personnel using GA-2 Adhesive. Mr. Enrique Medina installed Measurement Group strain gages. He installed type CEA-06-125UN-350 on the Titanium beam and type CEA-130135UN-350 strain gages on the aluminum. These gages were obtained from VASV's available stock that were the closest match to the material coefficient of thermal expansion (CTE) of the beams. Mr. Enrique Medina used M-Bond 200 to mount the strain gages to the beam on the side opposite of the FBG sensor mounting.

Laboratory Beam Experiment Data Collection

8

Data were collected during the month of February 2006 as described in the following charts. VASV analyzed the data collected during these experiments with Excel and MATLAB® software development by MLLP.

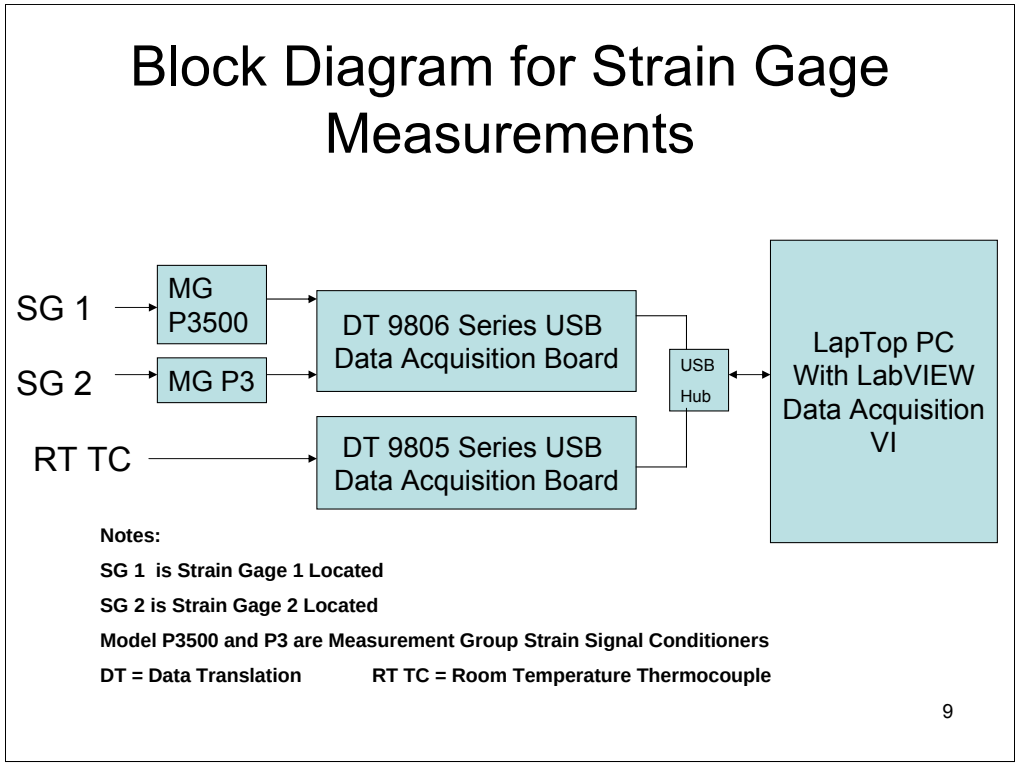

The block diagram for the data acquisition system used to measure the data from the strain gage is shown. The laptop PC used a AFRL/VASV developed LABVIEW® virtual instrument (VI) to collect data from the strain gage and thermocouples at a rate of 10 samples per second. In addition, VASV engineers used exisiting VIs to convert the raw binary data to Excel spreadsheet compatible files. Before beam deflection, the strain gage data acquisition system was started to record data for about 1200 seconds (20 minutes).

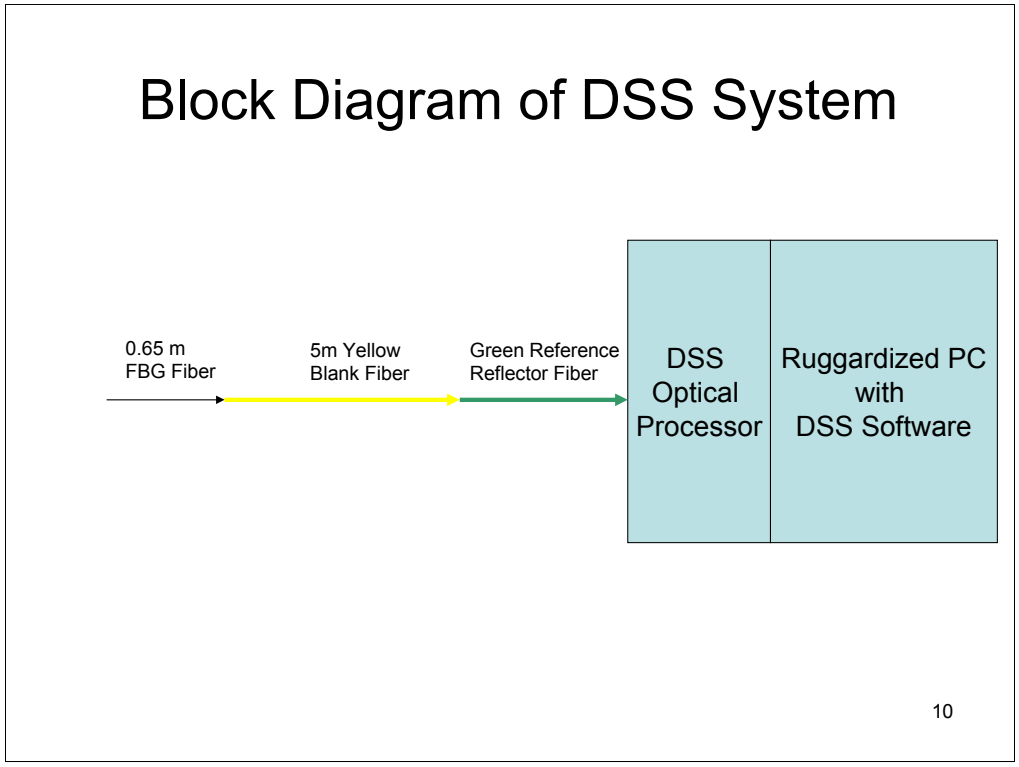

The block diagram for the Luna Innovations DSS system, used to measure the data from the optical FBG strain sensors mounted on the beams is shown above. The DSS system did all the conversion from optical light sensing using Optical Domain Frequency Reflectometry (ODFR) techniques and conversion to a strain measurement stored into an ASCII computer file on disk in the PC. The DSS acquisition rate was set for continuous before the start of the 20 minute recording for each beam deflection sequence. This file was then analyzed by compute programs such as Excel and MATLAB.

Bending 7075T6 Beam for FBG Tension Display on DSS System (10 Feb 06)

Bending 7075T6 Beam in Tension

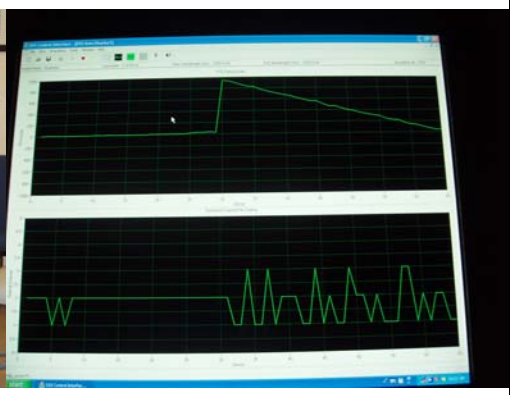

DSS System Displays Beam Tension

11

The beams were clamped on a lab workbench and loaded in bending and flexed to induce strain at a quasi-static rate. For example, the FBG sensor on top of the above beam is in tension while the SGs on the bottom of the beam are in compression. The FBG data and SG data were measured using different data acquisition PCs. The two PCs did not have a common time reference. It was decided to synchronize the FBG sensors and SG data by using the mechanical peaks induced by the manual deflection at the free end of the beam for comparison to evaluate the operation of the FBG sensors versus the conventional strain gages. For future experiments, VASV recommends either a Network Time Protocol (NTP) or a common time signal be recorded on both PCs.

For FBG measurements, the engineer must first ensure that the FBG sensor is initialized in accordance with the DSS User's manual before the first time of data collection. Once this initialization is complete, the fiber is usually zeroed before the start of each run. Operator instructions for the DSS system are in the User's Manual.

Note in the DSS display above that the maximum strain is indicated at the clamped edge of the beam as expected.

Log Sheets for Data Collection on Each Beam

Feb 10, 2006 7075-T6 Data Log for 20 Minute Test
GF = 2.125
2006-02-10-1003-24_0.00-1200.tim
7075t6-062110.txt

1. CAL Strain Gage(SG) 1 → 4699 → - 4 με
2. CAL Strain Gage 2 – 13 – **4728** – 9 με
3. Slow Tension < 1000 με ≈ ± 800 με
4. Slow Tension < 1000 με ≈ ± 800 με – Photo
5. Slow Compression < 1000 με ≈ ± 800 με
6. PLUCK 1 Tension Start ≈ 600 με to start
7. PLUCK 2 Compression Start ≈ - 700 με to start
8. PLUCK 3 Tension Start ≈ + 700 με to start
9. Slow Compression > 1000 με ≈ - 1000 με to start
10. Slow Tension > 1000 με ≈ t = 60 seconds
11. Hold 30 sec @ -1000 με
12. Hold 10 sec @ + 1000 με
13. CW&CCW Torsion at t = 818 seconds
14. Slow Tension ≈ 1000 με at t ≈ 1042 seconds
    Hold 10 seconds at peak and valley
    Photo taken
15. CAL SG 1 30→ 4730 → - 33 με at t ≈ 1100 seconds
16. CAL SG 2 19→ **4732** με stuck on calibrator

Feb 16, 2006 - TI-64 Data Log for 20 Minute Test
2006-02-16-1349-43_0.00-1200.00.tim
060216TI64Test1.TXT

1. Strain Gage(SG) 1 CAL - - 1→ 4840 → - 1 με
2. Strain Gage(SG) 2 CAL - + 1 → **4854** → 2 με
3. Slow Tension 1st – 0 → 1000 → 0 → - 1000 → 0 με
4. Slow Tension Repeat - 0 → 1000 → 0 → - 1000 → 0 με
5. Slow Compression 1st – 0 → - 1000 → 0 → + 1000 → 0 με
6. PLUKE 1 → i.e. Tension -Release – 0 → + 1000 με & release
7. PLUKE 2 + Compression-Release – 0 → - 1000 με & release
8. PLUKE 3 + Tension Release – 0 → 1000 με 4 release
9. Slow Compression → 0 → - 1500 → 0 → + 1500 → 0 με
10. Slow Tension → 0 → + 1500 → 0 → - 1500 → 0 με
11. Hold 30 Second Compression
    i.e. - 1000 με for 30 seconds then back to 0 με
    Hold 30 Second Tension
12. i.e. + 1000 με for 30 seconds then back to 0 με
13. CW & CCW – Torsion ➔ Very Low Level
14. Slow Tension First → 0 → 2000 με → 0 → - 1500 με → 0
    t=778 seconds
15. SG 1 Cal 0 → 4840 → - 1 με
16. SG 2 Cal 0 → 4854 → - 2 με t = 861 seconds
17. Slow Heat gun – t=870 seconds
    Pass gun from end center then back to end at t = 963
18. PLUKE 4 → - 1500 με PLUKE
19. PLUKE 5 → + 1500 με PLUC
20. SG1 → CAL → - 15 με 4825 με – 15 με
21. SG 2 → CAL – 15 με – 4840 με – 15 με

Feb 23, 2006 2024-T3 Data Log for 20 Minute Test
2006-02-23-1451-47_0.00-1200.00.tim
060223-2024-T3.txt

1. SG1 CAL – 1 → 4703 με → 1 με
2. SG2 CAL - -4 → **4712** με → 3 με (Turned off/on once)
3. Slow Tension 1st → 0 → + 1000 → 0 → - 1000 → 0 με
4. Slow Tension Repeat → 0 → + 1000 → 0 → - 1000 → 0 με
5. Slow Tension → 0 → + 1000 → 0 → - 1000 → 0 με
6. Slow Compression 1st → 0 → - 1000 → 0 → + 1000 0 → 0
7. PLUCK 1 → Tension Release → 0 → + 1000 με 4 release
8. PLUCK 2 → Compression Release → 0 → - 1000 με & release
9. PLUCK 3 → Tension Release → 0 → + 1000 με & release
10. Slow Compression → 0 → - 1500 → 0 → + 1500 → 0 με
11. Slow Tension → 0 → + 1500 → 0 → - 1500 → 0 με
12. Hold 30 sec Compression at – 1000 με
13. Hold 30 sec Tension at +1000 με
14. CW & CCW Torsion Lower Level
15. Slow Tension – 0 → 2000 με – 0 → - 2000 με → 0
    at t = 786 seconds
16. SG 1 CAL 1→ 4703 → 2 με
17. SG 2 CAL -3 → 4712 → -3 με
18. PLUCK 4 → - 1500 με → Release
19. PLUCK 5 → + 1500 με Release t = 1045 → 1128
20. Heat Gun Test at t = 1045 to 1128 seconds –
    Heat end to root of beam and then return
21. Did quick CAL 1 → 0 → 4702 → 0 με and
    CAL 2 → -3→ 4713 → -3 με

7075-T6 10 Feb2006 Ti-64 16 Feb 2006 2024-T3 23 Feb 2006

12

A log sheet of the manual deflection types conducted by the engineer were compiled as shown for the three beams. For example on the 7075-T6 beam, first an initial SG shunt calibration was recorded on the laptop PC for each of the two strain gages. Unfortunately, there is not yet a known way to do a shunt system calibration on the fiber sensor. Initially, the beam was slowly and manually moved through a cycle of tension to about 800 με and compression to about -800 με to induce one slow cycle of strain. In addition to additional tension and compression cycles, there were pluck and quick release events and other events as shown in the log sheets. The sample rate for the SG data acquisition system was 10 samples per second (sps) and the sample rate for the LUNA DSS system was approximately a maximum of 1.5 sps. This difference in sampling rate increased the difficulty of comparing the FBG and SG data.

Results from the 3 Beams

- 7075-T6 Beam on 10 Feb 06
- TI-64 Beam on 16 Feb 06
- 2024-T3 Beam on 23 Feb 06
- Results Presented using Excel
  - Time History of Strain Gages
  - Time History of FBG Sensors
- AVI Files of FBG Sensors using MATLAB®
- Merge FBG and Strain Files using MATLAB®

13

Based on the sequence of events, we can now look at the SG and FBG outputs from the three beams, 7070T6, TI-64 and 2024-T3. The following charts will show the time histories using Microsoft ® Office Excel spreadsheets. Next we will look at movie files (.avi files) for each of the three beams. Finally we will look at merges FBG and Strain Gage Files for comparison.

Time History of Strain Gage Sensors on 7075-T6 10 Feb 2006

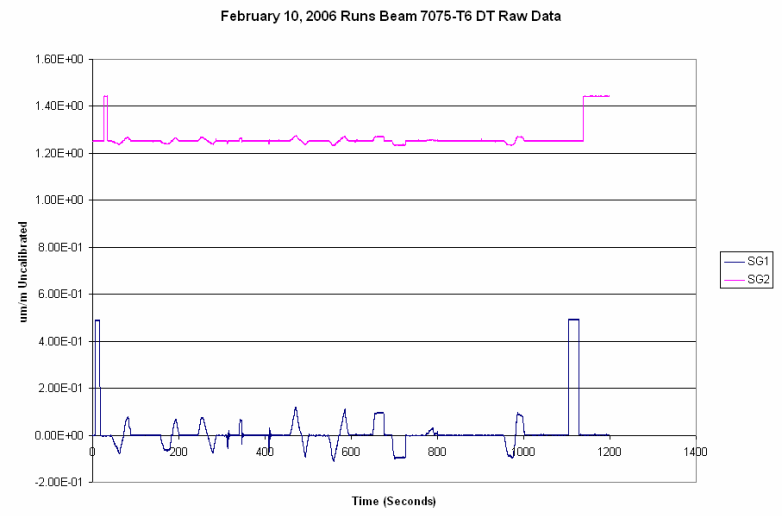

14

For the 7075-T6 test beam, we see here raw data for the two strain gages as plotted using Excel. Note that for both strain gages we still need to apply the calibration factors. One advantage of using the strain gage is that a shunt system calibration value can be applied (at the beginning and end of each recording) to each gage as showed in the log and the time histories. SG 1 uses the P3500 signal conditioner so has a 0um/m value of about 0 volts. The calibration data is applied for SG 1 for the MATLAB® routines developed by MLLP. Also for strain gage 2, the P3 signal gave a value of 1.2 volts offset for a strain level of 0 um/m. Also shown on the charts is the system shunt calibration (equivalent to about 4800 με) using the shunt calibration resistors built into the Measurement Group P3500 and P3 Strain Gage conditioners. Looking at the time histories, we can easily correlate the events in the logs with the cycles seen in the time histories.

Time Histories of FBG Sensors on 7075-T6 10 Feb 2006

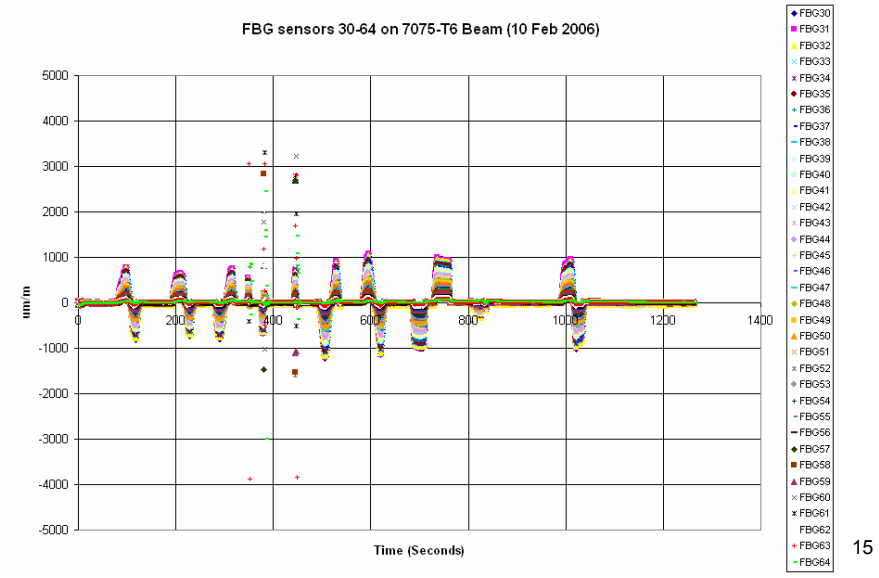

15

Above, we see a time history plot of the FBG sensors in locations 30 to 64 on the 7075 T-6 beams. Since the FBG sensors and Strain Gages are on opposite sides, we observe that the SG strains are 180 degrees out of phase from the measured FBG strains. In addition, the data in the DSS computer file has already done the necessary conversion to engineering units in a way transparent to the operator.

Time History of Strain Gages on Ti-64 16 Feb 2006

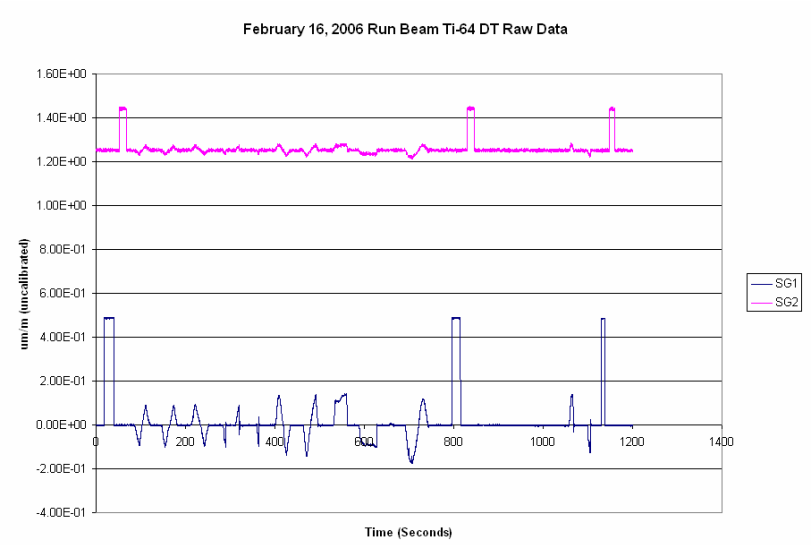

16

For the Ti-64 test beam, we see here raw data for the two strain gages as plotted using Excel. Again both strain gages need applications of the calibration factors. The system shunt calibration shown in the time log sheets can be applied to get true strain. Again, looking at the time histories above, we can easily correlate the events in the logs with the cycles seen in the time histories.

Time Histories of FBG Sensors on Ti-64 16 Feb 06

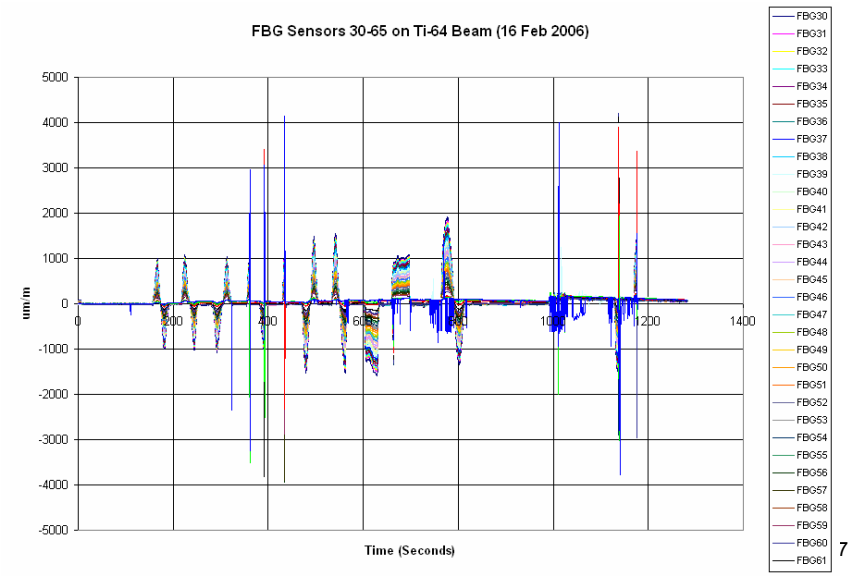

7

Above, we see a time history plot of the FBG sensors in locations 30 to 64 on the Ti-64 beam. Again, since the FBG sensors and Strain Gages are on opposite sides, we observe that the SG strains are 180 degrees out of phase from the measured FBG strains. For example, during the first SG cycle, the first indicates compression first and the FBG sensor indicated Tension first. Also, for location 64 at the root of the beam the strain is higher that at location 30 at the end of the beam. Again, FBG data in the DSS computer file is store in terms of engineering units (um/m).

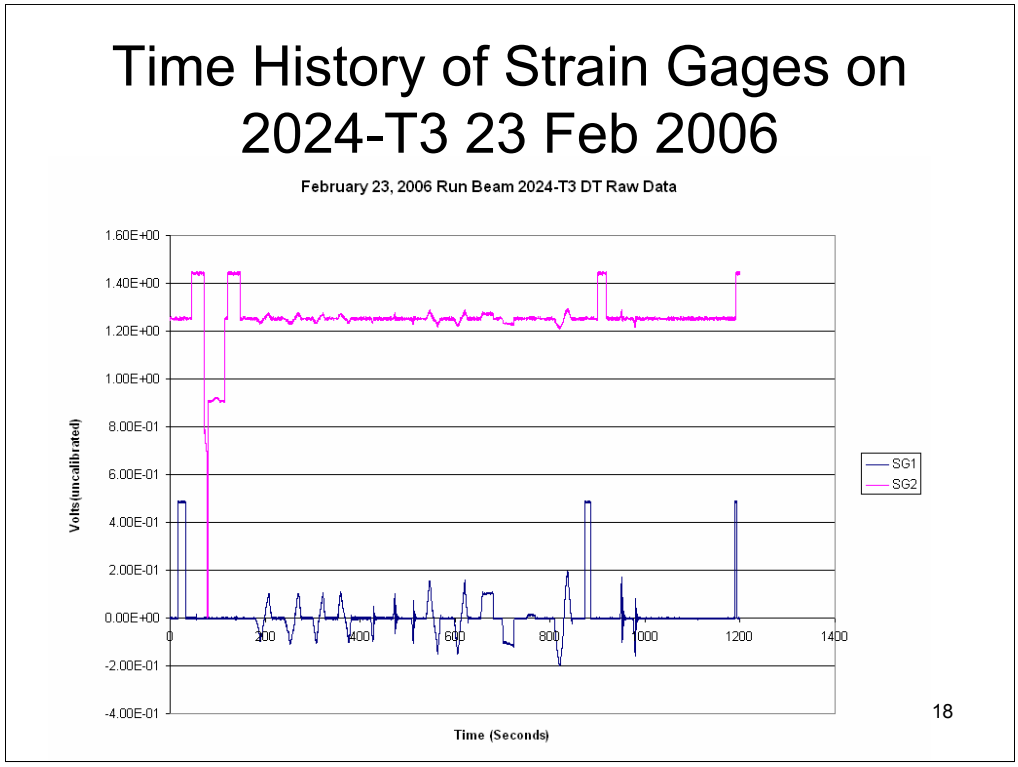

For the 2024-T3 test beam, we see here raw data for the two strain gages as plotted using Excel. Again both strain gages need applications of the calibration factors. The system shunt calibration shown in the time log sheets can be applied to get true strain. Again, looking at the time histories above, we can easily correlate the events in the logs with the cycles seen in the time histories.

Time Histories of FBG Sensors on 2024-T3 23 Feb 2006

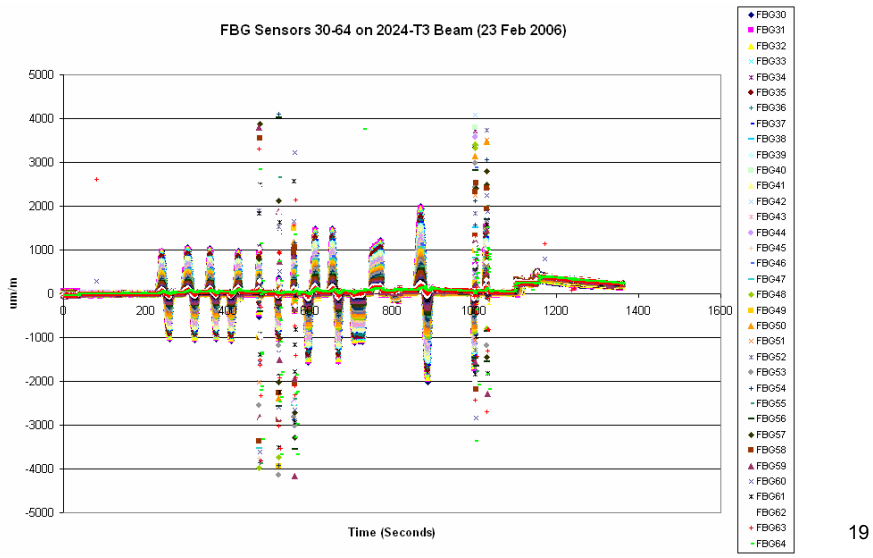

19

Above, we see a time history plot of the FBG sensors in locations 30 to 64 on the 2024-T3 beam. Again, since the FBG sensors and Strain Gages are on opposite sides, we observe that the SG strains are 180 degrees out of phase from the measured FBG strains. For example, during the first SG cycle, the first indicates compression first and the FBG sensor indicated Tension first. Also, for location 64 at the root of the beam the strain is higher that at location 30 at the end of the beam. Again, FBG data in the DSS computer file is stored in terms of engineering units (um/m).

Also, note that in the above figure we can see the effect of the heat gun as it passed over the fiber as indicated in the log for the 2024-T3 beam. This indicates that more study is needed on the operation of the FBG sensor at other than room temperature.

Comments on Raw Time Histories

- Strain Gage Data Acquisition System
  - Shunt calibrations available
  - Need to validly convert volts to microstrain
  - Certain sample rate
    - 10 Samples per Second (i.e. 0.1 Second between Samples)
- FBG Data
  - System converts files to engineering units
  - Uncertain sample rate
    - 1.488 to 1.54 Samples per Second during 7075-T6 run
    - i.e. 0.656 to 0.672 seconds between samples
  - Hard to convert time to seconds
  - Excel not usable for files with more that 255 sensors
- Need to synchronize start times

20

From a measurement view point there are advantages and disadvantages of each system. For the strain gage system, we can apply shunt calibrations to get a system calibration. Also, the LabView VI used to collect data samples the data at an exact rate of 10 samples per second or one sample every .1 second.

It is necessary to convert volts to engineering units using the LabView or Excel software.

For the FBG Data, the DSS system does all the signal conditioning and stores the data directly to the computer in terms of engineering units. There is some uncertainty on what the exact sample rate will be. For example in continous, time sampling on the DSS the time between samples varied from .656 to .672 seconds (1.524 to 1.488) for collection of data on the 7075-T6 Beam on 10 February. In addition, it was not a straight forward process to convert the DSS time code into seconds.

An method to synchronize the start time between the two data systems would also be helpful.

Lastly, for bigger fibers, there may be more that 255 locations which is greater than Excel software can currently handle.

Develop MATLAB® Routines

- Need to Merge Raw Time History Files
  - Read FBG data and SG data and merge
  - Initial start time (Recommend NTP server)
  - Different and uncertain sample rates
    - i.e. hard to set as multiples of each other
  - Difficult and time consuming in Excel
  - Request to ML to develop MATLAB® routines
- Get Better Representation of FBG Data
  - Generate video files from FBG data

21

To compare the data, it is necessary to merge the SG files and the FBG files. AFRL/MLLP (Enrique Medina) developed MATLAB® software routinges to merge the strain gage files from the laptop PC and the FBG data files to a common time base. Then the data can be compared between the FBG and the SGs for desired events in the two strain time history records. The data are synchronized by matching the peak reading from the FBG sensors with the peak readings from the SGs. In addition the conversion to engineering units was applied to SG1 based on the system calibrations. This can be done for all the events of each beam, but for this report, the comparison is done only for the first recorded cycle. This gave reasonable results, but there is still some concern about the different sampling rates.

An NTP server would help synchronize the start time between the two data systems but would not easily eliminate the complexities due to the differences in sampling rates.

Also as shown earlier, looking at multiple FBG locations using Excel did not provide very easy to read displays. MLLP offered to write very useful MATLAB programs to generate video files recreating the sequence of events for the 3 test beams.

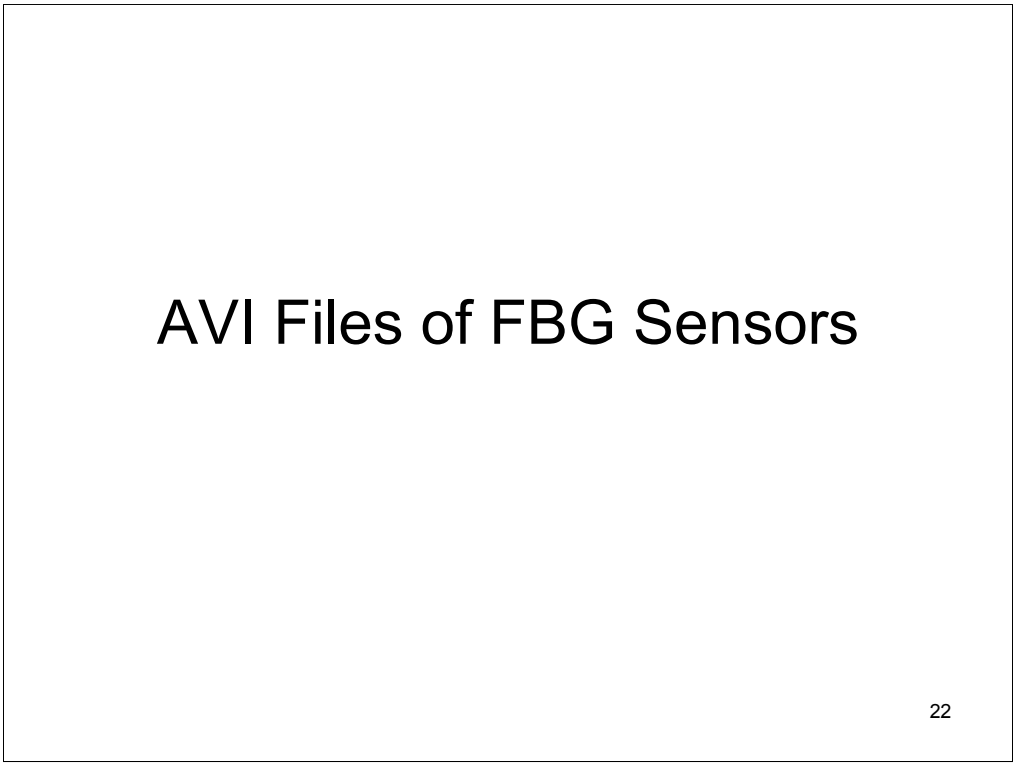

The following video files can be viewed and the events easily compared to the sequence of events in the logs for the three beams.

Video of Beam 7075-T6 Events

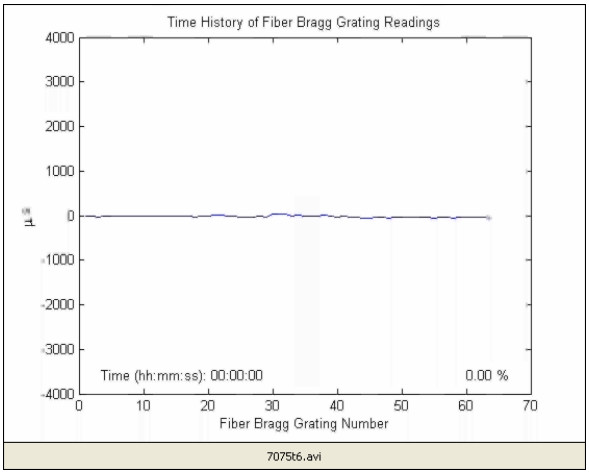

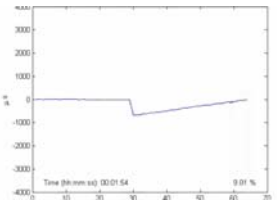

Single Frame Showing Beam Compression

23

This video shows the sequence of events for the 7075-T6 beam.

Note that for the first event we see a maximum of 800 με tension and then 800 με compression as indicated on the log sheet. One can easily trace all the events showed in the log sheet. Again, the strain distribution across the beam is easily seen. For the still frame shown during beam bending to create compression, one can easily see the strain distribution along the length of the beam.

Video of Beam TI-64 Events

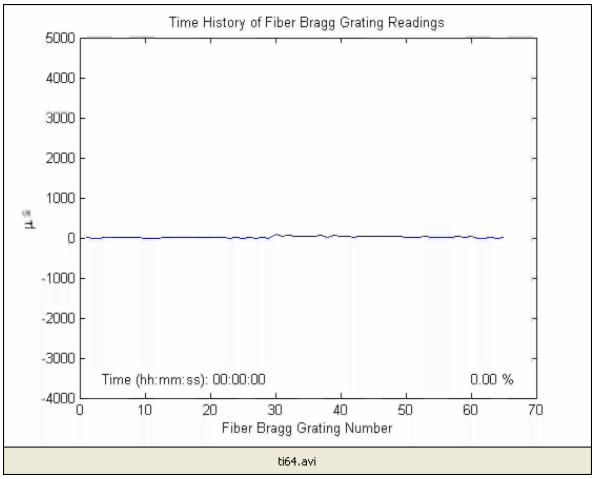

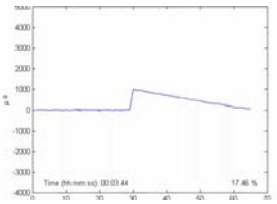

Single Frame Showing Beam in Tension

24

This video shows the sequence of events for the TI-64 beam.

Note that for the first event we see a maximum of 1000 με tension and then 100 με compression as indicated on the log sheet. Again, one can easily trace all the events showed in the log sheet and again, the strain distribution across the beam is easily seen. For the still frame shown during beam bending to create tension, one can easily see the strain distribution along the length of the beam.

Video of Beam 2024-T3 Events

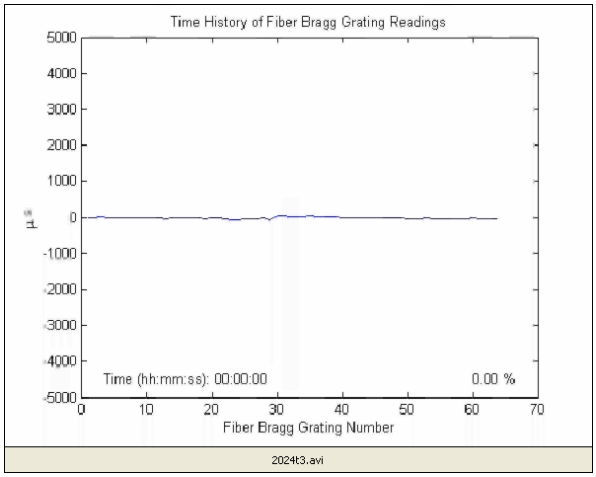

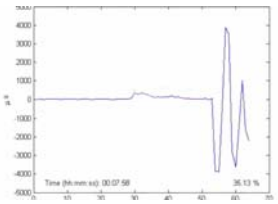

Single Frame Showing a Beam Pluck Event

25

This video shows the sequence of events for the 2024-T3 beam.

Note that for the first event we see a maximum of 1000 με tension and then 1000 με compression as indicated on the log sheet. Again, one can easily trace all the events showed in the log sheet and again, the strain distribution across the beam is easily seen. At the end one can also see the result on the FBG fiber as a heat gun is passed back and forth across the beams. For the still frame shown for a pluck event, more study is needed to explain the resultant response.

Merging FBG and Strain Time History Files using MATLAB®

- Beta Version of m files by Enrique Medina
  - Read FBG Data
  - Read SG Data
  - Merge Data
  - Plot Data
- Need to refine SG2 = Ch 8 still 1.2 VDC
- Merged Data-Plot FBG # versus SG1
  - Looking for slope close to 1

26

The difficult task of merging the FBG and SG files is being undertaken by Enrique Medina. To date we can present the following plots for this report.

The MATLAB® m-files can read the FBG data and the SG data and merge them into a new data file so that different FBG locations can be plotted versus SG 1. Future modifications include fitting the best fit straight line (BFSL) and slopes for the plotted data to see when FBG location versus SG1 give the slope closest to one. From the drawing we expect FBG #37 to give the best results. In the following plots, FBG #34 seems to give the best results.

More software refinements are needed to determine the BFSLs and the correlation coefficients and can be done at a later date. Also, the deviation and apparently slight hysterisis in the following comparison may be attributed to the differences in sampling rates.

Merging FBG and Strain Files using MATLAB®-7075 T-6

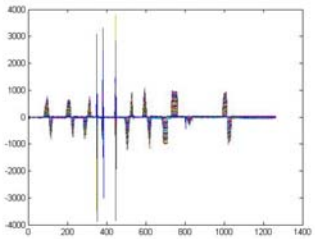

TH of all FBG Sensors on 7075T6

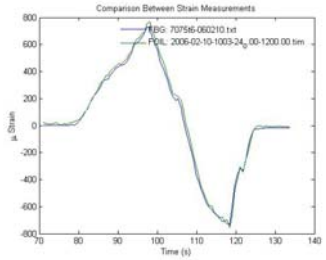

Comparison of FBG Sensor 34 and SG1 Inverted

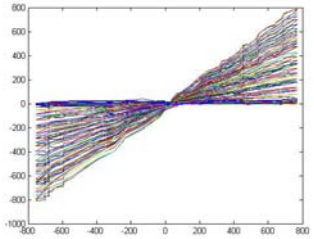

Plot of FBG Sensor 2-65 vs SG1 Inverted

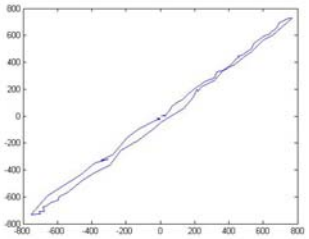

FBG34 vs -SG1 (Slope Closer to 1 than FBG 37)

27

The above plots show some of the displays used to merge the data for the first tension-compression event for the 7075-T6 beam. The plot in the upper left shows the time history for all the FBG sensors. The time histories for SG1 look similar to the raw data plots shown earlier except now the units are in με (um/m). In addition the sign of SG1 is inverted since it is 180 degrees out-of-phase from the FBG data. By utilizing a pick and select process for an event, the engineer can get a overlaid plot of the FBG and the SG1 as shown for the first compression event for beam 7075-T6 in the top right plot. The plots overlay nicely. The lower left plot shows all of the FBG sensors versus SG1. FBG34 looks like it has a slope close to one.

Merging FBG and Strain Files using MATLAB®- TI-64

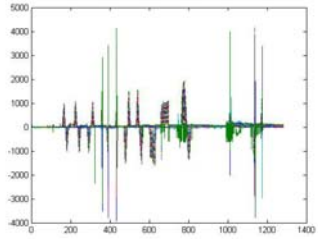

TH of all FBG Sensors

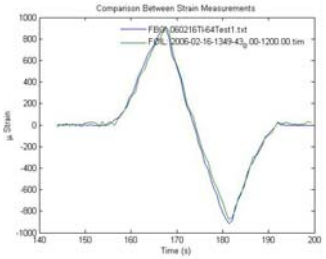

Comparison of FBG Sensor 34 and SG1 Inverted

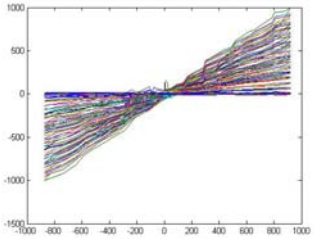

Plot of FBG Sensor 2-65 vs SG1 Inverted

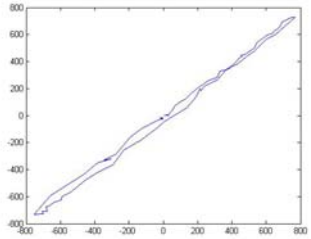

FBG34 vs -SG1(Slope Closer to 1 than FBG 37)

28

The above plots show some of the displays used to merge the data for the first event for the Ti-64 beam. The plot in the upper left shows the time history for all the FBG sensors. The time histories for SG1 look similar to the raw data plots shown earlier except now the units are in um/m. In addition the sign of SG1 is inverted since it is 180 degrees out-of-phase for the FBG data. By utilizing a pick and select process for an event, the engineer can get a overlaid plot of the FBG and the SG1 as shown for the first compression event for beam TI-64 above. The plots overlay nicely. The lower left plot shows all of the FBG sensors versus SG1. FBG34 looks like it has a slope close to one.

Merging FBG and Strain Files using MATLAB®- 2024-T3

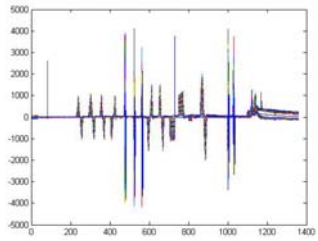

TH of all FBG Sensors on 7075T6

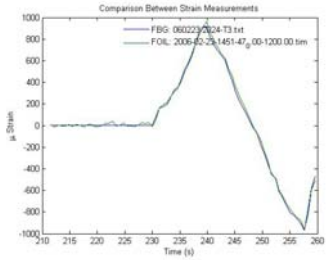

Comparison of FBG Sensor 34 and SG1 Inverted

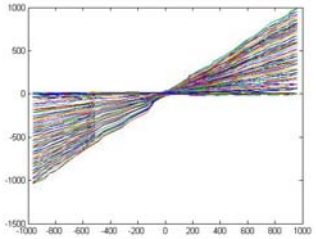

Plot of FBG Sensor 2-65 vs SG1 Inverted

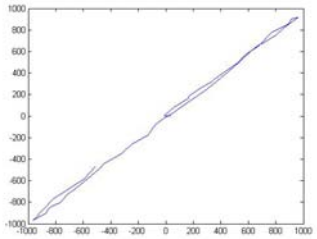

FBG#34 vs -SG1(Slope Closer to 1 than FBG 37)

The above plots show some of the displays used to merge the data for the first event for the 2024-T3 beam. The plot in the upper left shows the time history for all the FBG sensors. The time histories for SG1 look similar to the raw data plots shown earlier except now the units are in um/m. In addition the sign of SG1 is inverted since it is 180 degrees out-of-phase for the FBG data. By utilizing a pick and select process for an event, the engineer can get a overlaid plot of the FBG and the SG1 as shown for the first compression event for beam TI-64 above. The plots overlay nicely. The lower left plot shows all of the FBG sensors versus SG1. FBG34 looks like it has a slope close to one.

Concerns

- DSS Slow Sampling Rate (1.5 SPS Max)
- Sample Rate in File does not match Setup
- Hard to Synchronize LUNA PC with SG PC
  - SG PC 10 SPS Exact -LUNA Sample Rate Uncertain
  - Time Code hard to convert to seconds
- Maximum Sensors in Excel is 255
- Need to Zero at Start of Each Run
  - Software Appears to Remember Last Condition
- Need Calibration Techniques?
- Evaluations need at Different Temperatures

30

Currently the DSS system's slow sampling rate restricts it's use to quasi-static structural test. Also the DSS sample rate does not appear to match exactly the rate entered in the setup. The DSS time should be synchronized to data in other data systems for comparison. For example on a recent VASV tests, only hand signals were used to set data acquisition clocks and the DSS clocks. Better time synchronization techniques such as NTP need to be utilized. Without good time synchronization, a larger time burden is placed upon the data processing end of comparing FBG data with other sensors such as strain gages, load cells, and thermocouples.

Right now the large number of sensors measured by the DSS system are not easily handled by Microsoft Excel. Thus special routines and thought processes need to be developed.

Also, the DSS User's manual suggests that FBG sensor be zeroed before each measurement. VASV is unsure how to handle possible cumulative stress issues. In addition the software appears to remember when it left off during the last record.

There are no recommended calibrations techniques other than comparison of FBG sensors with strain gages. Research should be conducted to develop new calibration techniques to check the fiber at know strain levels. Also further evaluations need to be conducted to look at the impact of temperature (i.e. apparent strain) on the FBG fibers and potential thermal compensation methods.

Conclusions

- DSS System Impressive
  - Beam Results only at Room Temperature
  - Provides Many Strain Sensors on a Fiber
  - Provides View of Stain Distributions
- Low Installation Labor Time
  - 30 SGs x 3-1/2 hours = 105 hours
  - 1 FBG sensor with 30 sensors = 2 hours
- Improve Rates, Zeros, Synchronizing, Calibration
  - Hard to Compare FBG sensors with sensors
  - Need to implement NTP Server
- VAS should purchase this extremely useful tool

31

The DSS system is a very impressive way to measure strain. So far only beam results at room temperature are evaluated, but the FBG sensors provides many strain sensors on a single 125 um diameter fiber and displays strain distributions with a minimum amount of labor time. One of the big advantages is the reduced labor time to install many sensors. For example, VASV estimates about 3.5 hours per SG installation which results in a total of 105 hours for 30 SGs. For the FBG fiber only about 2 hours of installation time is required.

Suggestions include increased sampling rates, retaining cumulative strain, synchronizing time and developing system end-to-end calibration techniques. Utilizing an NTP server may help to make it easier to compare FBG sensors with other structural measurement sensors.

VAS should definitely consider purchasing its own DSS system for future structural tests.

Future Planned Work

- Appears Successful on recent VASV SIXA Test
  - 2.5 meter fiber on AL (244 strain Locations)
  - 5.0 meter fiber on Astro-Quartz (321 strain locations)
  - Mechanical Strain up to 4500 με
  - Temperatures from -160 to 60°F(-51.1 to 71.1°C) .
- Will use on Master Thesis Test of Steel Blocks
- Return DSS system to ML in December
- Pursue Purchase of DSS System for VAS

32

In addition to evaluation of the provided beams, the MLLP loan of the DSS system allowed VASV to evaluate the FBG sensors on the SIXA test program to record 244 strain sensors on Aluminum and 320 strain sensors on astro-quartz during mechanical loading up to 4500 με and temperature cycling from -60 to 160 °F (-51.1 to 71.1°C). A new laboratory version of this unit would cost $135,000 if purchased directly from Luna, which is more that VASV has in it current instrumentation budget. The current return date for the DSS system is 1 December 2006, so if possible some more data will be taken on some tests of steel blocks for VASM.

References

- SBIR Topic AF# SD01-CBM04
- LUNA Draft Marketing Manual
- Luna Innovations, Inc, (2006) The Flight Capable Distributed Sensing System User's Manual Revision Version 4.0, Blacksburg, VA.
- Medina, Enrique MATLAB Software Routines
- Banaszak, Kretz, Fisher, (2006) " Exploring Fiber Optic Strain Sensors for Testing Future Aerospace Structures ", 22nd Transducer Workshop, June, Forth Worth, TX.
- Banaszak, D. and Kretz, Larry , 2005, "Lab Evaluation of Fiber Optic EFPI Sensors for Extreme Environment Tests", ASA 2005 Proceedings of the Section on Physical and Engineering Sciences,,Minneapolis, MN, 7-11 August 2005.

33

A brief summary of suggested references is show above. The last two papers give an overview of past evaluations of using fiber optic EFPI and FBG sensors by AFRL/VASV.

Acknowledgements

- AFRL/VAS

  Ray Fisher, Larry Kretz, Hannah Peterson,

  Dave Preston Mason, Chris Thompson, RickRolfes, Cindy Swanson, Rob Reuter, Doug Schneider, Melissa Rihm, Tim Smith, Bill Baron
- Luna Innovations, Inc.

  Mike Nuckles, Trevor Rice, Roger Duncan
- Special Thanks to AFRL/MLLP

  Lt. William Freemantle, Enrique Medina

34

Special thanks is extended to the above persons for their help, advice and support in completing this evaluation. Special thanks are extended to the fine personnel in AFRL/MLLP who allowed VASV to experiment with their newly develop DSS system and help develop software to process the data.

Section 3.10

Evaluation of a Distributed Sensing System with Simple Bending Beams

Presentation by Enrique Medina at 2ND DESS

DESS = Dayton Engineering Sciences Symposium
At Wright State University, Fairborn OH
October 30, 2006

(NOTE: In the digital version of this report, see original PowerPoint attachment, 2NDDESS.ppt)

Exploring Fiber Optic Strain Sensors for Testing Future Aerospace Structures

Air Force Research Laboratory
Air Vehicles Directorate-Structures Division
Wright Patterson AFB, OH
David.Banaszak@wpafb.af.mil
Larry.Kretz@wpafb.af.mil
Burton.Fisher@wpafb.af.mil

June 20, 2006

22nd Transducer Workshop - Forth Worth, TX

Texas Christian University

Thanks for Allowing us to participate in this 22nd Transducer Workshop.

- It is always a privilege to be a speaker here. This paper will provide an overview of current work by AFRL/VAS in the area of evaluating and using fiber optic strain sensors. Some of the High Temperature Work were summarized in a paper given by Banaszak and Kretz(2005) at the 2005 Joint Statistical Meeting in Minneapolis, MN during August, 2005.

The talk will discuss

(1) Specimen tests of high temperature EFPI sensors,

(2) Heat and mechanical testing using the EFPI fibers on a structural test item,

(3) Thermal environmental testing (-60 to +160F) of COTS EFPI strain sensors and strain gages mounted on astro quartz and graphite,

(4) And initial evaluation of FBG sensors on test beams and an aluminum structural test item.

Exploring Fiber Optic Stain Sensors

- **Current AFRL Fiber Sensor Evaluation Efforts**
- **Extrinsic Fabry-Perot Interferometer (EFPI) Sensors**
  - **Specimen test using Aluminum and C-C coupons subjected to high temperature using different adhesives.**
  - **To measure strain on structures experiencing temperatures up to 2000ºF (1093.3 ºC)**
  - **COTS sensors specified to 350 ºC.**
- **Fiber Bragg Grating (FBG) sensors**
  - **Supplement conventional strain gages.**
  - **Provide many strain measurements on a single fiber.**
- **Present Plans, Efforts, and Results to Date.**

ABSTRACT: AFRL engineers are evaluating high temperature instrumentation including Extrinsic Fiber Fabry-Perot Interferometer (EFPI) fiber optic sensors for measuring strain on structures at temperatures up to 2000 ºF (1093.3 ºC) under applied mechanical loads. AFRL is also evaluating Fiber Bragg Grating (FBG) fiber optic sensors for measuring multiple strains using one fiber. This presentation will review recent AFRL laboratory test results using fiber optic strain sensors. The presentation will also describe new AFRL testing capabilities for testing fibers mounted on test specimens subjected to high temperatures and mechanical loads and the new thermal spray capability for in-house investigation of attachment techniques for fiber, thermocouples, strain gages and other high temperature instrumentation since often standard adhesive techniques fail due to extreme thermal environments as encountered in reentry vehicles and hot jet engine exhaust of high performance aircraft. The EFPI sensors utilize gold coated optical fibers to hand make sensors that measure gaps (L) of 30-80 μm (1.18-3.15 mil) between in-line fibers in a quartz tube. Technicians attach the fibers to the structures at end points using thermal spray techniques or high temperature adhesives to provide a gage length (GL). Using the measured change in gap (ΔL) the strain is determined as strain (ε) = ΔL/GL. FBG fibers utilize etched gratings that reflect at specific wavelengths of light. The reflected wavelength of each grating period responds to thermal and mechanical environmental changes. AFRL is investigating the many control variables that affect the performance and uncertainty of these sensors for high temperature strain measurement on future aerospace structures by performing in-house experiments using fiber optic sensors mounted on advanced materials and test objects.

Introduction to EFPI Sensors

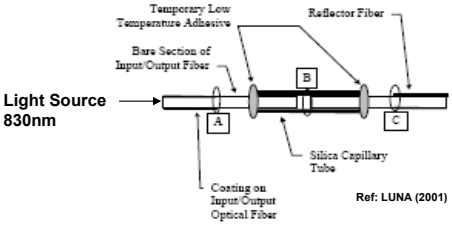

- **EFPIs consist of reflector and incoming fiber in quartz tube**
- **Bond to specimen with high temperature adhesive or flame spray**
- **Distance between attachments is gage length (GL)**
- **Nominal gap in tube is 50μm (1.97 mil)**
- **Multiple light waves reflect from the incoming and reflector fibers**
- **Interference pattern is used to measure the gap length (L)**
  - **Gap varies between 30-80 μm (1.18-3.15 mil)**
- **EFPI conditioner output is an analog voltage proportional to strain**
- **Strain =ΔL/GL, where ΔL is the change in gap length**
- **Strain unit-less- often expressed in microstrain(με) = (ΔL/GL) x 10^{-6}**

EFPIs consist of a fiber reflector and an incoming fiber, which are threaded through a quartz tube and bonded to the test specimen using a high temperature adhesive or flame spray technique. The distance between the fiber attachment points on the test specimen is known as gage length (GL). The fibers within the tube are separated by a nominal gap of 50μm (1.97 mil). As the operator sends a light source down the incoming fiber, multiple light-waves reflect between the incoming and reflector fibers. The result is an interference pattern that can be used to measure the gap length (L), which varies between 30-80 μm (1.18-3.15 mil) as the test specimen expands or contracts due to stress and thermal loads. EFPI signal conditioner output is an analog voltage proportional to the strain (ΔL/GL, where ΔL is the change in gap length). Strain is a unit-less quantity that is usually expressed in terms of microstrain, (i.e. microstrain = με = (ΔL/GL) x 10-6). Yu and Yin (2000) provide explanations of interferometer measurement techniques. Beyond the basic theory, there are many variables involved. Some of these variables are the type of fiber material, installation techniques, and adhesives. Control variables include test type, specimen material, specimen shape or size, attachment techniques, fiber and strain gage location, specimen side, test temperature, maximum test strain, and atmosphere.

Introduction To EFPI Studies

- **Extreme aerospace environments up to 3000˚F (1648.9ºC)**
- **Above 1800 ºF (i.e. gold's melting point) Bhatia, V, Green, J., et. al. (1996) experimented with sapphire fibers**
- **Bhatia, V., Greene, J., et. al. (2000) outline theory of an EFPI extensometer and describe equations to determine the gap**
- **EFPI sensor manufactures can provide technical details:**
  e.g. Luna, Blue Road, and Fiso
- **AFRL engineers examining EFPI sensors' potential to measure strain on aerospace at temperatures up to 2000 ºF (1093.3 º C).**

Shull and Wright (2002) discuss the use of conventional strain gages designed for dynamic strain measurements for extreme environments. Poland (2002) discusses fiber optic strain gage techniques and applications. Luna Innovations (2001) discussed the theory of commercial extensometer EFPI strain sensor operation. This commercial sensor operates at temperatures up to 350ºC (662ºF). However, extreme aerospace thermal environments often require operations at temperatures up to 2000ºF to 3000˚F (1093.3ºC to 1648.9ºC). Therefore, Piazza (2004), Moore (1997), Moore and Hart (2002), and Hart and Moore (2000) attempted to extend the temperature range of commercial EFPIs during numerous experiments at the National Aeronautics and Space Administration (NASA) Langley Research Center (LARC) and NASA Dryden Flight Research Center (DFRC). They manually fabricated EFPI extensometers using Luna-manufactured gold plated optical fibers with a Nextel jacket, quartz tubes, and new attachment techniques. For temperatures above 1800ºF (i.e. gold's melting point) Bhatia, V, Green, J., et. al. (1996) experimented with sapphire fibers. Bhatia, V., Greene, J., et. al. (2000) outlined the theory behind an EFPI extensometer and described the techniques and equations to determine the gap between the two fiber pieces. In addition, EFPI sensor manufactures, such as Luna, Blue Road, and Fiso, provided technical details

Building upon this work, AFRL engineers are examining EFPI sensors' potential to measure strain on aerospace structures at temperatures up to 2000ºF (1093.3ºC).

Preliminary Thermocouple Tests

- **July 2004**
- **Used ceramic adhesive Zircon Potting Cement No. 13 to bond K-type thermocouples (TCs) to Carbon-Carbon (CC) flame sprayed with a base coat**
- **Subjected TC attachments to 2000ºF (1093.3ºC) in approximately 40,000 seconds (about 11.1 hours)**

- **August 2004**
- **Sauereisen 13 successfully bonded about 40 thermocouples simultaneously to a CC test Article**

A prerequisite for full EFPI evaluation is finding reliable methods of bonding the EFPI sensor to the test structure at high temperatures. During preliminary experiments in July 2004, AFRL engineers used the ceramic adhesive Zircon Potting Cement No. 13 (made by Sauereisen and known as Sauereisen 13) to bond several K-type thermocouples to Carbon-Carbon (CC) material flame sprayed with a base coat by Roth (2004). Next, they subjected the attachments to temperatures up to 2000ºF (1093.3ºC). The temperature profile increased to 2000ºF (1093.3ºC) in approximately 40,000 seconds (about 11.1 hours). Sauereisen 13 also successfully bonded approximately 40 thermocouples simultaneously to a CC test article during August 2004.

Overview

- **2 methods of bonding EFPI Sensors**
  - **flame spray**
  - **high temperature adhesives**
- **Estimate GL by formula:**
  - **GL= (2*inner+outer)/3,**
  - **"inner" and "outer" are distances in millimeters (mm) of the end attachment bonds**
- **e.g. Adhesive Mount on Item 4 (C-C)**
  GL = (2*6.056+9.294)/3 = 21.406/3 = 7.135 mm (.281 inches)

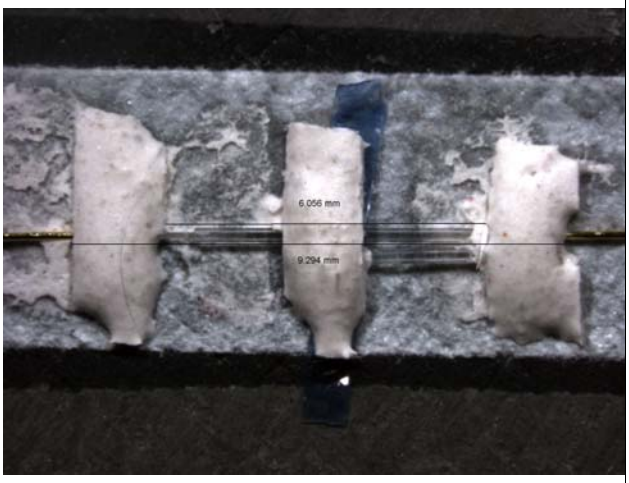

This figure is a close up view of a Sample Adhesive Mount of EFPI Sensor on Test Item 4 (CC). Fiber 3 is shown. This chart gives an overview of EFPI Strain Sensor Mounting and Installation Techniques. Engineers are exploring two methods of bonding EFPI sensors to test materials: flame spray techniques and high temperature adhesives. AFRL is still developing flame spray capabilities. AFRL engineers developed an in-house flame spray capability facility, which became operational during December 2005. Meanwhile, they are experimenting with using ceramic adhesives, like Sauereisen 13, to attach the EFPI sensors. For their initial attempts, AFRL engineers bonded EFPI sensors to Aluminum and CC using Sauereisen 13. The photograph shows initial attempts to mount the EFPI sensors.

Engineers estimated GL by using the formula GL= (2*inner+outer)/3, where "inner" and "outer" are the inner and outer distances in millimeters (mm) of the end attachment bonds. Luna (2001) recommends this formula when bond widths at the end points are not an infinitesimal point. In Figure 2 above, the GL = (2*6.5+10.0)/3 = 23/3 = 7.67 mm (.302 inches), where the inner distance is 6.5 mm (.256 inches), and the outer distance is 10.0 mm (.394 inches).

AFRL Requirements and Past Results

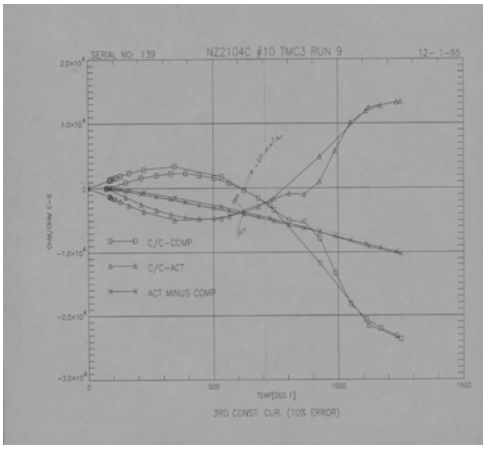

- **Engineers expect temperatures exceeding 1832ºF (1000ºC) in extreme thermal environments and high vibratory strain loads**
- **High apparent strain curves obtained using valid strain measurements at temperatures up to 1250 ºF (667.7 ºC)**
- **Convert ΔR/R to strain by using the strain gage factor (GF) for conventional resistance gages**

Apparent Strain-Conventional Gages (1 Dec 95)

This figure (make on December 1, 2005) shows typical apparent strain results using Conventional Strain Gages). Engineers expect temperatures exceeding 1832ºF (1000ºC) on structures experiencing extreme thermal environments and high vibratory strain and loads. For example, a conventional foil strain gage will be incinerated when heated to 1600ºF (871.1ºC). A conventional foil strain gage is limited to 550ºF (287.8ºC) continuous, 700ºF (371.1ºC) for short term such as seconds. The figure illustrates the output of a high temperature free filament strain gages. The data presented shows the output of each leg of the strain gage, active and compensating as well as the combined results. Note, the extremely large output of the active gage, and yet when combined with the compensating gage, there is still significant apparent strain signal that has to be corrected. High temperature, free filament gages can be heated and corrected to 1600ºF (871.1ºC), however as illustrated in the figure, a practical valid strain measurement for compensated gages should be limited to 1250ºF (676.7ºC). Apparent strain is expressed as ΔR/R and is converted to strain by using the appropriate strain gage factor (GF) used for conventional resistance gages.

Lab Test Measurement System

- Acquired data using a read data virtual instrument (VI)
- Sampled each channel 10 times per second.
- VI “overlayer” creates Microsoft® Excel readable file.
- Import data to Excel-generate time history and apparent strain plots

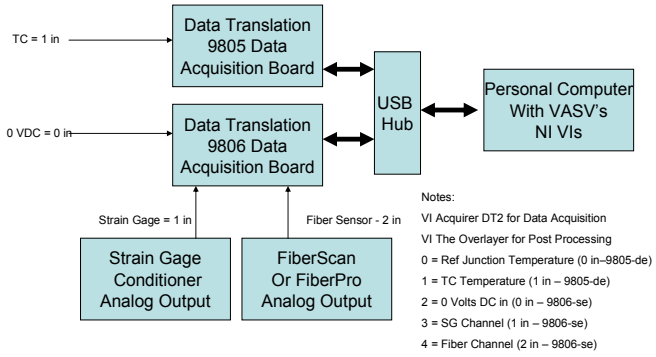

The quick response measurement system in these tests used a personal computer USB data acquisition board, designed by AFRL personnel, that measured outputs from the fiber optic signal conditioners, strain gage conditioners, and thermocouples in a timely manner. AFRL engineers acquired the test data using a read data virtual instrument (VI), which sampled each channel 10 times per second. They then used a VI titled “overlayer” to create an ASCII and Microsoft® Excel readable file. Finally, they imported all the data into an Excel workbook to generate time history and apparent strain plots. Engineers did not use anti-aliasing filters; however, these filters are highly recommended for a sampling based data acquisition system. For the oven portion of this test, engineers used a VAX based data acquisition system to record data from the thermocouples and strain sensor signal conditioners once per second.

Preliminary Design of Experiments (DOE)

Experimental Outputs

1-Correlation between EFPI and Strain Gages at room temperature using bending and axial loading

2-Apparent Strain Curves up to 1600ºF (871.1ºC)

3-Combined Strain Correlation & Apparent Strain at high Temperature

Test Items

1 - rectangular Aluminum 2024 (1.5 x 8.25 "(38.1mm x 209.6mm))

2 - rectangular CC-1 (1.25 inches x 4 inches (31.8mm x 101.4mm))

4 - round CC (69.8mm in diameter)

Engineers needed experiments that validated the correlation between conventional strain gages and EFPI sensors at room temperature, high temperatures, and under in-plane and out-of-plane mechanical loading (bending). A Design of Experiments (DOE) was the ideal solution because many control variables were required to account for all possible strain output signal variations. Ideally, engineers should use a checklist like the one recommended by Dean and Voss (1999) to determine objectives, sources of variation, rules for assigning experimental units to treatments, measurements to be made, experimental procedure, pilot experiments, a statistical model, type of analysis, and other important experimental considerations. When evaluating EFPI sensors for high temperature strain measurements, determining which control variables and response variables to measure was a challenge. Experimental outputs for this paper included strain correlation and apparent strain measurements on Test Item 1 (a rectangular piece of Aluminum 2024 measuring 1.5 inches by 8.25 inches (38.1mm by 209.6mm)), Test Item 2 (a rectangular piece of CC-1 measuring 1.25 inches by 4 inches (31.8mm by 101.4mm)), and Test Item 4 (a round piece of CC 69.8mm in diameter) in a large test matrix.

Preliminary Design of Experiments (DOE) Control Factors

Test Type	Specimen Material	Specimen Shape/Size	Attachment Techniques	Fiber & SG Location	Specimen Side	Test Temperature	Max Test Strain	Atmosphere
Room Temperature Load	C-C Samples With Flame Spray	Round Diameter 2.75 “inches	LaRC Flame Spray	Center For In-Plane	Top	Room Temperature	0με	Normal Air
Apparent Strain	2024-T3 AL	Rectangular 1.5x8x.125 ”	Ceramic Cements (e.g. Sauereisen 13)	Near End For Bending	Bottom	Low 550 F	500με	Nitrogen Purged
Combined	Inconel 718	Rectangular 1x12x.125	M Bond 610		Both	Medium 1100 F	2000με	
	Rene 41		AE 10			High (1945F=1063C)		
	Ti64							
	ScrapC-C							

Many possible control factors were determined as shown in the table of preliminary control factors. Experiments run to date are considered pilot experiments in an attempt to complete this test matrix with different test types, materials, sizes, attachments, locations, ages, atmospheric environments, oven types, temperatures, and strains.

Preliminary Design of Experiments (DOE)
Partial Test Matrix

No.	Test Type	Material	Size	Attachments	Location	Gages	Atm	Oven	Temp.	Strain
1	Bending	AL2024	1.5x8.25	Sauereisen 13 or Ceramic Cements	Center	Fiber Optic & Foil & TC	None	None	Room Low	1000 με
2	Apparent Strain	X-37 #1	1-1/4x4	Flame Spray & Sauereisen 13	Center	Fiber Optic & Foil & TC	N2	L & L	500F 2000F	None
4	Apparent Strain	Round	2.75	Flame Spray – Then Cements	Center	Fiber Optic & Foil & TC	N2	Lamp Bank (L&L)	2000F	None
11	Apparent Strain	Round C-C	2.75	Flame Spray	Center	Fiber Optic & Foil & TC	N2	Lamp Bank (L&L)	2000F	None

The actual test items studied to date are included in the above partial design test matrix. As time and manpower becomes available, more test specimens should be tested.

Preliminary Design of Experiments (DOE)

- Correlation between EFPI and Strain Gages at room temperature using bending loads.
  - **Technician opportunity to practice mounting EFPI sensors on known materials i.e. Aluminum and CC with flame sprayed base coat**
  - **Measure outputs to determine correlation between EFPI sensors & strain gages**
- *Apparent Strain Curves*
  - **Measure apparent strain curves up to 1600ºF (871.1ºC) on Test Item 2**
    - **EFPI sensors attached to CC with a flamed sprayed base coat**
    - **TC and 2 EFPI sensors mounted with Sauereisen 13**
    - **Convention strain gage mounted using M-Bond 600 adhesive**
  - **Heat specimens but not strain in 2 types of heat tests**
    - **Clamp specimen to lab bench-heat it to about 500 ºF (260 ºC) using a heat gun**
    - **Placed specimen in oven for apparent strain up to 2000°F (1093.3 ºC)**
- *Combined Strain Correlation and Apparent Strain at High Temperatures*
  - **Building a combined temperature and mechanical loading test chamber**
  - **Correlation between the EFPI sensor and strain gages at low, medium and high temperatures**
  - **Subject specimens to 2100ºF (1148.9 ºC) and 1000 με of in-plane or out-of-plane loads**
  - **Chamber will have nitrogen purge capabilities**
  - **Attain set temperature in less than 1 hour- simulate thermal transient**

1. Engineers correlated EFPI sensors and standard strain gages using bending and axial loading at room temperature. AFRL technicians practiced mounting EFPI sensors and foil strain gages on materials, such as aluminum, steel, and CC with a flame sprayed base coat. Piazza (2004) provided AFRL the NASA-DFRC recommended installation instructions for flame spraying EFPI sensors onto test items. In the laboratory, engineers measured the strain outputs for bending loads to determine the strain correlation.
2. AFRL engineers conducted limited testing to measure apparent strain curves up to 1600°F (871.1°C) for fiber optic EFPI sensors attached to sample CC materials with a flamed sprayed base coat provided by NASA-LARC. A later chart shows the layout for the sensors on Test Item 2 (CC rectangular coupon), where there are two EFPI Sensors(Fn-42 and Fn-37) and one thermocouple (TC) mounted with Sauereisen 13 and a convention strain gage mounted using M-Bond 600 adhesive. To measure apparent strain, engineers heated these specimens but did not strain them in two types of heat tests. First, they clamped the test specimen to the laboratory bench and heated it to about 500ºF (260ºC) using a heat gun. Next, they placed it in an oven for measuring apparent strain curves at temperatures up to 2000°F (1093.3ºC). Engineers purged the chamber with nitrogen to prevent subjecting the test article to an oxidizing environment, which would have destroyed it at temperatures above 800°F (426.7ºC).
3. AFRL built a combined temperature and mechanical loading test chamber, which will enable correlation between the EFPI sensor and strain gages at low, medium and high temperatures. It will be capable of subjecting specimens to 2100°F (1148.9ºC) and 1000 με of in-plane or out-of-plane loading. The chamber will have nitrogen purge capabilities and attain a set temperature in less than 1 hour, which will simulate thermal transient environments. The chamber encloses a high temperature quartz lamp bank.

Test Item 1 Laboratory Bending and Heat Tests (2024-T3 Al)

- **Room temperature tests**
- **Approximately equal bending strain on strain gage and EFPI sensors by clamping Al beam to a lab bench**
- **Bent to stimulate tension and compression then compare the strain gage and EFPI sensor outputs**
- **Outputs slightly different**
- **After corrections for GL, the EPFI sensor and strain gage outputs correlated well**

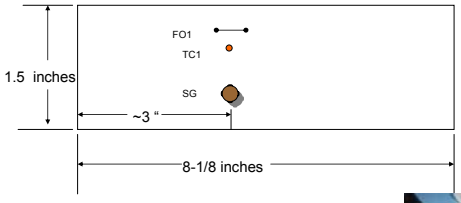

F1- EFPI fiber sensor Attached using Saureiensen #13.
TC- ThermoCouple Attached using Saureiensen #13
Route TC wires & fibers toward Right Hand Side of Plate
SG – Document SG Type and Bonding

Low Heat Setup

Test Item 1(2024-T3 Al) Layout

Next we will present test results to date on Carbon-Carbon (CC) and Aluminum specimens. Using the Test Item 1(2024-T3 Al) layout shown in the figure, engineers conducted several quick look tests at room temperature. For the simple bending test, they achieved approximately equal bending strain on both the strain gage and EFPI sensors by clamping the aluminum beam to a laboratory work bench. As the beam was bent to stimulate tension and compression, engineers compared the strain gage and EFPI sensor outputs. These values were slightly different. After small corrections for Test Item 2's GL, the EPFI sensor and strain gage outputs correlated at room temperature.

This correlation was similar to the results for more extensive experiments conducted by Hare and Moore (2000). The correction most likely involved gage length measurement uncertainty since the bond area is not infinitesimal small.

Engineers heated the aluminum specimens to approximately 500˚F using a heat gun. As predicted by the adhesive manufacture, the ceramic Sauereisen 13 adhesive detached from the aluminum during heating.

Test Item 2(CC) Laboratory Bending, Heat Gun and Oven Heat Tests

- **Rectangular piece of CC**
- **Designed for 2000ºF (1093.3ºC)**
- **4 sensors on Test Item**
- **Circular spots flame sprayed by Roth (2004) so that ceramic adhesives would bond to item at high temperatures**
- **Sauereisen 13 to bond EFPI sensors and thermocouple (TC) on the flame spray spots**
- **Mounted strain gage (SG) using M-Bond 610 adhesive**
- **Comparisons to 500ºF (260ºC)**

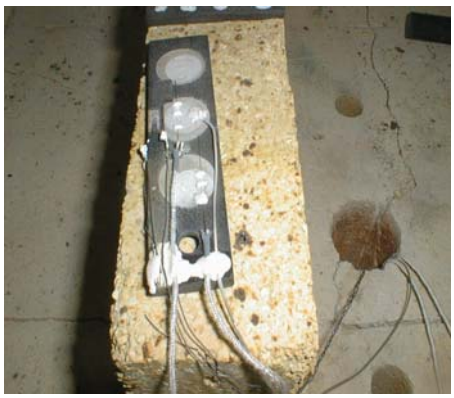

Test Item 2 (CC2) After 1600ºF Hest Test (F-42, TC, SG-Center & F-37-Hole)

- Next we will discuss test item 2(CC) laboratory bending, heat gun and oven heating tests. Test Item 2 was a rectangular piece of CC material designed to withstand temperatures up to 2000ºF (1093.3ºC). The photograph above shows the sensors on Test Item 2 on January 7, 2005. The circular spots on the CC were flame sprayed by Roth (2004) so that ceramic adhesives would bond to Test Item 2 at high temperatures. As shown in the figure, engineers used Sauereisen 13 to install an EFPI sensor (F-37) on the flame spray spot near the hole and an EFPI fiber sensor (F-42) and thermocouple (TC) on the center spot. They then mounted a conventional strain gage (SG), type WK-00-350, along side the flame sprayed spot using M-Bond 610 adhesive for comparison at temperatures up to 500ºF (260ºC).

- F-42 was reattached following the initial bending test and the first heat gun test because the reflector end of F42 detached. Unfortunately, GL was not re-measured following this adjustment, so engineers used the nominal value, GL=10.0, for F42 for later tests. For F37, the gage length was 8.921. The GL for F42 was 9.824 mm before it was reattached.

Test Results on Test Item 2 (CC)

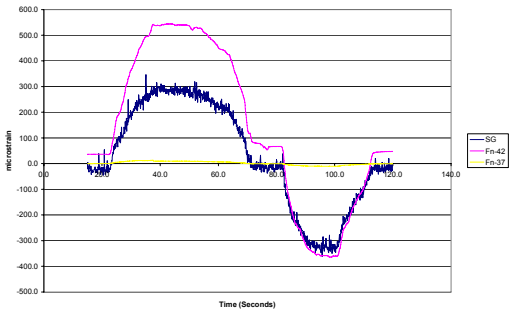

- Clamped beam to lab bench to form a cantilever beam
- Bent manually to induce tension and compression of roughly equal magnitudes into each of the sensors.
- Outputs for fiber F-42 and the strain gage in the center of the beam and fiber ID F-37 located at the end of the beam
- F-42 and strain gage output correlated, but have significant different readings

Lab Bending F-42 (Red) and Strain Gage (Blue) – F-37 (Yellow)-no Correction

During December 1, 2004, engineers clamped the beam to a laboratory work bench to form a cantilever beam that could be bent manually to induce tension and compression of roughly equal magnitudes into each of the strain sensors. The graph shows the outputs for fiber ID Fn-42 and the strain gage in the center of the beam and fiber ID Fn-37 located at the end of the beam. Although fiber Fn-42 and the strain gage output appear to be correlated, they have significant different readings.

Test Results on Test Item 2 (CC)

- **Plot of output of fiber Fn-42 versus strain gage confirms high correlation**
- **Best fit straight line (BFSL), (y=1.4993x+95.962 with correlation R^2 = .99) relates the fiber output to the strain gage output**
- **BFSL should have slope=1**
- **Correct fiber out by dividing GL by slope (1.4993)**

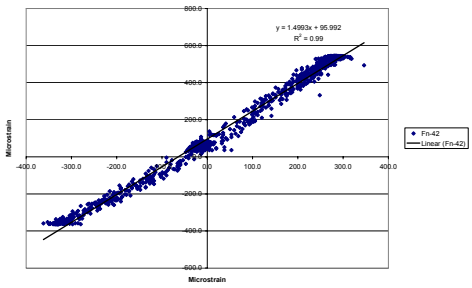

Lab Bending - F42 versus Strain Gage

The plot of the output of fiber Fn-42 versus the strain gage in the plot of fiber F42 versus strain gage reading confirms this high correlation. Using regression for the best fit straight line (BFSL), engineers obtained the equation (y=1.4993x+95.962 with a correlation R^2 = .99) relating the fiber output to the strain gage output. Ideally, the BFSL readings for the strain gage and EFPI sensor should be equal. Thus, we can correct the fiber output by dividing GL by the slope (1.4993) of the BFSL shown on the graph. Since this is a significant correction, signal conditioning and other factors may also need to be considered.

Test Results on Test Item 2 (CC)

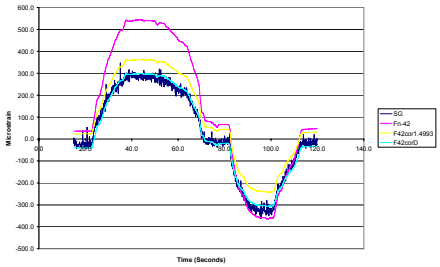

Lab Bending F-42 (Corrected) and Strain Gage

- **Figure shows the original fiber F-42 output, strain gage output, and corrected F-42**
- **Correction results much closer agreement, even without applying the offset term**
- **Same technique worked for bending tests on Item 1**
- **Note: Output of F-37 was much lower as expected since it's further from the clamped edge of the beam**

This figure shows the original fiber Fn-42 output, strain gage output, and corrected fiber Fn-42. The correction resulted in much closer agreement, even without applying the offset term. This same technique worked well for the bending tests on Test Item 1. Note that the output of fiber F-37 near the end of the beam was much lower; engineers expected this result because fiber F-37 was further away from the clamped edge of the beam at the flame spayed circle farthest from the hole.

Test Results on Test Item 2 (CC)

- **Heat Item to about 500ºF (260ºC) using heat gun for the apparent strain curve**
- **F42 did not return to zero με**
- **F37 had small response**
- **Strain gage had noisy signal**
- **Mixed results**
- **Continue to heat specimen in an oven to search for new insights.**

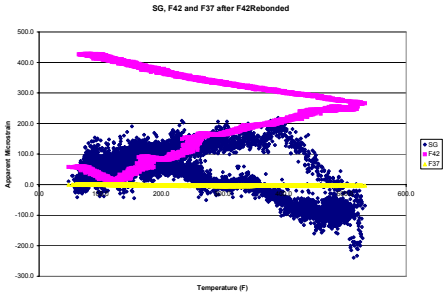

After Heat Gun Test to 500ºF

Next, engineers heated Test Item 2 up to approximately 500ºF (260ºC) using a heat gun. This figure shows test Item 2 (CC2) after Heat Gun Test to 500ºF on December 1, 2005(F42, TC, SG-Center&F37 Hole).

The apparent strain curve in the plot shows the EFPI sensors F42 and F37 and Strain Gage versus temperature. F42(on the center) did not return exactly to zero microstrain, and F37 (near the hole) had very small response. Also, the standard strain gage had a noisy signal. These mixed results caused AFRL engineers to continue to heat the specimen in an oven to search for new insights.

Test Results on Test Item 2 (CC)

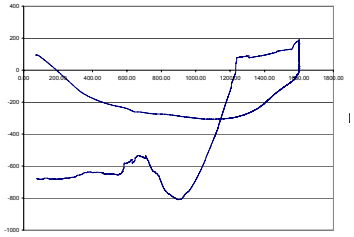

F-42 vs Temperature for 2 hour soak at 1600°F

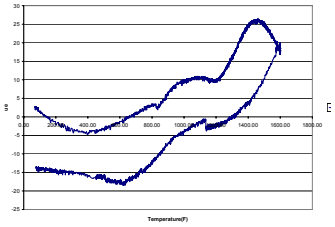

F-37 vs Temperature for 2 hour soak at 1600°F

- **Fiber 42 has large step changes**
- **F-37 lower apparent strain reading**
- **Strain gage fails at ≈ 800ºF(426.7ºC)**

First, AFRL engineers conducted oven tests using thermal profiles with a maximum of 500ºF (260ºC) and 600ºF (315.6ºC) before proceeding to the profile with a maximum temperature of 1600ºF (871.1ºC) during January 2005. The earlier photo showed Test Item 2 after it was heated to 1600ºF (871.1ºC). Successful completion of this test required over 40 hours, a much longer time than originally planned. Engineers set the oven controller for a half hour ramp and a two hour soak at 1600ºF (871.1ºC). However, the actual ramp time was about four hours; the soak time was two hours, and the cool down time was almost 40 hours. At 24 hours, engineers opened the oven door to decrease cool down time. The top figure shows the result of plotting apparent strain versus temperature for fiber F42, and the bottom figure shows the result of plotting apparent strain versus temperature for fiber F37. Note that fiber 42 has large step changes in jumps and that fiber 37 has much lower apparent strain reading. The conventional strain gage output started to fail at about 800ºF (426.7ºC). At failure the conventional strain gage had an apparent strain reading exceeding 6000 microstrain.

At a later date it may be useful to also look at the strain gage data as it got heated up to failure.

Test Item 4 (Round CC) Laboratory Bending and Heat Gun Tests

- **Round CC coupon**
- **Strain gage and commercial EFPI strain sensor mounted with M-Bond 610 adhesive**
- **3-EFPI sensors and 1-TC mounted with Sauereisen 13**

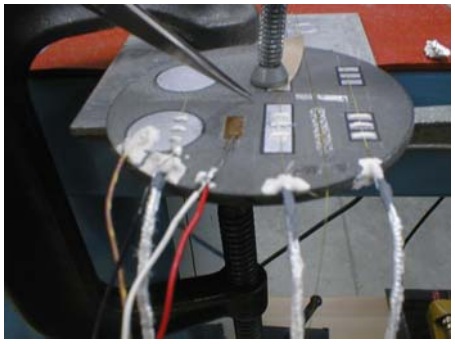

Lab Bending & Heat Gun Tests
(Sensors: L-R)
TC, F3-52, SG, F2-47, COTS-K01025, F1-No ID

The following preliminary data are from laboratory testing of Test Item 4, shown in the photograph. Test Item 4 was a round coated CC coupon with a strain gage and commercial EFPI strain sensor (Serial number K010125), both mounted with M-Bond 610 adhesive. Engineers mounted three additional EFPI sensors (F3 for serial number F52, F2 for serial number F47, and F1--a sensor with no serial number), and a thermocouple with Sauereisen 13.

Apparent Strain Results-Test Item 4 (CC)

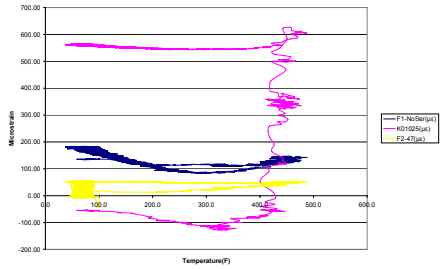

Test Item 4 Apparent Strain versus Temperature during Heat Gun Test

- Apparent strain to 450ºF using heat gun
- F3-optical signal conditioner displayed "CHECK SENSOR," - connector failed
- Bending tests does not demonstrate good correlation since the round specimen did not produce equal strains
- Commercial sensor (k01025) did not return to zero after heat gun removal
  - May indicate improper cure time
  - Found sensor unbonded at one end
- F2 and F3 show similar apparent strain
  - Apparent strains < 120 με up to 440ºF (226.7 ºC)
  - F2 much lower response than F1.
  - Zero shifts for F2 and F3 after bending test

Figure 13 shows apparent strain for temperatures up to 450ºF using the heat gun on test item 4 on February 3, 2005. For EFPI sensor F3, the optical signal conditioning displayed "CHECK SENSOR," and optical tests indicate that the connector most likely failed. As expected, the round specimen did not produce equal strain during the bending test. A point load was applied to the end of the round test item 4 to generate a bending load. This was only applied to generate some output from each of the strain gages. To analyze the exact strain field would be extremely difficult plus note that in the figure, there was a single point reaction by the C-clamp which further complicates the strain field. The apparent strain showed the commercial sensor did not return to zero after heat gun removal. The large shift in commercial EFPI strain sensor (K01025) may have indicated improper curing time for the M-Bond 610 adhesive. A post inspection of this sensor showed it became unbonded at one end. EFPI fiber F1 and F2 show similar apparent strain characteristics with apparent strains less than 120 με at temperatures up to 440ºF (226.7ºC). F2 had a much lower response than F1. The zero shifts for F2 and F3 began after bending test completion. Additional evaluations are needed to determine the validity of these results. The next step will be to quickly heat Test Item 4 to temperatures as high as 2000ºF (1093.3ºC) in AFRL's new high temperature chamber.

Results of High Temperature EFPI Sensors Test on Specimens

- **EFPI sensors operate to 1600ºF(871.1 ºC)**
- **GL needs correction for ideal correlation between EFPIs and SGs**
- **Need to understand physics of using Sauereisen 13 with the CC**
- **Need evaluations of attaching EFPI sensors using the flame spray**
- **Large number of control factors needed**
- **Testing is slow and tedious**
- **Goal: Measure strain on structures exceeding 2000 ºF (1093.3 º C)**
- **EFPI strain sensors can survive extreme thermal environments**
- **Preliminary experiments using ceramic adhesives are not conclusive**
- **Effort requires more practice and experimental iteration**
- **Developed oven to evaluate high temperature strain measurement techniques in timely and realistic manner**
  - **i.e. heat specimen to 2000 ºF (1093.3 º C) in less than a half hour**
- **Future High Temp Tests May Use Flame Spray Attachment Technique**

-In limited testing to date, the EFPI sensors successfully operated throughout a thermal heating cycle up to 1600ºF (871.1ºC). However, a number of questions about apparent strain and correlation between EFPI sensors and conventional gages require resolution.

-Room temperature test comparisons between the EFPI sensor and conventional strain cage indicated that in order to achieve good correlation, the gage length (GL) requires correction in a manner similar to that shown by Hare and Moore (2000).

-As predicted by its manufacturer, Sauereisen 13 adhesive did not bond well to a heated Aluminum specimen. However, further evaluation is needed to understand the physics involved with using Sauereisen 13 adhesive with the CC specimens. AFRL will conduct more evaluations by attaching EFPI sensors using the flame spray techniques.

-A very large number of control variables are involved. Preliminary control factors should be expanded and reviewed to include additional control variables of interest. Because this type of testing is slow and tedious, efficiency is very important. An EFPI sensor test matrix will be expanded as new material test requirements evolve.

New Thermal Spray Chamber and Quartz Oven

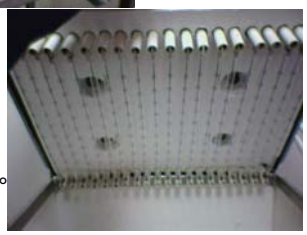

- Flame Spray Capability activated December 2005
- Developed Quartz Lamp Oven for tests over 3000°
- Finish Item 4 Testing in New Oven Soon
- Plasma Spray Capability planned for September 2006
- Continue to Study Attachment Techniques

-AFRL engineers are determined to find a method to measure strain on aerospace structures at temperatures up to 2000ºF (1093.3ºC). They are confident that the EFPI fiber strain sensors will successfully take strain measurements in extreme thermal environments where many previous sensors failed. Preliminary experiments with mounting sensors using ceramic adhesives are not conclusive. The sensors appear to survive and give outputs at temperatures up to 1600ºF (871.1ºC) whereas conventional strain gages incinerate at temperatures exceeding 700ºF (371.1ºC). AFRL engineers hope that attaching the sensors by using flame spray or plasma spray techniques pioneered by NASA-LARC and NASA-DFRC will enable accurate apparent strain curves. This effort will require additional practice and experimental iteration. The photograph on the left shows AFRL personnel being trained to use the new flame spray capability.

-In addition to developing a flame spray capability, AFRL developed an oven to evaluate high temperature strain measurement techniques in a timely and realistic manner. The oven will heat a test specimen to 2000ºF (1093.3ºC) is less than a half hour and cool the specimen down in less than a half hour. Currently, the heat gun can raise the specimen to about 500ºF (260ºC) in a couple of minutes, and then, the air cools the specimen quite rapidly. The other photos on the right show the oven and it's quartz lamps that will heat test specimens to very high temperatures over 2000 °F.

Survival Results of EFPI Sensors on a C-C Test Item during Aug04

- EFPI Sensors and TCs installed on a high temperature structure.
- Test Item heated with no mechanical loads
- Use the high temperature EFPI sensors
  - Sensors flame sprayed on by LaRC
  - Fibers are gold plated
- Nine of Ten EFPI Sensors on C-C Survived
- EFPI Sensor on Inconel Failed

Survival results of EFPI Sensors installed on a C-C test item during August 2004 are optimistic. Eleven EFPI Sensors and a number of thermocouples (TCs) were installed on the test item and monitored while the item was heated to temperatures as high a 2000 F. The following table shows temperatures achieved near the EFPI sensors during testing on several test runs and a typical plot of apparent strain versus temperature for one of the more extreme cases. Ten of the EFPI fibers were installed on CC material and one of the EFPI sensors was installed on Inconel material.

Highest Temperatures and Apparent Strain on C-C Test Item

Max Temperature (°F) from Time History Plots

	1000	1001	1002	1003	1004	1005	1006	2000
T8 - F1 & 2	170	490	880	1150	1200	1275	1050	1275
T35 - F3 & 4	90	170	370	590	510	630	950	780
T6 - F5 & 6	162	255	450	605	620	750	1420	800
T12 - F7 & 8	115	290	605	870	900	1050	1100	1190
T17 - F9 & 10	95	120	230	390	390	420	970	610
T29 - F11	70	120	180	250	240	280	880	850
T38SH - F11	78	110	170	230	220	280	810	380

Fiber F9 went bad during run 1001
Fiber 11 went bad during run 1006 at T = 469 °F
Maximum Temperature on Specimun was 2290 °F

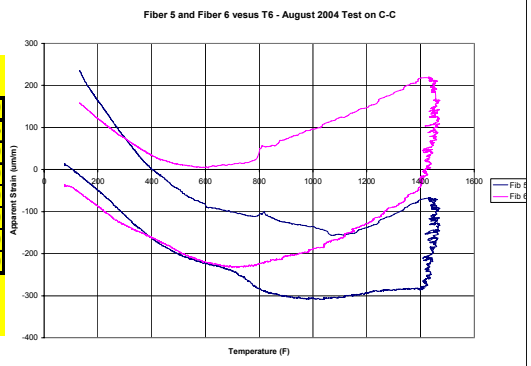

The above table summarizes the highest temperatures reached by the EFPI sensors during a several runs on the test item during August 2004 (Base2006). There are still many questions about material properties, adhesive properties and other concerns that still need to be answered. For a low CTE material such as C-C the high temperature sensors did have a high survival rate (i.e. 9 out of 10 survived). The plot on the right shows the apparent strain curve for run 1006 where fibers 5&6 reached a temperature of 1420 °F. As seen in the plot, during a temperature soak at 1420 °F the two fiber sensors shown had a shift in its reading. Engineers are still trying to determine whether or not this is due to adhesive or material properties or some combination. Perhaps someone in the audience will be able to shed light on what is happening.

Highest Temperatures and Apparent Strain on Inconel

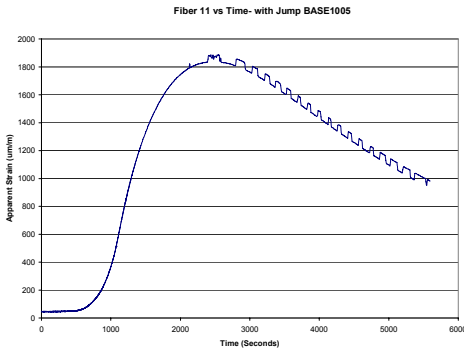

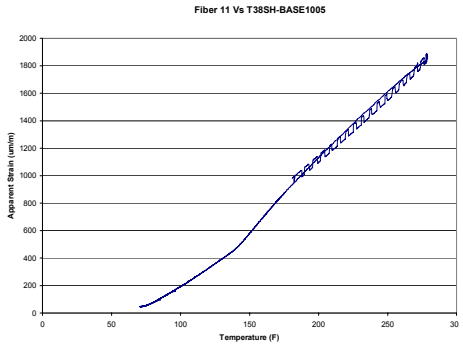

As noted earlier, one of the EFPI sensors was mounted on Inconel, which has a higher CTE. The data above show data for this sensor on the final run before failure. During the next run at higer temperature the fiber failed. Notice that sometimes there is a 50 microstrain jump in the fiber output. This is somehow related to ½ of the 850 nm wavelength of light being used in the signal conditioning software algorithm. That is for a given gage length of 7.81 mm, we find a jump error of 425 nm/7.81mm or about 54.4 microstrain. This is one unresolved difficulties of using the EFPI sensors.

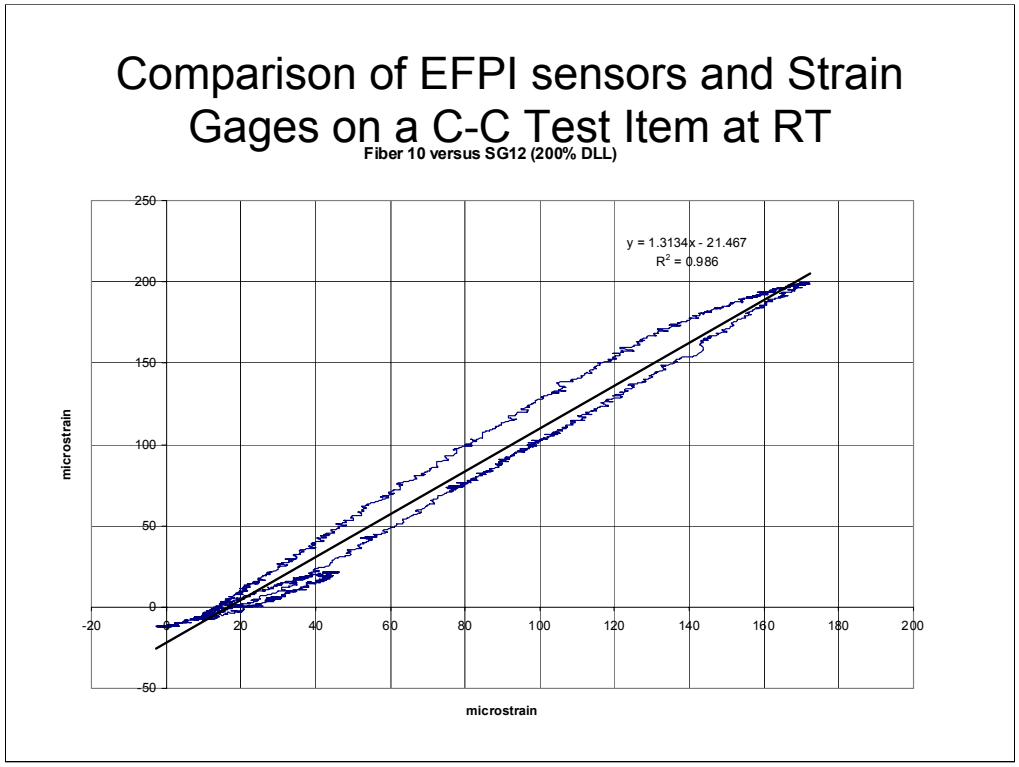

Four strain gages were mounted next to the flame sprayed EFPI sensors on the C-C test item at room temperature during August 2004. During this testing the item was mechanically loaded to induce strain at room temperatures. As shown in the graph, there is good corelation between the strain gage and the EFPI sensor, but the strain levels were very low. Ideally the slope should be one, but as mentioned earlier, the discrepancy may be due the difficulty in determining the gage length precisely. The plot shows the highest strain level attained during the testing and is very low for static testing. The slope of the fiber being greater than 1 indicates that the fiber gage length may need to be adjusted to get a slope of 1.

However, the slope being more than 1 might also indicate equipment signal conditioning may also be a concern.

Initial EFPI COTS Sensor Evaluations in Small Chamber

- COTS EFPI Sensors and Strain Gages
- 18 Runs Heat&Cool (Usually -60 to +160° F)
- Free End of Astro Quartz and Graphite Side
- SG , EFPI Fiber and TC adjacent to each other)

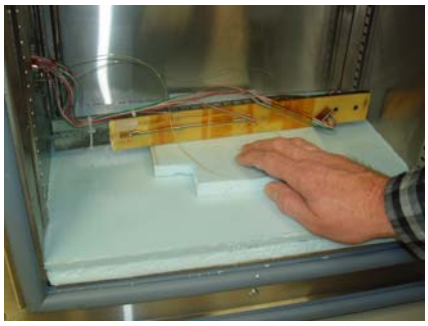

During January of 2006, AFRL started evaluation of commercial-off-the-shelf (COTS) EFPI strain sensors that are specified to work up to 350°C. A quick introduction to this work will now be given. AFRL engineers had two LUNA Commercial Off the Shelf EFPI Sensors mounted adjacent to foil strain gages as shown in the above figure. The fibers were LUNA stain sensors and the strain gages were CEA-03-250UW-350 on the graphite and CEA-06-250UW-350 on the astro quartz. A strain gage, strain sensor and T-Type TC were mounted on each material. The EFOU sensors are rated to operated at temperatures up to 350 °C. These COSTS EFPI sensors are mounted differently than the high temperature sensors discussed earlier. They were mounted with AE10 adhesive in accordance with the manufacture's instructions. The AE 10 adhesive rather than a higher temperature adhesive was used due to other testing constraints. Most of the 18 runs were accomplished from -60 to + 160 °F but some later runs were used to try to destroy the sensors using a heat gun as shown in the right hand photograph.

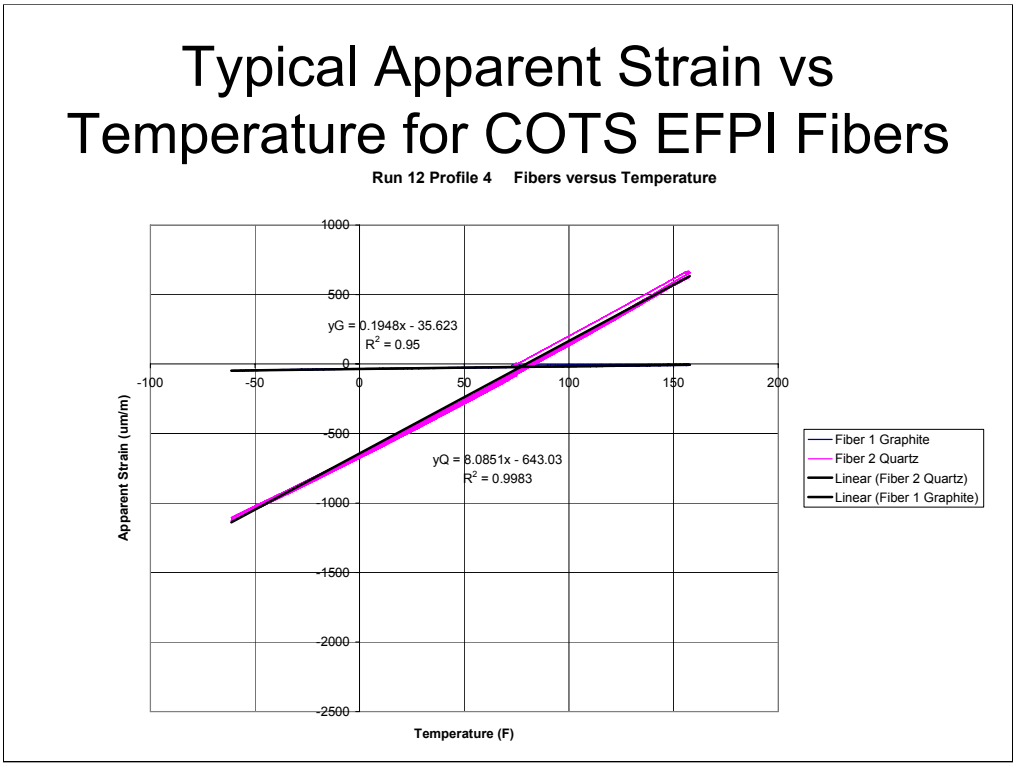

A total of 18 temperature profiles were run during December to January of 2006.

A table of these runs is listed below for the our reference. This typical graph shows the apparent strain versus temperature for the fiber sensor on the Quartz and the Graphite specimen's free end. As seen in the graph, the apparent strain versus temperature was very linear over the temperature range of -60 °F to 160°F. This was true for all the runs where the adhesive temperature were not exceeded.

Run Number	Profile Number	1stSoak Temp	Number Soaks	High Temp	Low Temp	Test Items
1	1	Heat	2	160	-60	Spec
2	2	Cool	2	160	-60	Spec
3	1	Heat	2	160	-60	Spec
4	1	Heat	2	160	-60	Spec+Quartz
5	2	Cool	2	160	-60	Spec+Quartz
6	2	Cool	2	160	-60	Spec+Quartz+Al
7	2	Cool	2	160	-60	Spec+Quartz+Al
8	3	Cool	4	160	-60	Spec+Quartz+Al
9	4	Heat	4	160	-60	Spec+Quartz+Al
10	3	Cool	4	160	-60	Spec+Quartz+Al
11	0	None	0	74	74	Spec+Quartz+Al
12	4	Heat	4	160	-60	Spec+Quartz+Al
13	5	Cool	4	250	-100	Spec
14	5	Cool	4	250	-100	Spec
15	6	Heat	4	300	-100	Spec
16	HeatGun	Heat	0	600	70	Spec-End Only
17	7	Heatonly	2	160	74	Spec+Quartz+AL
18	3	Heat	4	160	-60	Spec+Quartz+Al

Apparent Strain-COTS EFPI Sensors Compared to Strain Gages

- Fiber Linear but not Compensated
  - Graphite - Lower CTE - 9.3 x 10^{-7} m/m/°F
  - Quartz Composite - Higher CTE - 3.1 x 10^{-6} m/m/°F

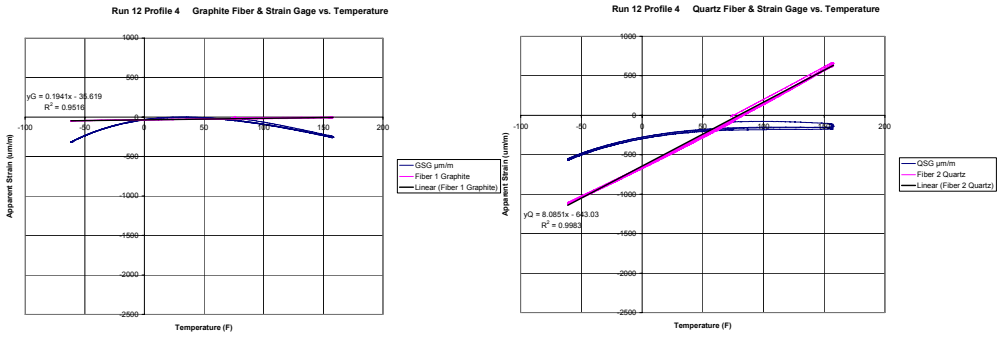

The above graphs compare the apparent strain of the strain gages and of the EFPI fiber strain sensors. All of the strain sensors were mounted with AE-10 adhesive. Note that apparent strain is linear versus temperature for the fibers. The fiber output appears to correlate with the CTE of the material. Graphite has a low CTE of 9.3 x 10-7 m/m/°F and the CTE for the Cyanada-Ester Astro Quartz is 3.1x10-6 m/m/°F. However the slope of 1.948x10^{-6} for the graphite and 8.0851x10^{-6} do not match the expected values of CTE for the two materials. Other factors such as fiber material properties and adhesive properties may account for the differences.

For metals, such as aluminum, there will probably be even a larger apparent strain due to thermal expansion which must be compensated or accounted for. Strain gage material is usually made of a special alloy to provide some thermal compensation. Refer to the Measurements Group (1992) technical note (TN-504-1) titled “Strain Gage Thermal Output and Gage Factor Variation with temperature” for information on self-temperature Compensated Strain Gages.

Initiatial Evaluation of Fiber Bragg Grating (FBG) Fibers

- Evaluating a DSS Systems by LUNA Innovations, Inc.
- Allows Viewing of of Strain Profile
- FBG Fiber Gratings Detect Strain every Centimeter.
  - e.g. 50 Sensors per .5m on 3 Test Beams
  - 7075-T6, 2024-T3, Ti-64

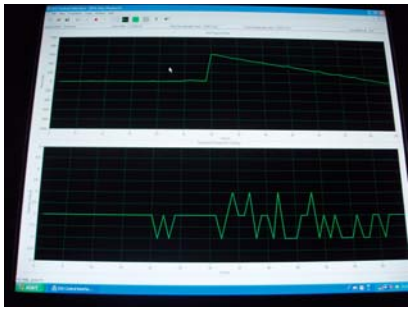

AFRL is currently evaluating a DSS Systems made by LUNA Innovations, Inc.

FBG fibers have gratings on fibers to detect strain every centimeter. The photo on the left shows a beam with two strain gages and a FBG fiber being bent in the laboratory for comparison. The right hand photograph show how the fiber displays the strain profile along the beam as it is compressed using simple bending.

Per LUNA(2006) “The sensing element of the Luna DSS is the Fiber Bragg Grating (FBG) that is etched into the core of an optical fiber by a laser. An FBG reflects like a mirror, but only a specific wavelength of light gets reflected. The reflected wavelength is directly related to the grating period. The grating period is affected by changes in the environment such as thermal or mechanical changes. Thus, temperature, strain, and other engineering parameters can be calculated by measuring the normalized change in wavelength of the grating.

An optical fiber may contain any number of gratings, each acting as a sensing element. In this manual, grating and sensor are synonymous. Because the Luna DSS provides one channel that can handle up to 500 sensors each, the system can acquire up to 500 measurements per scan. Multiple sensors in a small, rugged package are key advantages of fiber optic sensors over their electrical-based counterparts. “

Comparing FBG to Strain Gages

- Each FBG Detects Strain every 1 Centimeter
- Need to Correlate SG position with Fiber Sensor
- Hard to Correlate Fiber & Strain Gage Time.

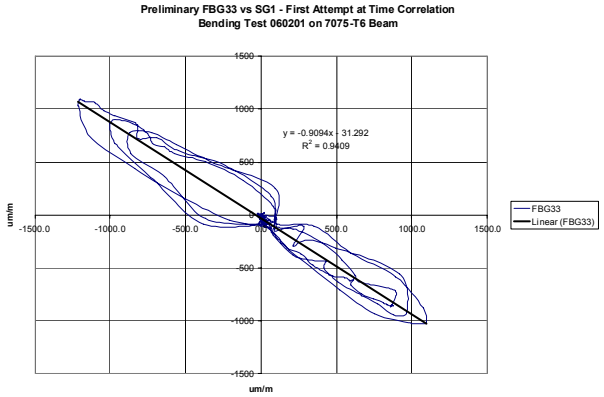

Since the data system used to record and process the optical strain data from the fiber is usually separate from the strain gage signal conditioning and recording system , it is hard to correlate the data between the strain gage and FBG fiber as the test beam is bended. In addition the strain gage system sample rate (set for 10sps exactly) is not an even multiple of the FBG system sample rate of about 1.56 samples per second. The graph shows an initial attempt to plot the strain output of the a FBG sensor versus the strain gage output. The above figure shows a slope of close to -1 between the FBG sensor opposite of the strain gage but the apparent hysteresis may be the result on time synchronizations difficulties. This is a difficulty that is currently being worked.

The above plot was very time consuming to generate using a spreadsheet so MatLab routines are being developed to help process the collected data more efficiently.

2.5 Meter FBG Fiber on Structural Aluminum Test Item (1.25×10^{-5} m/m/°F)

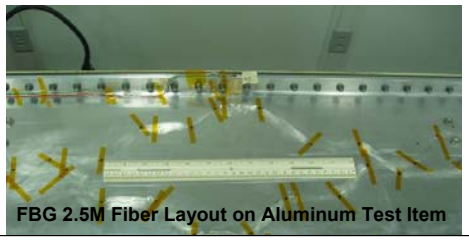

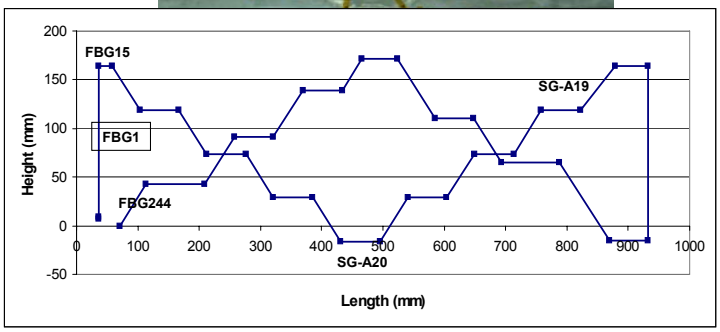

The chart shows a 2.5 meter fiber installed on an Aluminum(Al2024-T3&7050-T7651 with 12.5 x 10^{-6} per °F expected CTE) test item during a May 2006 AFRL/VA structural test. The FBG fiber is bonded to a base coat of AE10 adhesive with a covering layer of AE 10 adhesive per the fiber manufacturer's instructure. The bottom chart show the layout of the fiber on the structure.

Basically there is a strain sensor every 1 cm. The top left link is the location of FBG sensor #15 and the final diagonal leg on the bottom is the location of the final FBG #244. Additional strain gages were added at the bottom center (A20) and near the top right (A19). Isolating the FBG number in this installation posed a interesting geometric challenge. A heat gun was used to verify the FBG number as indicated above. Correlating the time base of the strain gage recording system and the FBG recording system is in the process of being solved by AFRL engineers.

244 FBG Sensors
Sample Thermal Test From RT to 160°F

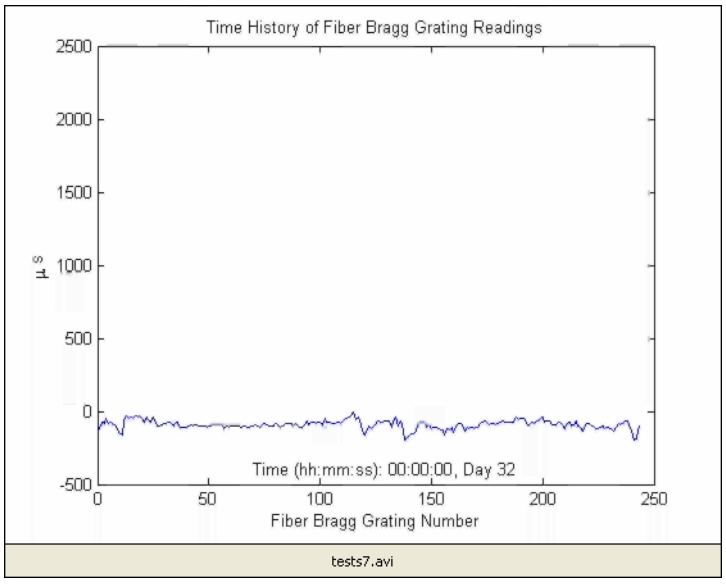

The FBG sensors was zeroed at room temperature (about 70 F) and then the temperature elevated to about 160 F. The apparent strain for all the FBG grating appeared to be about 1300 x 10-6 which is approximately the expectation using the CTE for aluminum(S7). This video (tests7.avi) shows the impact of heating only from room temperature to 160 °F. These analyis is due to the efforts of Enrique Medina from Materials Directorate, who is helping to evaluated data files larger than Excel can handle efficiently. (i.e. tests with fibers handling more that 256 gratings,)

244 FBG Sensors
Sample Fatigue Cycling at Room Temperature

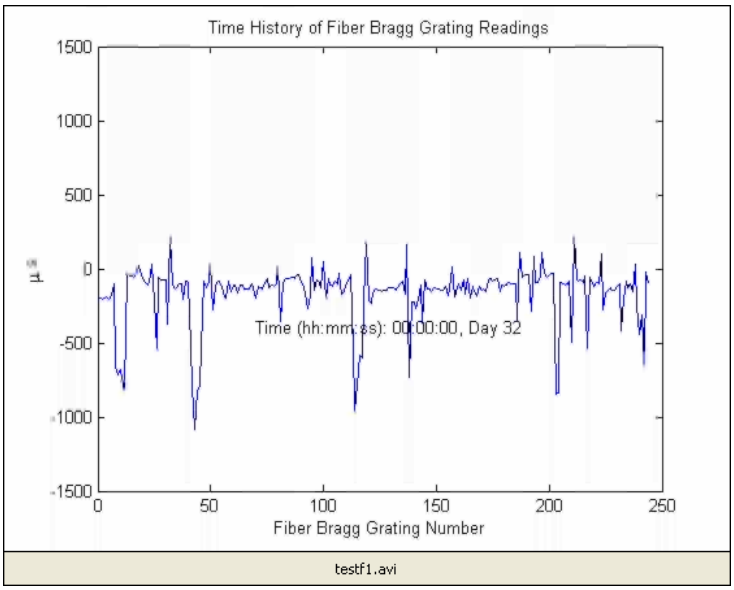

The display above shows the initial appearance of the 240 FBG sensor gratings as the test item cycles though a number of fatigue excursions. The preliminary video (testf2.avi) shows how the fiber works during mechanical cycles. You can easily see the strain distribution along the length of the fiber.

Conclusions

- Tests using EFPI High Temperature
  - Results on survivorability looks promising.
  - Needed more study of material, adhesive and fiber interactions and properties at high temperature.
  - Attachment techniques are very experimental.
- COTS EFPI Sensors operate satisfactory
  - May need compensation for high CTE Materials
- Initial FBG seem to work at Room Temperature
  - Need to complete more detailed evaluations
- So far all fiber sensors evaluated operate at very low frequency response (i.e. less than a few hertz).
- Displays on aluminum test item are very interesting.

As shown earlier, high temperature EFPI sensors show promise for making strain measurements at high temperatures, however, more study of materials and attachments techniques are needed.

The COTS EFPI sensors operated satisfactory but may need thermal compensations techniques similar to strain gages for high CTE materials such as aluminum.

AFRL need to complete more detailed analysis of bending beam data using FBG sensors. Most difficult is accounting for the different data acquisition systems used by fibers and convention strain sensors and other instrumentation.

So far all fiber sensors evaluated operate for static type of structural testing. The displays generated by the Aluminum are very interesting.

AFRL will definitely continue to evaluate the development of fiber optic based sensors.

References

- Bhatia,V., Murphy, K.A., May, R.G.,Claus,R.O.,Tran,T.A.,Greene,J.A. and Coate, J.E. (1996), "High Temperature Sapphire Optical Fiber Interferometer Strain Sensor", High Temperature and Materials Science, Vol.35, pp 31-41, Humana Press Inc., Totowa, NJ.
- Banaszak, D. and Kretz, L., "Lab Evaluation of Fiber Optic EFPI Sensors for Extreme Environmental Tests", JSM 2005, Minneapolis, MN, August 2005.
- Dean, A.and Voss, D. (1999), Design and Analysis of Experiments,Springer-Verlag, NY,NY.
- Hare, D.A. and Moore, T.C., (2000), Characteristics of Extrinsic Fabry-Perot Interferometric (EFPI) Fiber-Optic Strain Gages, NASA/TP-2000-210639, December, Langley Research Center, Hampton, VA.
- Luna Innovations, (2001), Application Notes "Extensometer EFPI Strain Gages", Blacksburg, VA.
- Luna Innovations, (2005), The Flight Capable Distributed Sensing System User's Manual Version 4.0, Blacksburg, VA.
- Moore, T.C., (1997) Recommended Strain Gage Application Procedures for Various Langley Research Center Balances and Test Articles', NASA Technical Memorandum 110327, March, NASA Langley Research Center.
- Moore, T.C. and Hart, D.A., (2002) "Performance Evaluation of Commercially Available High-Temperature Fiber-Optic Extensometer on Inconel 100 Test Beams at Elevated Temperatures" Western Regional Strain Gage Committee-2002 Winter Meetings, Society Experimental Mechanics, Bethel, CT.
- Poland, Steve (2002), "Luna Fiber Optic Strain Gages and their Applications" Western Regional Strain Gage Committee-2002 Winter Meetings, Society Experimental Mechanics, Bethel, CT.
- Piazza, Anthony, (2004), Conversions, NASA-Dryden Flight Research Center, CA.
- Roth, Mark, (2004), Conversions, Modern Machines & Tool Co., Inc., Newport News, VA.
- Shull, L.C. and Wright, C.P., (2002) "Strain Gages for Extreme Temperatures", Experimental Techniques, January/February, pp39-41.
- Vishay, Measurements Group, (1992) "Strain Gage Thermal Output and Gage Factor variation with Temperature", TN-504-1, Raleigh, NC.
- Yu, Francis T. and Yin Scizhue Editors (2002), Fiber Optic Sensors, Marcel Dekker, inc., New York.

Above is a list of references used in compiling this presentation. They Include information about high temperature strain measurement using EFPI sensors, statistics and general information on EFPI and FBG fiber sensing systems.

Acknowledgements

- **NASA-LARC**
  - **Trent Kite, Tom Moore, Mark Roth, and David Hare**
- **NASA-DFRC**
  - **Anthony Piazza**
- **Luna Innovations**
  - **Trevor Rice, Larry Vicari, Roger Duncan, Mike Nuckels**
- **AFRL Government and Contractor Personnel**
  - **Air Vehicles Directorate: Ken Leger, Mathew Leonard, Roderick Moore, Mark Clapper, Mike Morando, Dale Gerken, Paul Brown and Jim Taylor, Gerry Ewing, Ken Koverman, Melissa Withrow and Eric Brewster, Chris Thompson, David Preston-Mason, Todd Busey, Rueben Meeks, Hannah Peterson, Cindy Swanson, Dave Hart, Doug Schneider, Bob Schneider and other support personnel.**
  - **Materials Directorate: William Freemantle, Enrique Medina**
- **HPI - Vince Wnuk**

Acknowledgements are extended to the many personnel who helped the authors gather data and prepare this presentation. The authors thank the personnel at NASA-LARC and at NASA-DFRC for their help during numerous conversations regarding the use of EFPI fiber optic sensors. In addition, Luna Innovations personnel were very helpful in initiating AFRL personnel to fiber sensor technology. Most importantly, many AFRL structural test facility experts (governments employees and SelectTech contractors and AdTech contractors) provided an abundance of labor and helpful advice. Special thanks are extended to Melissa Withrow for providing technical editing expertise for the earlier paper. Also, Vince Wnuk helped to train VA personnel on using the new flame spray capability. Bill Freemantle loaned VA the DSS system procured from LUNA on a SBIR contract and Enrique Medina helped immensely with software development using Matlab.

4.0 SUMMARY AND CONCLUSIONS

In summary, this report contains papers and presentations in section 3.0 that illustrates the use of advanced instrumentation in a number of air vehicle applications.

Papers 2, 3, 5, 6 and 8 illustrates the application of an autonomous dosimeter data acquisition system for defining the environment of a C-130 during flight.

Papers 1 and 4 describe laboratory experiments utilizing a visual crack measurement system to observe cracks growing in structure while excited with an electrodynamics shaker.

Papers 7 discusses initial evaluation of Extrinsic Fiber Fabry-Perot Interferometer (EFPI) fiber optic strain sensors at high temperature.

Paper 9 gives an overview of initial AFRL work with EFPI and Fiber Bragg Grating (FBG) sensors.

Paper 10, gives a more detailed summary of experiments using a FBG sensor using simple beams.

This in-house work unit provided the Air Force with advanced instrumentation capability and knowledge of state-of-the-art techniques to measure static and dynamic strains for several applications including some at very high temperatures. This included use of a damage dosimeter on a flying C-130, computation of crack growth curves using a patented visual crack measurement system and evaluation of optical fiber sensors for measuring strain in extreme environments. Additional papers are in progress but will not be finalized until after the close out of this in-house work unit. In conclusion, this work unit titled "Versatile Measurement Techniques to Validate Analytical Structural Mechanical Models", resulted in effective and efficient instrumentation and analysis techniques to efficiently and quickly acquire strain, high temperature and visual crack data for a number of Air Force applications.